Penny Sarchet

Lincoln College

University of Oxford

The Developmental and Genetic Basis of Explosive Pod-Shatter in *Cardamine hirsuta*

Trinity Term, 2012

Thesis submitted for the degree of Doctor of Philosophy

Penny Sarchet **Lincoln College**

The Developmental and Genetic Basis of Explosive Pod-Shatter in *Cardamine hirsuta*

Thesis submitted for the degree of Doctor of Philosophy, Trinity term 2012

Abstract

Dispersal is a key trait across biology. Within plants, a variety of explosive seed dispersal mechanisms are seen. Whilst ecological and mechanical studies have described this important evolutionary adaptation in many species, a genetic and developmental understanding of explosive seed dispersal is lacking.

In this thesis, the morphology and development of the explosive seed pods of *Cardamine hirsuta* – a member of the Brassicaceae – are characterised in detail, with reference to its close relative, the model organism *A. thaliana*. Comparison of fruit morphology between these two species and across other Brassicacean species generated hypotheses regarding the function and polarity of morphological features.

In order to identify genes that are necessary for *C. hirsuta* fruit development, a genetic screen was conducted and a range of mutants identified and subsequently characterised. Analysis of the indehiscent *valveless (val)* mutant revealed a loss of valve tissue and an expansion of valve margin identity in the silique. Mapping and sequencing identified a mutation in the MADS-box gene *FRUITFULL (FUL)*, which results in a truncated protein, as the likely cause of the *val* phenotype. Consideration of *ful* mutants in *C. hirsuta* and *A. thaliana* allowed comparison of the genetic patterning of the fruit dehiscence zone in these two species.

The genetic interactions between fruit mutants characterised in this thesis and mutants in shoot patterning genes revealed common regulatory networks underlying leaf and fruit development in *C. hirsuta*.

Together, comparison of wild-type and mutant *C. hirsuta* siliques with those of *A. thaliana* and other Brassicacean species suggests that specialised cell layers within the valve silique region are of key importance to *C. hirsuta*'s explosive dehiscence mechanism.

Acknowledgements

I really appreciate the opportunity Angela Hay gave me to work in her research group, and for her invaluable training, supervision and support. Many thanks also to my second supervisor Miltos Tsiantis for all his ideas and advice.

I learned a great deal from the Hay and Tsiantis research groups, and I particularly value the mentorship that Sarah McKim and Gemma Bilsborough gave me. I am grateful to Maria Cartolano and Bjorn Pieper for sharing their molecular mapping expertise.

I was fortunate that many members of Oxford's Department of Plant Sciences took an interest in my work and were generous with their advice and time. I am especially grateful to Hugh Dickinson for his TEM work and histological advice, and to John Baker for photography. Specific contributions, from researchers from both Oxford and elsewhere, are named throughout this thesis.

I would also like to mention my examiners, Jane Langdale and Naomi Ori, for such an interesting and thorough discussion of my work.

I am grateful to the Newton Abraham board for their Biological Sciences Studentship, which funded me for the majority of my DPhil. I am also grateful for additional funding from the University of Oxford's Department of Plant Sciences, and for two senior scholarships from Lincoln College.

I want to thank Louise Durning and Carmella Elan-Gaston at Lincoln College for their support during my time there, and the Lincoln College MCR for being a constant source of enthusiasm, understanding, and camaraderie.

Most of all, I want to thank my parents and sister for their support and encouragement over the course of my DPhil, and for all the shared laughs that sustained me throughout this time.

List of Abbreviations

35S	Cauliflower Mosaic Virus 35S promoter
A. americanum	*Arceuthobium americanum*
AGL8	AGAMOUS-LIKE 8
A. halleri	*Arabidopsis halleri*
ALC	ALCATRAZ
A. lyrata	*Arabidopsis lyrata*
AMAS	Analysis of Multiply Aligned Sequences
A. quadripartita	*Adriana quadripartita*
ARF	auxin response factor
AS1	ASYMMETRIC LEAVES1
AS2	ASYMMETRIC LEAVES2
A. suecica	*Arabidopsis suecica*
A. thaliana	*Arabidopsis thaliana*
A. tumefaciens	*Agrobacterium tumefaciens*
BEAST	Bayesian evolutionary analysis by sampling trees
bHLH	basic helix-loop-helix
B. juncea	*Brassica juncea*
B. napus	*Brassica napus*
B. nigra	*Brassica nigra*
B. oleracea	*Brassica oleracea*
BP	BREVIPEDICELLUS
B. rapa	*Brassica rapa*
CAPS	cleaved amplified polymorphic sequence
cas1-1	*cardamine asymmetric leaves1-1*

cbp	*cardamine brevidpedicellus*
C. bursa-pastoris	*Capsella bursa-pastoris*
C. canadensis	*Cornus canadensis*
cetl	*cardamine ettin-like*
C. corymbosa	*Cardamine corymbosa*
C. grandiflora	*Capsella grandiflora*
C. hirsuta	*Cardamine hirsuta*
CLSM	confocal laser scanning microscopy
CLV1	CLAVATA 1
CLV2	CLAVATA 2
CLV3	CLAVATA 3
cM	centiMorgans
Col-0	Columbia-0
CRN	CORYNE
C. rubella	*Capsella rubella*
C. scutata	*Cardamine scutata*
dCAPS	derived cleaved amplified polymorphic sequence
D. biarmipes	*Drosophila biarmipes*
D. bipectinata	*Drosophila bipectinata*
dfo	*delayed fruit opening*
DIC	differential interference contrast
D. kikkawai	*Drosophila kikkawai*
D. melanogaster	*Drosophila melanogaster*
D. pseudoobscura	*Drosophila pseudoobscura*
D. santomea	*Drosophila santomea*

D. subobscura	*Drosophila subobscura*
EMS	ethyl methane sulphonate
en*a*	endocarp *a*
en*b*	endocarp *b*
EtOH	ethanol
ETT	ETTIN
F_1	first filial generation
F_2	second filial generation
FIL	FILAMENTOUS FLOWER
FUL	FRUITFULL
GFP	green fluorescent protein
GUS	β-glucuronidase
H. crepitans	*Hura crepitans*
het	heterozygote
I. capensis	*Impatiens capensis*
I. floridanum	*Illicium floridanum*
I. glandulifera	*Impatiens glandulifera*
IND	INDEHISCENT
JAG	JAGGED
KNAT2	KNOTTED-LIKE FROM ARABIDOPSIS THALIANA 2
KNAT6	KNOTTED1-LIKE HOMEOBOX GENE 6
KNAT7	KNOTTED-LIKE HOMEOBOX OF ARABIDOPSIS THALIANA 7
KNOX	KNOTTED1-LIKE HOMEOBOX
LB	Luria Broth

L*er*	Landsberg *erecta*
lig1	*less lignin1*
M_1	first generation of mutagenised seed
M_2	second generation of mutagenised seed
M_3	third generation of mutagenised seed
MAFFT	Multiple Alignment using Fast Fourier Transform
M. alba	*Morus alba*
MRCA	most recent common ancestor
MS	Murashige & Skoog
MYA	million years ago
MYB46	MYB DOMAIN PROTEIN 46
MYB52	MYB DOMAIN PROTEIN 52
MYB58	MYB DOMAIN PROTEIN 58
MYB63	MYB DOMAIN PROTEIN 63
MYB103	MYB DOMAIN PROTEIN 103
NAC	NO APICAL MERISTEM/ATAF/CUP-SHAPED COTYLEDON
NPA	N-1-napthylpthalamic acid
NST1	NAC SECONDARY WALL THICKENING PROMOTER1
NST3	NAC SECONDARY WALL THICKENING PROMOTER3
NUB	NUBBIN
oli	Oligosperma
O. pumila	*Olimarabidopsis pumila*
ORF	open reading frame
O. sativa	*Oryza sativa*
ox	Oxford

PAS	periodic acid-Schiff
PAT	polar auxin transport
PBS	phosphate buffered saline
PCR	polymerase chain reaction
P. hybrida	*Petunia hybrida*
PID	PINOID
R. islandica	*Rorippa islandica*
RPL	REPLUMLESS
SAM	shoot apical meristem
SEM	scanning electron microscopy
SHP1	SHATTERPROOF1
SHP2	SHATTERPROOF2
S. martensii	*Selaginella martensii*
SND1	SECONDARY WALL-ASSOCIATED NAC DOMAIN 1
SND3	SECONDARY WALL-ASSOCIATED NAC DOMAIN 3
SNP	single nucleotide polymorphism
SOC	Super Optimal Broth with Catabolite repression
SPT	SPATULA
STM	SHOOT MERISTEMLESS
T_1	first generation of transformed seed
TAIR	The Arabidopsis Information Resource
TBO	toluidine blue O
TEM	transmission electron microscopy
TILLING	Targetting Induced Local Legions in Genomes
twi	*twisted*

val	*valveless*
WT	wild type
YAB3	YABBY 3
YEB	Yeast Extract Broth

Contents

1. Introduction

Dispersal is a widespread process throughout biology. The success of a species depends upon its ability to find a suitable habitat. Similarly, the future of a species is dependent on its ability to disperse its offspring to favourable environments. In stationary organisms, such as plants, dispersal of the next generation provides a valuable opportunity to move.

A variety of seed dispersal modes and mechanisms are seen across the Angiosperms. The explosive propulsion of seeds from their parent is a forceful and dramatic trait, seen in many flowering plant families. Explosive pod shatter and seed dispersal is interesting as an evolutionary adaptation, an ecological process, and as a morphological feature. Whilst a number of studies have sought to observe and describe the mechanics and ecology of various explosive seed dispersal mechanisms, a developmental and genetic understanding of such mechanisms is lacking.

This thesis aims to establish a genetic handle on explosive seed dispersal. Genetic and developmental approaches are used to examine the process of explosive pod shatter in the Brassicacean species *Cardamine hirsuta*. A close relative of *Arabidopsis thaliana*, this species is amenable to the methods of molecular genetics, and is the ideal model organism for investigating the genetic networks and developmental pathways that coordinate explosive seed dispersal.

1.1. Dispersal and the Angiosperms

1.1.1. Dispersal: a widespread biological process

Dispersal can be defined as the “unidirectional movement of an individual away from its place of birth” (Clobert et al. 2001; Bullock et al. 2002; Nathan 2006). This process is widespread throughout biology, occurring across animals,

plants, fungi and prokaryotes. As a life-history trait, the movement of offspring away from their parent or parents has strong implications for a species' population biology, affecting its distribution, abundance, dynamics, persistence and community structure (Dieckmann et al. 1999).

In 1977, W.D. Hamilton and Robert M. May showed that simple mathematical models suggested that dispersal was important for organisms even in predictable, uniform environments, stating that a parent could be expected to send a high proportion of its propagules away from its own locality even when the mortality for these propagules is extremely high (Hamilton & May 1977).

A number of ecological factors are posited to drive the evolution of dispersal. These can be divided into five main pressures: habitat extinction risks, competition among kin, spatial and temporal variability within a habitat, cost of dispersal, and inbreeding (Dieckmann et al. 1999). Dispersal is seen as beneficial in unstable or fluctuating habitats or to avoid competition or inbreeding amongst an individual's offspring, however these benefits are offset against the costs of dispersal, which include dispersal morphology investment and dispersal mortality risks. This trade-off between dispersal costs and benefits is one faced by all biological organisms.

Seed dispersal is one form of dispersal, and is exhibited by all Spermatophyte plants (seed plants). A variety of seed dispersal mechanisms are seen across the Spermatohytes, particularly in the Angiosperms, where fruit morphologies adapt to enable different modes of seed dispersal. The fruit of *C. hirsuta* is adapted for explosive seed dispersal, and uses a rapid and powerful mechanism to propel its seeds from the fruit.

1.1.2. Turgor pressure powers rapid dispersal mechanisms in fungi and land plants

When compared with animals, fungi and the land plant organisms appear static, growing only through slow and gradual movements. Dispersal can therefore be seen as a more critical life stage for plants and fungi, allowing sessile organisms a rare opportunity to spread into new environments. In both fungi and plants, the dispersal of spores, pollen, propagules and seeds is often associated with some of the most sudden, rapid and forceful movements seen in these normally stationary organisms.

Rapid movements in both kingdoms, such as the snapping of carnivorous plants, the sudden release of fungal spores, or the expulsion of pollen at anthesis, are usually the result of hydraulics, and the cell walls possessed by both kingdoms are key to building the differential turgor pressures required for these processes. Analyses of these hydraulic processes in terms of their duration and the distance that fluid is transported allows for their classification into two categories – fluid transport-limited and inertia-limited (Skotheim & Mahadevan 2005). This latter category utilises elastic instabilities to store up elastic energy, which is then suddenly released, powering movements of greater speeds than are seen in the former category, which move only by using turgor pressure to swell or shrink (Skotheim & Mahadevan 2005).

1.1.2.1. Explosive spore release is common throughout the Ascomycota

An example of rapid dispersal driven by turgor pressure is seen in the fungal phylum *Ascomycota*. The phylum is named for its asci, tubular sacs which house sexual spores, called ascospores, and each of the three subphyla of the *Ascomycota* contains species which forcibly expel these ascospores (Trail 2007).

Since 1887, turgor pressure has been believed to power the upwards stretching of asci and the forceful pushing of the ascospores through a pore at the apex of the ascus (De Bary 1887; Trail 2007).

The acceleration measured inside the *Gibberella zeae* asci is the highest recorded in any organism (Trail 2007), with ascospores accelerating to 8 500 000 ms^{-2} (Trail et al. 2005). A proposed model for this process comprises two phases of pressure increase, with turgor pressure initially displacing ascospores towards the ascus apex (Trail 2007). This turgor pressure may be built by the accumulation of the osmolyte mannitol which has been detected in these asci (Trail et al. 2002). The second phase, in which the asci stretch and discharge at high speed, is thought to occur when the mannitol-initiated movement of water into the ascus stimulates a hypothesised proton pump (Trail 2007). It is proposed that the action of this pump results in the additional influx of water that underlies the hydrostatic pressure that drives the stretching and firing of the asci (Trail 2007), however this is an untested hypothesis.

1.1.2.2. Violent spore discharge occurs in non-seed plants

Rapid discharge mechanisms are seen in a variety of forms across the Embryophytes (land plants), and are not limited only to the reproductive functions of the Angiosperms. A range of non-seed plant lineages show explosive spore release, including mosses and liverworts (Bryophytes), *Selaginella* (a Lycophyte) and some ferns (Monilophytes).

A key model for rapid dispersal in basal plant lineages has been the moss *Sphagnum* genus. Mosses belong to the paraphyletic grouping of non-vascular plants which are most basal in the land plant phylogeny, the Bryophytes. The *Sphagnum* capsule, which contains the spore sac, contracts longitudinally as it

dries, facilitated by a large number of pseudo-stomata which are positioned only in the middle regions of the capsule (Duckett et al. 2009). The capsule has a thick, firm epidermis of four or five cell layers (Sundberg 2010). As the capsule dries, pressure builds inside an air-filled cavity which lies below the spore sac, leading to bursting of the capsule along a line of weakness and release of the spores (Ingold 1965; Sundberg 2010).

Many liverwort species also show violent spore dispersal mechanisms. Liverworts are another basal land plant lineage placed within the Bryophyte grouping. Liverwort capsules are typically smaller than moss capsules, and sudden dispersal is achieved through hygroscopically-induced twisting and splitting of this capsule (Ingold 1965; Sundberg 2010). As well as explosive spore dispersal, some liverworts such as *Conocephalum conicum* also violently release sperm (Shimamura et al. 2008).

The Lycophytes, which emerged after the lineages of the Bryophytes, are the most basal grouping of the Tracheophytes (vascular plants). Within the Lycophytes, rapid dispersal mechanisms are seen in the spikemoss *Selaginella*. Upon maturity, the megasporangium of *S. martensii* splits distally down both sides, exposing two basal and two apical megaspores (Webster 1995). As the flaps of the megasporangium bend backwards, the two apical megaspores are carried with them (Webster 1995). When the thin-walled cells of the flaps' basal hinges collapse, along with the internal chamber that houses the two basal megaspores, these spores are suddenly expelled from the megasporangium. The flaps are then jolted towards each other, releasing the apical spores (Webster 1995).

Within the Monilophytes too, some ferns show rapid spore dispersal. In *Angiopteris*, it is the drying of the spore itself that results in its sudden movement

(Hovenkamp et al. 2009). The forces required are generated by shrinking of the spore during dehydration, which results in deformation of the spore wall. The spore wall progressively deforms until it buckles inwards, creating a cavity between two of its layers. When this cavity forms, the outer of these two layers is no longer under tension and returns to its original shape, releasing elastic energy which expels the spore (Hovenkamp et al. 2009).

1.1.2.3. Rapid expulsion is seen in Angiosperm pollen release mechanisms

Parallels to the rapid mechanisms of spore release in fungi and non-seed plants can be seen in the Angiosperms during the process of anthesis. In *Cornus canadensis*, the flower explodes open in under half a millisecond, releasing its stamens which reach speeds of around 3.1 ms^{-1}, which propel the pollen grains from the plant (Edwards et al. 2005). Like other rapid movements in plants and fungi, this mechanism is dependent upon turgor pressures.

The changes in turgor that underlie most rapid movements in plants are frequently facilitated by ion pumps, which actively alter the hydrostatic pressures of parenchyma cells (Simons 1992; Taylor et al. 2006). It is thought that such ion pumps are responsible for the parenchymal pressures that build within the filament of the stamens of *Morus alba* (Taylor et al. 2006). High levels of humidity appear to increase turgor within the filaments of this species, building a store of elastic potential energy in the stamens, which are held in tension by a restraining organ (Taylor et al. 2006). When humidity drops, the anthers dehisce and slip past the restraining organ, causing them to rapidly straighten-up, and propel pollen from the flower in a rapid motion similar to that described in *C. canadensis* (Edwards et al. 2005; Taylor et al. 2006). The speed of pollen expulsion in *M. alba* is one of the fastest speeds recorded in biology (Taylor et al. 2006), and is a high-performing

example of the “explosive fracture” mechanism described by Skotheim and Mahadevan (2005), in which tearing of tissues occurs within an intertia-limited system. It is worth noting that explosive pollen dispersal in *M. alba* consists of two tightly-coupled processes: anther dehiscence, followed by pollen launching.

1.1.3. The Angiosperms are a highly successful and morphologically diverse clade of land plants

All flowering plants, including *C. hirsuta*, belong to the largest group of land plants, the Angiosperms. Compared to other major land plant groups, whose fossils date back to at least the Early Mesozoic, the Angiosperm fossil record is relatively young – the earliest undisputed flowering plant fossils date from the Early Cretaceous (Friis et al. 2006). Despite their recent emergence, the Angiosperms are incredibly species rich, with estimates of the total number of extant species ranging from 223 300 (Scotland & Wortley 2003) to 422 127 (Govaerts 2001). The Angiosperms therefore represent one of the greatest radiations on land in recent geological history (Davies et al. 2004). Angiosperms dominate almost all the terrestrial vegetation zones, are found in nearly every habitat on Earth, and exhibit huge diversity, particularly in reproductive morphologies (Friis et al. 1987; Soltis & Soltis 2004).

Defining synapomorphies of the Angiosperms include ovules enclosed within a carpel, the growth of the pollen tube through the carpel, a highly reduced gametophyte stage, endosperm formation following double fertilisation, stamens that posses two pairs of pollen sacs, and phloem elements comprising sieve tubes and companion cells (Friis et al. 1987; Soltis & Soltis 2004). Whilst many of the Angiosperms’ defining synapamorphies relate to reproductive features, the reproductive structures of the Angiosperms also provide some of the most stark

examples of morphological variation within the group. Flowers range in size from the minute (*Hedyosmum*) to over a metre wide (*Rafflesia*), whilst seeds range from the dust-like in orchids to giant coconuts (Friis et al. 2006).

1.1.4. Angiosperm fruits are defined by morphology and dehiscence

The flowering plants are named Angiosperms after the carpel or “vessel” that encloses their seed (Sporne 1974). Together, the Angiosperm fruit and seed function to protect and nurture the developing plant embryo and ultimately to disperse it, functions which render them evolutionarily sensitive components of a plant’s life cycle (Tiffney 1984; Ferrandiz 2011). Because fruits enable seeds to travel, they are seen as a key contributor to the evolutionary success of the Angiosperms (Ferrandiz 2011).

The fruit and seeds develop from the carpel and ovules after fertilisation. During this process, the ovary wall develops into the fruit wall and this pericarp is divided into three layers – the exocarp, mesocarp and endocarp. Simple fruits develop from one carpel or a fusion of several (a syncarpous pistil), whilst aggregate fruits develop from multiple separate flowers, and complex fruits comprise additional floral organs, for example the receptacle or bracts (Ferrandiz 2011). Fruits can be further classified by whether they are fleshy or dry and if they are dehiscent or indehiscent (Ferrandiz 2011).

The majority of fruits fall into three broad groups – fleshy indehiscent, dry indehiscent, and dry dehiscent (Heywood et al. 2007; Ferrandiz 2011). The fruit of *C. hirsuta* is a type of dry and dehiscent fruit, called a silique. Siliques are characteristic of the Brassicaceae, developing from a syncarpous pistil comprised

of two fused carpels, opening along two lines, and retaining a persistent central partition (Heywood et al. 2007; Ferrandiz 2011).

1.1.5. Seed dispersal in the Angiosperms

Naturalists took an interest in the wide diversity of seed dispersal morphologies and mechanisms as early as the 3rd and 2nd centuries BC, when Aristotle and Theophrastus described various seed-dispersing animal-plant interactions in the 'Historia Animalium' (Aristotle) and 'Historia Plantarum' and 'De Causis Plantarum' (Theophrastus). In 1785, Holmberger published his *Theory on the Dispersal of Plants over the World*, and Darwin investigated the ability of seeds to survive digestion by birds, sticking to vertebrates' feet, and immersion in salt water (Darwin 1860).

Research by these early investigators of seed dispersal, and by many scientists since, has delineated the modes of Angiosperm seed dispersal, their morphological adaptations, and the factors driving dispersal evolution.

1.1.5.1. Seed dispersal is adapted to abiotic and biotic modes

Seed dispersal can be described by two phases, where Phase I describes the mechanisms that transport a seed from its parent to a new surface and Phase II describes subsequent movements from that surface, either into the soil or to a second location (Chambers & MacMahon 1994).

Seeds can be dispersed either by abiotic or biotic agents (Levin et al. 2003). The abiotic dispersal of seeds can be by hydrochory (water) or anemochory (wind), whilst the biotic dispersal syndromes are either zoochory (dispersal by animals), autochory (dispersal by a plant's own mechanisms) or barochory (dispersal by the weight of the diaspore alone) (Van der Pijl 1972). Generally,

biotic dispersal has tended to attract more scientific attention than abiotic mechanisms (Chambers & MacMahon 1994).

The huge diversity seen in fruit morphologies allows for a wide variety of adaptations for dispersal. Hydrochorous fruits possess water-repellent surfaces and buoyancy mechanisms, whilst wings, hairs, feather and parachutes assist flight during anemochory (Ferrandiz 2011). Epizoochory – dispersal on the exterior of animals – can be facilitated by sticky surfaces or barbs and hooks (Sorensen 1986; Chambers & MacMahon 1994), whilst fleshy fruits are adapted for endozoochory – dispersal via an animal's digestive tract (Ferrandiz 2011).

Autochory, as is seen in *C. hirsuta*, is achieved by explosive fruits. These often use hydrostatic pressure to eject their seeds, like the squirting cucumber (*Ecballium*) whose seeds spurt out of a hole left by the former pedicel (Ferrandiz 2011). However, dry explosive mechanisms are seen too, and include the explosive mechanism of *C. hirsuta*. Further examples of explosive and ballistic fruits will be discussed in section 1.1.6.

1.1.5.2. Dispersal is usually beneficial, but carries associated risks

Hamilton and May noted that dispersal attempts can often appear to be suicidal or, in the case of seeds that fall only a few feet away from their parent after it dehisces, "too feeble to be worthwhile" (Hamilton & May 1977). With such a wide variety of Angiosperm adaptations for seed dispersal, there must be real and significant benefits to dispersal for the plants that possess them.

In their 1982 review, Howe and Smallwood summarised three hypotheses describing possible advantages to local seed dispersal: the Escape Hypothesis (to avoid high mortality near parents), the Colonisation Hypothesis (to colonise newly-suitable habitats) and the Directed Dispersal Hypothesis (to discover additional

microhabitats suitable for establishment (Howe & Smallwood 1982). Seed dispersal is also beneficial for minimising the effects of unpredictable temporal fluctuations in condition, allowing a plant to hedge its bets (Nathan et al. 2009).

Even in a homogeneous, stable habitat, a certain degree of dispersal will always be beneficial, as it reduces kin-competition by instead spreading offspring to compete with non-genetically similar individuals (Hamilton & May 1977; Rousset & Gandon 2002). However, the extent of the benefit of a specific dispersal strategy is dependent on the other dispersal strategies used within the population, as these affect both the number of competitors and their relatedness amongst non-dispersing and dispersing individuals (Levin et al. 2003).

There are high risks to seed dispersal and most seeds are ultimately eaten by predators or are dispersed to places in which they are unable to establish themselves (Nathan et al. 2009). The benefits to dispersal are also offset against the costs to the parent disperser (Rousset & Gandon 2002).

1.1.5.3. Seed dispersal mechanisms evolve amid trade-offs with other factors

The seed dispersal strategies of flowering plants heavily influence a species' fitness, so we can expect dispersal-related traits to experience strong selective pressures (Levin et al. 2003). The ancestral dispersal mechanism of the Angiosperms is thought to be the consumption of fleshy fruits by vertebrate frugivores (Van der Pijl 1972; Howe & Smallwood 1982). However, the fact that a single Angiosperm family can exhibit many different dispersal mechanisms suggests that fruits have since been subjected to varied and effective pressures that led to divergent selection (Howe & Smallwood 1982).

It has been argued that the main factors driving dispersal are kin competition and the spatiotemporal variability of the environment (Levin et al.

2003). These drivers reflect the dispersal benefits described in the Escape, Colonisation, and Directed Dispersal hypotheses. An optimal dispersal strategy, however, is also dependent on its trading-off against and coevolution with other traits and characters (Levin et al. 2003).

One such trade-off is that between seed size and seed number, two properties which show an inverse relationship (Ferrandiz 2011). Larger seeds are better adapted for enabling a new, individual seedling to become established, providing more resources for the next generation. However, these resources are expensive and cannot be dealt out generously across many seeds. Smaller seeds are therefore less supportive but can be produced in much greater numbers, providing more opportunities for dispersal. Whether a species produces few large seeds or many small seeds therefore represents a life history trade-off, with each species evolving a compromise adapted specifically to their niche and life habit.

1.1.6. Explosive seed dispersal in the Angiosperms

The seed dispersal mechanism of *C. hirsuta* is autochorous. Autochory – also referred to as ballistic or explosive seed dispersal – is seen in many families across the Angiosperms. Like the other rapid movement mechanisms that are found in land plants and fungi, these processes utilise turgor pressure to build tension and store energy, either through drying and dehydration, or through the mounting of hydrostatic forces.

Explosive seed dispersal is influenced by a range of physical and mechanical factors. The distance a seed is propelled is affected by the height of the fruit from the ground, its angle from the horizontal, its efficiency at transferring stored energy to the seeds, and the air resistance and drag experienced by the seeds in flight (Beer & Swaine 1977). It has been argued that it is the variations in

air drag (influenced by seed mass and shape) and the initial velocity (determined by the energy imparted by the parent fruit) that have the greatest effect on dispersal (Beer & Swaine 1977). Smaller seeds are subject to more drag than larger ones, as are faster-travelling seeds compared to slower ones (Vogel 2005). Unlike wind-dispersed seeds, which benefit from increased drag, ballistically-dispersed seeds seek to reduce relative drag, usually by minimising the surface area-to-volume ratio through a compact shape, large size, and high density (Stamp & Lucas 1983; Vogel 2005).

1.1.6.1. Explosive dispersal by fleshy fruit is often hydrostatic

An example of a fleshy fruit explosive mechanism is provided by a species of dwarf mistletoe *Arceuthobium americanum* (Viscaceae). As summarised by Friedman and Sumner (2009), the *A. americanum* seed is forcibly expelled from the pseudoberry fruit by hydrostatic pressure that builds in a mucilaginous tissue called viscin. Undertaking a morphological study of the *A. americanum* fruit, they found that the endocarp and lower mesocarp of the berry becomes flattened and filled with tannin-like substances to form a pseudo-seed coat, whilst the remaining layers of mesocarp form the viscin tissue (Friedman & Sumner 2009). They observed that this tissue comprised two types of cells, vesicular cells and viscin cells, the latter of which elongate and secrete a pectic mucilage. They hypothesised that the hygroscopic nature of these pectic acids is important in generating the hydrostatic pressure used to expel the seed, whilst the largely hydrophobic vesicular cells may play a role in abscission. The accumulation of tannins in the inner exocarp may impart high tensile strength to this layer, allowing it to resist the hydrostatic pressures that build up inside the fruit (Friedman & Sumner 2009).

1.1.6.2. Dry explosive dispersal utilises drying tensions

The silique of *C. hirsuta* is not fleshy, and is an example instead of a dry explosive fruit. Beer and Swaine (1977) describe the generation of potential energy for explosive dispersal by the deformation of fruit structure by drying as the most common method used for explosive seed dispersal. Structural tissues maintain the fruit form until their strength can no longer contain the generated stress, resulting in sudden rupture, removal of the seed from the fruit wall, and its propulsion out of the fruit (Beer & Swaine 1977).

Several examples of dry explosive dehiscence have been studied, including that seen in *Illicium floridanum* (Illiceae), a shrubby Magnoliid. Its fruit comprises a bowl-shaped aggregation of follicles, each of which splits along its ventral suture when it dehydrates (Roberts & Haynes 1983). The fruit is 83% water but loses approximately 20% of this prior to dehiscence (Roberts & Haynes 1983). Each follicle contains a single seed which appears to be propelled out through the follicle suture by the tensions formed by mesocarp dehydration and possibly the columnar sclerenchyma cells of the endocarp (Roberts & Haynes 1983). Roberts and Haynes also observed that mature fruits did not dehisce explosively if damaged by an herbivore or if dehydration was artificially slowed, and that gentle, artificial heating could be used to accelerate the onset of explosive dehiscence. They observed that the mean distance travelled by expelled seeds was 1.26 m with maximum distances of 3.5 m (without bouncing) and 5.8 m (with bouncing). Roberts and Haynes argue that the explosive dispersal mechanism seen in *I. floridanum*, a member of the Magnoliidae, suggests that early Angiosperms may have exhibited a range of dispersal mechanisms rather than depending upon the relatively basic fauna of the Cretaceous for seed dispersal.

Dry, dehiscent explosive seed dispersal has also been described in *Erodium* (Geraniaceae) (Stamp 1989; Jacobs & Lesmeister 2012), *Viola* (Violaceae) (Beattie & Lyons 1975) and in several species of the Euphorbiaceae (Swaine & Beer 1977; Narbona et al. 2005; Beaumont et al. 2009). To a limited extent, the genus *Impatiens* (Balsaminaceae) has served as a model for studying explosive seed dispersal (Schmitt et al. 1985; Hayashi et al. 2009; Jacobs & Lesmeister 2012).

Impatiens capensis is an annual plant growing in moist habitats, commonly referred to as jewelweed or touch-me-not (Schmitt et al. 1985). The *I. capensis* fruit appears to store energy in its five valves in the form of turgor pressure (Hayashi et al. 2009). When dehiscence occurs, these five valves coil suddenly, transferring some of this stored energy to the seeds which are propelled from the fruit (Schmitt et al. 1985; Hayashi et al. 2009). In their study of the mechanics of *I. capensis* dehiscence, Hayashi *et al*. observed that, due to the absence of connections between the fruit tissue and the mature seeds, many seeds gain only limited energy from the fruit and are not dispersed effectively.

Schmitt *et al.* (1985) studied *I. capensis* because of its ability to produce both chasmogamous (outcrossing) and cleistogamous (selfing) flowers. The seeds from these different flowers are, however, morphologically indistinguishable. They observed that the majority of *I. capensis* seeds travel 20 cm or less but that the seeds from chasmogamous flowers travelled nearly twice as far as those from cleistogamous flowers, with approximately 15% of these seeds travelling 100 cm or more (Schmitt et al. 1985). The result is that outcrossed seeds are more commonly dispersed further from their maternal parent, whilst self-fertilised seeds

are more likely to experience a similar environment to their parent (Schmitt et al. 1985).

A more recent study sought to model the energy required for the fruit to open in a related species, *Impatiens glandulifera* (Deegan 2012). This study focussed on the energetical cost of tissue fracture during the explosive dehiscence of *Impatiens*, and found that the fruit morphology is optimised to minimise the amount of energy lost in tissue fracture, thus transferring most of its stored energy to kinetic energy. The seeds were found to be propelled at speeds of up to 4 ms^{-1}, a property the author suggests may have helped the species to successfully invade Europe and North America (Deegan 2012).

1.1.6.3. Explosive models in Cardamine

Two recently published papers have examined the dry dehiscent explosive dispersal mechanism of the *Cardamine* genus of the Brassicaceae. The first of these focussed on describing the dispersal characteristics of the *Cardamine parviflora* silique (Hayashi et al. 2010), whilst the second sought to explain the explosive opening of *C. hirsuta* siliques in terms of cell layer morphology (Vaughn et al. 2011).

Hayashi *et al*. proposed that the *Cardamine parviflora* explosive opening mechanism arises from the differing properties of a bilayer, formed from the innermost tissues of the fruit wall. They observed the innermost cell layer of the fruit valve tissue to be mucilaginous, proposing that it absorbs water and becomes swollen. Hayashi *et al.* suggest that deposition of lignin, a rigid polymer, within the cell layer immediately above this functions to compress this endocarp *a* layer, until dehiscence occurs along a seem that runs down the fruit from top to bottom,

resulting in the sudden expansion of the mucilaginous layer, causing the explosive outward curling of the fruit wall.

Hayashi *et al*. hypothesised that a layer of water may exist between the fruit wall and the seeds which is responsible for imparting energy from the fruit to the seeds in *C. parviflora*. They observed the mean acceleration of seeds launched by the fruit's explosive mechanism to be 4.7ms^{-1}.

Vaughn *et al.* (2011) observed that the deposition of lignin in the second-most inner cell layer of the fruit wall in *C. hirsuta* occurs in a U-shaped pattern. They hypothesised that in *C. hirsuta*, shrinking of the middle cell layers of the fruit wall generates the explosive force for silique opening. They proposed that the U-shaped pattern of lignification ensures that when the fruit wall curls explosively, it curls outwards rather than inwards.

Vaugh *et al.* suggested that the innermost cell layer of the fruit wall functions to keep the lignified cells moist by trapping mucilage between the two cell layers. They hypothesised that this is necessary either to maintain the flexibility of the lignified cells, or to hold them together whilst the rest of the fruit wall dries.

1.1.6.4. Explosive dispersal is seen in multiple habitat and plant types

From their comparison of selected species from the *Geranium* (Geraniaceae), *Phlox* (Ploemoniaceae), *Viola* and *Impatiens* genera, Stamp and Lucas observed that no pattern regarding habitat, generation time or plant morphology is evident amongst those species that exhibit ballistic dispersal (Stamp & Lucas 1983). Explosive species include annuals like *Erodium* species (Stamp 1989; Jacobs & Lesmeister 2012) and perennials like *Cardamine scutata* (S. Yano 1997). They include epiphytic parasites like *A. americanum* (Friedman &

Sumner 2009), understory shrubs like *I. floridanum* (Roberts & Haynes 1983), thorny evergreen trees like *Hura crepitans* (Swaine & Beer 1977) and, in the case of *C. hirsuta*, fast-growing weed species.

In their study of *H. crepitans* (Euphorbiaceae), Swaine and Beer note that larger seeds are usually dispersed by animals or autochory, in contrast to small seeds which are better able to be dispersed by wind (Swaine & Beer 1977). They suggest that large seeds are beneficial to tree species as they improve the ability to establish successfully in deep shade. Harper *et al.*, however, assert that most arable weeds (which typically have small seeds) either use anemochory or explosive dispersal (Harper et al. 1970), whilst van der Pijl states that autochory is a common mode in arid regions (Van der Pijl 1972). In his study of *I. glandulifera*, Deegan notes that it is one of the most invasive alien species in both Europe and North America (Deegan 2012) and *Erodium cicutarium* too is also an invasive species (Jacobs & Lesmeister 2012).

Ideas about common traits of explosive dispersers therefore seem to be mixed. The trait is not definitively linked to a particular habitat or plant type, but does appear to show loose correlations with invasive plants or weeds, arid habitats, and large-seeded trees and shrubs, however, none of these are to the exclusion of alternatives. *C. hirsuta* is a highly invasive weed, so falls into this first category.

1.1.6.5. Reliability or predation response may be more significant advantages to explosive dispersal than distance

The seemingly high occurrence of ballistic dispersal amongst weeds, pioneer and invasive species appears to implicate explosive mechanisms as a tool for spreading into new territories. However, it has been noted that in many studies, ballistic mechanisms achieve dispersal distances of less than 5 m (Beaumont et

al. 2009). It was found that the ballistic mechanism of *Adriana quadripartita* (Euphorbiaceae), a spreading shrub, dispersed seeds a mean of only 27.1 cm from the edge of the shrub's canopy (Beaumont et al. 2009). *Erodium moschatum* (a semi-arid annual) has a mean dispersal distance of 55.6 cm (Stamp 1989) and the mean seed dispersal distance of chasmogamous flowers in *I. capensis* is 51.0 cm (Schmitt et al. 1985). Trees, rather than weedy colonisers, appear to achieve the furthest distances of explosive dispersal, with *H. crepitans* showing a maximum dispersal of 14 m (Swaine & Beer 1977) and van der Pijl naming *Bauhinia purpurea* (Fabaceae) as holding the record for maximum explosive dispersal distance at 15 m (Van der Pijl 1972). Even these distances are relatively small when compared with the potentials of wind and animal dispersal to spread seeds away from their parents (Swaine & Beer 1977), and in their study of the chasmogamous and cleistogamous flowers of *I. capensis*, Schmitt *et al.* state that it is unclear how the limited dispersal of explosive methods could be sufficient to propagate weedy, colonising species to new areas (Schmitt et al. 1985).

If explosive dispersal does not achieve particularly notable dispersal distances, the question arises of what the evolutionary advantages of such mechanisms might be. One reason might be reliability. In their study of *H. crepitans*, Swaine and Beer suggest that the limited dispersal distances reached by explosive mechanisms are better than those achieved by gravity alone at reducing parent-offspring competition, whilst being more reliable than depending upon animals or wind (Swaine & Beer 1977).

Perhaps then, explosive seed dispersal is not so often a mechanism for invading new regions, but instead a reliable mechanism used to reduce the degree of kin competition experienced amongst offspring and with their parents.

Alternatively, explosive seed dispersal may be a reliable mechanism for achieving a range of dispersal distances, safeguarding against all of a plant's offspring suffering from the same environmental fluctuations in the parent's microhabitat.

It has been suggested that an additional advantage of explosive seed dispersal may be as a response to predation. *Impatiens* species can be heavily grazed by predators including beetles, which can lead to reduced seed production (Schemske 1978; Stamp & Lucas 1983), and it has been suggested that these plants use the limited dispersal distances of ballistic mechanisms to reduce predation of their seeds, as the touch of an animal could potentially increase the pressure within the fruit and trigger seed release (Stamp & Lucas 1983). In this way, seeds can be protected from immediate predation and also form a type of escape-defence, dispersing offspring away from an attacked parent.

In his study of *Cardamine scutata*, Yano suggests that the explosive silique opening seen throughout the *Cardamine* genus may have originally evolved for seed dispersal, but in *C. scutata* has acquired a role in caterpillar defence (Yano 1997). He observes that *C. scutata* loses most of its foliage to decay or herbivore consumption and that, as in *Impatiens*, immature siliques can be triggered to open by physical stimuli including, perhaps, herbivores. He proposes that the sudden curling of *C. scutata*'s pericarp valve in response to a caterpillar results either in the propulsion of the larva away from the plant or its capture within the tightly coiled detached valve (Yano 1997).

1.1.6.6. Explosive dispersal is often followed by a secondary mechanism

It should be noted that explosive dispersal is commonly used in combination with a secondary dispersal mechanism (Stamp 1989), a feature termed diplochory. These secondary dispersal mechanisms can both increase the

dispersal distance and allow more directed dispersal. For example, in *A. quadripartita*, secondary dispersal by ants adds an average of an additional 76 cm to the mean ballistically-achieved distance of 27.1 cm from the canopy edge, and around 77% of diplochorously dispersed seeds escape their parental canopy, compared with just 45% in seeds that are only explosively dispersed (Beaumont et al. 2009). Ants can be attracted to seeds by elaiosomes, resulting in their transportation to the ants' nest – a habitat which may be suitable for germination – and hygroscopic seed awns, like those seen in *Erodium*, offer another method for directed seed dispersal, uncoiling and recoiling in response to moisture and desiccation, and moving the seeds they are attached to before burying them when a crevice or dead plant material are encountered (Stamp 1984; Stamp 1989).

Although diplochory enables dispersal over greater distances, in these cases seed morphology is a trade-off between the optima for explosive and secondary dispersal. *Impatiens* species exhibit secondary dispersal, using water to achieve greater dispersal distances, and Hayashi *et al.* suggest that the poor dispersal distances achieved ballistically (with many seeds travelling less than 20 cm) could be a consequence of seed buoyancy adaptations to secondary dispersal (Hayashi et al. 2009).

1.1.6.7. Summarising explosive studies

So far, most studies of ballistic seed dispersal have been purely descriptive and from an ecological viewpoint. More recently, mechanistic and modelling approaches have begun to be adopted (Hayashi et al. 2009; Deegan 2012). Excepting work on *A. americanum* (Friedman & Sumner 2009), the development of explosive morphologies has been largely ignored. The genus *Impatiens* is the closest the field has come to a model organism for studying the biology of

explosive seed dispersal. However, until a genetically tractable laboratory model for explosive dehiscence has been established, we will be unable to investigate the genetic regulation of this fascinating trait, nor will we be able to study it from an evolutionary developmental perspective.

Recently, studies have begun to use histological techniques to describe the morphology of explosive fruits from the *Cardamine* genus. In this DPhil thesis, a detailed developmental and genetic approach are used to develop *Cardamine hirsuta* into a genetically tractable model for understanding explosive seed dispersal.

1.2. The Brassicaceae and its models

The Brassicaceae is a monophyletic dicotyledenous family of Angiosperms, formerly referred to as the Cruciferae, after their cruciform flowers, and commonly known as the mustard family, because production of mustard oils is a synapomorphy of the family. This large family is distributed worldwide and comprises roughly 3709 species in 338 genera (Al-Shehbaz et al. 2006). Agricultural plants include the *Brassica* genus of oil-seed crops, cabbages and other vegetables, whilst other farmed species include *Lepidium sativum* (cress), *Raphanus sativus* (radish), some *Sinapis* species (table mustard), *Eutrema wasabi* (wasabi) and the bittercress *Cardamine amara* (Koch et al. 2003). Popular ornamental genera include *Matthiola, Hesperis* and *Lobularia*, and many Brassicaceans are familiar as weeds, including *Lepidium* and *Capsella* (Couvreur et al. 2010).

The Brassicaceae are a natural group and family members usually show a cruciform arrangement of four petals, the possession of six tetradynamous stamens (in which there are two outer, short stamens and four inner, long

stamens), and a silique fruit (Koch et al. 2003; Beilstein et al. 2006). The Brassicacean silique is bicarpellate, with parietal placentation, and usually comprises two locules, separated by a septum (Koch et al. 2003; Beilstein et al. 2006).

The Brassicacean fruit, however, shows considerable variation within and around these characteristics and traditionally this diversity of structure, shape and size has been used to delimit taxa at multiple ranks within the family (for example de Candolle 1821; Schulz 1936). Brassicacean siliques can lack septa, they can be dehiscent or indehiscent, and they can be classed as silicles when their length is less than three times their width (Koch et al. 2003). Most Brassicacean fruits are not flattened (terete) or are flattened in parallel to the septum (latiseptate), but some groups are flattened perpendicular to the septum (angustiseptate) (Koch et al. 2003). In addition to fruit form, trichome structure, the position of the cotyledons relative to the radical during embryonic development, and a range of other morphological features have been used to distinguish different Brassicacean taxa (Koch et al. 2003).

1.2.1. Emergence and relationships of the Brassicaceae

Estimates of the date of the emergence of the Brassicaceae include (amongst others) 50 million years ago (MYA) (Koch et al. 2001) and 19 MYA (Franzke et al. 2009). As noted by Al-Shehbaz *et al.* (2006), analyses of a range of molecular markers have been unable to provide sufficient resolution to determine the relationships amongst the basal region of Brassicacean phylogeny, which suggests the occurrence of one or more major adaptive radiations early in the history of the Brassicaceae (Al-Shehbaz et al. 2006). The emergence and adaptive radiation of the core Brassicaceae is thought to have coincided roughly

with both a cooling event (around 33 MYA) in the Irano-Turanian region where they originated, and with the family's most recent whole genome duplication (around 37-32 MYA) (Couvreur et al. 2010).

Because the Brassicaceae are particularly diverse in fruit morphology, it is possible that the genetic foundations for this diversity might have arisen during this whole genome duplication event, and perhaps played a role in the rapid adaptive radiation of the family.

Early classifications of the Brassicaceae by de Candolle and Schulz were heavily based on this diversity of fruit and seed morphology (De Candolle 1821; Schulz 1936). However, with the onset of molecular data, it has become clear that genetically similar taxa can exhibit strongly divergent seed and fruit morphologies (for example Beilstein et al. 2006). As noted by Al-Shehbaz *et al.* (2006), results like these suggest that large changes in fruit morphology can arise from alterations in only a few genes, as is seen in *Arabidopsis thaliana* mutants, and that fruit evolution can occur in sudden bursts, independently of other characters, and are therefore an unreliable indicator of phylogenetic relationships (Al-Shehbaz et al. 2006).

The advent of molecular phylogenetics has provided alternative methods for determining Brassicacean family relationships and for calculating the timings of their divergence history. A simplified phylogeny of the Brassicaceae is given in Figure 1.1. The date estimates included in this phylogeny were selected from a suite of papers using different estimation methods (Koch et al. 2000; Koch et al. 2001; Franzke et al. 2009; Beilstein et al. 2010; Couvreur et al. 2010). The studies of Koch *et al.* (2000, 2001) used chalcone synthase, alcohol dehydrogenase and the choloroplast gene *matK*. Franzke *et al.*, Couvreur *et al.*, and Beilstein *et al.* all

used the technique of Bayesian evolutionary analysis by sampling trees (BEAST), on NADH subunit 4 (Franzke et al. 2009; Couvreur et al. 2010), and on NADH dehydrogenase subunit F and nuclear phytochrome A (Beilstein et al. 2010). The analyses of all these studies, with the exception of Beilstein *et al.*, were conducted under a single constraint, such as a single fossil. The Beilstein *et al.* study, however, uses four fossil constraints, in conjunction with both a nuclear (phytochrome A) and a plastid (NADH dehydrogenase subunit) gene, so may offer the most reliable age estimates.

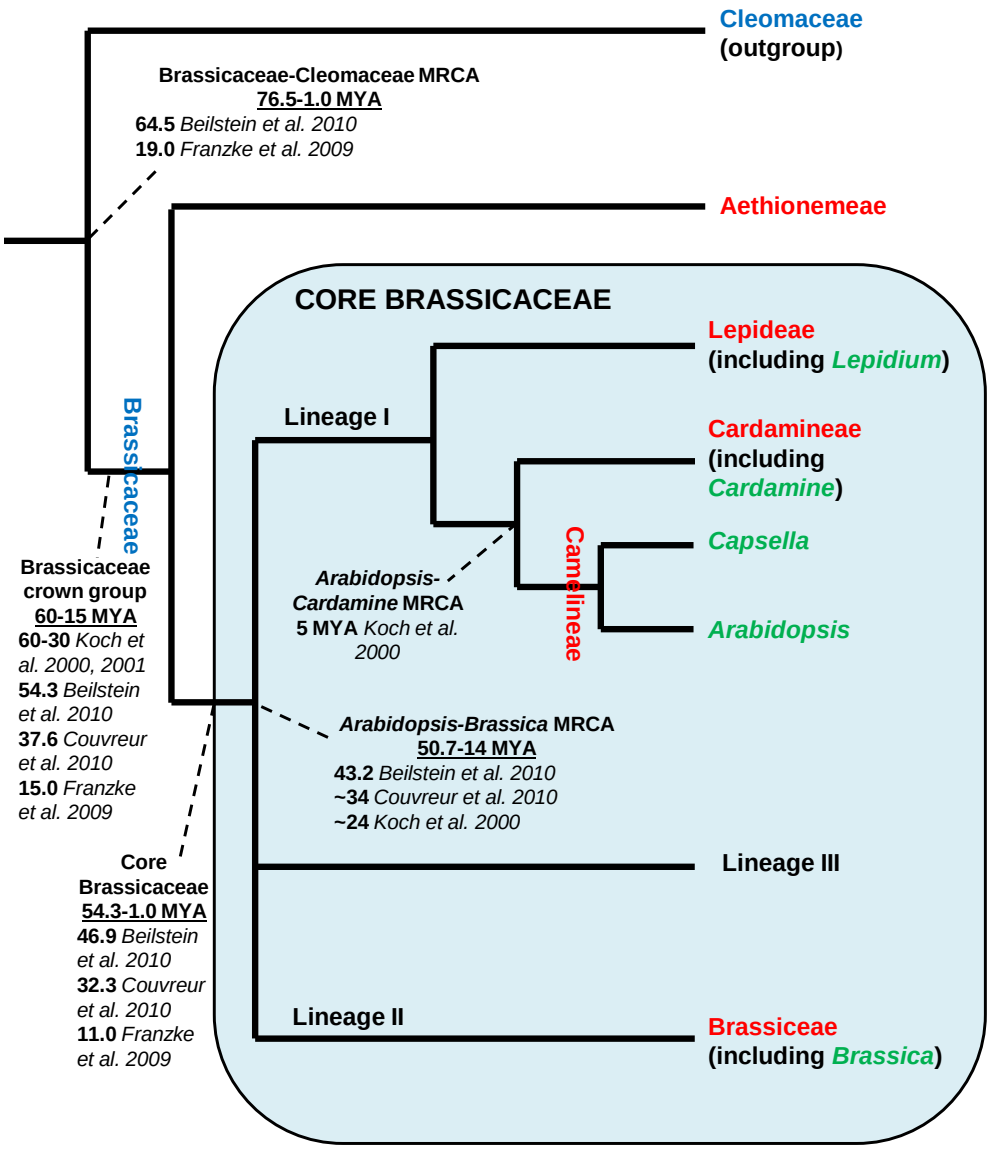

Figure 1.1 Simplified phylogeny of the Brassicaceae. Phylogeny simplified to show key phylogenetic divergences of the family and relationships of particular genera of interest. Families are denoted by blue, tribes by red and genera by green. Branches indicate relationships but are not scalar representations of genetic distance or evolutionary time. Underlined date estimates indicate total range of age estimates from references listed. Optimal date reconstructions and narrower age estimates are listed underneath with specific references. MYA stands for millions of years ago, MRCA most recent common ancestor.

1.2.2. Model Systems and the Brassicaceae

Within the Brassicacean family, a growing number of species from a range of genera are being developed into model species. Of these, the most important is *Arabidopsis thaliana* (tribe Camelineae), which is the genetic model for all flowering plants and has been used for almost every field of plant biology, ranging from genetics and development to physiology and pathology (Koch et al. 2003). In addition to *A. thaliana*, the *Brassica* crops (tribe Brassiceae) are important agricultural crop models that have also been used in a range of genetic studies.

Other mustard family model systems that have been adopted or are being developed include additional *Arabidopsis* species and members of the genera *Arabis, Boechera*, *Capsella, Cardamine, Diplotaxis, Iberis, Lepidium, Noccaea, Thellungiella* and *Thlaspi* (Schranz et al. 2006; Bailey et al. 2006; Franzke et al. 2011). These newer Brassicacean models have largely been developed for studying in conjunction with *A. thaliana*, in order to exploit the genetic resources already available in this species and to extend conclusions made using *A. thaliana* to other species, particularly those that differ from *A. thaliana* in a specific trait of interest.

Alternative *Arabidopsis* species in use include *A. halleri, A. lyrata* and *A. suecica*. *Arabidopsis* species share the experimental advantage of a high degree of similarity to *A. thaliana*'s fully-sequenced genome, whilst offering limited opportunities to investigate slightly different traits not seen in *A. thaliana*. *A. lyrata*, for example, shares over 80% sequence identity with the genome of *A. thaliana*, and has been used as a model for studying self-incompatible mating systems, and for investigating rapid genome expansion and changes in the regulation of transposable elements within the *Arabidopsis* genus (Kusaba et al. 2001;

Schierup et al. 2001; Hu et al. 2011; He et al. 2012). Other *Arabidopsis* study species include *A. halleri*, which shows heavy metal tolerance (Macnair et al. 1999; Bert et al. 2000; Küpper et al. 2000; Zhao et al. 2000), and *A. suecica,* which is an allopolyploid (Säll et al. 2004).

The *Capsella* genus, like *Arabidopsis*, is also a member of the Camelineae tribe, so provides further opportunities for studying traits in species sharing a high degree of genetic similarity with *A. thaliana*. Genome structure and evolution has been investigated in *C. rubella* (Koch & Kiefer 2005), *C. grandiflora* is another model for the study of self-incompatibility (Paetsch et al. 2006), whilst some populations of *C. bursa-pastoris* provide evolutionary examples of homeotic floral morphologies (Hintz et al. 2006; Nutt et al. 2006).

1.2.2.1. Analysing the molecular bases of morphological diversity in **Drosophila**

To understand the changes in developmental genetics that underly morphological diversity, a study system is required which shows both a range of morphological variation, and genetic tractability. A successful example of this has been the use of the *Drosophila* genus. Comparison of the genetic model *D. melanogaster* with other *Drosophila* species showing different morphological traits has allowed investigation of the molecular changes to regulatory networks that have enabled the evolution of novel morphologies within the genus (Prud'homme et al. 2007).

The use of molecular and genetic approaches in *D. melanogaster* has been combined with comparative analyses with other *Drosophila* species, including *D. santomea, D. biarmipes, D. kikkawai, D. bipectinata, D. subobscura,* and *D. pseudoobscura* (Gompel et al. 2005; Jeong et al. 2006; Prud'homme et al. 2006). An example of how this approach has been used is the investigation of the

different wing and abdomen pigmentation patterns that are seen in these species. This work found that changes in the *cis*-regulatory elements of the *yellow* pigmentation gene have facilitated the recent evolution of these divergent pigmentation patterns (Gompel et al. 2005; Jeong et al. 2006; Prud'homme et al. 2006).

This study system has several key strengths. *Drosophila* species share the same body plan, but show enough morphological diversity (such as different pigmentation patterns) to be interesting. *D. melanogaster* is a well-developed and extensively studied genetic model, and findings in *D. melanogaster* can easily be compared across its relatives because they are sufficiently closely related. Because these *Drosophila* species are so closely related, together they form a suitable system for investigating the molecular changes that underly the recent evolution of specific morphological divergences.

To understand the genetic bases of plant morphological diversity, such as explosive versus non-explosive fruit opening, similar study systems are needed in plants. By many criteria, *Arabidopsis thaliana* is the plant equivalent of *D. melanogaster*, being a convenient laboratory organism, amenable to genetic manipulation, and fully sequenced. Its close relative *Cardamine hirsuta* differs in a range of morphological features, including leaf shape, floral organ number and seed dispersal mechanism. Together, *A. thaliana* and *C. hirsuta* provide an opportunity to investigate the recent molecular changes underlying morphological traits like explosive pod shatter.

1.2.2.2. The utility of **Cardamine hirsuta** *as a model system*

The tribe Cardamineae is closely related to Camelineae, with some estimates placing the time of their divergence as more recent than 8 MYA

(Franzke et al. 2009). Within the Cardamineae, *Cardamine hirsuta* is being developed as a genetic model for comparative genetic and developmental studies with *A. thaliana. C. hirsuta*, which carries the common name hairy bittercress, is an invasive weed found in ruderal habitats on every continent except Antarctica (Lihová et al. 2006). As summarised by Lihová *et al.*, the species is thought to have originated in Europe, but has spread across the world, through introduction in the case of Africa, America, New Zealand, Australia and Japan, the latter case of which appears to have happened during or since the 1950s (Yatsu et al. 2003).

The real strength of *C. hirsuta* as a model organism comes from the combination of its experimental suitability, its close genetic similarity with *A. thaliana*, and its range of morphological traits that differ from *A. thaliana*. *C. hirsuta* is self-compatible and diploid, unlike many *A. thaliana* relatives, and is well suited to experimental genetics, producing many seeds, having a relatively short life cycle (approximately 10 weeks from germination to seed dispersal) and being amenable to mutageneses and genetic transformation (Hay & Tsiantis 2006; Canales et al. 2010). The high degree of genetic similarity between the two species means that the *A. thaliana* genome could be used as a guide to identify, sequence, clone or manipulate genes of interest in *C. hirsuta,* and through multiple sequencing efforts, the Tsiantis and Hay laboratories now have access to 295x coverage of the *C. hirsuta* genome, as well as a suite of SNP markers in a range of different *C. hirsuta* accessions that can be used for mapping mutant and quantitative trait loci (for example Jenkins & Tsiantis 2010).

Perhaps most importantly, *C. hirsuta* is sufficiently different from *A. thaliana* to study the evolution and development of morphological divergences. So far, work has focussed on the differences in *A. thaliana* and *C. hirsuta* leaf

architecture, with the former possessing simple leaves and the latter compound leaves (Hay & Tsiantis 2006; Barkoulas et al. 2008). However, *C. hirsuta* differs from *A. thaliana* too in shoot branching, floral organ morphogenesis, and trichome morphology (Hay & Tsiantis 2006; Canales et al. 2010), and by having an explosive seed dispersal mechanism.

The power of *C. hirsuta*, therefore, really comes into its own in studies of the genetic and developmental processes underlying recently diverged morphologies. *A. thaliana* and *C. hirsuta* diverged recently enough to minimise phylogenetic noise, which would make genetic changes of interest harder to detect, and for the *A. thaliana* genome sequence to provide a valuable framework for understanding *C. hirsuta*. However, the two species have been separated long enough for them to exhibit a range of different, interesting morphological features.

1.2.2.3. Brassicacean model species for fruit development

Silique dehiscence has been well studied in both *A. thaliana* and in agriculturally important *Brassica* species (Spence et al. 1996). A number of genes have been identified in both systems that influence and control correct fruit development and dehiscence zone patterning, and these will be discussed in the section 1.3. These studies have provided a good framework for the understanding of fruit development and dehiscence in *A. thaliana* (for example Liljegren et al. 2004), opened the way for genetic improvement of seed losses in *Brassica* crops (Østergaard et al. 2006), and in some instances provided insights into the evolutionary history of a specific gene both within the Brassicaceae and between the Brassicaceae and the Poacean crop plant, rice (Arnaud et al. 2011).

It has been suggested that the *Lepidium* genus (tribe Lepidieae) is well suited for evolutionary developmental studies of fruit development. *Lepidium*

campestre possesses dehiscent fruits, whilst the fruits of its very close relative *Cardaria pubescens* (synonymously called *Lepidium appelianum*) are indehiscent (Mummenhoff et al. 2009). Together, the two species therefore provide a tool for investigating the recent emergence of an indehiscent phenotype and an understanding of the *A. thaliana* dehiscence zone-patterning genes has been used to clone candidate genes in both species, alongside basic histological studies of silique morphology (Mummenhoff et al. 2009). Study systems like these are important for allowing us to begin to view the genetic networks uncovered in *A. thaliana* from an evo-devo perspective. However, the use of *C. hirsuta* carries an advantage. The *Cardamine* and *Arabidopsis* lineages are more closely related to each other than either are to the Lepidieae. *C. hirsuta* and *A. thaliana* are sufficiently similar, both genetically and morphologically, that they can be used together as a comparative system, without the need for an additional *Cardamine* species, simplifying the number of genes that need to be cloned and histological comparisons that need to be conducted. In addition, the striking explosive mechanism of silique opening in *C. hirsuta* provides a rare opportunity to use genetic and developmental approaches to consider the control, patterning and evolution of ballistic seed dispersal in the Angiosperms. This trait is both more dramatic and more complex than indehiscence, and ballistic seed dispersal morphologies are unlikely to be induced by a mutation in a single gene, in contrast to indehiscence. As a consequence, when considering how genetic networks evolve to pattern divergent morphologies, the difference in silique dehiscence between *A. thaliana* and *C. hirsuta* is an interesting problem for investigation.

1.3. Brassicacean silique development

1.3.1. Gynoecium development in *A. thaliana*

The carpel, which encloses the ovules and develops into a fruit as they form seeds, is a lateral organ, thought to be derived originally from leaf or bract tissue (Bowman et al. 1999). In *A. thaliana*, the silique develops from a gynoecium that comprises two congenitally fused carpels (Roeder & Yanofsky 2006). This gynoecium is the inner most floral organ and forms as a cylinder within the floral bud (Smyth et al. 1990). On top of this cylinder, the stigmatic surface forms above a style. It is the epidermis of the stigma that receives pollen during pollination, and when pollen grains germinate on the stigmatic surface, their pollen tubes grow between the stigmatic papillae cells to reach the centre of the style (Kandasamy et al. 1994; Sessions & Zambryski 1995). Together, the stigma and style form the first two components of the transmitting tract.

Inside the gynoecial cylinder, a septum later fuses postgenitally, bisecting the ovary to form the two locules within which the ovules form (Sessions & Zambryski 1995). The axial centre of this septum forms the third stage of the transmitting tract (Sessions & Zambryski 1995). That the *A. thaliana* gynoecium is derived from two fused carpels can be seen in the tissues of the mature gynoecium, in which the two valves are formed from carpel tissue, whilst the stigma, style and septum are formed from the fused carpel margins and submarginal placentae (Sessions & Zambryski 1995).

The two valves are the outer carpel walls of the gynoecium and comprise three tissue layers – the exocarp, mesocarp and endocarp (Roeder & Yanofsky 2006). The endocarp is split into two layers. The endocarp *a* (en*a*) is the innermost

carpel tissue layer, lying below the endocarp *b* (en*b*), which is in contact with the mesocarp and has a role in silique dehiscence (Roeder & Yanofsky 2006).

Between the two valves on either side of the gynoecium sit the two repla, which comprise the outermost portions of the septum tissue (Roeder & Yanofsky 2006). The medial vascular bundles run through the repla, and the placentae, from which the ovules and their funiculi form, sits on the inner surfaces of each replum (Roeder & Yanofsky 2006). In the four interface regions between the two valves and two repla, the four valve margins form, and each of these are important for silique dehiscence (Roeder & Yanofsky 2006). At the bottom of the gynoecium sits the stipe or gynophore. The tissues of the gynoecium are annotated in Figure 1.2.

Müller provided the first thorough characterisation of the development of the *A. thaliana* gynoecium and the subsequent development of the fruit and dehiscence of the silique (Müller 1961). Some thirty years later, Smyth *et al.* used scanning electron microscopy to take a closer look, splitting floral development into 12 stages (Smyth et al. 1990). Pollination occurs at stage 13, and all following stages describe fruit development and are numbered 14 to 20 (Roeder & Yanofsky 2006). The morphological changes occurring throughout these stages of gynoecium and fruit development will be discussed further in Chapter 3.

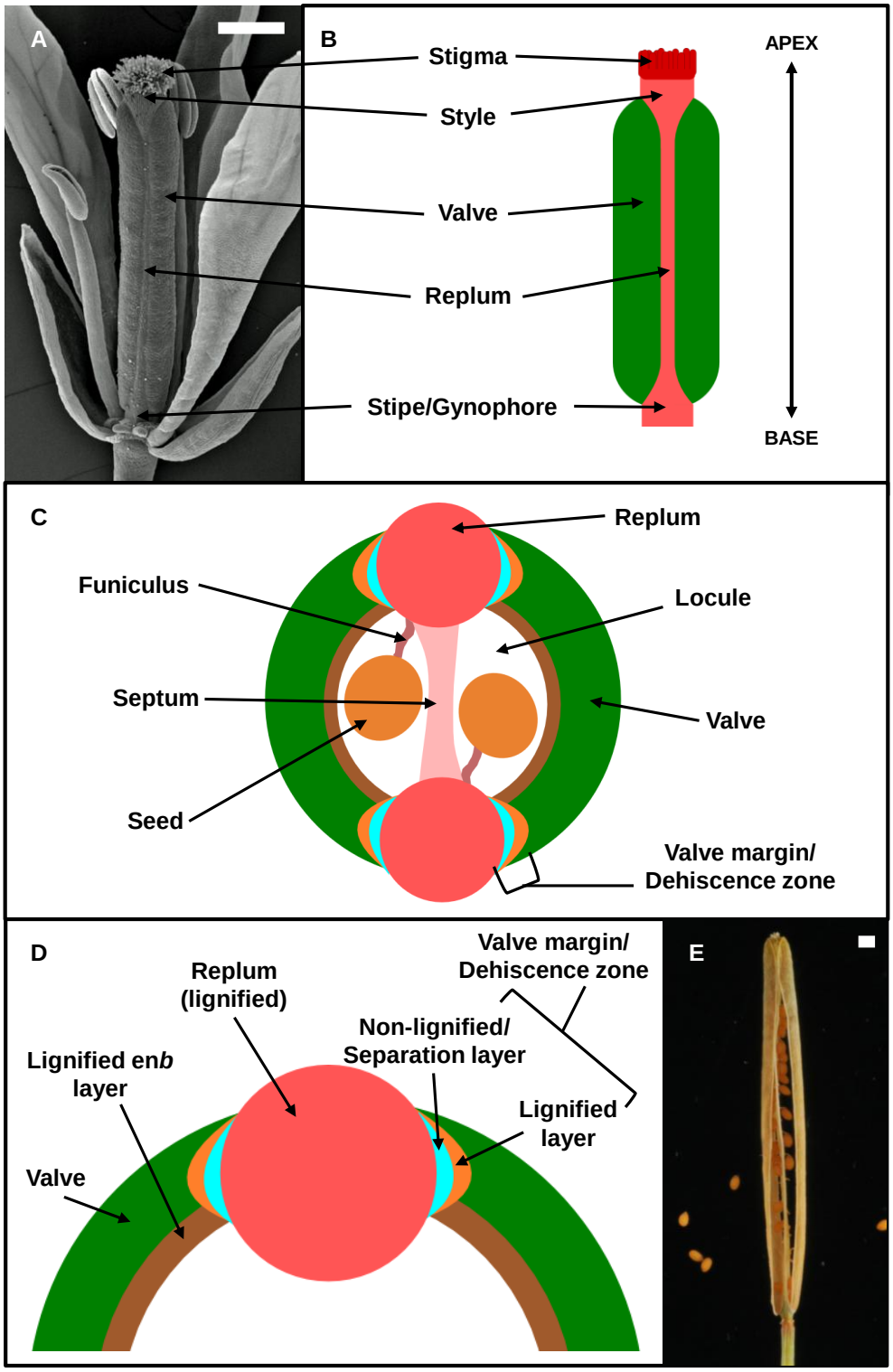

Figure 1.2 *A. thaliana* gynoecium and fruit morphology. Anthesis and fertilisation-stage gynoecium morphology shown in scanning electron microscopy (A) and diagram (B). Transverse section along apical-basal axis shown in (C), illustrating housing of seeds within two locules, separated by a septum formed from medial tissues and surrounded by the carpel valves. Tissues of importance for dehiscence illustrated in (D). Photograph of a dehiscing silique (E). Scale bar represents 500 µm.

1.3.2. Patterning Silique Dehiscence

The genetic patterning of the *A. thaliana* gynoecium has been extensively studied and reviewed (including Dinneny & Yanofsky 2004; Robles & Pelaz 2005; Roeder & Yanofsky 2006; Girin et al. 2009). This section will instead focus on the later differentiation of fruit tissues that were initiated during carpel development.

1.3.2.1. *Silique dehiscence in* Brassica

Brassicacean silique dehiscence was described by a number of studies throughout the twentieth century that looked at pods of the *Brassica* genus. By the start of the 1990s, yield losses due to *Brassica* oilseed pod dehiscence was an important agricultural problem, warranting a detailed characterisation of silique dehiscence in *Brassica napus*.

Electron and light microscopy of transverse silique sections revealed that the valve becomes separated from the replum during silique dehiscence due to cell wall breakdown in a layer of cells situated between the two, called the dehiscence zone (Meakin & Roberts 1990b). This dehiscence zone is a well-defined layer, one to three cells thick, which becomes enclosed by lignin on either side, as the cells of the valve edge and the replum lignify. The dehiscence zone cells, however, do not undergo secondary wall thickening (Meakin & Roberts 1990b).

After cell separation has taken place in the dehiscence zone, the dehiscence zone cells remained somewhat intact, attached either to valve or replum tissues, rather than being completely degraded, indicating that opening of the fruit along the dehiscence zone shares some similarities with conventional abscission processes (Meakin & Roberts 1990b). This degradation of the cell wall matrix was found to coincide with a rise in the activity of cellulase in the

dehiscence zone, implicating this enzyme in loosening this cell layer prior to dehiscence (Meakin & Roberts 1990a). An enhancement of the production of ethylene by seeds occurs immediately prior to this observed increase in cellulose, and ethylene can be used to accelerate dehiscence zone breakdown (Meakin & Roberts 1990a).

Spence *et al.* compared the dehiscence of *B. napus* with the model *A. thaliana* and lines of *Brassica juncea* which showed reduced dehiscence and pod shatter (Spence et al. 1996). From their studies, they suggested that dehiscence resulted from weakening of the middle lamella of the dehiscence zone following the differentiation of the valve into exocarp, mesocarp and endocarp *a* and *b* layers. They observed that the endocarp *b* layer forms a rigid, convex arc which is put under tension when the exocarp and mesocarp shrink through desiccation. This store of potential energy is maintained until the separation layer within the dehiscence zone weakens, at which point this tension can be released by the valve coming away from the replum. They suggested that the occurrence of dehiscence in this manner would often be assisted by environmental stimuli, including external pressure experienced during commercial harvesting (Spence et al. 1996).

Comparisons of *B. napus* and *A. thaliana* morphology with that of *B. juncea* lines which show reduced dehiscence suggested a role for endocarp *b* lignification in silique dehiscence (Spence et al. 1996). Whilst the endocarp *b* cells of *B. napus* and *A. thaliana* undergo secondary thickening and lignification prior to dehiscence, Spence *et al.* noted that the endocarp *b* cells of *B. juncea* failed to completely lignify. They observed that whilst the endocarp *b* secondary walls in *B. napus* do lignify, the primary walls and middle lamellae between cells do not, and the

authors suggested that the pectin remaining in these regions would provide flexibility in the endocarp *b* layer, preventing the generation of high levels of tension seen in *B. napus* and *A. thaliana* as the valve tissue desiccates. The tissues involved in *A. thaliana* dehiscence are illustrated in Figure 1.2 D and E.

1.3.2.2. A model that describes the patterning of the dehiscence zone in A. thaliana

As *A. thaliana* was developed into the preeminent genetic model for plant developmental studies, it provided an opportunity to uncover the genetics underlying the dehiscence process first described in *B. napus*.

The current model, put forward by the Yanofsky group, describes the network of discovered genes that specify the tissues involved in dehiscence (Figure 1.3A). *INDEHISCENT (IND)*, an atypical bHLH transcription factor acts to specify the valve margin region which sits between each valve and replum, and misexpression of *IND* in the valve has been shown to result in the ectopic lignification of this tissue (Liljegren et al. 2004). *IND* appears to be upstream of the unequal cell divisions required for formation of the valve margin (Wu et al. 2006), and interacts with another bHLH transcription factor, SPATULA (SPT) (Girin et al. 2011). IND has been shown to directly upregulate *SPT* expression and together IND and SPT are involved in coordinating auxin efflux from the valve margin, a process necessary for the specification of the dehiscence zone separation layer (Sorefan et al. 2009; Girin et al. 2011).

Also active in the valve margin is *ALCATRAZ (ALC)*, a myc/bHLH gene, evolved from a *SPATULA*-like ancestor after a gene duplication event (Rajani & Sundaresan 2001; Groszmann et al. 2011). *ALC* is required to specify the nonlignified cell layer of the valve margin which lies immediately adjacent to the replum (Rajani & Sundaresan 2001). This nonlignified cell layer corresponds to the

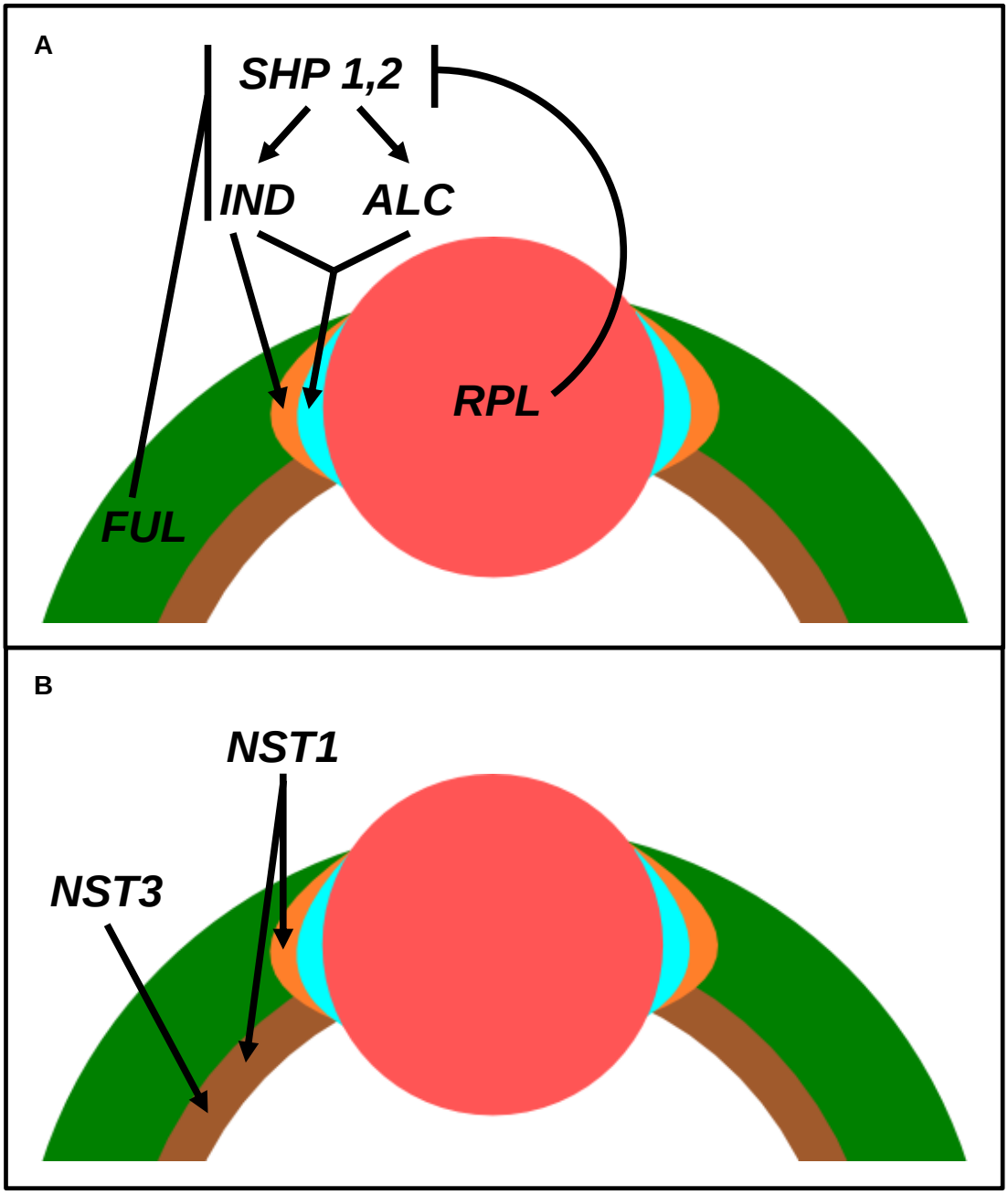

Figure 1.3 Patterning the dehiscence zone in *A. thaliana*. (A) The dehiscence zone patterning genes *FUL, RPL, SHP1, SHP2, IND* and *ALC* together specify the cells of the dehiscence zone. (B) *NST1* and *NST3* function in patterning the lignification of the valve margin and en*b* required for dehiscence.

separation layer observed in the *B. napus* dehiscence zone (Meakin & Roberts 1990b; Meakin & Roberts 1990a; Spence et al. 1996). Loss of function of either *IND* or *ALC* results in an indehiscent phenotype. *ind* valve margins fail to lignify, so the fruit cannot open, whilst in contrast, *alc* valve margins completely lignify, failing to produce the necessary layer of nonlignified cells whose autolysis is crucial to enable the fruit valves to separate from the replum. *IND* and *ALC* therefore pattern two specific stripes within the valve margin, one of lignified cells, the other of nonlignified.

This specification of the valve margin and patterning of its lignified and non-lignified layers by *IND* and *ALC* is thought to function via the gibberellin/DELLA pathway. IND directly activates *GA3ox1*, a gibberellin biosynthesis gene, a process necessary for valve margin formation. This IND-induced synthesis of gibberellin then releases ALC from DELLA-repression, enabling specification of the non-lignified separation layer within the valve margin (Arnaud et al. 2010).

As well as loss of *IND* or *ALC* function, indehiscent fruit phenotypes have also been found as a result of the loss of function of four other genes involved in dehiscensce zone cell specification. *SHATTERPROOF1* and *2* (*SHP1, 2)* encode two functionally redundant MADS box proteins (Liljegren et al. 2000) which function in the valve margin, upstream of *IND* (Liljegren et al. 2004). As a consequence, *shp1, shp2* double mutant valve margins fail to lignify.

FRUITFULL is a MADS box gene (Mandel & Yanofsky 1995; Gu et al. 1998) which is expressed in the valve and negatively regulates *SHP1* and *2* (Ferrandiz et al. 2000) and *IND* (Liljegren et al. 2004). In *ful* mutants, SHP, IND and ALC activity spread from the valve margin and into the valve causing a severe phenotype, including lignification of the valve mesophyll and stunted silique

growth. Loss of SHP, IND and ALC activity largely rescues the *ful* phenotype, with the quintuple mutant *ind alc shp1 shp2 ful* showing no lignification of the valve (Liljegren et al. 2004).

Whilst *FUL* acts in the valve tissue to restrict the domain of valve margin-specifying genes, *REPLUMLESS (RPL)*, which encodes a BEL1-like homeodomain protein, negatively regulates *SHP* expression in the replum (Roeder et al. 2003). Thus, FUL and RPL function to restrict valve margin specification and lignification to a thin stripe between the valve and the replum through their negative interactions with the valve margin specifying genes.

1.3.2.3. **FRUITFULL** *plays a key role in silique patterning in A. thaliana.*

The *ful* mutants isolated in *A. thaliana* (Landsberg *erecta* ecotype) exhibit a suite of morphological aberrations in the silique, including indehiscence. Most striking is the stunted growth seen in *ful* mutants, resulting in siliques which are around 80% shorter than WT (Gu et al. 1998). This stunted growth appears to arise from a failure of valve cells to expand after fertilisation, during which time WT valve cells expand in both the apical-basal and transverse planes (Gu et al. 1998). Weaker mutants, including alleles isolated in the Colombia-0 ecotype, show less stunted valve elongation, as well as an increase in style tissue (Ferrandiz et al. 2000). The stunted silique length of *ful* mutants can also be largely rescued by *ind* loss of function (Liljegren et al. 2004).

In addition to failing to expand, the valves of *ful* fruits also show ectopic lignification, with lignin being deposited in the mesophyll tissue layers of the valve (Ferrándiz et al. 2000). This is usually interpreted as a spreading of valve margin-like “identity” into the valve, another phenotype which can be rescued by *ind* (Liljegren et al. 2004). Loss of *IND* function also restores some guard cell

development to the *ful* valve. It is these findings that have led to the interpretation that *FUL* functions not to specify valve tissue but instead to suppress the expansion of IND and valve margin identity into the valve (Liljegren et al. 2004).

In contrast to the valve cells, the *ful* replum cells do expand after fertilisation, growing to approximately the same length as is seen in WT (Gu et al. 1998). However, these cells appear to be constrained by the stunted growth of the valve, and instead of expanding along the apical-basal axis as part of longitudinal growth, the cells “zig-zag” back on each other in a wavy arrangement running roughly perpendicular to the apical-basal axis (Gu et al. 1998). In addition to this “twisted” arrangement of the *ful* replum, the repla in these mutants are also wider, a phenotype which is partially rescued through loss of *RPL* function (Roeder et al. 2003; Alonso-Cantabrana et al. 2007).

Due to the drastic alterations in valve and replum morphology seen in *ful* mutants, the locules within the mutant siliques are much reduced, causing seed crowding within the fruit, which frequently results in the seeds bursting through the valve only a few days after they are fertilised (Gu et al. 1998). It is this striking phenotype that inspired the gene name *FRUITFULL*. As well as increased crowding, *ful* seeds are also smaller in size, but otherwise appear normal (Gu et al. 1998).

Differences in *ful* and WT *A. thaliana* morphology are described as first being detectable at stage 12, when cell types specific to the valve and replum tissues become visible in the carpel. At this stage in *ful* mutants, the valve cells are small and undifferentiated, with guard cell precursors absent from the epidermis, and no clear boundary is visible between the replum and valve tissues (Gu et al. 1998).

FUL expression within the floral bud was originally described as being confined to inflorescence meristems and later to the valve tissue (Gu et al. 1998). Gu *et al*. described expression as being seen through all cell layers of the valve but as completely absent from the replum. However, FUL-GFP fusion proteins have more recently been detected, prior to stage 12, in the epidermal and subepidermal layers of the valve margin and replum tissues too (Urbanus et al. 2009).

1.3.2.4. Fruit development genes in Brassica

FUL, ALC, IND, and *RPL* have all been studied in *Brassica* genus species including *B. napus, B. juncea* and *B. oleracea* (Østergaard et al. 2006; Hua et al. 2009; Girin et al. 2010; Arnaud et al. 2011). Constitutive expression of *FUL* in *B. juncea* results in a less defined dehiscence zone, the complete absence of the non-lignified separation layer within this zone, and indehiscent pods (Østergaard et al. 2006), whilst loss of *IND* function in *B. napus* can also lead to indehiscent siliques, through a lack of valve margin differentiation (Girin et al. 2010). Whilst completely indehiscent siliques are not commercially desirable, both these findings hint at means for fine-tuning silique dehiscence using genetic manipulation to reduce crop seed losses.

Studies of fruit development genes in the Brassicaceae have also provided evolutionary insights, both within the family and across the Angiosperms, particularly in the case of *RPL*. The *B. oleracea* replum is much reduced compared to *A. thaliana*, and resembles that of *A. thaliana rpl* mutants. This difference in replum morphology has been found to result from a one base difference (cytosine to thymine) in a *RPL cis*-element (Arnaud et al. 2011). This base-pair change pre-dates domestication of the *Brassica* crops and appears to

have had a role in the evolution of replum morphological diversity in the Brassicaceae, with *Capsella rubella* and *Lepidium campestre* both possessing *A. thaliana*-like repla and the C-form of the *cis*-element, whilst *Sinapis alba* and other *Brassica* species possess the reduced replum seen in *B. oleracea* and the T-form of the *cis*-element (Arnaud et al. 2011). Because the C-form of the *cis*-element is also found in the wild rice relative *Oryza rufipogon* (Konishi et al. 2006), in the soybean *Glycine max,* and in *Brachypodium distachyon*, the T-form seems likely to have arisen by mutation from an ancestral C-form after the divergence of the *Arabidopsis* and *Brassica* lineages (Arnaud et al. 2011).

This same C-to-T *cis*-element mutation appears to have also occurred, independently, during rice domestication. The mutated *cis*-element causes a loss of an abscission zone beneath each rice grain and appears to have been artificially selected for in order to produce a seed-shatterless rice crop (Konishi et al. 2006; Arnaud et al. 2011). This one-base pair mutation affecting *RPL* has therefore played a key role both in the evolution of diversity in Brassicacean replum morphology and in rice domestication.

1.3.2.5. NST1 *and* NST3 *pattern lignification for dehiscence*

Whilst the genes described above are crucial for correct silique development and dehiscence, additional downstream genes are necessary for the correct cellular morphologies and chemical activities that facilitate the dehiscence process. An example of this is the lignification of the endocarp *b* layer and the non-separation layer cells of the valve margin.

The *NAC SECONDARY WALL THICKENING PROMOTERS (NST) 1* and *3* provided a first example of genes which function downstream of the dehiscence zone patterning genes. The *NST1* and *NST3* transcription factors have been

shown to act as master regulators of secondary cell wall formation (Mitsuda et al. 2005; Mitsuda et al. 2007; Zhong et al. 2007b). During silique development, *NST1* and *NST3* , the latter of which is also referred to as *SECONDARY WALL-ASSOCIATED NAC DOMAIN1 (SND1),* are expressed in the en*b* layer, whilst *NST1* is also expressed in the valve margins (Mitsuda & Ohme-Takagi 2008), where they regulate secondary wall formation (Figure 1.3B). Secondary cell wall formation is a key step prior to lignification of a cell, and disruption of *NST1* and *NST3* function results in a failure of the endocarp *b* cells and valve margins to lignify, preventing silique dehiscence. Due to redundancy between *NST1* and *NST3* in the endocarp *b* layer, *nst3* single mutants are not indehiscent. Because *nst1* is expressed in the valve margin without *nst3*, single *nst1* mutants are indehiscent (Mitsuda & Ohme-Takagi 2008).

The valve margin tissue in *nst1* and *nst1 nst3* mutants is correctly specified. It has been shown that in the *ful* mutant, the ectopic lignification observed throughout the valve tissue is correlated with expanded *NST1* expression, and in *ful nst1* this ectopic lignification is completely suppressed (Mitsuda & Ohme-Takagi 2008), indicating that *NST1* is responsible for this aspect of the *ful* phenotype and that *FUL* may normally function to directly or indirectly restrict *NST1* expression to the endocarp and valve margins.

Studies have identified many downstream regulatory targets of *NST1* and *NST3*, the majority of which are MYB domain transcription factors associated with secondary wall thickening and lignification (Zhong et al. 2007a; Zhong et al. 2008; Zhou et al. 2009). NST1 and NST3 appear to largely function redundantly with each other, directly upregulating expression of *SND3, MYB46, MYB103* and a Knotted1-like homeodomain transcription factor, *KNAT7* (Zhong et al. 2008).

MYB46, along with its activators *NST1* and *NST3*, acts as a regulatory master switch for secondary wall synthesis and lignin biosynthesis, (Zhong et al. 2007a; Ko et al. 2009). These three genes carry out this function via their regulation of a number of downstream genes, including *MYB52, MYB58* and *MYB63* (Ko et al. 2009; Zhou et al. 2009).

NST1 and *NST3* are therefore of key importance to silique dehiscence, functioning as master switches of the transcriptional regulators of the entire secondary wall biosynthesis pathway, including transcription factors which function to turn on the lignin biosynthesis pathway. Without this lignification of the en*b* layer and valve margin, the *A. thaliana* fruit is unable to build enough tension through desiccation to open the silique and undergo dehiscence (Mitsuda & Ohme-Takagi 2008).

1.3.2.6. Roles for auxin in patterning the gynoecium and dehiscence

The plant hormone auxin has also been implicated in patterning the *A. thaliana* fruit. *ETTIN (ETT)* functions in patterning the apical-basal axis of the gynoecium, and loss of function mutants exhibit an increase in style, stigma and basal stipe tissue, a reduction in valve size and the ovary region, and the proliferation of transmitting tract tissue outwards (Sessions & Zambryski 1995). Blocking polar auxin transport (PAT) using N-1-napthylpthalamic acid (NPA) is capable of mimicking this phenotype and provided a first indication that auxin gradients play a role in gynoecium and subsequent silique patterning, a finding which was supported by the identification of *ETTIN* as an auxin response factor (ARF) (Nemhauser et al. 2000). PAT is also thought to play a role in medio-lateral patterning of the gynoecium, and NPA treatment enhances the loss of adaxial

valve domains and medial ovary phenotypes of the *revoluta* single and *revoluta aintegumenta* double mutants (Nole-Wilson et al. 2010).

It has also been shown in *Brassica napus* that the levels of auxin observed within the dehiscence zone must decrease in order for the hydrolytic enzymes required for cell separation during dehiscence to be active (Chauvaux et al. 1997). This appears to be true too for *A. thaliana*, where IND coordinates auxin efflux from the separation layer to create an auxin minimum (Sorefan et al. 2009). Expression of a bacterial auxin biosynthesis gene, *iaaM*, driven by *IND* (*IND::IND:iaaM* construct), prevents formation of this auxin minimum in the separation layer and results in an *ind*-like phenotype of undifferentiated valve margins and indehiscent siliques (Sorefan et al. 2009).

The polar transport of auxin depends upon the correct localisation of its efflux carriers, the PIN proteins (Gälweiler et al. 1998; Petrasek et al. 2006). This required polarity of PIN proteins is controlled by PINOID (PID) family members, which act as protein kinases, modifying PIN proteins through reversible phosphorylation and thus regulating their apical-basal targeting and localisation (Benjamins et al. 2001; Friml et al. 2004; Galván-Ampudia & Offringa 2007; Michniewicz et al. 2007). Disruption of PAT through mutations such as *pid* results in a reduction in valve size and an expansion of the replum, thus mimicking NPA treatment (Christensen et al. 2000). Ectopic IND activity also mimics these effects and *ind-2* siliques fail to develop auxin minima in their valve margins (Sorefan et al. 2009). This data has led to a model (Sorefan et al. 2009) where IND promotes efflux of auxin from the valve margin through its regulatory actions on *PID* and the related kinase *WAG2* (Galván-Ampudia & Offringa 2007). It is proposed that IND directly inhibits *PID* expression and promotes *WAG2* expression, with the result

that PINs are no longer polarly localised at the basal plasma membrane of valve margin separation layer cells, but are instead localised to all sides of the cell, facilitating the drainage of auxin out of the separation layer into the surrounding tissues (Sorefan et al. 2009). Were auxin to regulate the activity of hydrolytic enzymes in *A. thaliana* valve margins as it does in *B. napus*, auxin would therefore provide a link between *IND* expression and the autolysis of the nonlignified layer of the valve margin which is required for dehiscence to occur.

1.3.2.7. Gynoecium patterning shares similarities with shoots and leaves

As discussed, the *A. thaliana* gynoecium consists of two fused carpels, and these arise from the floral meristem after the other floral organ whorls have been initiated. These carpels are modified leaves and, as such, are determinate structures. However, the medial tissues of the fruit maintain some meristematic activity, with the septum forming the seeds. The indeterminate tissue required for this process lies in the regions of the gynoecium which later form the repla (Sessions & Zambryski 1995), and it has been suggested that the *A. thaliana* silique can be seen as comprising two modified mersitems fused to two modified leaves (Girin et al. 2009). Expression of the meristematic gene *SHOOTMERISTEMLESS (STM)* (Long et al. 1996) is observed in the developing gynoecium and *BREVIPEDICELLUS (BP)* is expressed in the replum (Alonso-Cantabrana et al. 2007) along with its interacting protein partner RPL (also called BELLRINGER or PENNYWISE), which also plays a role in maintaining stem cell fate in the shoot apical meristem (SAM) (Byrne et al. 2003).

The complex formed by ASYMMETRIC LEAVES1 (AS1) and ASYMMETRIC LEAVES2 (AS2) promotes the formation of leaf primordia through the silencing of class I *KNOX* meristem identity genes *BP, KNAT2* and *KNAT6*

(Byrne et al. 2000; Ori et al. 2000; Pautot et al. 2001; Semiarti et al. 2001). In the shoot apical meristem, *AS1* is negatively regulated by *STM* (Byrne et al. 2000).

AS1 is also active in the fruit valve, where it represses *BP* (Alonso-Cantabrana et al. 2007). Loss of *AS1* function or *BP* overexpression leads to enlarged repla, a reduced valve width and enhancement of *ful*, whilst *bp* loss of function partially rescues these phenotypes (Alonso-Cantabrana et al. 2007). BP and RPL have been shown to restrict the activity of *KNAT6* and *KNAT2* to the valve margin, with loss of *KNAT6* function rescuing the defects in the replum and septum seen in *rpl* and *bp rpl* mutants. As RPL acts to restrict valve margin identity rather than specify the replum, and *knat2 knat6 rpl* triple mutants develop a normal replum, it has been suggested that an additional class I *KNOX* gene, *STM*, which is also expressed in both the meristem and the replum, may be responsible for specifying this tissue (Alonso-Cantabrana et al. 2007; Ragni et al. 2008). *STM* RNA interference lines show a decrease in *BP* and *KNAT2* expression in floral apices, and reduced *STM* expression results in a failure to develop carpels (Scofield et al. 2007).

AS1 is not the only leaf-patterning gene which is active in the fruit valve – *JAGGED (JAG), NUBBIN (NUB)* and members of the *YABBY (YAB)* transcription factor family also function. During leaf development, *JAG* and *NUB* act to promote leaf formation and regulate leaf shape (Dinneny et al. 2004; Ohno et al. 2004; Dinneny et al. 2006), whilst *FILAMENTOUS FLOWER (FIL)* and *YABBY 3 (YAB3)* promote abaxial leaf identity (Siegfried et al. 1999). YAB3 and FIL also function to repress class I *KNOX* expression in lateral organ primordia (Kumaran et al. 2002). In the fruit, JAG, FIL and YAB3 promote the formation of the valves and valve margins through positive regulation of *FUL* and *SHP* genes (Dinneny et al. 2005),

and have been proposed to act as valve promoting factors which oppose and repress replum promoting factors such as the class I *KNOX* genes (Alonso-Cantabrana et al. 2007; Schiessl et al. 2012). The expression and function of genes within the fruit which also act in the shoot apical meristem or leaf development imply a relationship between meristems and repla, and leaves and valves, where pre-existing developmental regulatory networks have been co-opted into fruit patterning (Figure 1.4).

As in the SAM, CLAVATA (CLV) and CORYNE (CRN) receptors appear to function in a signalling pathway in the gynoecium. In the SAM, the CLV3 peptide is recognised by the CLV1, CLV2 and CRN receptors, and this signalling pathway functions to restrict stem cell number in the SAM via regulation of the transcription factor *WUSCHEL* (Brand et al. 2000; Schoof et al. 2000). However, in the gynoecium, CLV1, CLV2 and CRN appear to function to repress STM, and disruption of this pathway results in the formation of additional medial tissue and valves as a consequence of increased cell proliferation in young gynoecia (Durbak & Tax 2011).

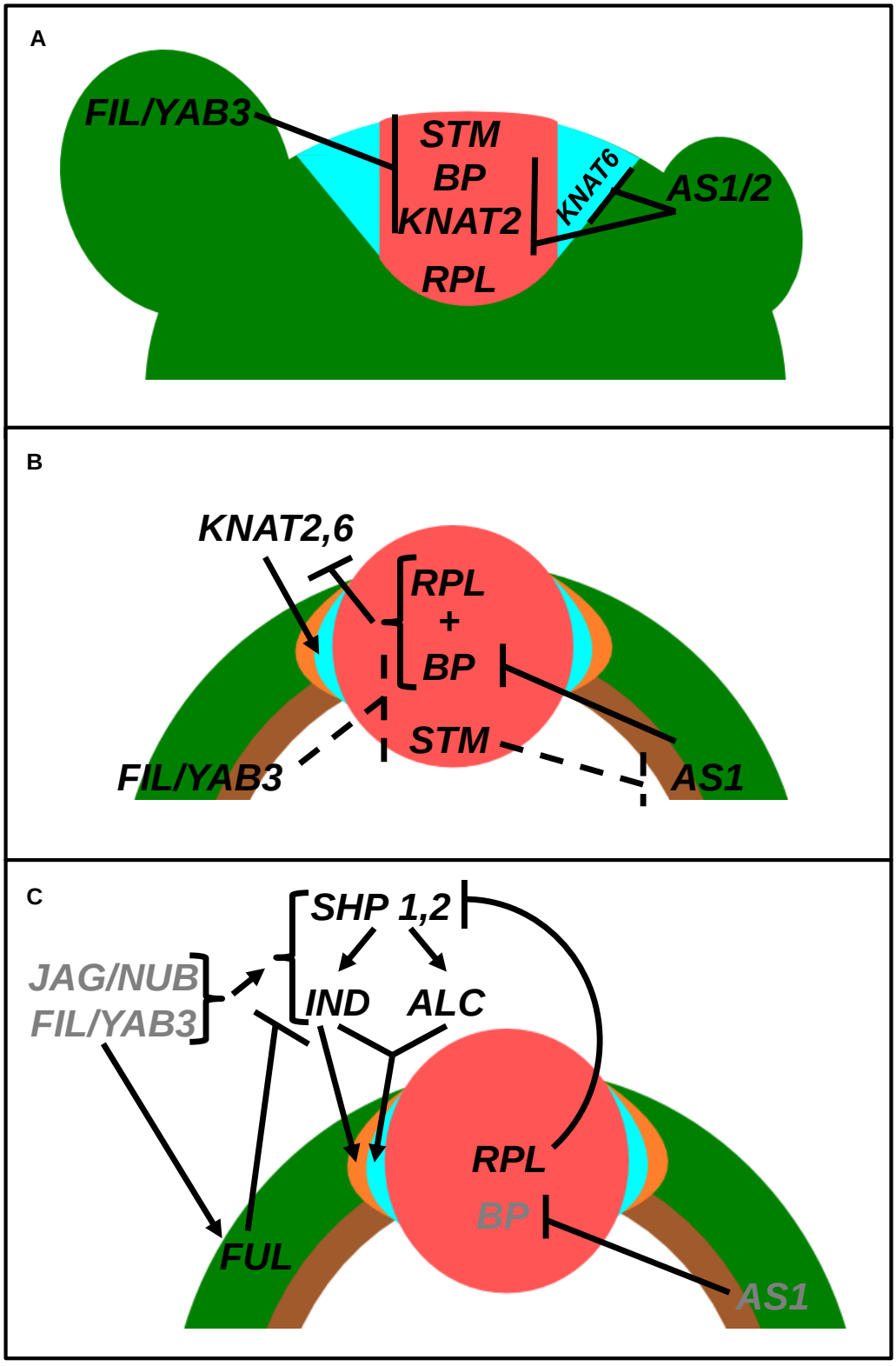

Figure 1.4 Genetic networks in the SAM and gynoecium. Outline of genetic regulatory interactions in the SAM (A) and gynoecium (B), where gene expression defines shoot versus leaf (A) and valve versus replum (B). Dashed lines represent hypothesised interactions. C) shows how some of these genes (grey) interact with the dehiscence zone patterning genes (black) to promote correct cell specification during gynoecium development.

Whilst the precise details of the expression, regulation and interaction of SAM and leaf patterning genes in the *A. thaliana* fruit requires further elucidation, evidence is accumulating that these genes function to promote determinacy versus indeterminacy in the valve and replum/medial fruit tissues, and that they tie-in with the network of known dehiscence zone patterning genes. JAG and FIL appear to promote *FUL*, *SHP1* and *2*, *IND* and *ALC* (Østergaard 2009), and RPL and the class I KNOX protein BP appear to interact in the replum (Alonso-Cantabrana et al. 2007), indicating that the leaf and meristem patterning genes may have a role in regulating the expression of the dehiscence zone patterning genes. The proposed role of SAM and leaf patterning genes in silique development are summarised in Figure 1.4. From an evolutionary context, the functions of leaf and meristem genes in fruit growth and patterning hint at the historical co-option of pre-existing developmental mechanisms to pattern a new and important Angiosperm lateral organ, the fruit. Indehiscent mutants in *A. thaliana*

1.3.2.8. *Indehiscent mutants in* A. thaliana

A suite of mutant alleles have been described in *A. thaliana* that reduce dehiscence or possess fully indehiscent siliques. The majority of these indehiscence phenotypes are caused by a failure of the valve margin tissues to differentiate correctly, but mutations affecting valve and replum formation also produce altered dehiscence phenotypes.

A high degree of morphological similarity is seen between *indehiscent (ind)* and *shatterproof 1, shatterproof 2 (shp1, shp2)* double mutants. Both show a lack of valve margin definition, resulting in indehiscence (Liljegren et al. 2000; Liljegren et al. 2004). These phenotypes arise too as a consequence of constitutive

FRUITFULL (FUL) expression, as is seen in transgenic *35S::FUL* lines (Ferrándiz et al. 2000). The indehiscent phenotypes arising from aberrant expression of these genes were key to developing the current model of dehiscence zone patterning in *A. thaliana*.

Indehiscence phenotypes similar to those seen in *shp* double mutants, *ind* and *35S::FUL* plants can also be mimicked by manipulating auxin distribution. An IND-mediated auxin minimum forms in the valve margin of WT plants, and expression of the bacterial biosynthetic auxin gene *iaaM* under the *IND* promoter has been shown to prevent formation of this minimum (Sorefan et al. 2009). The valve margins of the resulting siliques are similar to those of *ind* mutants, lacking a separation layer and showing poor definition under SEM.

Mutations in *NAC SECONDARY WALL THICKENING PROMOTER (NST)* genes also result in indehiscence as a consequence of valve margin defects. Whilst the valve margin does form in *nst1* mutants and *nst1, nst3* double mutants, it fails to lignify (Mitsuda & Ohme-Takagi 2008). This lack of valve margin lignification results in indehiscent siliques, similar to *shp1, shp2* fruits, however, because these *nst* mutants do possess valve margin, they can be opened by rubbing between two fingers, a technique which does not work with the valve margin-less siliques of *shp1, shp2* mutants (Mitsuda & Ohme-Takagi 2008).

Like *nst* mutants, *alcatraz (alc)* and *spatula (spt)* siliques also develop valve margin. However, *spt* shows reduced dehiscence (Girin et al. 2011), whilst *alc* is fully indehiscent (Rajani & Sundaresan 2001). These two genes are partially redundant (Groszmann et al. 2011), and the defects in dehiscence that both mutants show arises not from a failure to lignify the valve margin, as is seen in *nst* mutants, but from the absence in both of a correctly specified separation layer

within the valve margin (Rajani & Sundaresan 2001; Girin et al. 2011). The fact that *alc* mutants are fully indehiscent, whilst *spt* mutants are only partially indehiscent, reflects subfunctionalisation - *SPT* is key for the earlier development of carpel margin tissues, whilst *ALC* is more important for the later development of the dehiscence zone (Groszmann et al. 2011). The reduced dehiscence of both mutants shows, however, that without the correct specification of the layer of non-lignified cells within the valve margin, dehiscence in *A. thaliana* cannot take place.

Alterations in *YABBY 3 (YAB3)* and *FILAMENTOUS FLOWER (FIL)* also affect valve margin formation (Dinneny et al. 2005). The apex of *fil, yab3* double mutant siliques fails to develop valve margin, resulting in the indehiscence of this region of the silique. This phenotype appears to arise due to a failure of *fil, yab3* mutants to express *FUL* in the valve. *FIL* and *YAB3* are therefore necessary for the activation of *FUL* expression in the valve, and furthermore, are required for the maintenance at the valve margin of *SHP* expression (Dinneny et al. 2005).

FIL and *YAB3* activate *FUL* and *SHP* expression redundantly with *JAGGED (JAG)*, and *jag-5D* siliques, which possess a dominant activation tagged allele, also show reduced dehiscence (Dinneny et al. 2005). However, the reduced dehiscence seen in strongly affected *jag-5D* silique regions does not arise from alterations in valve margin specification and differentiation, but instead from a replum defect. In these siliques, *SHP* expression and valve margin tissues spread into the replum. This results in a much reduced replum, and the spreading of lignified valve margin cells across this tissue forms what Dinnenny *et al.* describe as a ‘lignified bridge’ which spans the distance between the two valves, preventing their separation and dehiscence.

Similar indehiscence phenotypes arising from replum defects can also be seen in strong *replumless (rpl)* mutants. Unlike in weaker alleles, *rpl-3* siliques show expansion of the valve margin lignified layer through the replum, forming a 'bridge' between the valves similar to that described in *jag-5D* mutants, resulting in reduced dehiscence (Roeder et al. 2003).

Indehiscence in *A. thaliana* can therefore arise from a lack of valve margin tissue, incorrect specification of the lignified and non-lignified layers within the valve margin, and from spreading of the lignified valve margin cells across the replum region. A fourth cause of indehiscence is seen in *ful* mutants. In contrast to *shp1, shp2* double mutants and *35S::FUL* transgenic lines, *ful* fruits show ectopic lignification of the valve (Ferrándiz et al. 2000). This phenotype suggests a spreading of valve margin identity into the valve tissue, similar to the valve margin identity observed in the replum in strong *rpl* mutants. Likewise, this spreading of valve margin identity into the valve results in indehiscence, as the valve fails to separate from the replum in *ful* mutants (Gu et al. 1998). Liljegren *et al.* (2004) propose that the indehiscence seen in *ful* mutants arises because *A. thaliana* dehiscence requires valve margin identity to be restricted to a narrow strip and not to spread into the valve.

1.4. Experimental aims and goals of this work

As discussed throughout this chapter, explosive seed dispersal is a dramatic and intriguing adaptation to a critical life cycle stage in flowering plants. Many factors influence this complex trait, which has evolved independently multiple times in different Angiosperm lineages, and mirrors the rapid dispersal movements of spores seen in more basal land plants and some fungi.

The development of *C. hirsuta* as a model for developmental and genetic studies provides an opportunity to investigate the mechanics, cell biology, developmental processes, and genetic patterning of explosive seed dispersal in this species. Its high genetic similarity with *A. thaliana* allows for capitalisation upon the extensive genetic analyses of fruit development that have been undertaken in this latter species, and allows us to ask how these networks in *A. thaliana* may have altered to pattern such a drastically different dehiscence mechanism in *C. hirsuta*.

The aim of this body of work is to characterise the developmental and genetic basis of explosive pod shatter in *C. hirsuta* in a comparative framework with *A. thaliana*, which exhibits non-explosive shatter. This will be done through detailed characterisation of the morphology of the wild-type *C. hirsuta* silique and its dehiscence, and its comparison both with other Brassicacean species and isolated *C. hirsuta* fruit mutants.

2. Materials & Methods

All chemicals were sourced from Sigma-Aldrich unless stated otherwise.

2.1. Plant Materials and Growth Conditions

2.1.1. Plant Growth Conditions

Plants were grown in soil medium made from two parts Scotts Levington M2 compost and one part Sinclair Vermicullite Medium (0.2 to 5.0 mm). Prior to seed-sowing, soil was watered with 0.2 mg/L Intercept ® 70WG. After 7 days in the dark at 4^{o}C, plants were moved to a long day greenhouse (18 hours 20^{o}C, 6 hours 16^{o}C) with supplemental lighting of 50 µmol photons $m^{-2}s^{-1}$ intensity. Propagator lids were removed post germination, and ungerminated pots were cycled between 4 days in the cold (dark, 4^{o}C) and 7 days in the greenhouse until germination.

2.1.2. Plant Growth Characterisation

All digital photographs of whole plant tissue and whole-mount phloroglucinol or GUS staining were taken by J. Baker, Department of Plant Sciences, University of Oxford.

C. hirsuta (Oxford accession) and *A. thaliana* (Columbia-0 accession) plants used for seed number and seed dispersal distance comparisons were grown in a large greenhouse without temperature and light control at Wytham Field Station, Oxfordshire. Each plant was grown at the centre of a large sheet of plastic, with radii of 5 cm intervals from the plant marked, and a total 21 *C. hirsuta* and 15 *A. thaliana* plants were analysed. A summer project undergraduate student, C. Rookyard, recorded how many seeds fell within each distance interval.

Seed weights for *A. thaliana* and *C. hirsuta* were calculated by taking the mean of 3 tubes of 40 *A. thaliana* (Columbia-0) seeds and 3 tubes of 20 *C. hirsuta*

(Oxford accession) seeds. Duration of fruit developmental stages in *A. thaliana* and *C. hirsuta* were measured in the Landsberg *erecta* (L*er*) and Oxford accessions, respectively. Data was collected from two fruits each from five L*er* and six Oxford plants, grown in the same greenhouse, at the same time-point each day. The duration of each developmental stage was measured in whole days, and individual data points were approximated to the nearest day when necessary. The data was then averaged by taking a mean for each developmental stage in each species. For both species, the number of data points at each stage (n) ranged between 4 and 10.

Silique lignin content was calculated by modified klason analysis (Rogers et al. 2005), conducted by A. Hay. WT and *valveless* silique lengths were measured at stage 17b, when siliques have reached their full length and the dehiscence tissues have lignified. Two mature siliques from each of 15 plants per genotype were measured, giving a total sample size of 30 for each genotype.

2.1.3. Plant Materials

The wild-type *C. hirsuta* accession used was 'Oxford', (specimen voucher Hay 1), originally collected in Oxford, United Kingdom (Hay & Tsiantis 2006). The 'Oligosperma' accession used for mapping crosses was collected in Clark County, Washington State, USA, and was a gift from K. Marhold. *A. thaliana* accessions used were Col-0 and L*er*. The *ful-1* mutant characterised was a L*er* allele (Gu et al. 1998), obtained from the *Arabidopsis* Biological Resource Centre (stock number CS3759).

Cardamine corymbosa was collected in Pukerua Bay, New Zealand by A. Hay and identified by internal transcriber sequence (ITS) sequencing. *Olimarabidopsis pumila* accession number N3700 was used, obtained from

Nottingham *Arabidopsis* Stock Centre. *Rorippa islandica* was identified when it grew as a weed in unsterilized soil and was identified by ITS sequencing. A selfing strain of *Arabidopsis lyrata*, donated by B. Mable (Mable & Adam 2007), was self-pollinated by M. Tsiantis. *Brassica nigra* and fast-cycling *Brassica rapa* were donated by R. Leimu Brown and N. Prill.

The *twisted (twi)* mutant was identified in a previous EMS screen by A. Hay. The *cardamine asymmetric leaves1-1 (cas1-1)* mutant was previously described (Hay & Tsiantis 2006). The *cardamine brevipedicellus (cbp)* mutant was identified simultaneously from two different EMS screens, the one described in this thesis, and one conducted by H. Jenkins (Jenkins & Tsiantis 2010). *valveless (val), delayed fruit opening (dfo), less lignin1 (lig1)* and *cardamine ettin-like (cetl)* alleles were all identified from the EMS screen described in Chapter 3.

Crosses between genotypes were accomplished by dissecting away all floral organs except the carpel in unopened floral buds (used as female) and brushing stamens (from plant used as male) against the stigmatic surface. Naked pollinated carpels were then protected with cling film until the carpel elongated, thus preventing pollination by contaminant pollen.

Crosses were used to determine the inheritance patterns of mutant alleles. *cbp* inheritance was characterised by H. Jenkins as recessive. *val* was crossed to the Oligosperma accession and the phenotypes of the second filial generation (F_2) were scored. Of 743 plants, 595 were WT and 148 were *val*, with a chi-squared test confirming recessive inheritance ($\chi^2 = 0.1561$, 1 degree freedom, not significantly different from expected at >10% level). Analysis of the F_2 generations of crosses between *cetl* and the WT Oxford accession found segregation of 160 WT to 54 *cetl*, confirming recessive inheritance ($\chi^2 = 0.006231$, 1 degree freedom,

not significantly different from expected at >50% level). Analysis of the F_2 generation between *twi* and the WT Oxford accession found segregation of 47 WT to 9 *twi*, confirming recessive inheritance ($\chi^2 = 2.18$, 1 degree freedom, not significantly different from expected at >10% level).

To determine inheritance of the *lig1* mutant, progeny of a selfed mutant identified in the second generation of mutagenised seed (M_2) were screened. Of 6 plants, none showed the bumpy replum or mutant lignification phenotype. Re-screening of the M_2 line in which the *lig1* mutant was identified did not identify any siblings showing the *lig1* phenotype. Out of 31 siblings, 4 were sterile, 27 showed the WT replum morphology, and 0 possessed a bumpy replum. Therefore, the *lig1* mutation was either not transmitted to progeny or the phenotype showed variable expressivity.

The *dfo* phenotype is quantitative and can easily be confused with developmentally delayed WT siliques. The *dfo* mutant was crossed to the Oligosperma accession. From the F_2 generation, consisting of 243 plants, 41 of the most delayed plants were identified as most likely to be *dfo*, and tissue was collected and frozen from 34 of these plants for future linkage mapping.

Genotypes of double mutants were determined using phenotype segregation analyses.

2.2. Histology and Microscopy Techniques

Phosphate buffers were made using NaH_2PO_4 from Melford and Na_2HPO_4 from AnalaR Normapur®.

2.2.1. Scanning Electron Microscopy (SEM)

Young flowers were fixed as whole inflorescences for SEM, whilst elongated siliques were cut into sections to aid fixative infiltration. These tissue

samples were vacuum infiltrated with 25 mM phosphate buffer pH 7 with 3% gluturaldehyde (Agar Scientific) for 10 minutes, and then left shaking overnight at 4^{o}C. Samples were rinsed in 25 mM phosphate buffer pH 7 and immediately replaced with a second 25 mM phosphate buffer pH 7 wash for 15 minutes, shaking at 4^{o}C. Samples were given a second 15 minute phosphate buffer wash, and then dehydrated through an ethanol series of 30%, 50%, 60%, 70%, 80%, 90%, 95% and three washes of 100%, each for 15 minutes, shaking at 4^{o}C. Samples were left in a fourth 100% ethanol wash at 4^{o}C overnight, followed by two more 100% washes the following day.

A Tousimis AutoSamDry 814 critical point dryer was used to critically point-dry the samples, which were then mounted and dissected on Agar Scientific Plain Stubs for Jeol coated with Agar Scientific Carbon Tabs. Samples were then coated with palladium using a Polaron SC7640 sputter coater. A Jeol JSM-5510 scanning electron microscope was then used to view and photograph the specimens.

2.2.2. Transmission Electron Microscopy (TEM)

TEM of *A. thaliana* and *C. hirsuta* developing and mature siliques was conducted by H. Dickinson, as previously described (Spielman et al. 1997).

2.2.3. Cryotome sectioning and Confocal Laser Scanning Microscopy (CLSM)

Silique tissue was free-sectioned using a razor blade and embedded in Sakura Tissue-Tek ® O.C.T.™ Compound. Tissue was then sectioned using a Leica Microsystems Cryostat 1720. Sections were mounted on slides and viewed using a Zeiss LSM 510 META confocal laser-scanning microscope. A 405 diode laser was used, at 21% output, to visualise chlorophyll, lignin and calcofluor white

fluorescence. Chlorophyll autofluorescence was visualised using a 78 µm pinhole diameter and a 411-753 nm filter. Lignin autofluorescence and calcofluor white fluorescence were visualised using a 63 µm pinhole diameter and a 435-485 nm filter.

2.2.4. Calcofluor White Staining

Calcofluor White M2R was used at a concentration of 0.05 mg/ml in pH7 phosphate buffer. The stain was pippetted under the coverslip of mounted cryotome sections and visualised using CLSM.

2.2.5. Plastic-embedding of tissue

Tissue was was vacuum infiltrated with 0.05 M phosphate buffer pH 7.2 with 1% gluturaldehyde (Agar Scientific) and 4% formaldehyde (Fisher Scientific) for 15 minutes and then left shaking at 4^{o}C overnight. Tissue was then washed for 30 minutes with 0.5 M phosphate buffer pH 7.2, shaking at 4^{o}C. Tissue was then dehydrated through an ethanol series of 10%, 30%, 50%, 70%, 95% and two 100% washes, each for 30 minutes shaking at 4^{o}C. Tissue was then incubated in Technovit/EtOH solution (1 gram of Hardener I per 100 ml Technovit 7100 liquid, diluted 2:1 with 100% ethanol) for 3 hours at room temperature. Technovit/EtOH solution was then replaced with Technovit 7100 liquid with Hardener I (1 gram of hardener I per 100 ml) and left shaking overnight at 4^{o}C. Tissue was then embedded with Technovit 7100 liquid with 6.25% hardener II. Embedded tissue was glued to rubber stubs with Araldite Precision (Blue) epoxy glue. 5 µm sections were cut using a glass knife mounted on a Microm HM 335 E microtome and floated onto Thermo Scientific Menzel-Gläser Superfrost glass slides using a water bath.

2.2.6. Toluidine Blue O (TBO) Staining

Slides of 5 µm plastic sections were placed on a 60^{o}C slide warmer. Filtered 0.05% toluidine blue O in 0.1 M phosphate buffer pH 5.7 was layered onto slides and left to soak between 20 to 180 seconds, depending on stage of fruit development. Slides were immediately washed twice (10 to 20 seconds each, depending on developmental stage) in distilled water and left to air dry. Young flower sections were soaked in TBO and washed for shorter periods, late silique sections for longer periods. Slides were then mounted using Agar Scientific DPX Mounting Medium.

2.2.7. Ruthenium Red Staining

Both free-hand fresh sections and plastic-embedded 5 µm sections were stained using a fresh 0.05% solution of ruthenium red (ruthenium oxychloride ammoniated) in 0.1 M phosphate buffer (pH 7.2). Sections were stained for 5 to 10 minutes. Fresh sections were mounted in glycerine, and plastic sections in Agar Scientific DPX Mounting Medium.

2.2.8. Paraffin-embedding of tissue

Samples were fixed with 4% paraformaldehyde (Agar Scientific) solution (0.2 mM NaOH from Fisher Scientific, 1X phosphate buffered saline, 4% DMSO from Fisher Scientific, 0.1% Triton® X-100), shaking over night at 4^{o}C. Samples were then given two 30 minute 1X phosphate buffered saline (PBS) washes, both shaking at 4^{o}C. Samples were then dehydrated for 30 minutes each in 30%, 50%, 60% and 70% ethanol, before being processed using a Sakura Tissue-Tek® VIP™ processor and embedded using a Sakura Tissue-Tek® TEC™ embedding station.

2.2.9. Periodic Acid Schiff Staining

8 µm sections of paraffin-embedded tissue were treated with National Diagnostics Histo-Clear and hydrated. Slides were then placed for 10 to 20 minutes in 0.5% periodic acid, washed with water for 5 to 10 minutes, stained in Schiff's reagent for between 10 and 15 minutes, and then rinsed with water for 5 to 10 minutes. This staining was conducted by S. McKim.

2.2.10. Clearing of whole-mount preparations

Embryos were prepared for microscopy by removing developing seeds and positioning them in drops of chloral hydrate solution (72.7% chloral hydrate and 9% glycerol in water) on microscope slides. The glycerol used for this was from Fisher Scientific. These slides were then regfrigerated at 4^{o}C for a minimum of 4 hours prior to microscopy.

To prepare tissue for whole-mount phloroglucinol staining, siliques were first fixed for 1 to 4 hours in 14.2% acetic acid (AnalaR Normapur®) in ethanol, shaking at room temperature, or overnight shaking at 4^{o}C. Siliques were rinsed in 100% ethanol and immediately washed with a second 100% ethanol wash, lasting 5 minutes. Siliques were then washed in 70% ethanol for 2 minutes before being cleared for 1 to 3 hours in chloral hydrate solution.

2.2.11. Phloroglucinol Staining

Fixed and cleared whole-mount siliques were stained with phloroglucinol solution (1.72% phloroglucinol, 81.9% ethanol, 13.8% hydrochloric acid in water) and inspected after 10, 20 and 40 minutes. When photographed, siliques were photographed within 30 minutes of first exposure to phloroglucinol.

2.2.12. β-Glucuronidase (GUS) Staining

Tissue was fixed in 90% acetone (Fisher Scientific) for 30 minutes, shaking at room temperature. Tissue was then washed, twice, in 1M phosphate buffer pH7, shaking at room temperature for 5 minutes.

5-Bromo-4-chloro-3-indolyl b-D-glucuronide (Invitrogen) was dissolved in dimethyl formamide to make a 100 mg per ml 'X-Gluc' solution. 'GUS solution' was made up from 1% X-Gluc solution, 2% 0.1 M ferricyanide, 2% 0.1 M ferrocyanide, 25% GUS buffer (20% sodium phosphate buffer pH7, 0.8% Triton® X-100, 79.2% water), and 70% water.

Tissue was incubated in GUS solution at 37^{o}C overnight (around 18 hours). GUS solution was removed and tissue rinsed with 95% ethanol, replaced immediately by a second 95% ethanol wash, and returned to 37^{o}C for 1 hour. 95% ethanol was replaced again and tissue left at 37^{o}C overnight (minimum 18 hours). The next day, tissue was moved to room temperature and 95% ethanol replaced daily until tissue was fully cleared (around 4 days). 95% ethanol was then replaced with 50% glycerol (Fisher Scientific).

2.2.13. Light Microscopy and Image Processing

Stained plastic and paraffin-embedded sections were observed using an Olympus BX50 microscope and photographed using a QImaging Retiga EXi camera and QCapture Pro 6.0 software. Differential interference contrast was used to observe whole-mount embryos. Where necessary, image contrast and light levels were adjusted using Adobe Photoshop Elements 10. MediaCybernetics ImagePro was used to measure the cross-sectional area of endocarp *b* cells.

2.3. EMS Mutagenesis and Screen Methods

Approximately 10 000 *C. hirsuta* Oxford seeds were washed for 15 mins in 0.1% Triton® X-100. Half the seeds were treated with 0.18% (15 mM) ethyl methane sulphonate (EMS) in water (treatment A), and half were treated with 0.36% (30 mM) EMS in water (treatment B), both for 10 hours. Seeds were rinsed with 12 water washes of 5 minutes each. The final wash was replaced with 0.1% agarose and M_1 seeds were pipetted onto soil, one seed per pot. 520 treatment A M_1s were grown and 484 of treatment B. Plants were allowed to self and seed collected from all fertile M_1s. 5 lower treatment A M_1s were sterile, as were 104 of the treatment B M_1s. Selfed M_1 seed gave a total of 895 M_2 lines. 27 seeds (9 seeds in each of 3 pots) were planted from each of the 515 treatment A lines, and 48 seeds (16 in each of 3 pots) were planted from each of the 380 treatment B lines. A total of 32 145 M_2 seeds were planted and screened for aberrant silique morphology, delayed silique opening, and indehiscence.

Siliques were screened for altered lignin deposition by high-throughput whole-mount lignin staining. Three pots were planted for each M_2 line. Stage 17b siliques, which have undergone lignification of the endocarp *b* and the dehiscence zone, were removed from each of the 9 (treatment A) or 16 (treatment B) plants growing in a single pot. These were then pooled in a single well of a 24-well histology plate. A maximum of 24 pots from 8 M_2 lines could then be processed together. Siliques were fixed, washed and stained following the procedures described in sections 2.2.10 and 2.2.11. When a mutant phloroglucinol-staining pattern was observed within a well, plants from the corresponding pot were individually screened to identify the mutant plant.

Selected mutants were selfed. M_3 lines of interest were backcrossed to Oxford accession 2 (*twi*) to 3 (*val*, *cetl*) times, with the exception of *dfo* and *lig 1*.

2.4. Molecular and Bioinformatic Methods

2.4.1. Genomic DNA Extraction

Leaf or inflorescence tissue was mechanically homogenised in 1.5 ml eppendorf tubes. 400 µl Extraction Buffer added (250 mM NaCl, 25 mM EDTA, 250 mM Tris-HCl pH 7.5, 0.5% SDS), followed by vortexing. Samples were spun for 1 minute at 13 000 rpm in a Heraeus Biofuge pico microcentrifuge. 300 µl of supernatant was removed to new eppendorf tubes and 300 µl isopropanol added. Tubes were mixed by inverting and left for 2 minutes at room temperature to allow precipitation. After a 5 minute centrifugation at 13 000 rpm, the supernatant was decanted away and the DNA pellets washed with 100 µl 70% ethanol and centrifuged for 1 minute. The supernatant was tipped away and tubes allowed to air dry for 10 minutes. 100 µl of TE pH8 (10 mM Tris, 1 mM EDTA) was added and tubes left shaking at room temperature overnight, so as to resuspend genomic DNA. 2 µl of genomic DNA was used as template in a PCR. EDTA was sourced from Melford, NaCl and SDS from Fisher Scientific.

2.4.2. Bioinformatic Tools

Primers were designed using Invitrogen Vector NTI Advance™ 11.0, NCBIPrimer-BLAST and Primer3 (Rozen & Skaletsky 1999). The online dCAPS Finder 2.0 was used to identify CAPS and dCAPS markers (M. M. Neff et al. 2002).

DNA sequencing data was analysed using ContigExpress (Invitrogen Vector NTI Advance™ 11.0). Sequence comparisons were conducted using ContigExpress, AlignX (Invitrogen Vector NTI Advance™ 11.0), CLUSTAL-W

(EMBL-EBI) (Larkin et al. 2007; Goujon et al. 2010), Multiple Alignment using Fast Fourier Transform (MAFFT, EMBL-EBI) (Katoh et al. 2009), and Analysis of Multiply Aligned Sequences (AMAS, http://www.compbio.dundee.ac.uk/www-amas/) (Livingstone & G. J. Barton 1993). Graphical mapping of marker and SNP positions was conducted by B. Pieper, using JoinMap 4 ® (Van Ooijen 2006).

DNA sequences and genome annotations for *A. thaliana* were retrieved from The *Arabidopsis* Information Resource at www.arabidopsis.org (Lamesch et al. 2011). Protein annotations were retrieved from UniProt at http://www.uniprot.org/ (The UniProt Consortium 2012). The sequences from other species retrieved from online databases are described in Table 2.1. *C. hirsuta* protein sequences were translated *in silico* from database and sequencing DNA data using Invitrogen Vector NTI Advance ™ 11.0.

2.4.3. Primers Used

The primers used throughout this thesis are listed in Table 2.2. All primers were synthesised by Eurofins MWG Operon.

Sequence	Species	Database	URL
FUL	*A. thaliana*	TAIR	http://www.arabidopsis.org/servlets/TairObject?id=134558&type=locus
IND	*A. thaliana*		http://www.arabidopsis.org/servlets/TairObject?id=128276&type=locus
FRUITFULL-like protein G0LEW0_LEPCM	*Lepidium campestre*	UniProt	http://www.uniprot.org/uniprot/G0LEW0
Ful-like protein Q1ZZV2_BRANA	*Brassica napus*	UniProt	http://www.uniprot.org/uniprot/Q1ZZV2
Floral binding protein 26 Q9SBQ0_PETHY	*Petunia hybrida*	UniProt	http://www.uniprot.org/uniprot/Q9SBQ0
TC23520	*Aquilegia formosa X pubescens*	The DFCI *Aquilegia* Gene Index (AgGI)	http://compbio.dfci.harvard.edu/cgi-bin/tgi/tc_report.pl?tc=TC23520&species=aquilegia
LOC_Os03g54160.2	*Oryza sativa*	Rice Genome Annotation Project	http://rice.plantbiology.msu.edu/cgi-bin/sequence_display.cgi?orf=LOC_Os03g54160.2
BraA.IND.a	*Brassica rapa subsp. pekinensis*	UniProt	http://www.uniprot.org/uniprot/D3Y275
INDEHISCENT	*Lepidium campestre*	UniProt	http://www.uniprot.org/uniprot/C5IFL1

Table 2.1 Table of sequences retrieved from online databases.

Function	Name	Sequence	Restriction Enzyme	Description
Species identification	ITS_4	TCCTCCGCTTATTGATATGC		(White et al. 1990)
	ITS_5	GGAAGTAAAAGTCGTAACAAGG		
Mapping *val*	m229F	TCCTTAGTTCGATATTTGCAAATC	Taq$^{\alpha}$I	Pre-existing
	m229R	GATTTGAGAAGGAACCGTTGA		
	m306F	TCCTTTGGGTCATCCTCTTG	DdeI	Newly designed
	m306R	CTTTCTCTTGCCGTGATGCT		
	fu04F	TATGGGTTGCGGATCGACCATTGGTCG	HinfI	
	fu04R	ATTCACGTCATCTGCAGCAC		
	fd04F	TATCGTGGTGTGCCGAGAACTG	PstI	
	fd04R	AGCTTGACAACCCCATTCAC		
	m102F	GAAGAGGGCTAAAGTGGAACC	DdeI	
	m102R	AAGTCAGGGGTGAACCCAAT		
Amplification of *cFUL* (used in pairs)	n11F	CGCGAAACCCAATAAGAGTC		Upstream from exon 1
	n11R	GGGCAATCAAATCGTGAGTC		In intron 1
	n17F	TGTGGACTCACCAAAAACTAGG		Upstream from exon 2
	n17R	CGATTTGATAAGCACGCAGA		In intron 3
	n19F	CAGGAATTTCATGGGGGAAG		Upstream from exon 4
	n19R	GTTGGACTAACCTTTTTGAGAAGC		Downstream from exon 6
	n20F	TTTGCGATTTGTGTCTTGGA		In intron 3
	n21F	GAGGAATTTGCGATTTGTGTC		In intron 3
	n20/21R	CGCAACTTTCAATCCCACTT		In intron 6
Sequencing *cFUL* (used singly)	n11F	CGCGAAACCCAATAAGAGTC		Upstream from exon 1
	n11R	GGGCAATCAAATCGTGAGTC		In intron 1
	n17F	TGTGGACTCACCAAAAACTAGG		Upstream from exon 2
	ex2R	CTTACACTCTGTGAAACTTCTCGGCC		Spans end of exon 2 and start of intron 2
	ex3F	GGGTTCTAGAACATGCTAAGCTCAAGG		In exon 3
	n19F	CAGGAATTTCATGGGGGAAG		Upstream from exon 4
	ex4F	TTTCATGGGGGAAGATCTTGATTCC		In exon 4
	ex6R	ATTGTGATCTTGCAAGGCCTTATCC		In exon 6

	n19R	GTTGGACTAACCTTTTTGAGAAGC		Downstream from exon 6
	n20R	CGCAACTTTCAATCCCACTT		In intron 6
cFUL marker	cful4F	GCTTCAAAGCTTGGAGCATC	DdeI	Genotyping marker to *cful* mutation in *val*
	cful4R	GCAAGGCCTTATCCTGTTTG		

Table 2.2 Sequences of Primers Used. 'F' and 'R' denote 'forwards' and 'reverse' primers. All sequences read from 5' to 3'.

2.4.4. PCR Marker Amplification

CAPS and dCAPS marker PCRs were conducted using Bioline Mango*Taq*™ DNA Polymerase in the following 15 µl reaction mix: 2 µl genomic DNA (approximately 100 ng), 0.1 mM dNTP, 2.67 mM $MgCl_2$, 1X Mango*Taq*™ Colored Reaction Buffer, 8 pmol forward primer, 8 pmol reverse primer,1U Mango*Taq*™ DNA Polymerase.

Reactions took place in an Applied BioSystems 2720 Thermal cycler, using the following programme: 94^{o}C (5 minutes); 40 Cycles of: 94^{o}C (15 seconds), 53^{o}C (15 seconds), 72^{o}C (30 seconds); 72^{o}C (7 minutes); 8^{o}C (indefinitely). 10 µl of amplified marker product was then treated with 3 units of the appropriate restriction enzyme, in a 15 µl mix of 1X buffer (and 1X BSA if required), at the optimum temperature for 4 hours and then visualised using gel electrophoresis. TaqαI, DdeI, HinfI and PstI restriction enzymes were all sourced from New England Biolabs.

2.4.5. PCR Amplification for Sequencing

Prior to sequencing, gene fragments were amplified using the proof-reading Promega *Pfu* DNA polymerase. A 50 µl reaction mix was used, comprising 1X Pfu DNA Polymerase Buffer (with magnesium sulphate), 10 nmol dNTPs, 25 pmol forwards primer, 25 pmol reverse primer, 1.25 U *Pfu* DNA Polumerase, and 2 µl genomic DNA (approximately 100 ng), in water.

Reactions took place in an Applied BioSystems 2720 Thermal cycler, using the following programme: 95^{o}C (3 minutes); 35 Cycles of: 95^{o}C (30 seconds), 51.5^{o}C (30 seconds), 72^{o}C (2 minutes per kb); 72^{o}C (10 minutes); 4^{o}C (indefinitely).

2.4.6. Gel Electrophoresis

Digested amplified markers were visualised on a 3.5% agarose (Invitrogen Agarose Electrophoresis Grade), 1X TAE gel containing 0.4 µg/ml ethidium bromide (Bio-Rad). Gels were run at 100 V for between 40 and 90 minutes, depending on amplified fragment lengths. Other PCR products, such as amplified gene fragments for sequencing, were confirmed on 1% agarose gels, run for 20 to 40 minutes.

2.4.7. Sequencing

The amount of amplified DNA used as template in sequencing reactions was determined as follows, as advised by Applied Biosystems BigDye ® Terminator v3.1 protocol: 100-200 bp (1-3 ng); 200-500 bp (3-10 ng); 500-1000 bp (5-20 ng); 1000-2000 bp (20-50 ng), more than 2000 bp (40-100 ng).

DNA was sequenced in 10 µl reactions, including 10 pmol of primer, 1X sequencing buffer, and 1 µl of Applied Biosystems BigDye ® Terminator Ready Reaction Mix. The sequencing reactions took place in an Applied Biosystems 2720 thermocycler, undergoing 25 cycles of: 94^{o}C (30 seconds), 50^{o}C (15 seconds), 60^{o}C (4 minutes), followed by an indefinite hold at 8^{o}C.

After the reaction, the product was precipitated for 15 minutes at room temperature in 83 mM sodium acetate (AnalaR Normapur®) in 66% ethanol and spun in a Heraeus Biofuge pico microcentrifuge at 13 000 rpm for 40 minutes. The supernatant was removed, the precipitated pellet washed with 70% ethanol and spun for 5 minutes at 13 000. The supernatant was then tipped away and the pellet allowed to air dry for 10 minutes. Sequencing products were stored at -20^{o}C prior to sequencing by the University of Oxford Department of Zoology

Sequencing Facility, using an Applied Biosciences ABI PRISM® 377 DNA Sequencer.

2.5. Genetic Constructs and Transformation

2.5.1. Transgenic Constructs Used

The *IND::IND:GUS* construct (pEGAD vector) was kindly provided by L. Østergaard (Sorefan et al. 2009). The *FUL::FUL:GUS* construct was adapted from the *gFUL:GFP* construct (pMDC204 vector) kindly provided by G. Angenent (Urbanus et al. 2009). Gateway Cloning (Invitrogen) was used to transfer the 5.3 kb *gFUL* fragment (including 2 kb of the promoter region upstream from the ATG start codon) to the pMDC163 GUS vector, via the the pDONR207 vector. The construct was verified at each stage by restriction digestion (with PstI for pDONR207 and XhoI for pMDC163) followed by gel electrophoresis.

2.5.2. Growth and Transformation of Bacterial Strains

Bacterial strains were cultured with the appropriate antibiotic in Luria Broth (LB) or Yeast Extract Broth (YEB), prepared by P. White. Super Optimal Broth with Catabolite repression (SOC) media, used during chemical transformations, was also prepared by P. White.

Cloning and plasmid amplifications were conducted in *Escherichia coli* (DH5α strain), cultures grown at 37^{o}C. For transformation, 100 ng of plasmid was mixed in 100 µl of 1X KCM solution (0.1 M potassium chloride, 0.3 M calcium chloride, 0.25 M magnesium chloride) and incubated with 100 µl of chemically competent DH5α cells on ice for 15 minutes. This incubation mixture was then heat-shocked for 30 seconds at 42^{o}C, prior to a further incubation of 2 minutes on ice. After the addition of 200 µl SOC liquid medium, the transformation mixture was shaken for 1 hour at 37^{o}C. The culture was spun for 30 seconds at 6000 rpm

in a Heraeus Biofuge pico microcentrifuge, and 800 µl of supernatant removed. Cells were resuspended in the remaining 200 µl by pippetting and then plated on LB agar plates containing the appropriate antibiotic (most commonly kanamycin, sourced from Melford, at 100 µg/ml) and incubated overnight at 37^{o}C.

Transformation of *C. hirsuta* was conducted using *Agrobacterium tumefaciens* (GV3101 strain), cultures grown at 28^{o}C. *A. tumefaciens* was transformed by adding approximately 100 ng of plasmid to 50 µl of electrocompetent GV3101 cells, and electroporating the mixture at 2 kV voltage, 200 Ω resistance, and 25 µF capacitance. 500 µl of LB liquid medium was added immediately, and the mixture was shaken for 2 hours at 28^{o}C. 200 µl of the mixture was then plated on LB agar plates containing the appropriate antibiotics for the plasmid. Plates were incubated for around two days at 28^{o}C.

For mid- or long-term storage of plasmids, glycerol (Fisher Scientific) stocks of both bacterial species (25% glycerol, 50% bacterial liquid culture, 25% water) were stored at -80^{o}C.

2.5.3. Transformation of *C. hirsuta* Plants

To transform genetic constructs into *C. hirsuta* plants, *A. tumefaciens*, containing the desired plasmid, was first cultured overnight in 5 ml LB liquid culture, containing the appropriate antibiotic, at 28^{o}C. This culture was then added to a 1 litre culture of YEB medium and grown overnight at 28^{o}C. This 1 litre culture was then pelleted by centrifugation at 4^{o}C for 20 minutes at 5000 rpm. Pelleted cells were then resuspended by agitation in 500 ml of infiltration medium (10 mM magnesium chloride, 100 ng/ml 6-benzylaminopurine, 1X Gamborg's vitamins, 5% sucrose from Fisher Scientific, 0.03% Vac-In-Stuff Silwet L-77).

One pot at a time of between 5 to 9 *C. hirsuta* plants were then dipped in the infiltration medium. Each pot was dipped for 15 seconds, and was continually moved around in the culture for the duration of this time. Plants which had only just started flowering and that possessed many young floral buds were used. The pots of dipped plants were then laid horizontally over trays lined with absorbant paper towels. These trays were covered with cling-film and left overnight at 4^{o}C. The following day, pots were moved to an upright position and returned to the greenhouse. After the transformed plants had set seed and dried out, this T_1 seed was collected and dried a further two weeks before selection.

2.5.4. Sterilisation and Selection of Transgenic Seed

For transgenic plants with hygromycin resistance, T_1 seed was sterilised and then cultured on hygromycin Murashige & Skoog (MS) plates. MS media was prepared by P. White, and hygromycin was sourced from Melford.

Prior to sterilisation, seeds were washed for 4 minutes in 95% ethanol. Seeds were then sterilised for 5 minutes in a 10% bleach and 0.05% sodium lauryl sulphate mixture. Seeds were then washed in four successive washes with water, before the addition of MS top agar. Seeds were then plated under aseptic conditions on 50 µg/ml hygromycin MS agar plates. These plates were wrapped in foil and stored at 4^{o}C for three days, then unwrapped and transferred to a tissue culture room (22^{o}C, 16 hour photoperiod). After one day, the plates were wrapped again in foil for an additional day to provoke an etiolation response. The plates were then unwrapped and left to grow in the tissue culture room. Resistant seedlings were then transferred to soil and moved to the greenhouse.

For transgenic plants with BASTA resistance, seedlings were sprayed with 400 µM BASTA (“Kaspar” from Aventis), two to three times a week.

3. *Cardamine hirsuta* fruit morphology

3.1. Introduction

For *C. hirsuta* to become a model for understanding the developmental genetics of explosive dehiscence and how this trait evolved, an understanding of the *C. hirsuta* silique morphology is required. In this chapter, *C. hirsuta* seed dispersal and silique morphology is examined with reference to its non-explosive relative, *A. thaliana*. The gross morphologies of these fruits are then compared with other siliques from the Brassicaceae family, enabling consideration of the wider context within which these features sit. To further investigate the contribution of silique morphology to the explosive phenotype of *C. hirsuta*, a screen for genetic mutants is conducted in order to provide more diversity for study.

3.1.1. Stages of *A. thaliana* fruit development

Gynoecium development in *A. thaliana* can be classified into twenty successive stages. The first twelve describe floral development, from initiation of the floral primordium to the development of a gynoecium that is ready to be fertilised (Smyth et al. 1990; Roeder & Yanofsky 2006). It is at this twelfth stage that the replum, style, valve and valve margin become discernible as gynoecium tissues.

Stage 13 is characterised by opening of the floral bud, anthesis and self-pollination. The seven subsequent stages (14 to 20) describe fruit development, as opposed to that of the carpel. This distinction is largely defined by the occurrence of ovule fertilisation at stage 14, and from this stage onwards the ovules are instead referred to as developing seeds.

Stage 15 sees the expansion of the gynoecium upwards out of the floral bud as a consequence of apical-basal growth. This elongation of the gynoecium

continues through stage 16, which is demarcated by withering and abscission of the stamens, petals and sepals from the fruit, and up until mid stage 17.

Throughout stage 17, a number of important processes occur and the stage is subdivided into two – stages 17a and 17b. Throughout stage 17a the silique continues to elongate until reaching its full length. The silique then broadens and the valve margin and endocarp *b* layers lignify, a process of key importance to dehiscence. By stage 17b, the silique is fully grown and the dehiscence tissues are fully developed.

The remaining three stages of silique maturation describe the subsequent desiccation, dehiscence and dispersal events. Stage 18 is characterised by yellowing of the silique and at stage 19 dehiscence occurs, the valves splitting from the replum along the valve margins. The valves then fall from the silique, leaving the seeds exposed along the fruit septum. The final stage, 20, sees the abscission of the seeds and their dispersal from the silique.

In this chapter, fruit development in *C. hirsuta* is approached from an understanding of stages 14 to 20 of *A. thaliana* gynoecium maturation.

3.1.1. Forward genetics screens in a post-genomic age

To generate morphological diversity for investigating explosive silique dehiscence in *C. hirsuta*, a forward genetics screen was conducted. This mutagenised population was also used to initiate a pilot experiment of the reverse Targetting Induced Local Legions in Genomes (TILLING) method in *C. hirsuta* (data not shown).

The forward genetics screen has been the traditional method for isolating mutants. This method proceeds by identifying phenotypes of interest in a mutagenised population, and then works to uncover the mutated gene responsible

by the process of map-based or positional cloning. With the availability of whole genome sequences, the procedure of forward screens has altered, however this pre-genomics technique remains an important tool for gene discovery. Instead of rendering forward genetics obsolete, the power of genomics has instead streamlined the process.

A key advantage to forward screens is their unbiased approach. Whilst newer, sequence-based reverse genetics techniques offer the chance to determine the consequences when a specific, chosen gene is disrupted, such targeted approaches can often be disappointing, resulting in no mutant phenotype, usually as a result of genetic redundancy (Peters et al. 2003). Forward screens, however, completely bypass this problem by starting from the position of a phenotype of interest. Because no genes are selected or prioritised in this technique, the approach is completely unbiased. This means that, by homing in on a gene from its mutant phenotype, any kind of genetic sequence that is important for this phenotype can be found, including gene families that we might find surprising, genes that have not been correctly inferred or that are poorly annotated, and even intergenic sequences (Jander et al. 2002).

Forward approaches therefore remain an important genetic method in spite of developments in genome sequencing methods and data. However, the procedures of forward genetics do not remain unchanged in the post-genomics age, and the wider availability of both sequencing technologies and sequence data itself have greatly boosted the speed and throughput of modern-day mutant screens. Traditionally, map-based cloning of a mutant gene was a long, drawn-out process, requiring the development of a physical map, the designing of markers and chromosome walking (Jander et al. 2002). However, chromosome walking is

no longer necessary in *A. thaliana*, where a physical map already exists, and a large quantity of sequence data across polymorphic accessions has been collected, enabling the easier design of markers. These benefits are not confined to *A. thaliana* and are now being exploited in numerous model species, including *Medicago trunculata,* rice, maize and tomato (for example Thoquet et al. 2002; Shen et al. 2004; Bortiri et al. 2006; Pei et al. 2011).

Map-based cloning in *C. hirsuta* also benefits from the genomic progress made in *A. thaliana*. Such is the genetic similarity between the two species that the Tsiantis and Hay laboratories were initially using the fully sequenced *A. thaliana* genome as a framework for genetic studies in *C. hirsuta.* Now, these research groups currently share access to 295x coverage of the *C. hirsuta* genome (sequence generated by X. Gan and R. Mott of the Wellcome Trust Centre for Human Genetics, University of Oxford).

Furthermore, a dense genetic map has been constructed for *C. hirsuta* and genetic markers have been developed for multiple *C. hirsuta* accessions, providing resources to begin the cloning of any *C. hirsuta* mutant gene.The width of the genetic interval to which a gene can be mapped depends upon the number of recombinants in a mapping population, the density of markers possible, and the recombination frequency in this region. By using the large amount of single nucleotide polymorphism (SNP) data available for multiple *C. hirsuta* accessions, new genetic markers can be designed and tested within any interval, providing an excellent level of resolution. The specifics of map-based cloning will be discussed in more detail in Chapter 4.

3.1.2. Mutagens for genetic screens

A range of mutagens can be deployed in forward genetics screens. T-DNA and transposon insertions are popular because they enable fast identification of the 'tagged' gene without the need for mapping (Lukowitz et al. 2000; Peters et al. 2003). However, these mutagens usually result in the complete knock-out of genes, with the potential for lethal consequences (Jander et al. 2002). Furthermore, the average number of insertions is around 1.5 per plant grown from a mutagenised seed (M_1), meaning that large numbers of plants need to be screened (Weigel & Glazebrook 2006).

Deletion mutageneses can be conducted through exposure to X-rays, gamma-rays, or fast neutron bombardment (Ino & Yourno 1974; Li et al. 2001; Sikora et al. 2011). Fast neutron bombardment is a highly effective means of mutagenesis and induces a wide range of deletion sizes, ranging from a few base pairs to over 30 kilobasepairs (Koornneeff et al. 1982; Li & Zhang 2002). Fast neutron-induced deletions tend, however, to be around 1 kilobase in size (Bruggemann et al. 1996), meaning that subtler genetic changes, such as reduced gene function, are less likely to be found using this mutagen. Unlike insertional mutageneses, deletion mutageneses involve no 'tag' with which to quickly identify the deletion site. Positional cloning must therefore be used to determine and narrow the genetic interval that contains the affected gene, although once the interval has been narrowed to a few hundred kilobases, DNA blot hybridisation can in some cases be used to more quickly identify the deletion (Weigel & Glazebrook 2006).

Chemical mutagens are advantageous because, unlike T-DNA, transposon, or fast-neutron mutageneses, they do not induce chromosomal rearrangements

(Grini et al. 1999; Kim et al. 2006). Furthermore, chemical mutagens more commonly induce the mutation of a single base-pair than they do DNA deletions or translocations (Sikora et al. 2011). As a consequence, chemical mutageneses result in a wider range of gene expression changes, including dominant gain of function, hypomorphic loss of function, and minor alterations in promoter regions (Jander et al. 2002).

The most widely used chemical mutagen, ethyl methane sulphonate (EMS), is more effective than many other mutagens and relatively easy to use (Lukowitz et al. 2000; Sikora et al. 2011). EMS induces point mutations by alkylating guanine bases, with the result that during DNA replication, DNA-polymerase preferentially pairs thymine instead of cytosine with alkylated guanine bases (Sikora et al. 2011). EMS mutageneses therefore result, 99% of the time, in basepair transitions from GC to AT (Krieg 1963; Kovalchuk et al. 2000; Greene et al. 2003; Kim et al. 2006; Sikora et al. 2011). The main disadvantage of EMS as a mutagen is that mutated genes must be identified by positional cloning (Weigel & Glazebrook 2006). Whilst genomic advances have enabled improvement of the process of mapping genetic mutants, this method is considerably more laborious than the technique of simply identifying the flanking regions of a T-DNA insertion in an insertional mutagenesis.

EMS-induced mutations can be missense, nonsense or silent, and can affect non-coding regulatory regions, coding sequence, mRNA splicing, mRNA stability, and protein translation (Sikora et al. 2011). A key advantage to EMS is that it can induce a wide range of mutant phenotypes that are unlikely to be induced by other mutagens (Weigel & Glazebrook 2006). The broad range of alleles that can be induced by EMS include null and hypomorphic alleles

(recessive loss of function phenotypes), antimorphic alleles (dominant loss of function phenotype), and hypermorphic and neomorphic alleles (dominant gain of function phenotypes) (Weigel & Glazebrook 2006; Sikora et al. 2011).

EMS was selected as the mutagen for the forward genetic screen for fruit and dehiscence mutants in *C. hirsuta*. In *A. thaliana*, approximately 125 000 lines or more of EMS-mutagenised seed (M_1) are required to achieve a saturation mutagenesis (Haughn & Somerville 1987; Kim et al. 2006). However, this number would also be influenced by the process being examined, the effectiveness of the screening methods used, and genomic factors, such as percentage guanine and cytosine content.

In their saturation mutagenesis for herbicide resistance, Jander *et al.* (2003) found that immersion of *A. thaliana* seed for 16 hours in a concentration of 0.2% EMS resulted in around 700 mutations per M_1 line. They calculated that to have a 95% likelihood of identifying a mutation of every GC basepair in the *A. thaliana* genome, a fewer than 50 000 M_1 lines would be needed (Jander et al. 2003). Their reasoning was that, given *A. thaliana*'s genome size of 125 Mb and its GC content of 35% (The Arabidopsis Genome Initiative 2000), it has 4.4×10^7 bp that are susceptible to EMS mutagenesis. From the mutants isolated from their mutagenesis, they calculated a mutation frequency of 1.6×10^{-5} per GC basepair. Multiplying the number of susceptible basepairs by the mutation frequency gives an approximation that each M_1 plant contained 700 mutations. Using a binomial distribution, Jander *et al.* calculated that 250 000 or 45 000 M_1 plants would be needed to have a 98% or 95% chance of finding a mutation in any specific GC basepair, respectively.

However, this would differ between species according to the size of the genome and the percentage GC content. A comparison of *A. thaliana* with *Arabidopsis lyrata* found that in genic regions, the two species had a GC content of 37.6% and 44.9%, respectively (DeRose-Wilson & Gaut 2007). Furthermore, *A. lyrata* has a larger genome size of 207 Mb (Hu et al. 2011). It would therefore take a higher concentration of EMS or a longer mutagen incubation period to have the same percentage likelihood of identifying a mutation in every *A. lyrata* GC basepair as it does in *A. thaliana*.

In general, EMS is usually used at concentrations sufficient to cause enough mutations per plant that a mutant allele for a gene of interest can be found by screening roughly 2000 to 5000 plants from the second filial generation (M_2) of mutagenised seed (Jander et al. 2002; Weigel & Glazebrook 2006).

3.2. Results

3.2.1. Seed dispersal in *C. hirsuta* and *A. thaliana*

To begin this study of the explosive silique of *Cardamine hirsuta*, its role in seed dispersal was first measured and compared with its non-explosive relative *A. thaliana*.

The seed number, weight, and dispersal distance of both species were measured (Figure 3.1). This work was conducted with the assistance of C. Rookyard, an undergraduate summer student who measured seed number and dispersal distance.

The seeds of *C. hirsuta* are markedly heavier than those of *A. thaliana* (Figure 3.1A). A one-tailed Student's T-test (assuming equal variance) gave a P-value of 0.06, which was significant at the 90% level. This difference in seed size could also be seen in scanning electron microscopy (SEM) images (from A. Hay,

Figure 3.1 B and C). These SEM images also revealed that *C. hirsuta* seeds are flatter and more disc-shaped than those of *A. thaliana*. The outward projections seen on the surface of the *A. thaliana* seed are replaced in *C. hirsuta* by sunken indentations in the seed epidermis.

Whilst *C. hirsuta* seeds were larger than those of *A. thaliana*, single plants produced far fewer of them (Figure 3.1D). The difference in seed number per plant was highly significant at higher than the 99% level, with a Student's T-test (two-tailed, unequal variance) giving a P-value of 0.00008.

Data from 21 *C. hirsuta* and 15 *A. thaliana* plants left to freely disperse in undisturbed greenhouse conditions showed that, despite the increased weight of *C. hirsuta* seeds, the vast majority were dispersed much further than *A. thaliana* seeds (Figure 3.1E). In these sheltered greenhouse conditions, where wind and animal disturbance was minimised, 99.9% of *A. thaliana* seeds were found to be dispersed less than 5 centimetres. *C. hirsuta* seeds were distributed over a wider range of distances, with 68.2% landing between 25 to 100 cm from their parent plant, 20.8% remaining within 5 cm from their parent similar to *A. thaliana* seeds, and 7.8% reaching distances of over 1 m.

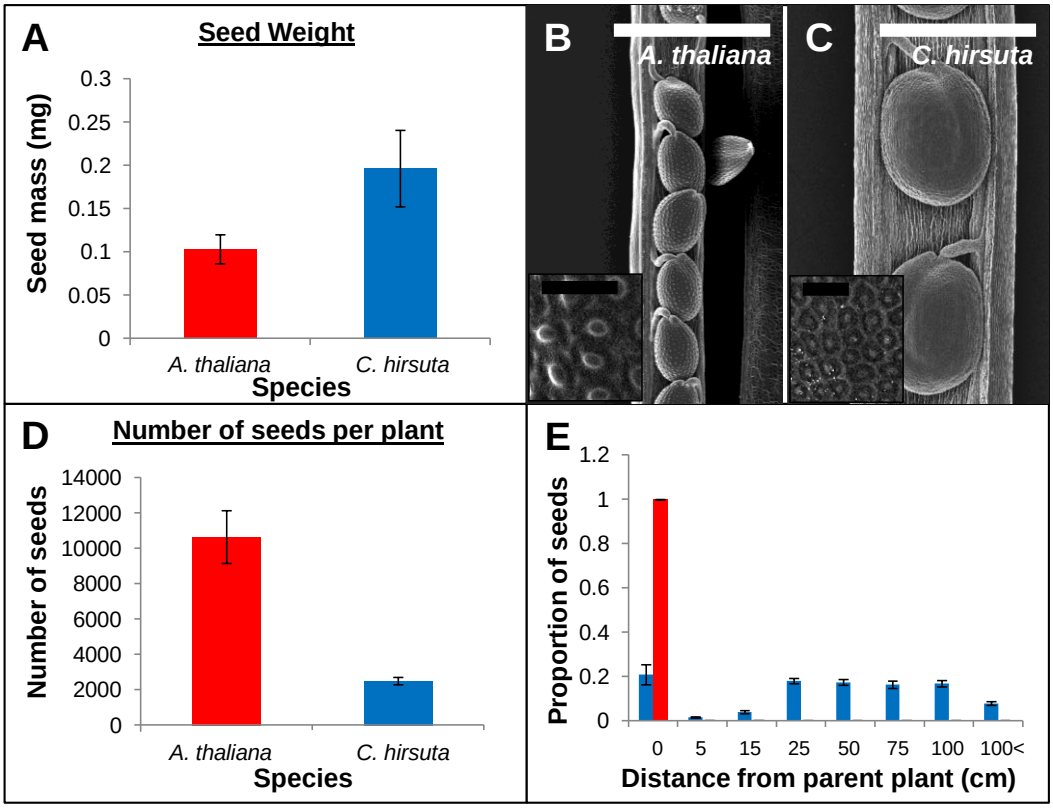

Figure 3.1 Differences in *A. thaliana* and *C. hirsuta* seed morphology and dispersal distance. (A) Difference in seed weight between *A. thaliana* and *C. hirsuta*. SEM of seeds of *A. thaliana* (B) and *C. hirsuta* (C). Inset SEMs in (B) and (C) show magnified seed epidermis. White bar represents 1 mm, black bar 50 µm. (D) Difference in the number of seeds produced per plant between *A. thaliana* and *C. hirsuta*. (E) Differences in seed dispersal distances from parent plant between *A. thaliana* (red) and *C. hirsuta* (blue). Error bars show standard error.

3.2.2. *C. hirsuta* and *A. thaliana* silique morphology

To identify features of the *C. hirsuta* fruit that may contribute to its explosive opening mechanism, *C. hirsuta* silique maturation and fruit structure were examined. Comparisons with *A. thaliana* were used to compare morphological features between an explosive and a non-explosive silique.

3.2.2.1. A. thaliana *and* C. hirsuta *fruit maturation stages are largely comparable*

It was found that *C. hirsuta* fruit development could be split into stages that are similar to those of *A. thaliana*. Gynoecium maturation and silique formation followed comparable developmental progressions, from stage 14 to 19 (Figure 3.2 A to F). Stage 14 saw fertilisation of the carpel and was followed by elongation of the gynoecium out from the floral bud (stage 15) and withering and abscission of the other floral organs (stage 16). Stage 17 was prolonged in both species (Figure 3.2G) and can be subdivided into stages 17a and 17b. During stage 17a the siliques reached full length. The siliques reached stage 17b when they had broadened to reach their full width and were ready to dehisce. Stage 18 was characterised by desiccation and yellowing of the silique and dehiscence occured at stage 19. Here the *A. thaliana* and *C. hirsuta* stages of silique maturation and dehiscence differed, as *A. thaliana* exhibited a final stage, stage 20, in which the seeds abscised from the fruit and were dispersed. In *C. hirsuta*, however, the removal of the seeds from the silique was instantaneous with silique dehiscence, and the seeds were propelled from the fruit when the valve curled suddenly upwards during dehiscence. Aside from this difference, fruit developmental stages were largely comparable between the two species, with some differences in stage duration, including a much shorter silique maturation (stage 17) in *C. hirsuta*. This stage is significantly shorter in *C. hirsuta*, with a two-tailed Student's T-Test (equal

variance) giving a P-value of 6.72×10^{-10}, a value significant at higher than the 99.9% level.

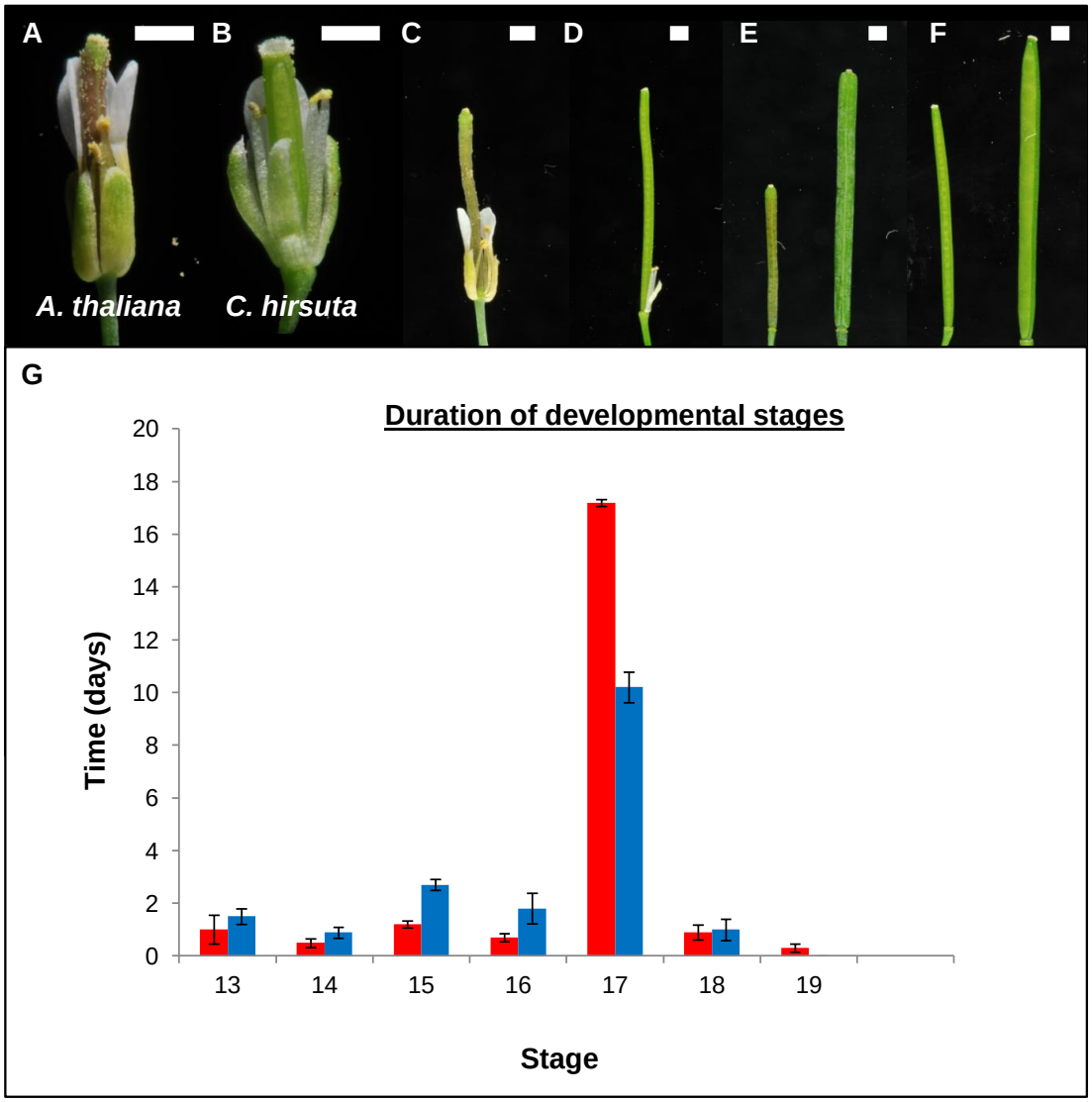

Figure 3.2 Fruit developmental stages in *A. thaliana* and *C. hirsuta*. (A) to (F) Photographs throughout fruit development. Bar represents 1 mm. (A), (C) and E) *A. thaliana*, (B), (D) and (F) *C. hirsuta*. (A) and (B) Stage 15: Elongation of carpel after fertilisation. (C) and (D) Stage 16: Continued fruit elongation, withering and abscission of sepals, stamens and petals. (E) and (F) Early and late stage 17. The silique reaches full length throughout stage 17a and broadens during the transition to 17b. (G) The duration of fruit developmental stages in *A. thaliana* (red) and *C. hirsuta* (blue). Error bars show standard error.

3.2.2.2. Comparison of A. thaliana *and* C. hirsuta *silique morphology*

Electron microscopy and histology gave a closer look at the morphologies of mature *A. thaliana* and *C. hirsuta* siliques at stage 17b (Figure 3.3).

Figure 3.3 panels A to D reveal that both siliques comprise the same tissues – valve, valve margin, replum, septum and seeds – but that the *C. hirsuta* silique is squarer with broader repla and flatter valves.

The valves of both species are examined in Figure 3.3 E and F. Both *A. thaliana* and *C. hirsuta* possess an exocarp layer (a single cell layer containing stomata and covered by a waxy cuticle), several layers of mesocarp cells (which are cuboidal and contain chloroplasts), and innermost endocarp tissues. However, the *C. hirsuta* valve is thicker than that of *A. thaliana*, and an additional tissue layer of sclerenchyma-like cells is present between the mesocarp and endocarp *b* tissues. The cells of this tissue are more irregularly shaped than those of the mesocarp, and this layer contains vascular bundles but lacks chloroplasts.

Both species possess endocarp *a* and *b* layers, however these two cell layers do differ between them. Cells in the endocarp *b* layer are much larger in *C. hirsuta* than in *A. thaliana*. In *A. thaliana*, the endocarp *a* layer disintegrates during stage 17, however the endocarp *a* is maintained through to fruit maturity in *C. hirsuta*. TBO stains lignin light blue, and this staining of lignin in *C. hirsuta* is localised to the innermost edge of the endocarp *b* cells, and is deposited in a U-shape. This differs from *A. thaliana*, where lignin is present in all endocarp *b* cell walls. The valve margin regions of the two species, however, share a close resemblance (Figure 3.3 G and H).

In models of *A. thaliana* silique dehiscence, lignin deposition is invoked as crucial for building the tensions required for pulling apart the valve from the

replum. Because dehiscence in *C. hirsuta* is explosive, it was hypothesised that this more forceful process might involve a greater deposition of lignin in the valve.

Phloroglucinol can be used to stain lignin pink in whole-mount preparations (Figure 3.3 I and J). Whole-mount staining of fresh *A. thaliana* and *C. hirsuta* stage 17b siliques revealed a stark difference in phloroglucinol staining intensity. Whilst pink stripes along the valve margins and repla of the *A. thaliana* fruit reflect lignification of the dehiscence zone, the entire *C. hirsuta* silique stained strongly pink. This suggested an increased deposition of lignin in *C. hirsuta* siliques. Figure 3.3F suggests that this increased lignin deposition is entirely localised in the endocarp *b* layer of the *C. hirsuta* valve.

The mature, opened fruits of both species are shown in photographs in Figure 3.3 panels K and L. Whilst the *A. thaliana* silique splits along the valve margin, creating seams through which its seeds can fall and disperse, the entire *C. hirsuta* valve curls outwards and upwards, away from the fruit body, propelling the seeds from the fruit in the process.

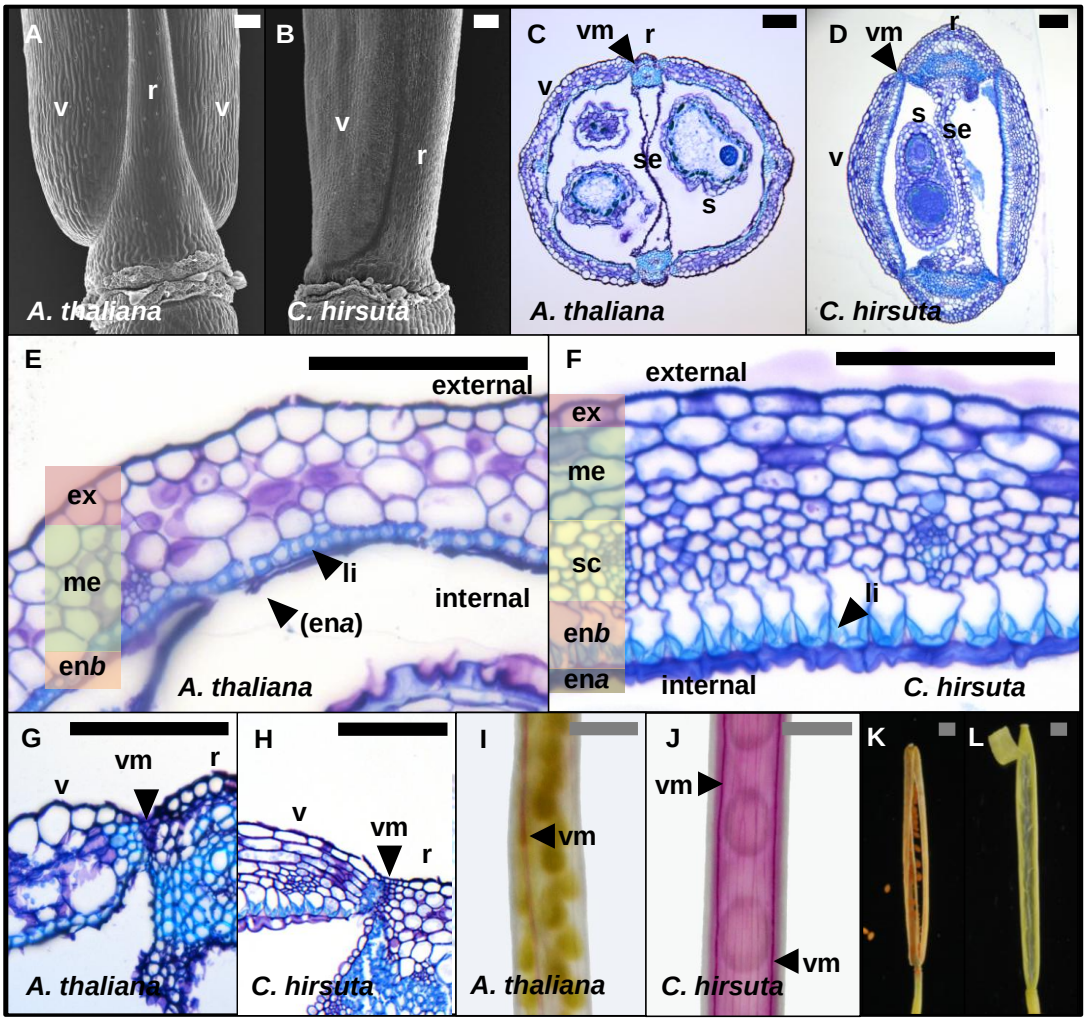

Figure 3.3 Similarities and differences in the silique morphology of *A. thaliana* and *C. hirsuta*. *A. thaliana* (A, C, E, G, I, K) and *C. hirsuta* (B, D, F, H, J, L), both at stage 17b. (A) and (B) SEM showing base of silique. v = valve, r = replum. (C) to (H) Toluidine Blue O stained transverse sections showing whole fruit (C and D), valve wall (E and F), and dehiscence zone (G and H). Cell walls and cytoplasm stain purple or darker blue, lignified walls stain light blue. s = seed, se = septum, vm = valve margin, ex = exocarp, me = mesocarp, sc = sclerenchyma, en*b* = endocarp *b*, ena = endocarp *a*, li = lignin (I) and (J) Photographs of whole-mount phloroglucinol staining of stage 17b siliques. Lignin stains pink. Valve margins are indicated. (K) and (L) Photographs of mature, open siliques. Bars represent 100 µm except (G) and (H): 10 µm, and (I) to (L): 1 mm.

3.2.3. Silique structure across the Brassicaceae

Comparison of the *A. thaliana* and *C. hirsuta* siliques reveals a number of silique features that differ between the two species. These differences include the broader replum, flatter valve, and larger seeds seen in *C. hirsuta*.

To investigate how common these gross morphological features are, these were compared across a range of other Brassicaceae family members. Fruit structure within the Brassicacean family is notoriously homoplasious, so firm evolutionary inferences should not be drawn regarding the occurrence and pattern of these features within the family. However, a tentative correlation of specific morphological features with aspects of silique opening phenotypes can contribute additional contextual information that can be used to help refine hypotheses regarding the roles of these features in shaping explosive silique dehiscence in *C. hirsuta*.

In total, eight Brassicacean species were selected for comparison (Figure 3.4). To add context for the comparisons between *A. thaliana* and *C. hirsuta* silique morphologies, an additional species from each genus was selected (*Arabidopsis lyrata* and *Cardamine corymbosa*), plus an additional species of the same tribe for each of these species (*Olimarabidopsis pumila* from the Camelineae and *Rorippa islandica* from the Cardamineae). Two *Brassica* species (provided by R. Leimu Brown and N. Prill) were included as examples of species of equal distance from both *C. hirsuta* and *A. thaliana*.

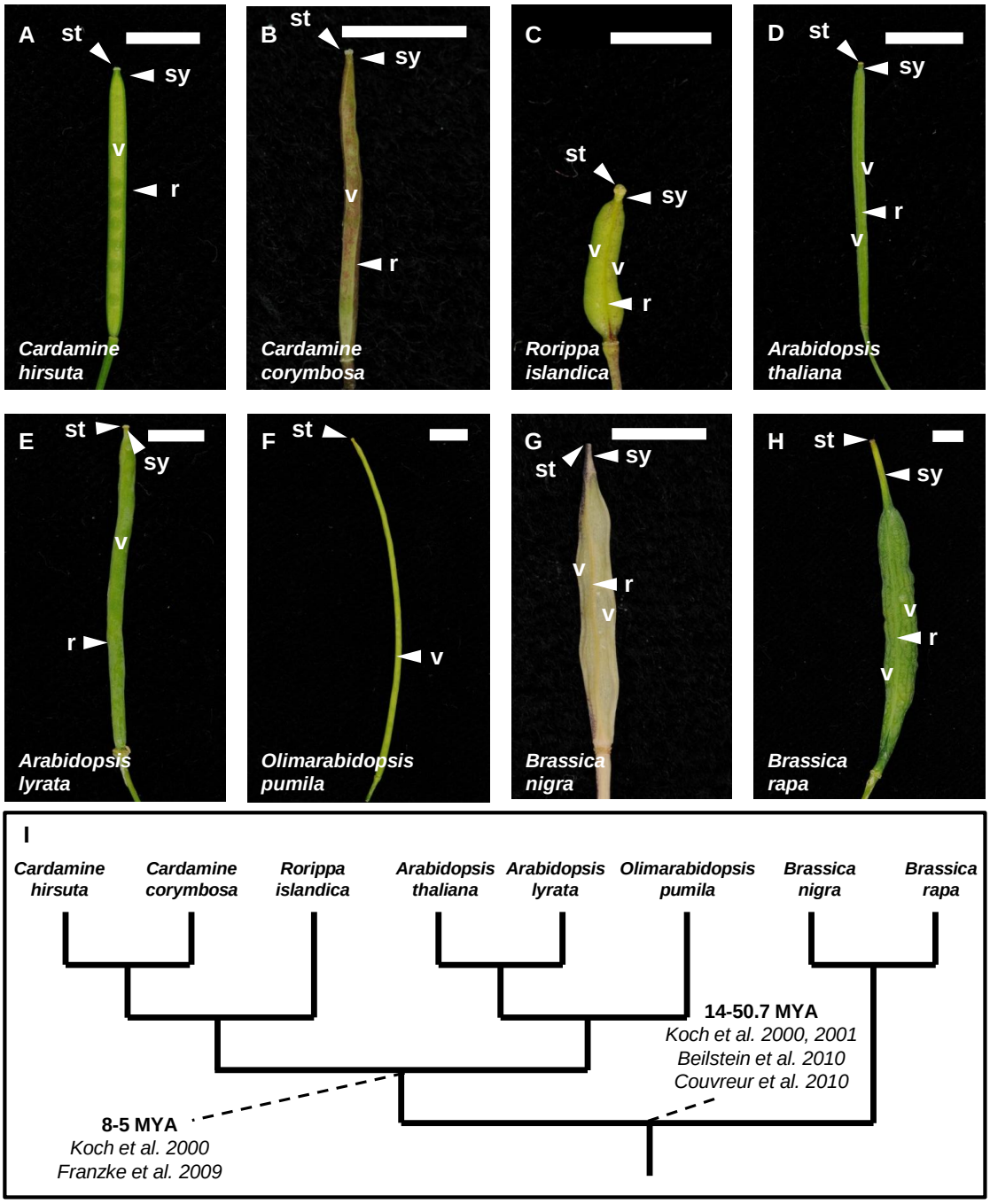

Figure 3.4 Siliques of sampled Brassicacean species. Bar represents 5 mm. 8 species of Brassicaceae were analysed (A-H), and their evolutionary relationships are indicated in (I). st = stigma, sy = style, v = valve, r = replum. Tree represents relationships only and not genetic or chronological distance. Date estimates are discussed in Chapter 1.

Across these selected species, a range of dehiscence phenotypes are visible following desiccation (Figure 3.5). Like *C. hirsuta*, *C. corymbosa* exhibits valve curling, although this was observed to be less forceful, less reliable, and less sensitive to triggering. *R. islandica* and *O. pumila* split along the dehiscence zone in a manner similar to *A. thaliana*, although the curved silique of *O. pumila* means that this results in a pulling away of the dried valves from the basal region of the silique, creating a wider region through which abscised seeds can fall downwards. In the greenhouse conditions in which all of these species were grown, none of the siliques of either *Brassica* species opened. Whilst dehiscence of *Brassica* siliques occurs frequently enough to be an agricultural problem, this is known to be influenced by environmental conditions such as heavy rain, so for the purposes of this work, both the *B. napus* and *B. rapa* siliques will be regarded as indehiscent when grown in these sheltered greenhouse conditions.

Figure 3.5 Dehiscence of sampled Brassicacean species. Dehiscence following desiccation in the sampled Brassicacean species. *A. lyrata* is not shown due to mould infection of siliques during this experiment. v = valve, r = replum, se = septum, s = seed. Bar represents 1 mm.

Transverse plastic sections of the eight species allowed comparison of silique morphological features (Figure 3.6). Like *C. hirsuta*, *C. corymbosa* and *A. lyrata* posses flattened valves, whilst all other species show more curved, *A. thaliana*-like valves. This appears to correlate with larger, flattened, disc-shaped seeds in these three species. However, only the two *Cardamine* species exhibit a broad replum, with all other species possessing round, narrow repla similar to those of *A. thaliana*. This perhaps represents a correlation between the broad repla of the *Cardamine* species and the curling of their valves that they exhibit during dehiscence.

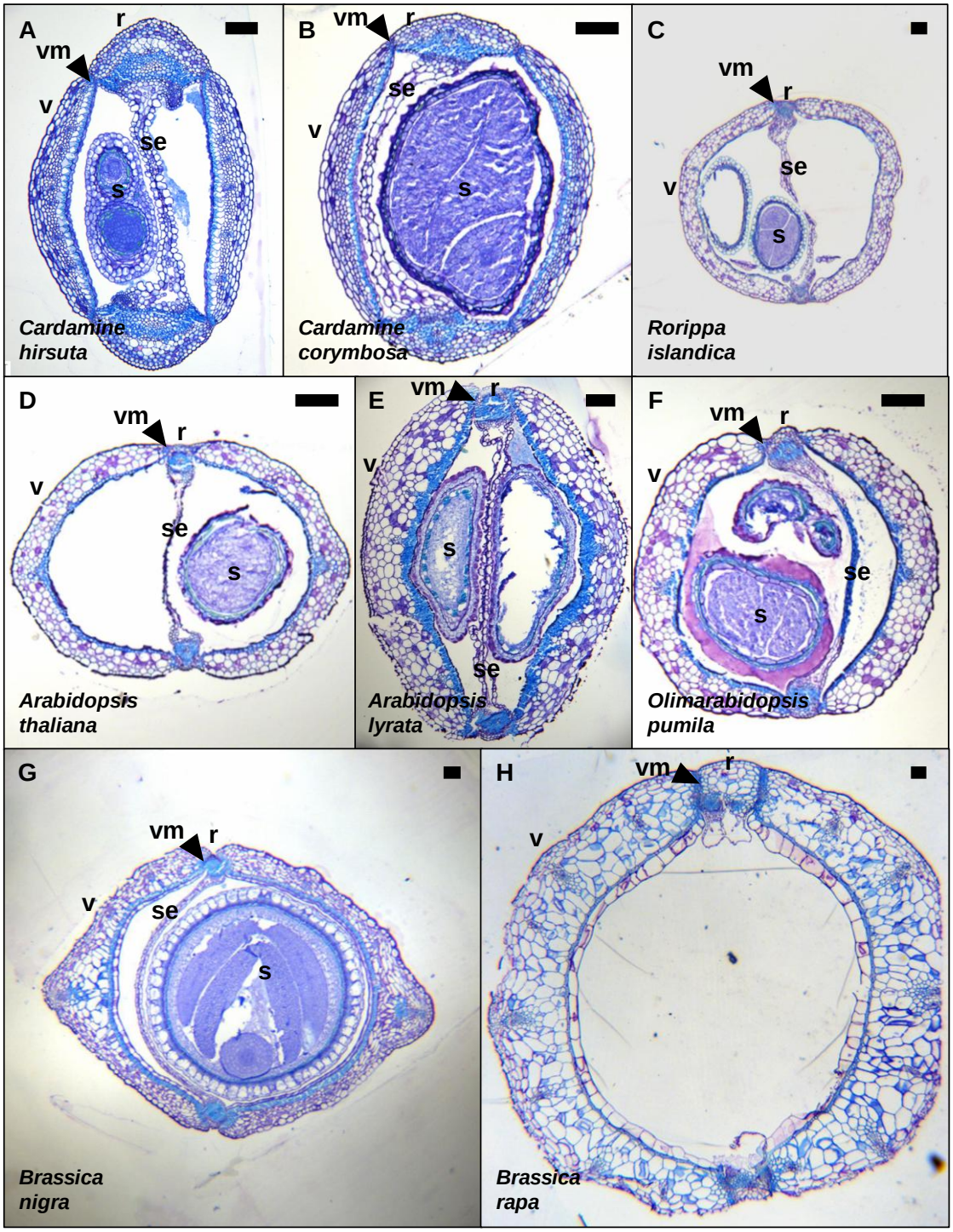

Figure 3.6 Transverse sections of Brassicacean fruits. Plastic sections of mature fruits, stained with TBO. r = replum, v = valve, vm = valve margin, s = seed, se = septum. Bar represents 100 µm.

3.2.4. Genetic screen for *C. hirsuta mutants*

Comparison of *C. hirsuta* siliques with other Brassicacean fruits reveals a number of morphological divergences, including a broad replum and flatter valves. However, the conclusions that can be drawn about such features from these observations are limited. To further investigate the role of *C. hirsuta* silique features in this species's explosive opening mechanism, these morphologies need to be experimentally perturbed.

To increase the morphological diversity available for studying explosive dehiscence in *C. hirsuta*, a genetic screen was conducted, using a population mutagenised with ethyl methane sulphonate. Because this mutagenesis was also used for a trial of TILLING (Targetting Induced Local Legions in Genomes) in *C. hirsuta* (data not shown), two different concentrations of EMS were trialled – a lower concentration of 15 mM (0.18% EMS, 'treatment A'), and a higher concentration of 30 mM (0.36% EMS, 'treatment B'). Seeds were incubated with EMS for 10 hours (see Chapter 2).

520 treatment A and 484 treatment B M_1s were grown to maturity, of which 5 treatment A M_1s and 104 treatment B M_1s were sterile. Seed was collected from all fertile M_1s, giving 895 M_2 seed families. 27 M_2 siblings were planted from each of the 515 treatment A families, and 48 M_2 siblings were planted from each of the 380 treatment B families to account for increased mortality as a consequence of their higher mutagenic load. A confounding factor in this experiment was the suboptimal greenhouse conditions that reduced fertility of even wild type plants.

A total of 32,145 seeds from 895 M_2 seed lines were planted and subsequently screened for phenotypes of interest. Three methods were used to screen these plants. Fruits were inspected visually for aberrant morphologies between stages 15 and 17. At stage 17b, whole siliques were treated with phloroglucinol to examine lignification in these plants. Finally, at full maturity, plants were screened for aberrant indehiscence.

Whilst screening methods were intentionally biased towards discovering fruit and lignification morphologies, other phenotypic abnormalities were recorded when recognised. A summary of the phenotypic categories observed is presented in Table 3.7.

As shown in Table 3.7, a broad range of phenotypic categories were observed. Seed was collected from every fertile mutant recorded as exhibiting a mutant phenotype, and a curated database of EMS lines and observed phenotypes was maintained so that this mutagenised population can be returned to in future studies.

Combined, 43 M_2 families were identified that contained mutants affecting inflorescence, floral, carpel or silique development. Out of these, a subset of informative mutants were chosen for study, highlighted in the last column of Table 3.7. Due to the high throughput procedure used to assay phloroglucinol staining, a high degree of variation in staining was seen in many M_2 lines. Each of these 39 lines was recorded, but it is likely that many of the observed abnormal staining patterns seen could be due to incomplete fixation or other variability within the bulk staining process. Rather than go back and re-screen these 39 lines, a single mutant with an *A. thaliana*-like pattern of lignin was selected for further study.

Mutant Category	Description	Number of M_2 plants	Example
Albino	Whole plants lacking pigmentation.	3	
Albino leaf sectors	Sectors of leaf tissue lacking pigmentation.	2	
Pale	Whole plants of a paler green	8	
Late-flowering	Typically shorter in stature, darker in pigmentation, and later to flower	21	
Long hypocotyls	Pale, elongated seedlings	1	
Semi and whole dwarfs	Plants showing medium to severe dwarfing in growth height	11	
Reduced apical dominance	Plants with increased branching and reduced dominance of central stem	5	
Vegetative meristem identity/determinacy	Plants showing defective meristems, indeterminacy or premature termination	5	
pin-like	Plants showing *pin*-like phenotypes (Barkoulas et al. 2008)	4	
Leaf phenotypes	Plants showing altered leaf shape or leaflet arrangement	31	
Inflorescence and floral phenotypes	Plants showing aberrations in inflorescence organisation or floral organs other than the carpel	10	*cbp*
....of which *leafy*-like	Mutants in the inflorescence/floral phenotype class closely resembled *C. hirsuta leafy* mutants	2	
Carpel	Altered carpel morphologies	18	*cetl*
Silique morphology	Altered silique opening at dehiscence	35	*val*
Silique opening	Perceived changes in openening of silique at dehiscence	10	*dfo*
Lignin deposition	Abnormal phloroglucinol staining	39 M_2 families	*lig1*

Table 3.7 Phenotypic mutant categories observed in forward genetic screen.

3.2.5.*C. hirsuta* mutant phenotypes

Out of the mutant categories described in Table 3.7, five mutants were selected as being of the most interest. To these, a mutant named *twisted* which was isolated in a previous EMS screen of *C. hirsuta* was added. This total of six mutants can be divided into three classes – *less lignin 1 (lig1)* and *delayed fruit opening (dfo)* affect mature fruit; *twisted (twi)* and *cardamine ettin-like (cetl)* affect fruit morphology throughout development; whilst *valveless (val)* is indehiscent (Figure 3.8). In addition, *cardamine brevipedicellus (cbp)* was selected for study because its gene product is known to interact with the fruit patterning protein RPL.

Compared to WT (Figure 3.8 A and B), both *lig1* (Figure 3.8 C and D) and *dfo* (Figure 3.8 E and F) show somewhat delayed dehiscence, remaining closed after yellowing at stage 18 (Figure 3.8 C and E). Phloroglucinol revealed a lack of lignin deposition in the valve of *lig1* (Figure 3.8D), implying a role for endocarp *b* lignin in normal dehiscence. However, *dfo* siliques showed normal lignin content (Figure 3.8F), suggesting an alternative cause of delayed dehiscence.

twi and *cetl* siliques show aberrant patterning of fruit tissues. In *twi*, a twisting of the replum and valve tissue around the apical-basal axis is visible (Figure 3.8 G and H). *cetl* siliques show varying degrees of severity. A milder silique is shown in Figure 3.8 I and J, with one side of the fruit appearing unaffected (Figure 3.8J), whilst the other side shows an apical shift of the valve towards the top of the silique and expansion of the stipe or gynophore (Figure 3.8I). In more severe *cetl* siliques (Figure 3.8K) the gynoecium splits open towards the apex. *cbp* was identified by its altered silique arrangement (Figure 3.8N). Whilst its siliques appear similar in morphology to wild type (Figure 3.8O), they are arranged around the stem differently, pointing further outwards from the plant.

The only indehiscent mutant identified in this screen was *valveless*, which appears to lack valve tissue (Figure 3.8 P and Q). Both repla are present, and between them spreads a thin, semi-transparent tissue resembling valve margin.

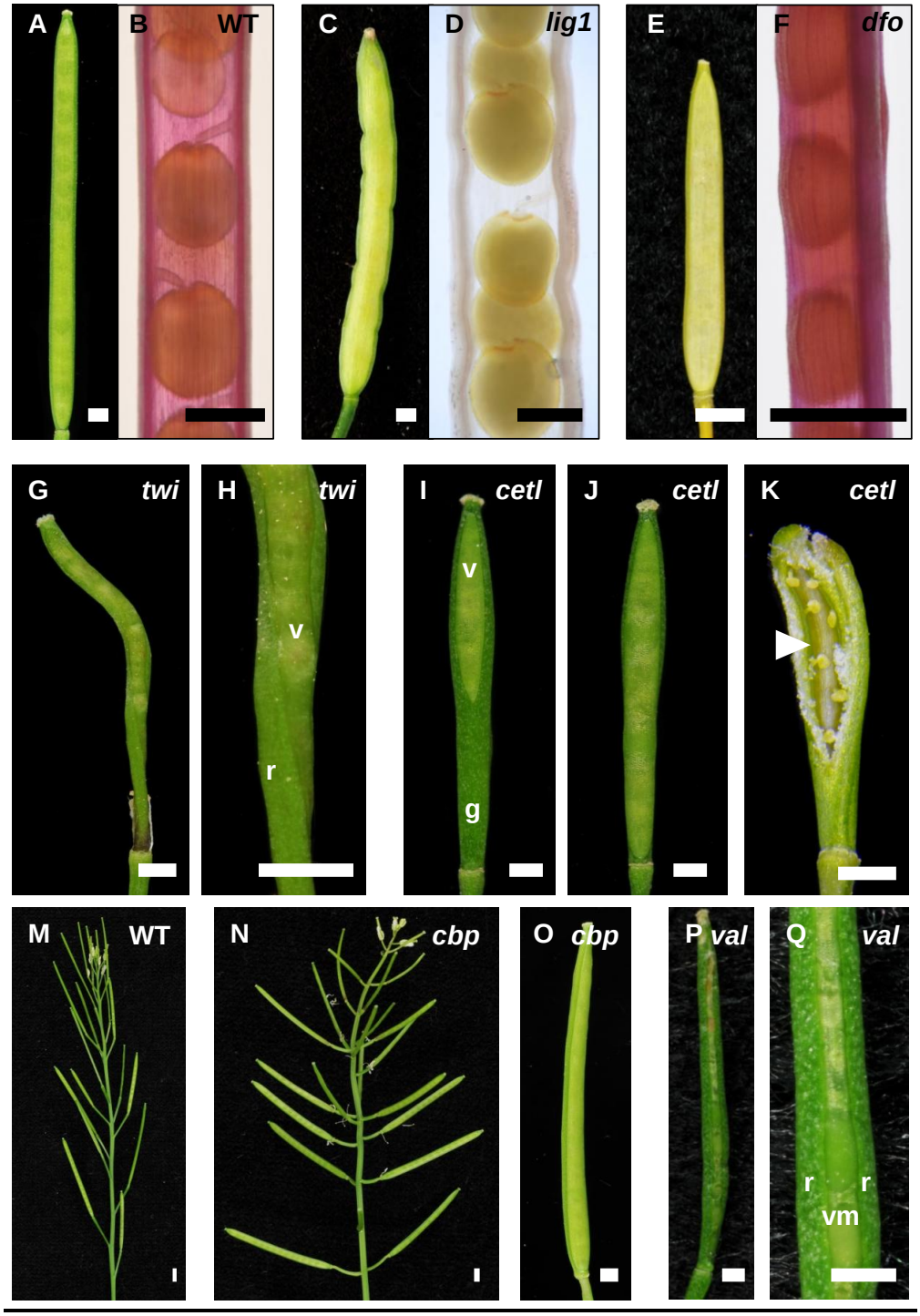

Figure 3.8 Mature mutant siliques. (A), (C) and (E) show wild type, *less lignin 1* and *delayed fruit opening* siliques, and (B), (D) and (F) show phloroglucinol treatment of these genotypes to reveal lignin content. (G) and (H) show the twisted siliques seen in *twisted* plants. (I) and (J) show opposite sides of the same *cetl* silique, with (I) showing apical-shifting of valve (v) position and expansion of the gynophore (g). (K) shows a more severe *cetl* silique, illustrating splitting of the gynoecium (arrow). Arrangement of siliques on stem is shown in WT (M) and *cbp* (N). (O) shows *cbp* silique. (P) and (Q) show a *valveless* silique, with replum (r) and valve margin (vm) indicated. Bar approximates 1 mm.

3.2.5.1. The valveless *mutant is indehiscent*

The only indehiscent mutant recovered in this genetic screen was *val*. The gross silique and seed morphologies of this mutant are compared with WT in Figure 3.9.

val siliques are thinner than WT at maturity (Figure 3.9 A and B). SEM (Figure 3.9 C and D) reveals an apparent absence of valve in *val* siliques, with valve tissue replaced by a depressed tissue similar to the depressed valve margin in wild type. Unlike wild-type valve tissue, this tissue is thin and semi-transparent, and seeds are clearly visible through it (Figure 3.9 E and F). In WT siliques, three cell types can be recognised in the dehiscence zone region – the replum, valve margin and valve cells (Figure 3.9G). However, in *val*, only replum and valve margin cells are visible (Figure 3.9H), indicating that valve tissue has been replaced by cells with valve margin identity. *val* seeds also differ from WT. Whilst WT seeds are a round, flattened disc-shape (Figure 3.9I), *val* seeds are narrow, cylindrical and slightly tapered at each end (Figure 3.9L).

Compared to WT (Figure 3.9J), replum size is increased in *val*, and the valve margin tissue is expanded (Figure 3.9K). Closer inspection of WT (Figure 3.9M) and *val* (Figure 3.9 N and O) “valve” regions show that, in place of valve tissue, *val* possesses layers of small, narrow, symmetrical cells reminiscent of the wild type valve margin. This region in both WT and *val* possesses the same number of cell layers (9). However, this tissue in *val* shows no differentiation into exocarp, mesocarp, sclerenchyma and endocarp, and instead exhibits 8 layers of non-lignified cells and an innermost, lignified layer (Figure 3.9 O). Unlike wild-type valve endocarp *b* tissue (Figure 3.9M), the cells in this lignified layer are small and

lignin is deposited in all walls. This innermost lignified layer in *val* is variable, with patches of non-lignified cells occurring throughout the silique.

The *val* mutant therefore appears to fail to correctly differentiate valve tissue. The fact that this mutant is indehiscent implies that this differentiated valve tissue is strictly necessary both for *C. hirsuta* dehiscence and its explosive opening. *valveless* was selected for further analysis to identify the gene responsible for the mutant phenotype and to understand the role of this gene in *C. hirsuta* fruit development. The data from these experiments are presented and discussed in Chapter 4.

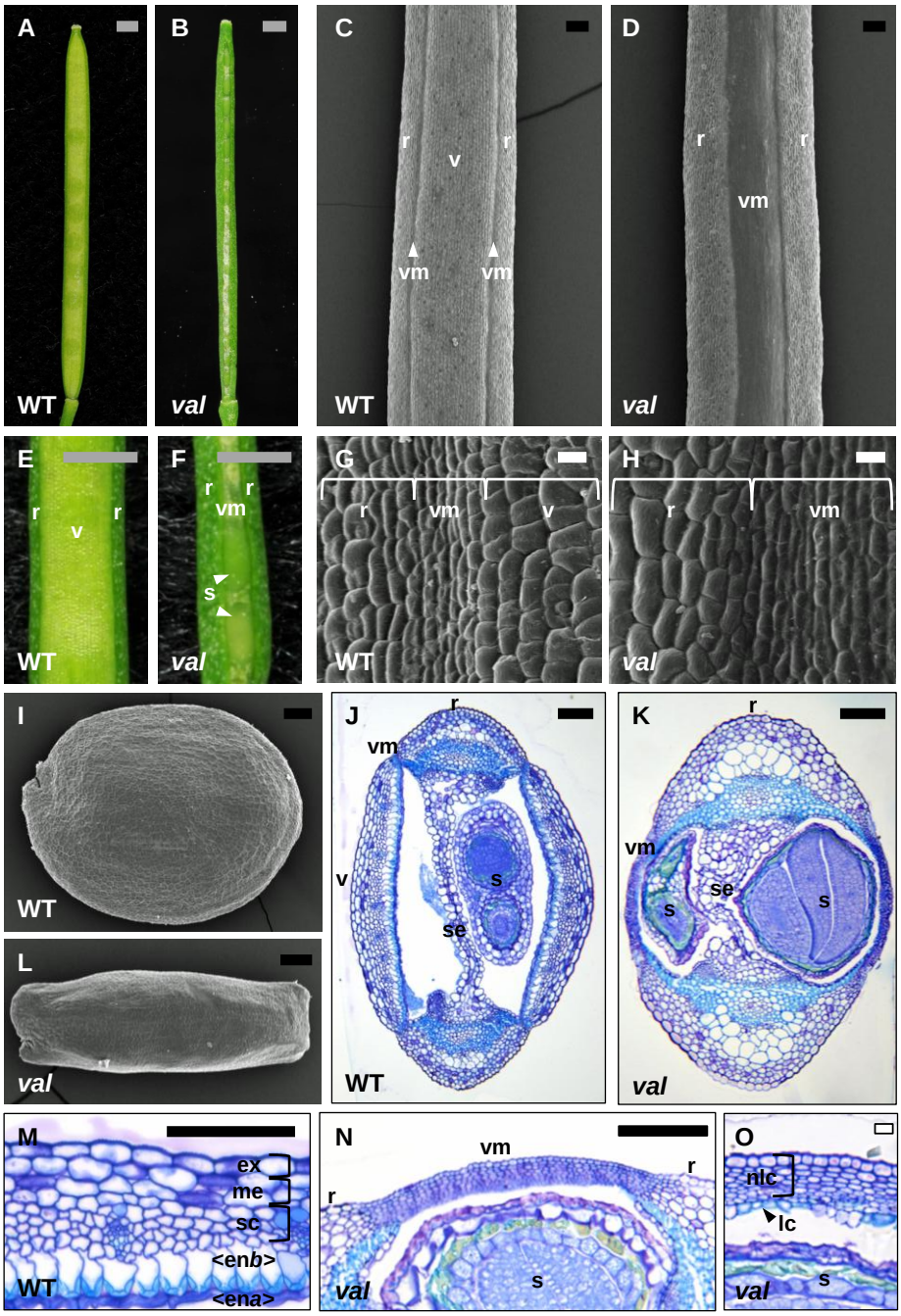

Figure 3.9 WT and *valveless* siliques and seeds. Photographs (A, B, E, F), SEM (C, D, G, H, I, L) and TBO-stained plastic sections (J, K, M, N, O) of WT and *val* seeds and siliques. All siliques shown at stage 17, except in (C), (D), (G) and (H), which show stage 15/16. Seeds shown in (I) and (L) were dissected from stage 17 siliques. (A) to (F) show external views of dehiscence zone tissues. Close-up of dehiscence zone tissue cells depicted in (G) and (H). WT and *val* seeds shown in (I) and (L). Internal tissue organisation shown in (J) and (K). (M) shows WT valve tissue, with (N) and (O) illustrating the equivalent region and constituent cells in *val*. Genotypes indicated on each panel. Tissues and cell types are labelled: replum (r), valve (v), valve margin (vm), seed (s), septum (se), excocarp (ex), mesocarp (me), sclerenchyma (sc), endocarp *b* (en*b*), endocarp *a* (en*a*), non-lignified cells (nlc) and lignified cells (lc). Grey bar indicates 1 mm, black bar 100 µm, white bar 10 µm.

3.2.5.2. Fruit morphology mutants

Two mutants showing alterations in fruit morphology were selected from the screen. The *cetl* mutant was isolated for its aberrant silique morphology and is a recessive mutant. *cetl* exhibits a number of characteristics reminiscent of *A. thaliana ettin* mutants, including apical shifts of the valve and the outward proliferation of medial tissues (Figure 3.8 I and K).

SEM of dissected inflorescences reveals a range of aberrant phenotypes in developing *cetl* gynoecia (Figure 3.10). Whilst WT gynoecia develop as a tube within the floral bud (Figure 3.10A), some *cetl* buds show severe aberrations, with one carpel showing a strong retardation in development (Figure 3.10B), leading to aberrant formation of the other, faster-growing, unfused carpel (Figure 3.10C).

In *cetl* gynoecia, the ovules are often exposed, due to the development of only one carpel (Figure 3.10 D to E). Whilst gynoecial tissues such as the stigmatic surfaces do differentiate, organ shape is frequently deformed (Figure 4.5E).

After anthesis and the onset of fruit development, developing *cetl* siliques show a spectrum of phenotypes of different severities. Fruits comprising only one carpel become curved (Figure 3.10G). Less severe fruits show differentiation of the valve and replum tissues (Figure 3.10H). However, compared with WT (Figure 3.10I), apical abnormalities in these fruits are visible, such as wider, misshapen stigmatic surfaces (Figure 3.10H), likely caused by the uneven growth of the two carpels.

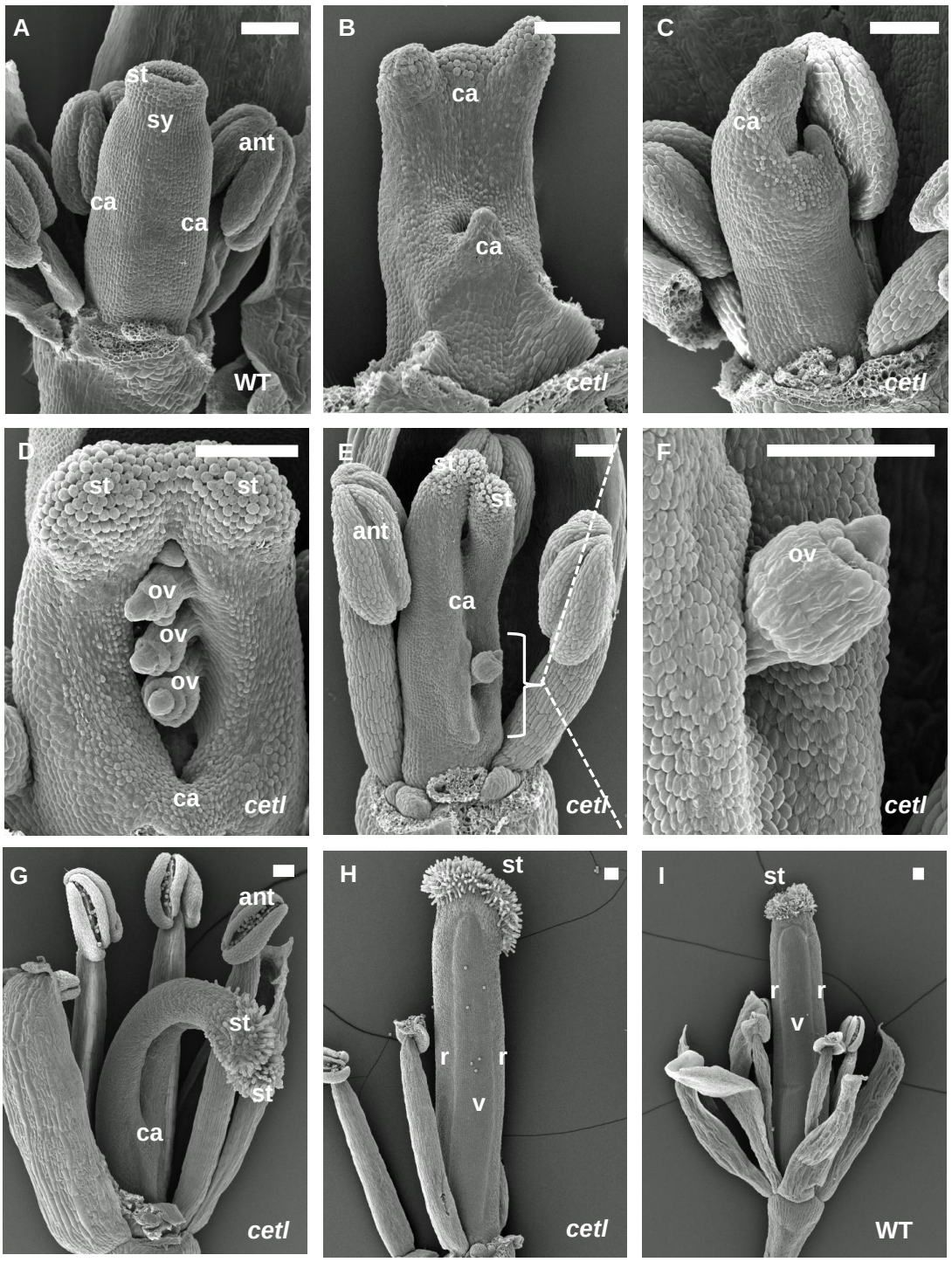

Figure 3.10 SEM of developing *cetl* gynoecia. SEM of dissected WT (A) and (I), and *cetl* (B) to (H) inflorescences, with annotation of style (sy), stigma (st), anther (ant), carpel (ca), ovule (ov), replum (r) and valve (v) positions. WT gynoecia shown at stage 10 (A) and stage 15 (I). Aberrant carpel development shown in (B) and (C). Exposure of ovules is seen in (D) and (F). Misshapen stigmatic surface shown in (E). After anthesis, severely affected gynocia show curving of a single carpel (G), whilst milder siliques are misshapen at the silique apex, possessing a wide and curved stigmatic surface (H). WT at stage 15 is shown in (I). Bar represents 100 µm.

The recessive *twi* mutant was previously isolated from another EMS screen of *C. hirsuta*. *twi* mutants possess twisted siliques of varying degrees of severity. Milder siliques are curved, with slightly bumpy valves which show less definition than wild type. Severe gynoecia show a complete twisting of replum and valve tissue. These siliques do not produce seed so may be infertile or represent carpels that happen not to have undergone pollination and subsequently miss out on a degree of rescue due to post-fertilisation carpel elongation.

Compared to WT (Figure 3.11A), *twi* siliques are curved or twisted (Figure 3.11B). Transverse sections of WT siliques show valve and replum morphology (Figure 3.11C), including a rounded replum (Figure 3.11D), and a highly organised valve, with abaxial lignification of the endocarp *b* layer (Figure 3.11E). In section, the arrangement of *twi* fruit tissues is largely similar (Figure 3.11F). However, replum morphology in these mutants is altered, showing indentations on the outer surface (‘a’, Figure 3.11G), and an internal, flattened expansion of the tissue (‘b’, Figure 3.11G). The *twi* valve mostly shows the same internal tissue organisation as WT (‘v’, Figure 3.11H), except in the regions which border the valve margin (‘abv’, Figure 3.11H). These abnormal valve regions show some disorganisation, with overexpansion of some exocarp and mesocarp cells, an absence of the sclerenchymal layer, and some adaxial lignification of endocarp *b* cells.

SEM of stage 12 (Figure 3.11 I and J), shows a ring of tissue at the apex of WT gynoecia, whilst the *twi* apex comprises several lobes (arrow, Figure 3.11J). Severe *twi* carpels fail to form a closed gynoecial tube, instead exposing the ovules (Figure 3.11K).

Severe gynoecia, which fail to produce seeds, show a twisting of valve and replum tissues around the apical-basal axis of the gynoecium (Figure 3.11L).

Milder mutants show reduced twisting, and mature siliques are frequently curved (Figure 3.11M).

At stage 15/16, the replum and valve tissues are clearly distinguishable at the silique apex in WT (Figure 3.11N), as the constricted valve margin forms a darkened boundary between them. This boundary is not visible in mild *twi* siliques at this stage (Figure 3.11O), and the valve tissue lacks clear definition and demarcation.

In WT, the valve margin is visible as a narrow constriction in the dehiscence zone, positioned between the replum and valve (Figure 3.11P). In *twi* siliques the valve margin is present but cells are larger and not all of valve margin identity, thereby forming a broader, flatter bridge between the replum and valve tissues (Figure 3.11Q). Additionally, presence of stomata within this valve margin suggests that this tissue is less clearly defined in these mutants.

In summary, the primary defect in *twi* mutants appears to cause twisting of the gynoecium. This twisting probably has its largest effect at cell boundaries that usually fuse post-genitally, such as the carpel margins, because the cell layers twist out of alignment. A failure to fuse after twisting would explain the unfused carpel phenotype seen in Figure 3.11K. In milder gynoecia, in which the carpels manage a degree of fusion, the subsequent differentiation of fruit tissues within a twisted context could be the cause of the observed disorganisation of cell types. This includes the absence of a broad, lignified band of cells across the replum, an aberrant mesocarp layer and an absent sclerenchymal layer at the periphery of the valves, and a broader valve margin that possesses stomatal pores (Figure 3.11G and H).

Figure 3.11 *twisted* mutants show aberrant patterning of the valve and dehiscence zones. Photographs of WT (A) and *twi* (B) siliques. (C) to (F) TBO staining of transverse sections. Transverse sections of WT whole silique (C), replum (D) and valve (E), compared with *twi* silique (F), replum (G) and valve (H). 'vm' in (E) and (H) indicates valve margin position. G) 'a' bracket marks indented outer shape of *twi* replum, 'b' bracket indicates internal expansion of replum in *twi*. (H) Arrows indicate aberrant, adaxial lignin deposition in endocarp *b*-like cells. *twi* valve comprises a normal region ('v'), and an aberrant region ('abv'). (I) to (Q) SEM of WT and *twi* gynoecia and siliques. At stage 12 (I and J), *twi* shows aberrant apical fusion of the gynoecial tube (arrow, J). Severe mutants (K) show a complete lack of apical gynoecial fusion, exposing the ovules ('ov'). Severe *twi* siliques (L) show a twisting of replum ('r') and valve ('v') tissues. Milder *twi* siliques are curved (M). At stage 15/16, valve and replum tissues are clearly discernible at the WT silique apex (N), whilst *twi* valve is less clearly demarcated (O). Mature WT dehiscence zones (P) show a contracted, indented valve margin ('vm') region between the replum ('r') and valve ('v') tissues. The *twi* dehiscence zone (Q) has a broader, flatter valve margin, which shows no indentation between the replum and valve tissues. Arrow indicates stomatal pore in valve margin. All bars represent 100 μm, except in (A) and (B), 1 mm.

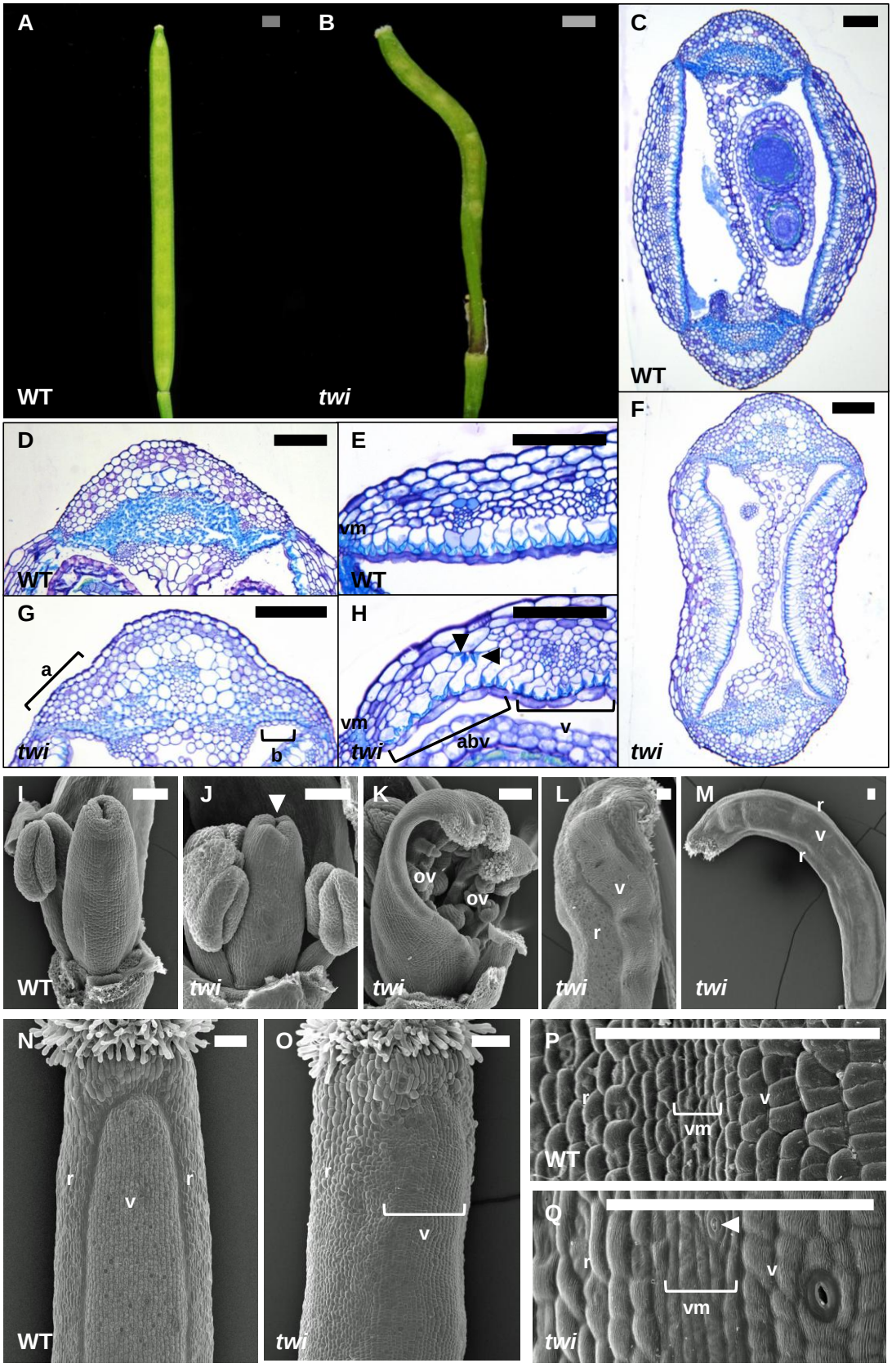
A
B
C
WT
twi
WT
D
E
F
WT
vm
WT
twi
G
H
a
b
vm
v
twi
abv
twi
I
J
K
L
M
WT
twi
ov
ov
v
r
r
v
r
twi
twi
twi
N
O
P
Q
r
v
r
r
v
r
v
vm
WT
r
v
vm
WT
r
v
vm
twi
twi

This *twi* mutant was crossed to the indehiscent *val* mutant. *twi val* double mutants (Figure 3.12) show a range of additive carpel phenotypes. Severely-affected carpels are similar to strong *twi* single mutant morphologies, showing aberrant fusion (Figure 3.12A). More weakly-affected carpels, however, appear normal at stage 10 (Figure 3.12B). After stage 13, the dehiscence zone tissues become visible, and a tissue comprising small epidermal cells are observed in the region that would be valve in wild type (Figure 3.12 C and D). Like the valve in *twi* mutants, this tissue lacks a clearly defined boundary (Figure 3.12E). At stage 15, the silique is curved and twisted, like those of *twi* single mutants (Figure 3.12F). Compared to WT, and *val* and *twi* single mutants, mature *val twi* siliques are shorter in length (Figure 3.12 G to J). A tissue resembling the expanded valve margin-like tissue of *val* single mutants is visible in these siliques, which are also twisted like *twi* mutants (Figure 3.12J).

Transverse sections of WT valve and the aberrant valve regions of *val* and *twi val* siliques are shown in Figure 3.12 K to M. These sections reveal that, like *val*, the *twi val* double mutants possess a thin tissue in the valve region which lacks the organisation of cell layers that is seen in the WT valve. However, the cells of this aberrant tissue are larger in *twi val* than in *val* single mutants. This cell layer in *val* will be discussed in further detail in Chapter 4.

The *twi val* double mutant siliques appear largely to show an additive combination of *twi* and *val* phenotypes, including *twi*-like silique twisting and aberrant valve development. Severe *twi* effects are visible during earlier stages of carpel development, whilst *val*-like abnormalities are not visible until after stage 13, suggesting that *TWI* functions earlier than *VAL* in fruit patterning. Sections reveal that *twi val* possesses an aberrant tissue in the valve region, which is

similar to *val* in its absence of organisation into WT-like cell layers. However, the aberrant cells in *twi val* expand more than in *val*, indicating that *TWI* loss of function can partially rescue the small size of these cells in *val* mutants.

Figure 3.12 Phenotypes of *twi val* double mutants. SEM of *twi val* (A) to (F). Ovules labelled ‘ov’, stigmatic surface ‘st’, gynophore ‘gy’. (A) An aberrant carpel showing unfused carpels and exposure of ovules. (B) A less severely affected carpel at Stage 10. (C, D, F) Bracket denotes small, valve margin-like cells. (E) Arrows indicate irregular shape of valve margin-like region. Mature siliques shown in (G) WT, (H) *val*, (I) *twi*, and (J) *twi val*. Arrow in (J) indicates aberrant valve margin-like tissue. TBO-stained sections of valve region in WT (K), *val* (L), and *twi val* (M). Bracket indicates the thickness of the tissue in the valve region. White and black bars represent 100 µm, grey bar represents 1 mm.


A
st
st
ov
twi val
B
C
D
E
st
st
F
G
WT
H
val
I
twi
J
twi val
K
WT
L
val
M
twi val

3.2.5.3. Mature fruit mutants

The *lig1* mutant shows delayed dehiscence, and decreased lignin deposition. However, a penetrant phenotype could not be recovered in successive generations of this mutant, so *lig1* was not pursued further.

The fruit morphology of *dfo* was characterised further and a mapping population was generated with the Oligosperma accession. However, plastic sections revealed no discernible polymorphic differences in mature fruit morphology from wild type. Furthermore, it was difficult to discern mutants in the F_2 mapping populations from environmentally or developmentally delayed dehiscence. However, leaf tissue was collected from 34 F_2 plants exhibiting severe delays and in future this tissue could be used for genetic mapping. Because *dfo* showed no obvious alterations in silique morphology and its inheritance was difficult to track by phenotype, this mutant was not pursued futher.

3.2.5.4. cBREVIPEDICELLUS

cbp was identified based on its dwarfed stature and altered arrangement of siliques (Figure 3.8N). Mutations in *REPLUMLESS* are also known to alter silique arrangement (Byrne et al. 2003). However, this mutant was found to contain a mutation in *BP*, not *RPL*.

Similarities were observed between this mutant and a *bp* allele identified by my colleague H. Jenkins in a different genetic screen. Dr. Jenkins genotyped this new mutant and found that it contained the same lesion as his original *bp* allele – a G to A mutation at the splice site at the start of the second intron of *cBP*. Curiously, the times at which the two different M_1 populations were at reproductive age did not coincide, making cross-pollination unlikely. Additionally, the two *cbp* alleles were isolated some months apart and furthermore , Dr Jenkins's screen was conducted as a suppressor screen in the *cardamine asymmetric leaves 1*

(cas1) mutant background. The fact that his *cbp* mutant showed segregation of the *cas1* allele in subsequent generations whilst mine did not rules out the possibility of seed contamination.

This raises the possibility that the same *cbp* mutation may have occurred twice. It is possible that the splice site between the second exon and intron of *cBP* is a mutational hotspot, particularly sensitive to EMS-induced mutations. Alternatively, mutations at this site may produce a more noticeable phenotype than mutations at other sites within the *cBP* gene, increasing the likelihood of independently isolating *cbp* mutants that share the same mutation.

The *cbp* silique exhibits no discernible differences in silique opening. However, because *BP* is known to function in the replum of *A. thaliana*, its role in patterning the replum of *C. hirsuta* is further examined in Chapter 4.

3.3. Discussion

Morphological characterisation of the siliques of WT *C. hirsuta*, mutant *C. hirsuta*, and *C. hirsuta* relatives allows the identification of structural features that may be of importance to the explosive dehiscence mechanism of this species. Whilst these comparisons implicate several *C. hirsuta* silique morphologies as being important for this process, they also reveal that *C. hirsuta* possesses the same organisation of fruit tissues that it shared across species of the Brassicaceae.

3.3.1. Explosive dehiscence does not arise from major alterations in silique structure

Comparison of seed weight, number, and dispersal difference between *A. thaliana* and *C. hirsuta* reveals significant differences between the two species (Figure 3.1). Whilst over 99% of *A. thaliana* seeds remain in the dehisced silique, this proportion is less than 21% in *C. hirsuta*. Of the 79.2% of *C. hirsuta*'s seeds that are succesfully expelled from the silique by its explosive mechanism, the majority (68.2%) were dispersed relatively evenly across the distance of 25 to 100 cm from their parent. By dispersing its offspring over a range of distances, the *C. hirsuta* explosive pod shatter mechanism reduces competition amongst its offspring. This range of dispersal distances would also maximise the chances of germination in a heterogeneous environment.

In plants, explosive dispersal mechanisms are typically correlated with larger seed sizes (Swaine & Beer 1977), and have been described in a number of highly invasive weed species, including *Impatiens glandulifera* and *Erodium circutarium* (Perrins et al. 1993; Clements et al. 2008; Jacobs & Lesmeister 2012). This correlation between larger seed size and an explosive dispersal mechanism

is seen too in *C. hirsuta*. Its larger, heavier seed likely fosters a large seedling which establishes quickly – a trait that would be valuable for an invasive weed species like *C. hirsuta*.

However, despite the starkly different seed dispersal modes observed between *C. hirsuta* and *A. thaliana*, comparison of their siliques reveals that the fruits of the two species share a common morphological plan. Their fruits comprise all the same tissues – two valves, two repla, a septum separating two locules, style, and stigma (Figure 3.3).

In both species, a valve margin region is distinguishable in the four regions of each silique where the valves and repla meet. As published work in *A. thaliana* has shown, the morphology of its valve margin is of crucial importance to correct dehiscence of the plant's silique. The valve margin of *C. hirsuta* is strikingly similar to that of *A. thaliana* (Figure 3.3 G and H), showing the same arrangement of lignified and non-lignified cells. This close resemblance suggests that the dehiscence mechanism of *C. hirsuta* could involve the sequential stages of lignin deposition, silique desiccation, and autolysis of the valve margin's non-lignified cells that are known to function in the dehiscence of *A. thaliana*.

It is surprising that the fruits of two species that exhibit such different seed dispersal mechanisms should be so similar. Comparison of fruit structure across eight Brassicacean species reveals that the same basic plan – a septum running between two repla, with two flanking valves meeting each of these repla at distinctive valve margin regions – is shared across each of these species (Figure 3.6). The species examined show a range of dehiscence phenotypes – *C. hirsuta*-like explosive opening, *A. thaliana*-like splitting along the valve margins to form seams, and *Brassica nigra* and *rapa*-like indehiscence. Across these species, no

entirely novel fruit tissue is seen. In *C. hirsuta*, we can see that a dramatically different mode of seed dispersal has evolved without the acquisition of whole new morphological features.

However, comparison of *C. hirsuta* silique morphology with *A. thaliana* and other Brassicacean species does reveal a number of alterations in phenotype within this shared fruit structure. Consideration of these features in other species and in *C. hirsuta* mutants allows the formation of hypotheses for the possible function of these differences in the explosive mechanism of *C. hirsuta.*

3.3.2. Altered morphologies of existing fruit tissues may contribute to explosive dehiscence

The replum of *C. hirsuta* is broader than is seen in *A. thaliana*. Of the other Brassicaceae species examined, all share the same thin, *A. thaliana*-like replum, except for the other *Cardamine* species, *C. corymbosa*. These are the only two species in which the fruits show outward curling of the valve tissue during dehiscence. In the other 6 species characterised, the valves either simply split apart from the replum at the valve margins, or do not come apart from the fruit at all. In these two *Cardamine* species, however, the valve springs away from the base of the silique, curling outwards and upwards towards the silique apex. It is possible therefore that the broad repla seen in both these species are related to this process.

Of the mutants selected from the genetic screen, *val* has a replum which appears to be wider still than that of WT *C. hirsuta* plants. However, the effect of this expanded replum on curling of the valve cannot be studied in this mutant, due to its aberrant valve development. All other mutants show repla that appear to be

of WT width, and each of these mutants continues to show outward curling of the valve.

Compared with *A. thaliana*, the valve of *C. hirsuta* is much flatter. Like *C. hirsuta*, *C. corymbosa* also possesses flattened valves, and a plausible hypothesis might be that this tissue needs to be flat in order to be able to curl outwards, the way that is seen in these *Cardamine* species. Comparison of valve morphology across the other 6 Brassicaceae species reveals that all species possess curved valves like *A. thaliana*, with the exception of *A. lyrata*. Like *C. hirsuta* and *C. corymbosa*, this species also has flatter, more disc-shaped seeds than the other species. This may therefore indicate a correlation between the flatter valves and disc-shaped seeds seen in *C. hirsuta*.

A correlation between valve and seed morphology is also seen in the *val* mutant. This mutant fails to correctly specify valve, possessing what appears to be expanded valve margin tissue in its place. This mutant also produces narrower, more cylindrical seeds. This could be the result of embryonic defects, or instead a consequence of the reduced locule size that arises from the wider replum and curved, aberrant flanking tissue of the *val* mutant. This will be investigated further in Chapter 4.

The *twi* and *cetl* mutants show that distortion of the *C. hirsuta* silique can perturb valve opening, but is not sufficient to prevent it. The valves of curved or twisted *twi* siliques are in some cases impeded from curling up the entire length of the fruit, but these valves still retain the ability to curl outwards, and to roll upwards when they are not obstructed by distortions further up the valve and replum tissue. *cetl* and *twi* siliques only show indehiscence in severely affected siliques, where valve has failed to develop or differentiate correctly.

A difference in lignin content is also seen between *A. thaliana* and *C. hirsuta* siliques (Figure 3.3 I and J). Because lignin is responsible for generating the tensions during silique desiccation that are then used to pull the valve away from the replum during dehiscence, increased lignin deposition could be responsible for generating the stronger forces required to power the explosive dehiscence mechanism of *C. hirsuta*.

The *lig1*mutant shows correct lignification of the dehiscence zone, but does not show the intense phloroglucinol staining of the valve that is seen in WT *C. hirsuta* but not in *A. thaliana*. However, this mutant does not show the drastically altered dehiscence phenotype that would be predicted by the hypothesis that increased lignification of the *C. hirsuta* valve provides the force for its explosive opening.

The siliiques of *lig1* still show explosive dehiscence, and its valves are still fully able to curl outwards and upwards from the fruit base. Alterations to dehiscence in this mutant are more subtle than predicted, and instead this mutant shows a delay in dehiscence, remaining unexploded into the yellowing of stage 18. The explosive opening of these siliques is also less sensitive to triggering by external stimuli. This suggests that the increased deposition of lignin in the valve of *C. hirsuta* is not necessary for the explosive opening of the fruit, but instead plays a role in the timing and sensitivity of the mechanism.

The *dfo* mutant, however, shows similarly delayed opening with reduced sensitivity, without any detectable alteration in valve morphology or lignin deposition. This suggests that factors other than valve lignification are also involved in fine-tuning the explosivity of the *C. hirsuta* dehiscence mechanism.

3.3.3. Conclusions

Through consideration of *C. hirsuta* silique morphology in comparison with other Brassicaceae species and with *C. hirsuta* mutants, features which may be of importance to explosive opening in *C. hirsuta* have been identified. This work suggests the broader replum, flatter valves, and increased lignification of *C. hirsuta* as candidates for features which help build its explosive phenotype, as labelled in Figure 3.13. Comparison of these features with other species and with mutants suggests that the broader replum may allow outward curling of the flatter valve, that the larger seeds of *C. hirsuta* may be correlated with this flatter valve, and that increased lignin deposition within the valve tissue may be important for fine-tuning the sensitivity of this mechanism. Throughout these hypotheses, the valve is of central importance, and the *val* mutant shows that without correct valve development, not only does the *C. hirsuta* silique fail to explode, it does not open at all.

The *val* mutant appears to completely lack valve tissue, instead showing an expansion of the valve margin. No mutant like this has been described in *A. thaliana*, as *fruitfull* mutants are thought to show a spreading of valve margin characteristics into the valve, rather than the entire loss of this tissue.

In the next chapter, the genetic locus of the *val* mutant is mapped, and the phenotypic consequences of mutation of this gene and other known fruit-patterning genes are characterised further.

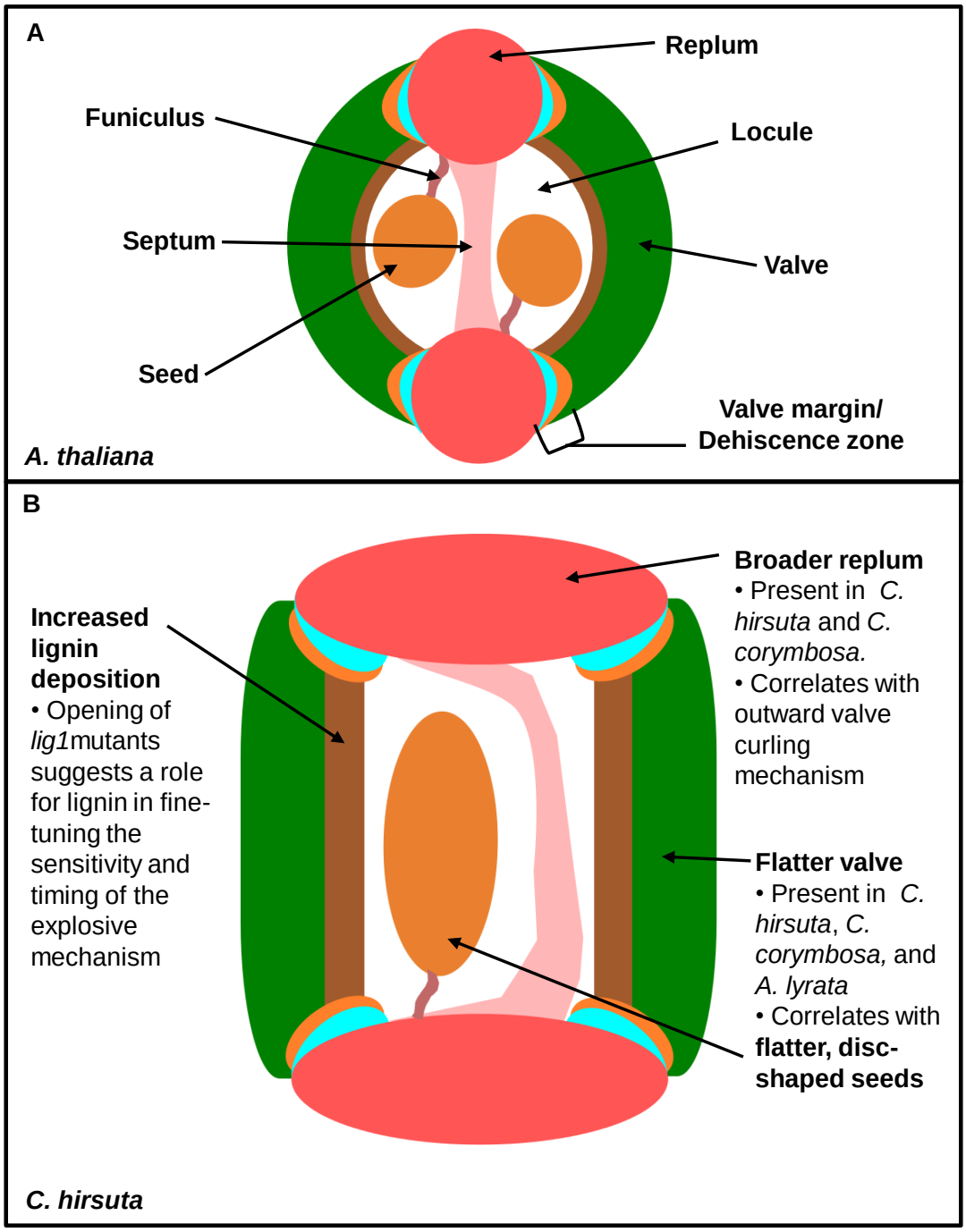

Figure 3.13 Diagram of *A. thaliana* and *C. hirsuta* siliques in transverse section. Diagrams showing the morphological organisation of *A. thaliana* (A) and *C. hirsuta* (B) siliques. Whilst the siliques share the same organisational plan and fruit tissues, there are some differences, labelled in (B). Comparison with other species and mutants identifies possible correlations with other traits.

4. Genetic effects on *C. hirsuta* silique morphology

4.1. Introduction

In this chapter, genetic mutants of known loci are used to begin investigating the underlying genetic networks that pattern the explosive fruit morphology of *C. hirsuta*. The locus of the *val* mutant is mapped, and its effect on silique development are examined further. In addition, the model of valve vs replum patterning by shoot genes in *A. thaliana* is tested in *C. hirsuta*.

4.1.1. Genetic mapping

To find the mutated locus underlying the *val* mutation, genetic mapping can be used to identify and narrow down the genomic region containing the mutation.

The method of mapping mutations of interest to a genetic map is a reliable procedure that uses recombination data to define a genetic interval, flanked by markers, which contains the mutated gene responsible for the phenotype of interest (Griffiths et al. 2012). The underlying principle of genetic mapping is that the number of recombination events that occur between non-sister homologous chromatids during meiosis increases with the distance between two loci (Peters et al. 2003; Bortiri et al. 2006; Griffiths et al. 2012). Recombination frequencies between two points can be expressed in centiMorgans (cM), and this measurement of genetic distance is related to the physical distance that separates these two loci on a chromosome (Peters et al. 2003; Bortiri et al. 2006; Griffiths et al. 2012). Whilst they are related, the genetic and physical distances between markers do not directly correspond to one another. This is because recombination frequencies vary depending on a number of factors, including species, gender, genetic similarity between parents, environment and chromosome region (Peters et al. 2003).

Prior to advances in DNA sequencing and genomic assembly, genetic mapping involved the laborious process of chromosome walking (Jander et al. 2002). Now, however, genetic mapping in species like *C. hirsuta*, which shares synteny with the fully sequenced genome of *A. thaliana*, and for which genome sequence and single nucleotide polymorphism (SNP) data is available, is a less time-consuming process.

4.1.1.1. Generation of mapping population

When a mutant phenotype of interest has been identified, the first step in mapping the mutated gene responsible is to construct a mapping population. The mutant is crossed to a different accession, which is polymorphic with the mutant's genetic background. This high degree of polymorphism is then used to track recombination events in the F_2 population, using markers designed to distinguish between the two parent accessions (Lukowitz et al. 2000; Jander et al. 2002; Page & Grossniklaus 2002; Peters et al. 2003; Bortiri et al. 2006). In *C. hirsuta*, the degree of polymorphism between 'Oxford' (the genetic background of the mutagenesis in this thesis) and 'Oligosperma' accessions has been used previously to successfully map mutations (Jenkins & Tsiantis 2010).

It is during gamete production in the F_1 generation that the recombination events between chromosomes of the two different accessions occur. This generation is allowed to self-fertilise to generate the F_2 mapping population. When the mutation is recessive and easily identified by phenotype, mapping utilises F_2 plants which show the homozygous mutant phenotype.

In order to map the *val* mutation, homozygous *val* mutants were crossed to the Oligosperma accession. F_1 plants were allowed to self, and their progeny formed an F_2 mapping population, segregating the *val* phenotype.

4.1.1.2. Marker design

The resolution and power of genetic mapping depends heavily on the density of markers available for mapping (Lukowitz et al. 2000), and since the development of high-throughput sequencing methods, a greater availability of sequence data from different accessions has boosted the strength of genetic mapping in species of interest (Peters et al. 2003), including in *C. hirsuta*.

PCR-based markers are frequently used because they are cheap and can utilise polymorphisms that occur more frequently between accessions, such as SNPs (Jander et al. 2002). PCR-detection of SNPs can be visualised using gel electrophoresis, and these markers are co-dominant, enabling both chromosomes of a plant to be genotyped for a given marker, thus providing the maximum amount of information (two data points) on recombination per locus (Lukowitz et al. 2000).

Two types of PCR-amplified DNA marker that make use of SNPs are cleaved amplified polymorphic sequence (CAPS) and derived cleaved amplified polymorphic sequence (dCAPS) markers. CAPS markers can be used when a polymorphism results in a restriction endonuclease site in one accession but not the other (Konieczny & Ausubel 1993). Primers are used to PCR-amplify the surrounding sequence and amplicons are then treated with the relevant restriction enzyme. Digestion products are visualised using gel electrophoresis. dCAPS markers are based on the same principle, and work by introducing a restriction endonuclease site into one but not the other of the accessions in a polymorphic region by using a mis-matched primer (Michaels & Amasino 1998; Neff et al. 1998).

CAPS and dCAPs are simple markers amenable to use in *C. hirsuta*, where a large amount of SNP data is available for the Oxford and Oligosperma accessions. These SNPs can be used to design CAPS and dCAPS markers, and comparison with the *A. thaliana* genome can be used as a guide for the genetic location of these markers. Marker location can then be confirmed by mapping to the *C. hirsuta* map.

4.1.1.3. Mapping procedure

A generalised procedure for mapping in *A. thaliana* is shown in Figure 4.1. First, linkage to a chromosome arm is established, followed by the definition and narrowing of a genetic interval through rough mapping, followed by further narrowing of the interval by fine mapping. Throughout these processes, a progressively larger number of mapping individuals are used to provide greater resolution.

Once the interval has been mapped to 40 kb it can be sequenced (Jander et al. 2002). Alternatively, gene annotations can be used to identify candidate genes within the region and these instead can be sequenced (Lukowitz et al. 2000). Jander *et al.* (2002) note that strong candidates often become clear before the interval has been narrowed to 40 kb and that it is common to finish mapping and move straight to sequencing of candidates at whichever point they become clear.

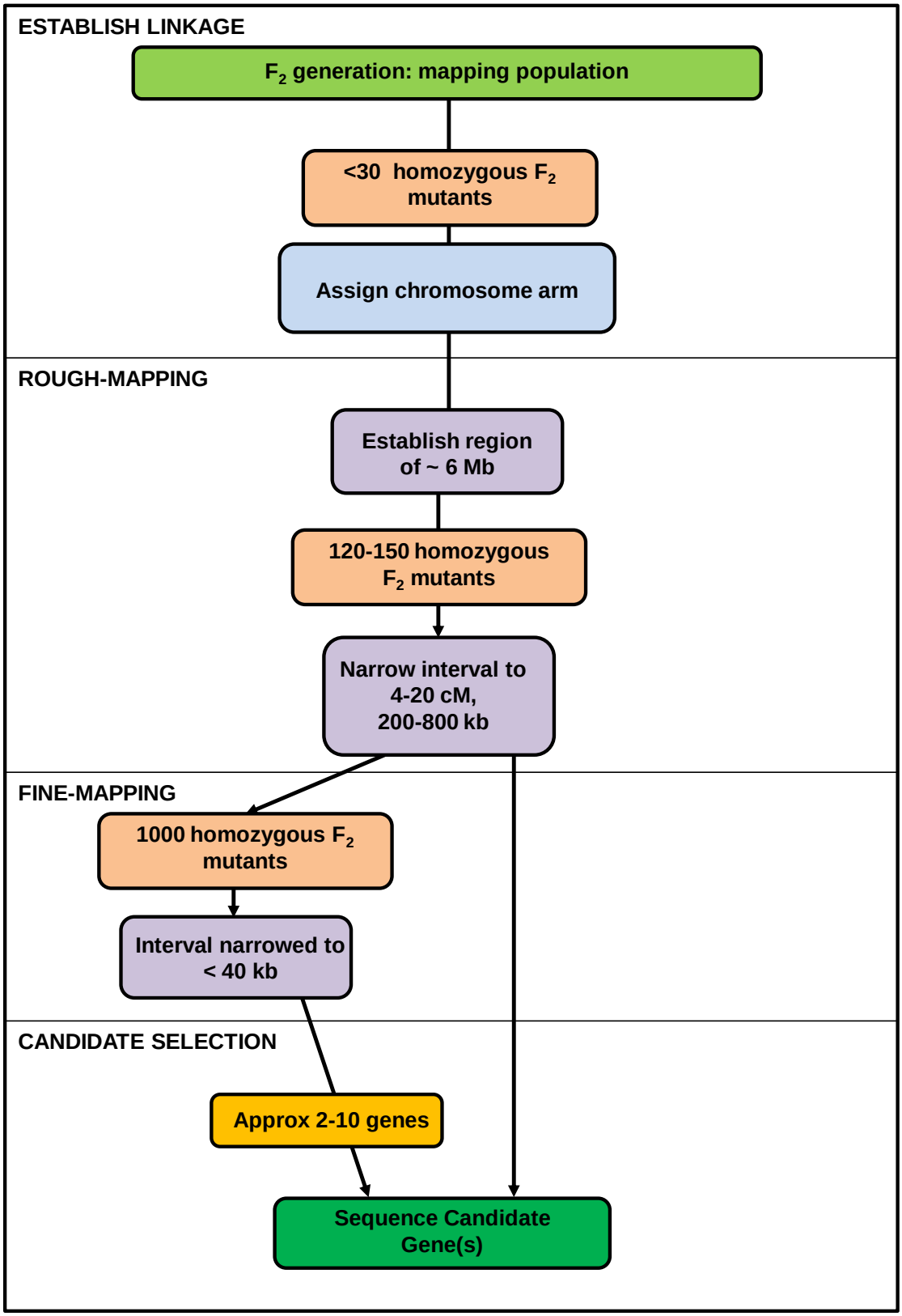

Figure 4.1 Generalised mapping procedure in *A. thaliana*. Summarised from *Lukowitz et al.* 2000; Jander *et al*. 2002; Peters *et al*. 2003; Bortiri *et al*. 2006.

When multiple mutant alleles exist, sequencing of a candidate gene in each strain will confirm whether it is responsible for the mutant phenotypes seen (Bortiri et al. 2006). In cases where there is only one mutant allele, confirmation of the identity of the mutant gene can be achieved through complementation of the mutant allele by transformation or by the generation of additional mutant alleles (Bortiri et al. 2006).

4.1.2. Shoot genes affect replum morphology

The fruits of the *valveless (val)* mutant possess wider repla than wild type. This phenotype is seen too in *ful* mutants in *A. thaliana* (Roeder et al. 2003; Alonso-Cantabrana et al. 2007). Manipulation of shoot-patterning genes also result in wider repla in *A. thaliana*, with loss of *AS1* expression or an overexpression of *BP* both causing broadened repla (Alonso-Cantabrana et al. 2007).

Because loss of *AS1* function rescues the replum of *rpl* mutants, it is thought that other factors, in addition to *RPL,* promote replum formation, including *BP* (Alonso-Cantabrana et al. 2007). Within the gynoecium, *AS1* and *JAG* repress *BP* expression in the valve, restricting *BP* to the wild type replum (Alonso-Cantabrana et al. 2007; Schiessl et al. 2012). In *as1* mutants and transgenic *BP* overexpression lines, *BP* expression spreads throughout the gynoecium (Alonso-Cantabrana et al. 2007). Whilst loss of *BP* partially rescues the broadened replum of *as1* mutants, and increases the severity of replum reduction seen in *rpl* mutants, *bp* null mutants show no alteration in replum width, suggesting that *BP* functions redundantly in the replum with other factors, possibly other class 1 *KNOX* genes (Alonso-Cantabrana et al. 2007).

AS1 is therefore thought to limit the expression of class 1 *KNOX* genes to the replum (*BP* and *STM*) and valve margins (*KNAT2* and *KNAT6*), and when this repression is compromised, it is hypothesised that the expression of the class 1 *KNOX* genes expands outwards, into the valve, where they promote expression of *RPL* (Alonso-Cantabrana et al. 2007). *FUL* functions to repress *RPL* expression in the valve, so loss of *FUL* expression enhances the *as1* fruit phenotype. *as1 ful* fruits show a more severe reduction of valve tissue and widening of the replum than is seen in either single mutant (Alonso-Cantabrana et al. 2007). These phenotypes are similarly seen when *ful* alleles are combined with transgenic lines overexpressing *BP*, and in both *as1 ful* and *ful 35S::BP* lines, loss of *RPL* expression reduces the severity of this phenotype (Alonso-Cantabrana et al. 2007).

In the previous chapter, the *val* and *cardamine brevipedicellus (cbp)* mutants were identified during an EMS screen for silique phenotypes. In this chapter *val* is mapped, and its affect on fruit development and morphology are characterised further. Then, in combination with a previously identified *cardamine asymmetric leaves (cas1)* mutant, the *val* and *cbp* mutants are used to investigate the influence on fruit morphology that the *A. thaliana* antagonistic model for valve versus replum patterning, proposed by Alonso-Cantabrana *et al*., has in *C. hirsuta*.

4.2. Results

4.2.1. Mapping *valveless*

A dense linkage map exists for *C. hirsuta* that was constructed using Oxford and Oligosperma recombinant inbred lines. To map *val*, the mutant (Oxford background) was crossed to the Oligosperma accession to generate an F_2

mapping population. 743 F_2 plants were grown to maturity, and tissue was collected from the 148 of these that showed the *valveless* phenotype. DNA was extracted from this tissue and used for mapping.

Linkage was identified between *val* and a pre-existing marker, m229, which is positioned on the bottom of chromosome 8 in *C. hirsuta* (Figure 4.2A). A range of novel CAPS and dCAPS markers were then designed using Oxford/Oligosperma SNP data (see Chapter 2). Using 39 homozygous *val* F_2 plants, the marker m306 was found, with m229, to flank the *val* locus, giving a genetic distance of 11.7 cM (Figure 4.2B). m229 flanks the *val* locus on the telomere side of the chromosome and is described as distal, whilst m306 flanks the locus on the side towards the centromere, and is described as proximal. Additional markers between m306 and m229 were designed and used to screen a total of 79 homozygous *val* F_2 plants, totalling 158 chromosomes. Out of these 79 plants, 10 showed recombination within the 11.7 cM interval (Figure 4.2C). Recombination break-points within these 10 plants indicated that the *val* locus lies between the distal marker fd04 and the proximal marker m690; a genetic interval of 2.7 cM.

The region homologous to the chromosome region lying between markers fd04 and m690 corresponds to a region of chromosome 5 in *A. thaliana* (Figure 4.2D). In *A. thaliana*, 33 genes are annotated in The Arabidopsis Information Resource (TAIR) Generic genome browser (version 1.70). These loci are listed in Table 4.3 and encode a range of different putative proteins, including nitrate transporters and several transcription factors, including REVOLUTA, a TCP protein and, most interestingly FRUITFULL, a strong candidate for the aberrant valve specification seen in *val* mutants.

Figure 4.2 Mapping *valveless*. (A) Genetic map showing the 8 chromosomes of *C. hirsuta* and rough mapping markers available. Marker m229 is circled. (B) Map of markers linked to *val* in *C. hirsuta*, numbers indicate centiMorgans from *val*. (A) and (B) constructed by Bjorn Pieper using JoinMap 4®. (C) Mapping population recombinants. 'ox' (green) indicates homozygous oxford genotype for a given marker, 'oli' and 'het' (red) indicate the recombined genotypes, homozygous oligosperma and heterozygous. Unlabelled green boxes indicate inferred homozygous oxford genotypes. (D) TAIR gbrowse view (The Arabidopsis Information Resource (TAIR), http://gbrowse.arabidopsis.org/cgi-bin/gbrowse/arabidopsis/, on www.arabidopsis.org). The *A. thaliana* region homologous to the interval between markers fd04 and m690 contains 33 gene-encoding loci, including *FRUITFULL*. AT numbers refer to loci in *A. thaliana*, equivalent markers in *C. hirsuta* annotated with linkage to *val* in centiMorgans.

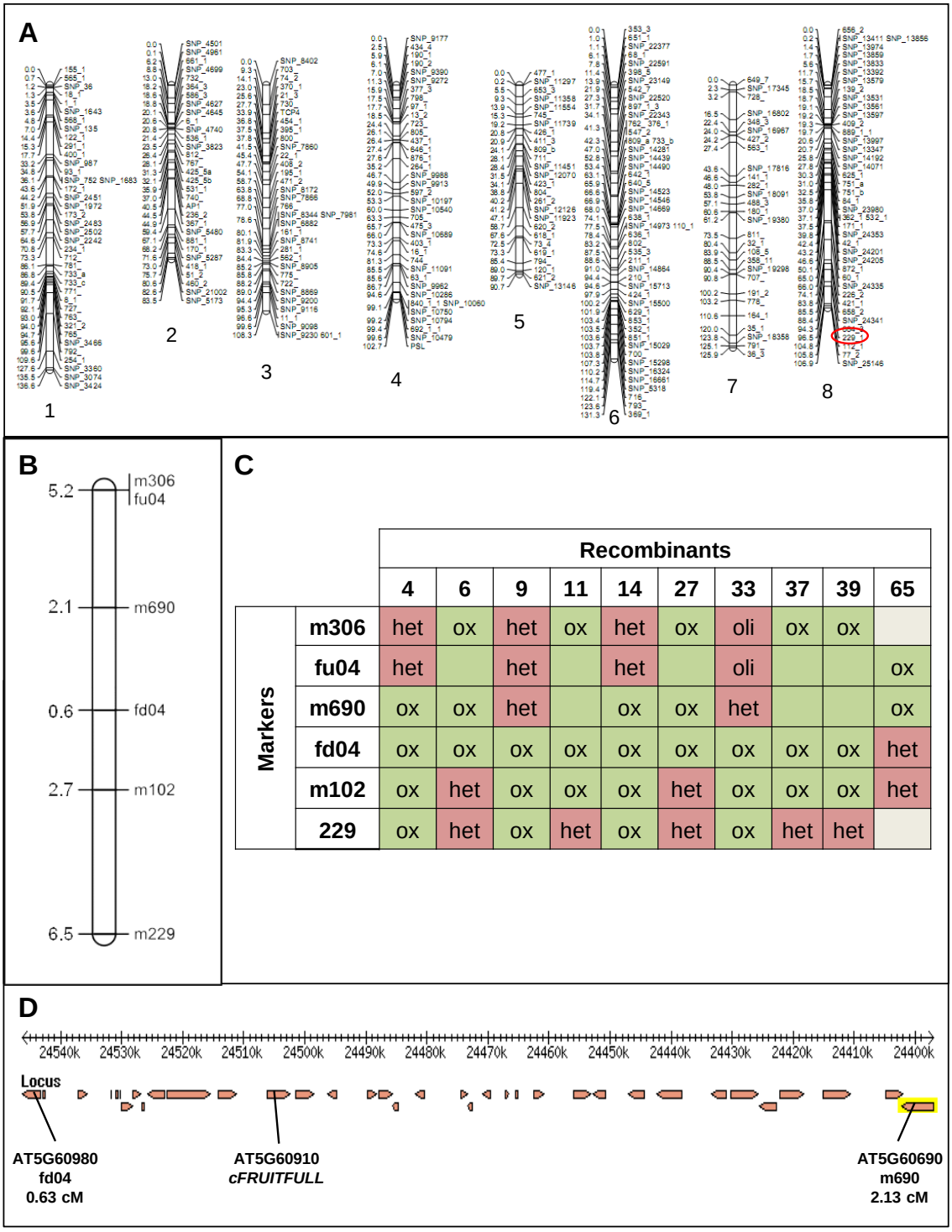
A
1
2
3
4
5
6
7
8
B
5.2
m306
fu04
2.1
m690
0.6
fd04
2.7
m102
6.5
m229
C
Recombinants
4 6 9 11 14 27 33 37 39 65
Markers
m306 het ox het ox het ox oli ox ox
fu04 het het het het oli ox
m690 ox ox het ox ox het ox
fd04 ox ox ox ox ox ox ox ox ox het
m102 ox het ox ox ox het ox ox ox het
229 ox het ox het ox het ox het het
D
24540k 24530k 24520k 24510k 24500k 24490k 24480k 24470k 24460k 24450k 24440k 24430k 24420k 24410k 24400k
Locus
AT5G60980
fd04
0.63 cM
AT5G60910
cFRUITFULL
AT5G60690
m690
2.13 cM

***A. thaliana* gene ID**	**Annotation**
AT5G60690.1	REVOLUTA
AT5G60700.1	glycosyltransferase family protein 2
AT5G60710.1	Zinc finger family protein
AT5G60720.1	Protein of unknown function, DUF547
AT5G60730.1	Anion-transporting ATPase
AT5G60740.1	ABC transporter family protein
AT5G60750.1	CAAX amino terminal protease family protein
AT5G60760.1	P-loop containing nucleoside triphosphate hydrolases superfamily protein
AT5G60770.1	member of High affinity nitrate transporter family
AT5G60780.1	member of High affinity nitrate transporter family
AT5G60790.1	member of GCN subfamily
AT5G60800	Heavy metal transport/detoxification superfamily protein
AT5G60805.1	Encodes a defensin-like (DEFL) family protein.
AT5G60810	Encodes a root meristem growth factor (RGF)
AT5G60820.1	RING/U-box superfamily protein
AT5G60830.1	basic leucine-zipper 70 (bZIP70)
AT5G60840.1	unknown protein
AT5G60850.1	Encodes a zinc finger protein.
AT5G60860.1	RAB GTPase homolog A1F (RABA1f)
AT5G60870	Regulator of chromosome condensation (RCC1) family protein
AT5G60880	Encodes BASL (BREAKING OF ASYMMETRY IN THE STOMATAL LINEAGE), a regulator of asymmetric divisions
AT5G60890.1	Myb-like transcription factor that modulates expression of ASA1, a key point of control in the tryptophan pathway
AT5G60900.1	Encodes a receptor-like protein kinase.
AT5G60910	**FRUITFULL**
AT5G60920.1	Encodes a glycosylphosphatidylinositol-anchored protein localized primarily in the plasma membrane of the longitudinal sides of root cells
AT5G60930.1	P-loop containing nucleoside triphosphate hydrolases superfamily protein
AT5G60940	Transducin/WD40 repeat-like superfamily protein
AT5G60945.1	Encodes a ECA1 gametogenesis related family protein
AT5G60950.1	COBRA-like protein 5 precursor (COBL5)
AT5G60960.1	Encodes PNM1 (for PPR protein localized to the nucleus and mitochondria 1)
AT5G60964.1	Encodes a ECA1 gametogenesis related family protein
AT5G60970.1	TCP gene involved in heterochronic control of leaf differentiation
AT5G60980	Nuclear transport factor 2 (NTF2) family protein with RNA binding (RRM-RBD-RNP motifs) domain

Table 4.3 Genes annotated within the *A. thaliana* genome region Chr5:24397023-24546062. Gene IDs and corresponding annotation descriptions from TAIR.

4.2.2. Sequencing *cFRUITFULL*

Out of the 33 genes annotated in the *A. thaliana* region that is syntenous with the *val* mapping interval, *FUL* is a strong candidate, due to its described role in *A. thaliana* valve patterning, and similarities between *ful-1* and *val* mutant phenotypes. *C. hirsuta* genomic sequence data for *cFUL* was retrieved from the current *C. hirsuta* genome assembly and used to design primers to amplify and sequence *cFUL* from both WT and *val* genomic DNA.

Sequencing of the *cFUL* ORF identified a cytosine to thymine mutation in the fourth base-pair of the fifth *cFUL* exon in *val* mutants (Figure 4.4 A to C). This mutation results in a premature stop codon giving a truncated protein of 143 amino acids. The protein sequences of the *A. thaliana* (aFUL) and *C. hirsuta* (cFUL) homologues are aligned in Figure 4.4D. The MADS-box and K-box domains are annotated using the AGL8 entry in the UniProt Protein Knowledgebase (http://www.uniprot.org/uniprot/Q38876) (The UniProt Consortium 2012). This alignment reveals that the premature stop codon in *val* does not affect the MADS-box but does disrupt the protein's K-box, resulting in a truncated K-box domain in the cFUL protein in *val* mutants.

Figure 4.4 Sequencing of *cFRUITFULL* in WT and *val*. Sequencing chromatograms from ContigExpress (Invitrogen) for WT (A) and *val* (B) show mutation of the 4th base-pair of exon 5 in *val*. (C) Visualisation of *cFUL* exons and introns, with C to T mutation annotated. (D) Alignment of FUL protein sequences from *A. thaliana* (aFUL) and *C. hirsuta* (cFUL). Amino acid differences are in red and boxed. MADS-box and K-box domains are annotated according to the "Agamous-like MADS-box protein AGL8" entry in the UniProt Protein Knowledgebase (The UniProt Consortium, 2012). Premature stop codon at position 144 in *val* is annotated '*'. Protein sequence in grey indicates amino acids missing from the truncated cFUL protein in *val* mutants.

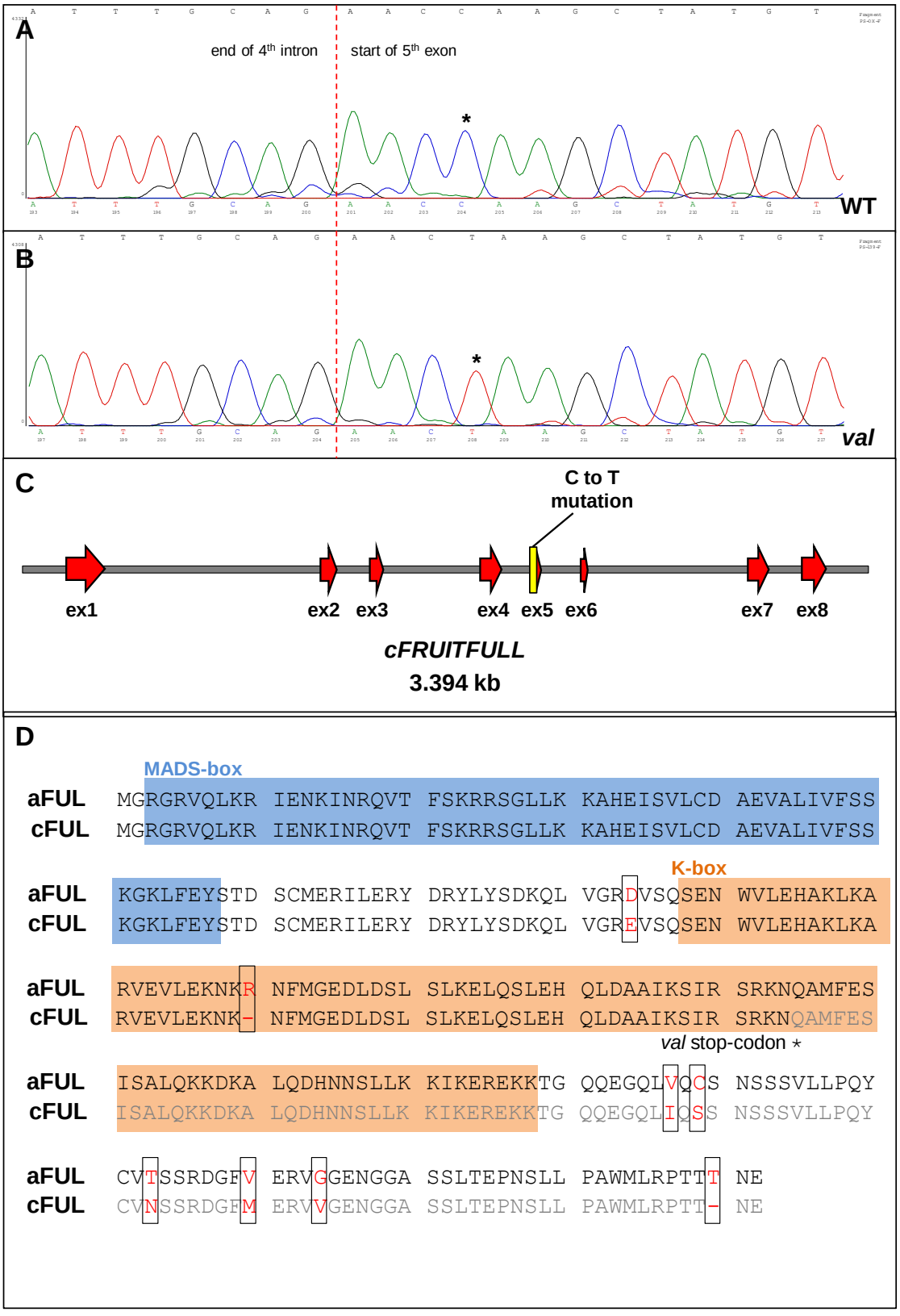
A
end of 4th intron
start of 5th exon
*
WT
B
*
val
C
C to T
mutation
ex1
ex2
ex3
ex4
ex5
ex6
ex7
ex8
cFRUITFULL
3.394 kb
D
MADS-box
aFUL MGRGRVQLKR IENKINRQVT FSKRRSGLLK KAHEISVLCD AEVALIVFSS
cFUL MGRGRVQLKR IENKINRQVT FSKRRSGLLK KAHEISVLCD AEVALIVFSS
K-box
aFUL KGKLFEYSTD SCMERILERY DRYLYSDKQL VGRDVSQSEN WVLEHAKLKA
cFUL KGKLFEYSTD SCMERILERY DRYLYSDKQL VGREVSQSEN WVLEHAKLKA
aFUL RVEVLEKNKR NFMGEDLDSL SLKELQSLEH QLDAAIKSIR SRKNQAMFES
cFUL RVEVLEKNK- NFMGEDLDSL SLKELQSLEH QLDAAIKSIR SRKNQAMFES
val stop-codon *
aFUL ISALQKKDKA LQDHNNSLLK KIKEREKKTG QQEGQLVQCS NSSSVLLPQY
cFUL ISALQKKDKA LQDHNNSLLK KIKEREKKTG QQEGQLIQSS NSSSVLLPQY
aFUL CVTSSRDGFV ERVGGENGGA SSLTEPNSLL PAWMLRPTTT NE
cFUL CVNSSRDGFM ERVVGENGGA SSLTEPNSLL PAWMLRPTT- NE

cFUL was sequenced in 6 homozygous *val* mutants from the mapping population, all of which possessed the same C to T mutation in the fifth exon. A CAPS marker was designed to this *cFUL* mutation which could be visualised using gel electrophoresis (Figure 4.5A). This PCR-amplified marker produces an amplicon of 415 bp in all backgrounds (Oxford, Oligosperma and *val*), which is digested to two 195 and 220 bp bands only in the *val* mutant, as a consequence of the introduction of a novel DdeI restriction enzyme site due to the mutation in *cFUL*. This 'cful' marker was found to co-segregate with the *val* phenotype in seven *val* mutants tested from the *val* mapping population. Its position relative to the other markers used is shown in Figure 4.5B.

To consider the importance of the mutated codon in *val*, FUL protein sequences were compared from species across the Brassicaceae (Figure 4.5C). Within the Brassicaceae, *A. thaliana, C. hirsuta* and *Lepidium campestre* all belong to Lineage I, whilst *Brassica napus* is in Lineage II. Within the core eudicots, these Brassicacean species are rosids, whilst *Petunia hybrida* is in the asterid clade. Outside of the core eudicots, *Aquilegia formosa X pubescens* is a basal eudicot, whilst *Oryza sativa* is a monocot species.

Comparison of FUL protein sequences from these species shows a high degree of conservation of the MADS-box. This comparison also shows that the amino acid mutated in *val* is conserved across the angiosperms. This suggests the codon has a strong functional importance, as evolution has conserved this codon in all 7 of these species.

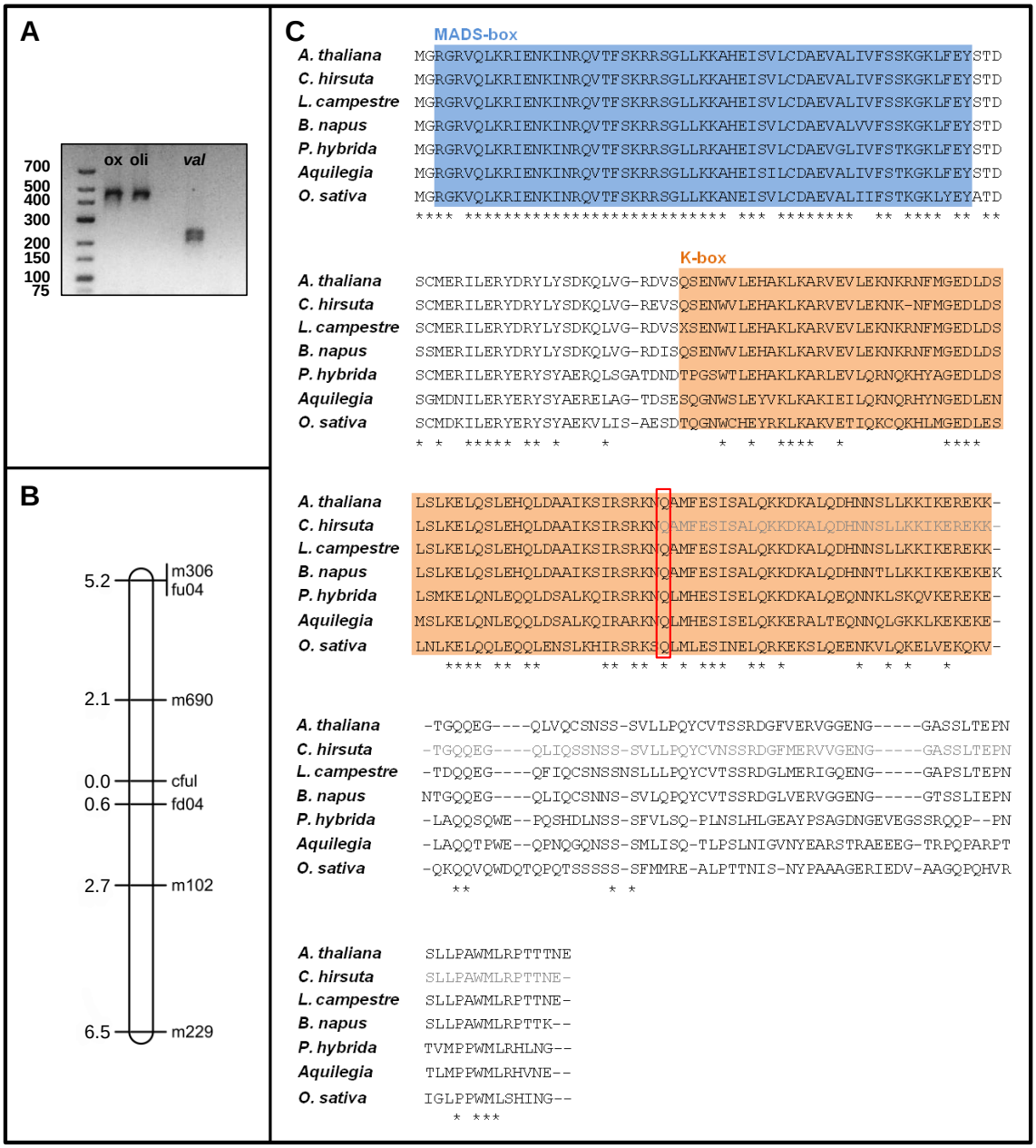

Figure 4.5 The *valveless* phenotype is tightly linked to a mutation in *cFRUITFULL*. (A) Gel-electrophoresis of PCR-amplified marker designed to *cFUL* mutation shows polymorphism between WT accessions (Oxford, 'ox' and Oligosperma, 'oli') and *val* mutants. (B) Linkage position of cful marker relative to other mapping markers used. Genetic distance shown in cM. Map constructed by Bjorn Pieper using JoinMap 4® (C) Alignment of FUL protein sequence from 7 angiosperm species. MADS-box and K-box are indicated in blue and orange, respectively. Conserved bases are indicated with '*'. The position of the premature stop codon in *val* is shown by the red box. Amino acids absent from truncated protein in *val* are indicated in grey.

4.2.3. Comparison of wild type and *valveless* morphologies

Wild type and *val* silique and seed gross morphologies were described in Chapter 3, and are shown in Figure 3.9. *val* siliques are thinner than WT, appear to lack valve tissue, produce narrow seeds, and are indehiscent. To examine the affect of the mutated FUL protein in *val* mutants, the development and mutant phenoptype of *val* was characterised further.

4.2.3.1. SEM of developing carpels and siliques

SEM of WT and *val* throughout carpel and silique maturation (Figure 4.6) revealed no visible differences between genotypes in carpel development prior to stage 12 (Figure 4.6 A to D) (in Figure 4.6, the carpels in panels C and D are viewed from different orientations, but are otherwise similar). Morphological differences are first visible at stage 12, when WT starts to show a flattened region which later becomes the replum (Figure 4.6E). This flattened region, however, is not visible in *val* at stage 12 (Figure 4.6F). By stage 13 (anthesis), replum and valve tissues, separated by valve margin, are clearly discernible in WT (Figure 4.6G). Replum tissue is also observed in *val* mutants at this stage, flanking two regions of the fruit that are slightly narrower than WT valves (Figure 4.6H).

At silique maturity, the WT dehiscence zone clearly possesses replum, valve margin and valve epidermal cells (Figure 4.6I), whilst valve epidermal cells are absent in *val* mutants (Figure 4.6J). Replum epidermal cells are straight, vertically elongated cells possessing surface striations, and stomata are present in this tissue (Figure 4.6K). No differences were observed between the repla of WT (Figure 4.6K) and *val* (Figure 4.6L). Valve epidermal cells are also elongated with a striated surface, and stomata are present, as in the replum (Figure 4.6M). These cells, however, are wavier and broader than replum epidermal cells. Valve margin

epidermal cells are elongated and very narrow, with unstriated walls, and unlike replum and valve tissue, the valve margin tissue possesses no stomata (Figure 4.6 I and O). In *val* mutants, the region where the valve is normally found contains very narrow, unstriated epidermal cells that clearly do not have valve identity, and stomata are conspicuously absent from this tissue (Figure 4.6N). These epidermal characteristics suggest that this tissue has valve margin identity.

Compared with WT (Figure 4.6P), SEM also reveals an expansion of style tissue at the silique apex in *val* mutants (Figure 4.6Q). When the WT valve is curled away, its round seeds are easily seen in an ordered arrangement (Figure 4.6R). By contrast, the narrower seeds of *val* are revealed by dissecting away the ectopic valve margin-like tissue (Figure 4.6S).

Figure 4.6 SEM of gynoecium growth and maturation in wild type and *valveless*. No differences are seen in WT and *val* gynoecial tissue arrangement in stages 8 (A and B) and 9 (C and D). At stage 12, a flattened gynoecial region (indicated by bracket), which later forms the replum, becomes visible in WT (E) but is less defined in *val* (F). At stage 13 (G and H), dehiscence zone tissues become clearly discernible. (I) and (J) shows the dehiscence zone at stage 17b. Epidermal cell types are shown in (K) to (O), arrows indicate stomata. (K and L) replum epidermal cells, (M) WT valve, (N) *val* expanded valve margin, (O) WT dehiscence zone. Stage 15/16 siliques show differences in apical tissue domains (P and Q). The arrangement of seeds within stage 17 siliques are shown in (R) and (S). Genotypes are indicated on each panel. Tissues are labelled: stigma (st), style (sy), replum (r), valve (v), valve margin (vm) and seed (s). Bar shows 100 μm in (A) to (J) and (P) to (R), bar shows 10 μm in (K) to (O).

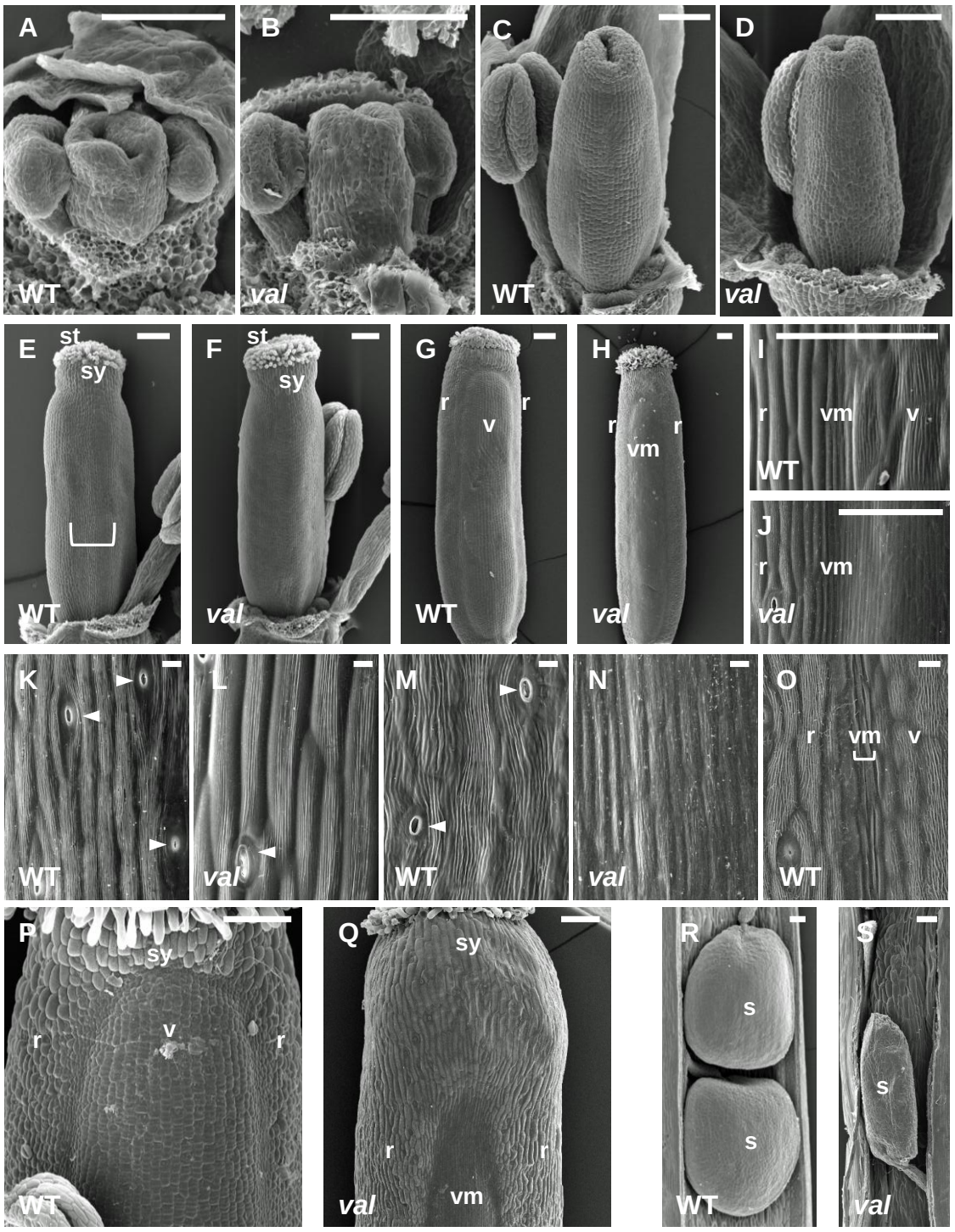
A
WT
B
val
C
WT
D
val
E
st
sy
WT
F
st
sy
val
G
r
r
v
WT
H
r
r
vm
val
I
r
vm
v
WT
J
r
vm
val
K
WT
L
val
M
WT
N
val
O
r
vm
v
WT
P
sy
r
v
r
WT
Q
sy
r
r
vm
val
R
s
s
WT
S
s
val

4.2.3.2. TBO sections of developing siliques

TBO-stained transverse sections (Figure 4.7) also show little difference between WT and *val* in early carpel stages (Figure 4.7 A to D). At stage 10/11, the replum region starts to become clearly pronounced in WT (Figure 4.7E), but protrudes less in *val* (Figure 4.7F). By stage 12, replum and valve regions are visible in WT as tissues separated by narrower, slightly constricted regions of valve margin (Figure 4.7G). At this stage in *val*, however, the carpel tissue remains largely undifferentiated, whilst the replum tissues have become clear (Figure 4.7H). Boundaries between the replum and the undifferentiated carpel tissue are visible in *val* at this stage (Figure 4.7H).

At stage 14 (fertilisation and the start of silique maturation), replum, valve and valve margin tissues are clearly differentiated in WT (Figure 4.7I). At this stage in *val*, replum tissue has differentiated normally but valve tissue is discernibly absent (Figure 4.7J). The replum in *val*, however, is wider and more rounded than in WT, and a tissue of small, square cells resembling valve margin is found in place of the missing valve tissue. At silique maturity it is clear that *val* mutants contain no cell types characteristic of the WT valve, such as large epidermal cells, chloroplast-containing mesocarp, or enlarged and lignified endocarp *b* cells (Figure 4.7L).

At maturity, the WT valve margin comprises four cell layers – two layers of lignified cells and two layers of non-lignified cells (Figure 4.7M). The tissue that is present in place of valve tissue in *val* siliques also comprises lignified and non-lignified cells (Figure 4.7N). Like the cells of the WT valve margin, these cells are small and square. However, the WT valve margin and aberrant *val* tissue show some differences. The WT valve margin is 8 cells wide from the outer to the inner

surface of the fruit, whilst the mutant tissue in *val* is 9 cells wide. This is the same number as in the WT valve, which comprises 7 layers of non-lignified exocarp, mesocarp and sclerenchyma cells, 1 layer of lignified endocarp *b* cells, and 1 layer of non-lignified endocarp *a* cells. The tissue in place of valve tissue in *val* mutants also differs from the WT valve margin in its pattern of lignified cells. In the WT valve margin, the lignified cells and non-lignified cells form two parallel stripes, of equal cell number, spanning from the outer surface to the inner surface of the silique (Figure 4.7M). The expanded tissue in *val*, however, is mostly non-lignified, and the lignified cells form only a single-cell layer along the innermost surface of the silique (Figure 4.7N). This lignified layer is variable and frequently interrupted with non-lignified cells (indicated by arrows in Figure 4.7N).

Comparison of the WT valve margin and the expanded tissue in *val* mutants therefore seems to suggest that the aberrant tissue in *val* is not simply overproliferated valve margin tissue, as indicated by the differences in lignification patterns and the number of cell layers. The number of cell layers in the *val* tissue suggests that this might be valve tissue which has acquired the valve margin-like characteristics of small cell size, organisation into only two cell types (lignified and non-lignified) and, in cells which are lignified, lignin deposition in all cell walls.

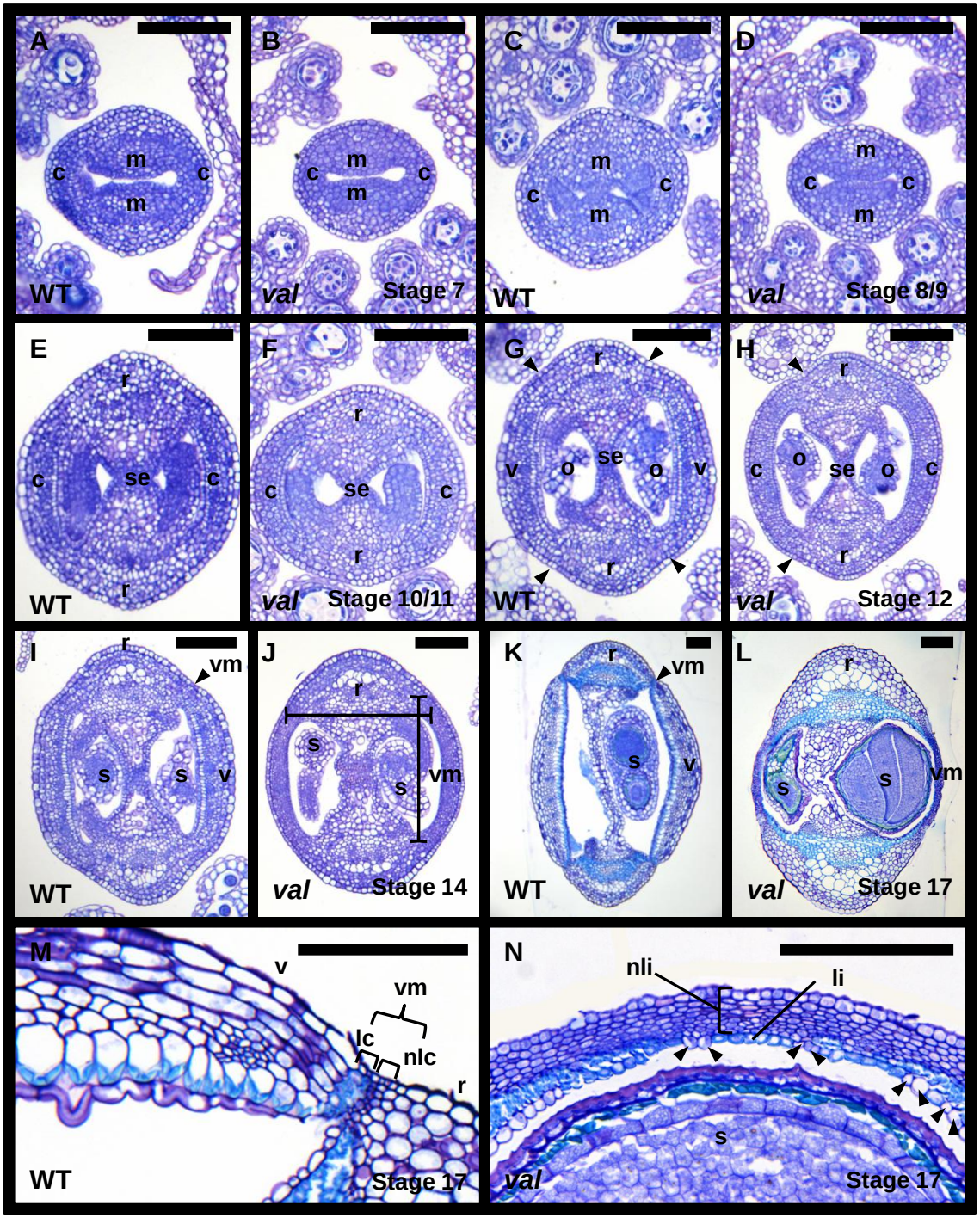

Figure 4.7 TBO-stained plastic sections of gynoecium growth and maturation in wild type and *valveless*. Genotypes and developmental stages indicated on panels. Tissues and organs are labelled carpel (c), medial tissue (m), replum (r), septum (se), valve (v), ovule (o), seed (s), valve margin (vm). Arrows in (G and (H) mark boundary between replum and flanking tissue. Brackets in (J) indicate the expanse of the replum and valve margin tissues visible in *val* at stage 14. (M) Shows valve margin lignified cell layer (lc) and non-lignified cell layer (nlc). (N) Shows lignified (li) and non-lignified (nli) cells of the tissue in place of valve in *val* siliques. Arrows indicate non-lignified cells in lignified cell layer. Bar represents 100 µm.

4.2.3.3. DIC of developing embryos

val mutants develop narrower, smaller, cylindrical seeds (Figures 3.9L and 4.6S), so seeds were cleared and visualised using differential interference contrast (DIC) microscopy, to examine whether *val* shows aberrant embryo morphologies (Figure 4.8). No differences in embryo morphology can be seen between WT and *val* at the globular and heart stages (Figure 4.8 A to L, O and P). The early torpedo stage in WT and *val* is comparable (Figure 4.8 M and Q), with both showing the development of cotyledon and hypocotyl regions. However bent-cotyledon stage embryos in *val* appear squashed within the narrower seed (Figure 4.8R). In comparison to WT (Figure 4.8N), *val* embryos frequently have a kinked hypocotyl (Figure 4.8R). This suggests that *val* embryos develop normally as WT, and that it is the altered silique structure of *val* mutants that causes their aberrant seed shapes.

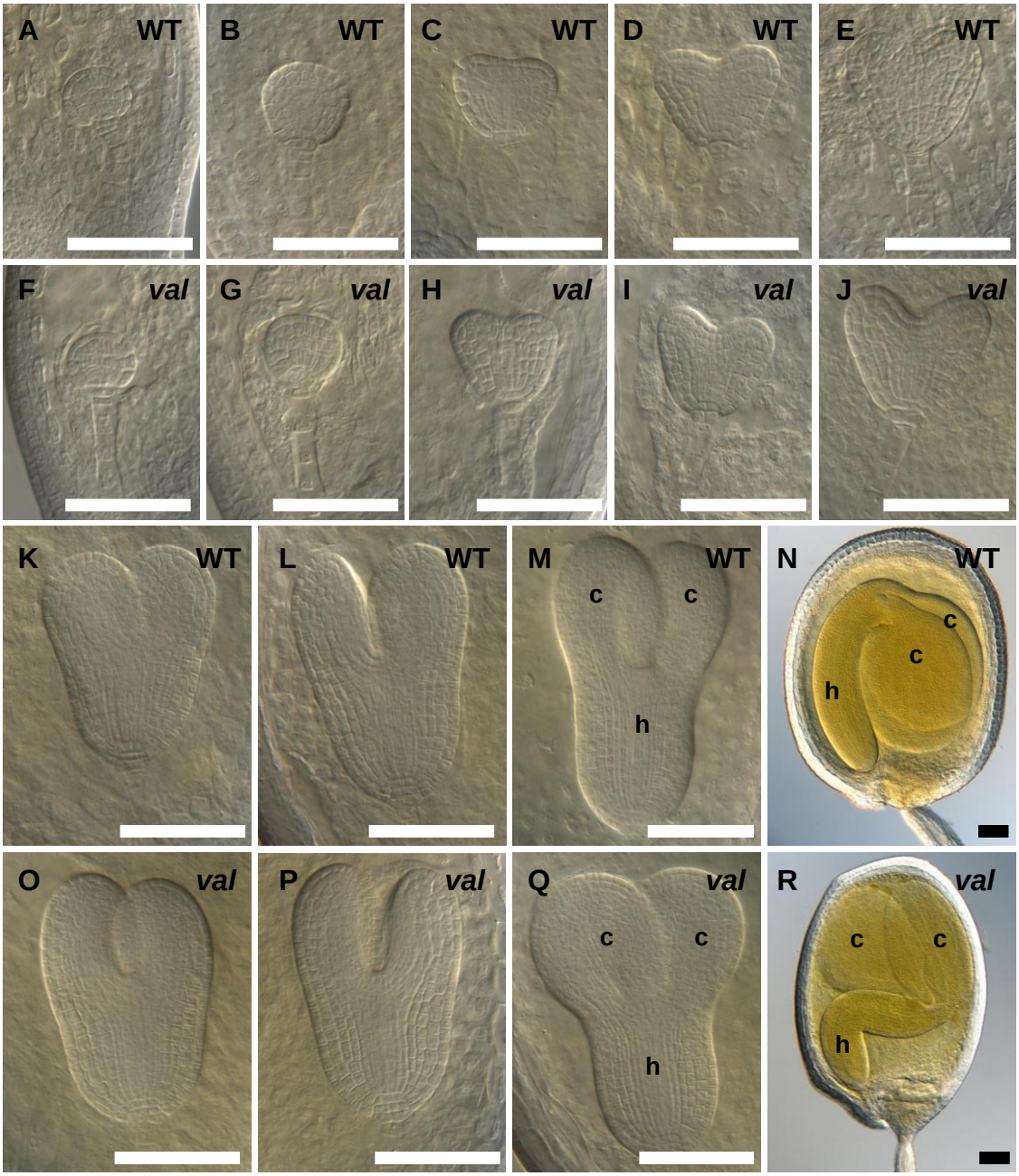

Figure 4.8 Differential interference contrast (DIC) microscopy of wild type and *valveless* embryos. Embryos photographed at globular (A, B, F, G), heart (C-E, H-J, K, L, O, P), torpedo (M, Q) and bent-cotyledon (N,R) stages. Genotypes indicated. In (M), (N), (Q) and (R), h indicates hypocotyl, c denotes cotyledon. Bar represents 100 µm.

4.2.3.4. Analysis of A. thaliana IND *and* FUL *expression in* C. hirsuta *WT and* val *gynoecia*

To further assess the identity of the ectopic valve margin tissue that appears to replace the valve in *val* mutants, expression of *A. thaliana INDEHISCENT (IND)* was examined. This was carried out using an *A. thaliana IND::IND:GUS* construct (gift from L. Østergaard) that comprises 2.7 kb of the *IND* promoter and the 0.5 kb IND open reading frame (ORF), fused to the uidA gene that encodes β-glucoronidase (GUS) (Sorefan et al. 2009).

WT *C. hirsuta* plants expressing this construct show GUS-staining patterns like those seen in *A. thaliana* (Sorefan et al. 2009)(Figure 4.9A), with blue staining clearly visible in the valve margin tissue at stage 12. This result is consistent with *IND* expression marking valve margin tissue identity. *val*, however, shows expression of β-glucoronidase throughout the entire tissue region that develops in place of valve (Figure 4.9B). This pattern of GUS staining is similar to that in *ful* mutants of both the valve margin enhancer trap marker YJ80 and the *in situ* staining of *IND* expression (Liljegren et al. 2004). Blue-stained pollen grains are a common artefact of GUS reporter constructs (for example Thoma et al. 1994)

The differences between WT and *val* GUS staining are shown clearly in cross section (Figure 4.9 C to H). At stages 12 and 14, GUS staining is observed only in the WT valve margin cells (Figure 4.9 C, E, G). However, the expanded expression seen in *val* is seen across all cell layers of the entire aberrant “valve margin-like” region (Figure 4.9 D, F, H). Using *IND* expression as a marker for valve margin identity, this result confirms the identity of the ectopic tissue which occupies the valve region in *val* as being expanded valve margin.

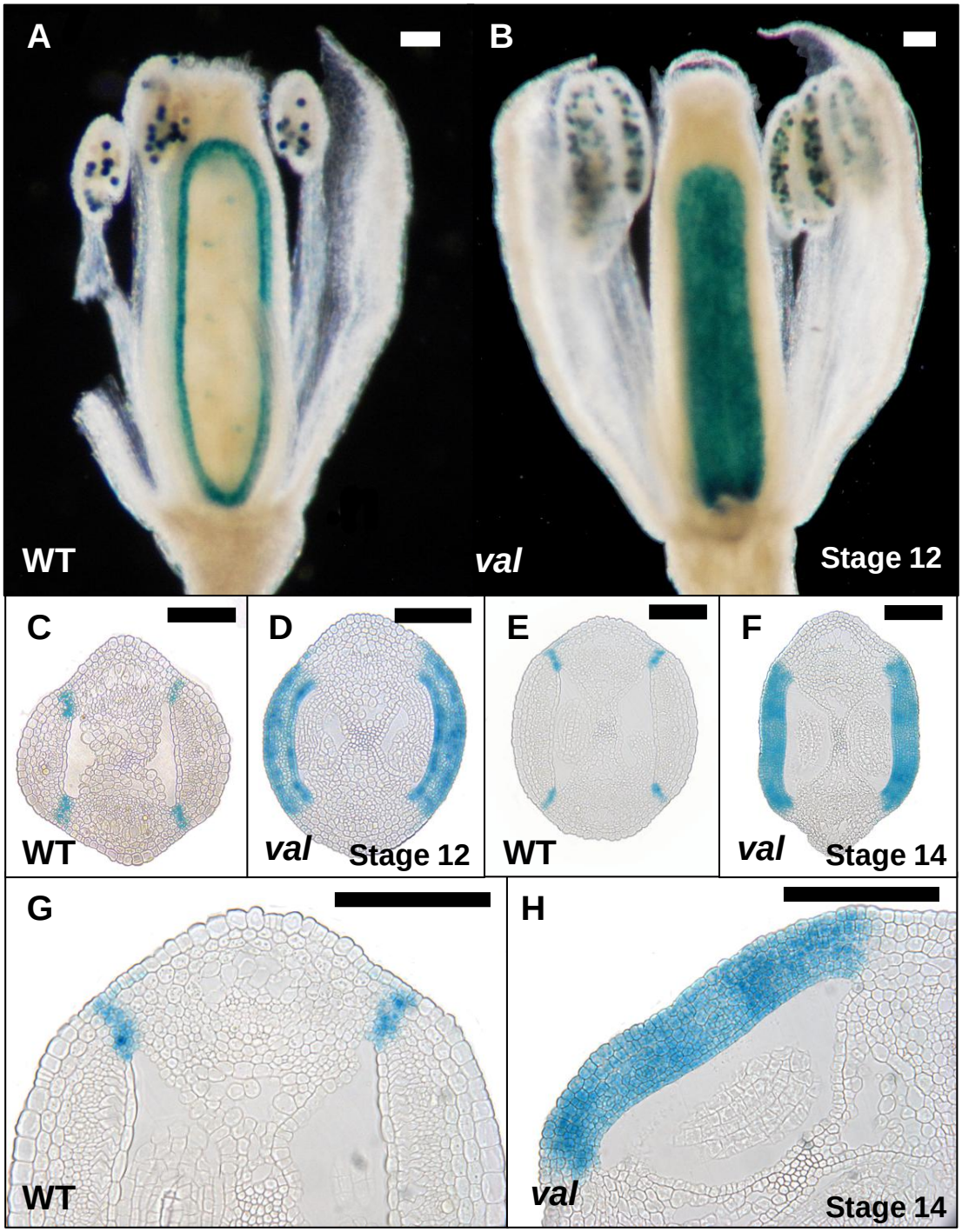

Figure 4.9 *AtIND::IND:GUS* expression in wild type and *valveless*. GUS expression marks valve margin indentity in WT and *val*, shown in whole mount carpels (A and B) and in transverse section (C-H). Stages and genotypes indicated. White bar indicates 1 mm, black bar 100 µm.

Clear, strong expression of *IND* is first visible at stage 12 in both WT and *val* (Figure 4.9 A to D). This coincides with the stage at which the boundaries between valve and replum, which later differentiate into valve margin tissue, first become clear in WT (Figure 4.9G), and at the stage when the replum first becomes discernible by SEM (Figure 4.9E).

Expression of the *A. thaliana FUL* gene, which marks valve tissue identity in *A. thaliana*, was analysed in *C. hirsuta*, in order to further investigate whether *val*fruits possess valve tissue, and to see if *A. thaliana FUL* could complement the *val* phenotype.

In order to carry out comparable GUS staining of *FUL* expression, an *A. thaliana FUL::FUL:GFP* construct (a gift from G. Angenent) that comprised a 5.298 kb genomic fragment, including a 2 kb promoter region upstream from the *FUL* start codon, and a green fluorescent protein (GFP) tag, was adapted (Urbanus et al. 2009). Using Gateway Cloning, this GFP tag was replaced with GUS.

At stage 12 in WT, the *AtFUL::FUL:GUS* construct is expressed strongly in two flanks along the gynoecia that mark the two valves (Figure 4.10A). By stage 15, this staining is fainter and is clearly restricted to the valve tissues (Figure 4.10B). At stage 12 in *val* gynoecia, *AtFUL::FUL:GUS* expression is drastically reduced compared to WT (Figure 4.10C), with very faint, patchy staining observed in similar tissues. At stage 16, odd, patchy GUS staining is found throughout the style and presumptive valve margin tissue that occupies the position of the WT valve in *val* (Figure 4.10D). Expression of *AtFUL::FUL:GUS* was also observed in the pedicels and a small domain in the receptacle in both WT and *val* (Figure 4.10 A and C).

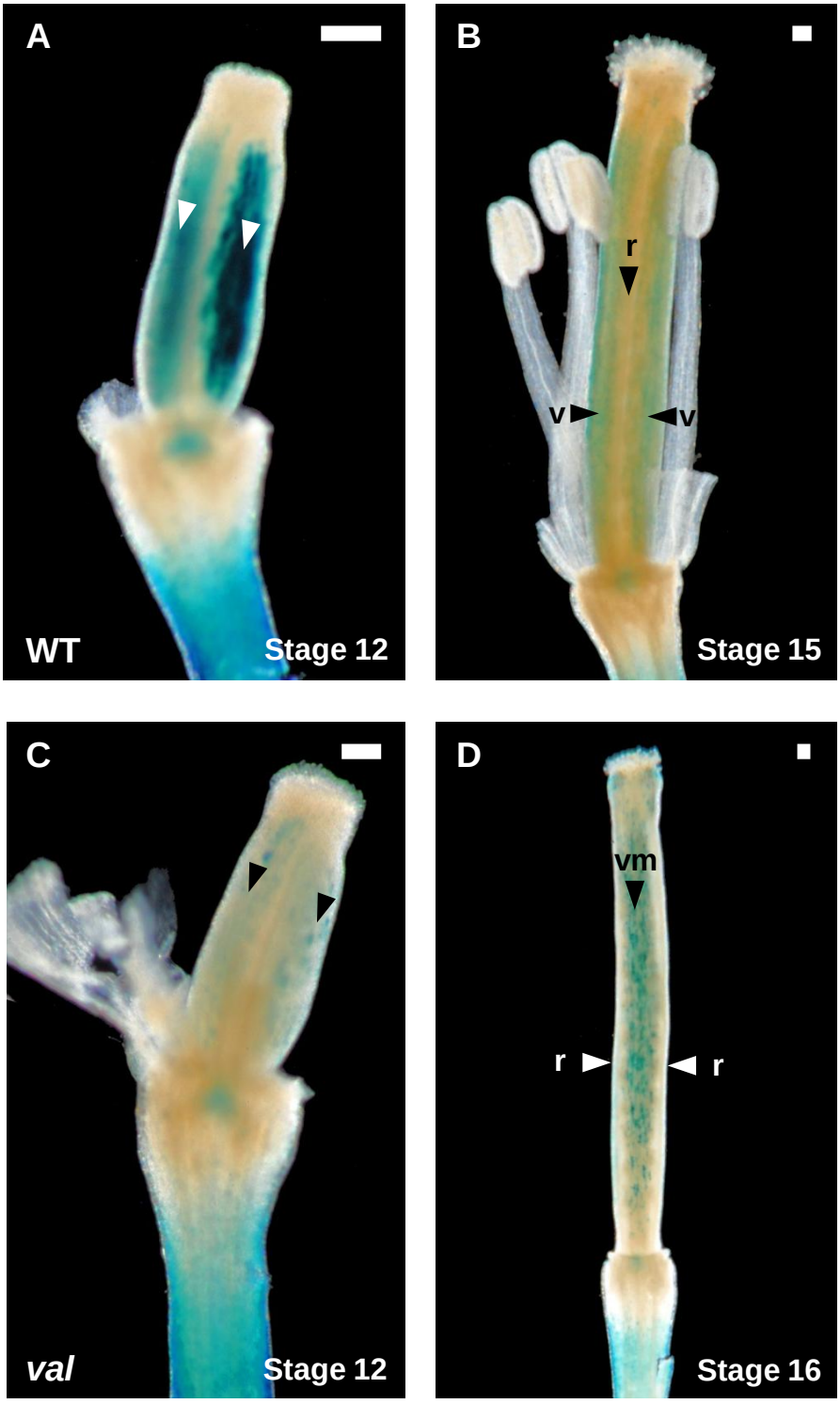

Figure 4.10 *AtFUL::FUL:GUS* expression in WT and *val C. hirsuta*. Expression of *A. thaliana FUL* construct in WT (A and B) and *val* (C and D). (A) WT stage 12, arrows indicate two stripes of expression.(B) WT stage 15. (C) *val* stage 12, arrows indicate two feint stripes of expression. (D) *val* stage 16. Tisses labelled 'v' (valve), 'vm' (valve margin), and 'r' (replum). Bar represents 100 µm.

These results show that *A. thaliana FUL* expression marks the WT valves of *C. hirsuta* fruit. The drastically reduced expression of *AtFUL::FUL:GUS* in *val* gynoecia is in line with morphological data that show that the fruit of *val* mutants lack valves. However, unexpectedly, no rescue of the *val* phenotype by expression of this *A. thaliana FUL* genetic construct was observed. This could be because the GUS tag interferes with FUL activity, or due to species-specific differences in FUL function.

4.2.4. Comparison of silique morphologies of WT and *val* in *C. hirsuta* and WT and *ful* in *A. thaliana*

The *val* mutant is tightly linked to a mutation in *cFUL* that results in a truncated cFUL protein. Like *A. thaliana ful* mutants, *val* siliques show incorrect specification of valve identity. It is therefore highly likely that this phenotype in *val* is caused by the mutation in the *cFUL* gene.

To investigate this further, *C. hirsuta* WT and *val* fruits were compared with those of *A. thaliana* WT (Landsberg *erecta* accession) and the *A. thaliana* null mutant *ful-1* (Gu et al. 1998), in order to compare the silique morphologies arising from *FUL* mutations in both species.Commonalities and differences between the two mutants were found (Figure 4.11).

The most obvious phenotype of *ful-1* siliques are their stunted growth (Figure 4.11A), compared with WT Landsberg *erecta* (L*er*) siliques, and *ful-1* siliques are around 80% shorter than WT (Gu et al. 1998). This severe stunting of apical-basal growth and expansion contrasts with *val* mutants. Whilst *val* siliques are significantly shorter than WT *C. hirsuta* siliques (P-value 1.68×10^{-20}, one-tailed T-test, assumed unequal variance), the difference between WT and *val*

silique length is much smaller, with *val* siliques showing a mean reduction in length of only 18.3%.

The stunted *ful-1* siliques comprise a valve-like tissue and a twisted replum that appears ‘bumpy’ (Figure 4.11B). This replum phenotype arises from the juxtaposition of normal growth of the replum tissue with the stunted growth of the valve, which causes the replum to repeatedly twist back on itself in a wavy arrangement (Gu et al. 1998). This too contrasts with *val*, where the repla remain smooth and untwisted, and are separated by a thin, semi-transparent layer of valve margin tissue, through which the seeds are visible (Figure 4.11C). However, the siliques of the weaker alleles *ful-4* and *ful-6* both possess less distorted repla, and are not as severely stunted in length (Ferrandiz et al. 2000). The severe reduction in silique length and the twisted replum of the *ful-1* silique, therefore, likely represent a null phenotype for *FUL* in *A. thaliana*, and the less severely stunted silique length and smooth replum of *val* mutants may be due to its being a hypomorphic allele. This hypothesis is supported by the fact that sequencing of *FUL* in *val* reveals that the entire MADS-box and a large portion of the K-box are upstream of the premature stop codon, which suggests that the resultant protein could still have some impaired, low-level function.

At stage 14 (Figure 4.11 D to G), transverse sections show that *ful-1* is largely similar to WT L*er*, showing only slightly less definition of the replum and slightly less differentiation of the valve, and this is also the case for *val* in *C. hirsuta*.

The WT and mutant morphologies are more clearly divergent at silique maturity (Figure 4.11 H to K). Like *val*, *ful-1* shows an altered fruit shape when compared with WT *A. thaliana* (Figure 4.11 H and I). The replum is much enlarged

in *ful-1* (Figure 4.11I), similar to what is seen in *val* (Figure 4.11K). The aberrant 'valve' tissue which curls around the *ful-1* fruit is thinner than the WT valve (Figure 4.11 H and I), which also is similar to what is seen between *C. hirsuta* WT and *val* (Figure 4.11 J and K).

Closer inspection of the replum of *ful-1* (Figure 4.11L) reveals some cellular similarities with that of *val* (Figure 4.11M). Like in *val* mutants, the *ful-1* replum shows an increased number of lignified cells which span the expanded replum and spread out from its edges. Aberrant large, circular cells that are not found in WT are also visible in the *ful-1* replum, and these bear some resemblance to the large replum cells which over-proliferate in *val*. However, the *val* replum shows much greater cellular organisation than is seen in *ful-1* mutants.

The greatest difference in tissue differentiation between *ful-1* and *val* fruits is seen where valve tissue normally develops (Figure 4.11 N and O). Both mutants possess a thin tissue composed of small cells, however this tissue differs in its lignification. In *ful-1* fruits, the three internal layers of the 'valve' are fully lignified (Figure 4.11N). However, only the innermost layer of the expanded valve margin tissue is lignified in *val* fruits (Figure 4.11O). In both mutants, this lignification resembles the thin lignin deposition seen in the *A. thaliana* valve margin and endocarp *b* tissues, and not the heavy lignin deposition along the innermost wall only that occurs in the *C. hirsuta* endocarp *b* layer.

Figure 4.11 Morphology of *A. thaliana* and *C. hirsuta* wild types and valve mutants. Genotypes labelled WT L*er* (wild type *A. thaliana* Landsberg *erecta*), *ful-1* (Landsberg *erecta fruitfull* null mutant), WT *Ch* (wild type *C. hirsuta*) and *val* (*C. hirsuta valveless* mutant). Photograph of WT and mutant siliques (A). Close-up photography of *ful-1* (B) and *val* (C) mutant siliques. Tissues labelled r (replum), 'v' (valve-like), vm (valve margin) and s (seed). TBO-stained transverse sections of stages 14 (D-G) and 17 (H-O). (D-K) Whole fruit sections. Position of repla is indicated by r. (L and M) Mutant repla. li indicates ectopic lignification. o indicates large, ectopic cells. (N and O) Mutant tissue in place of valve. li indicates lignified cells. White bar indicates 1 mm, black bar 100 µm.

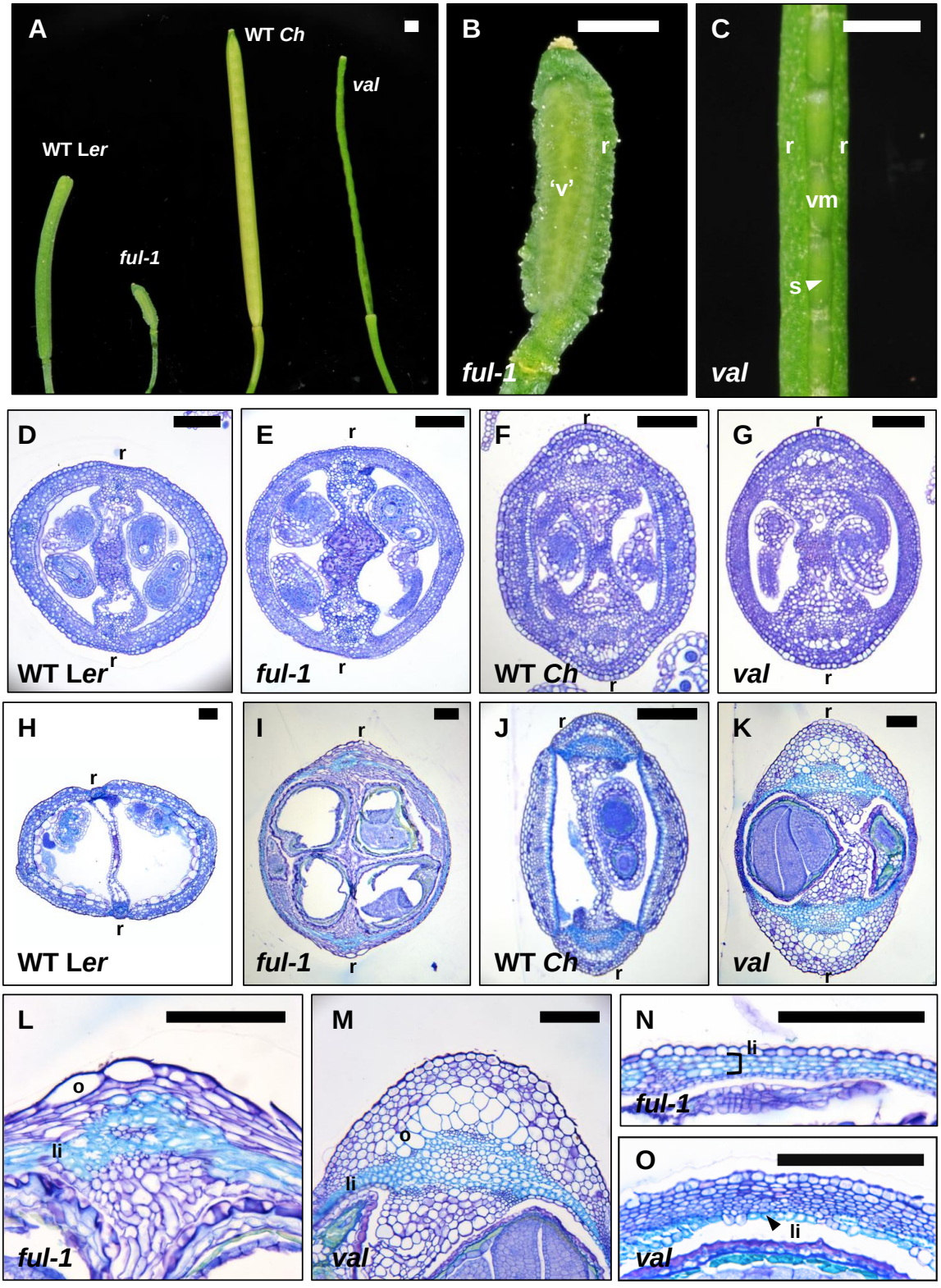
A
WT Ler
ful-1
WT Ch
val
B
r
'v'
ful-1
C
r
r
vm
s
val
D
r
r
WT Ler
E
r
r
ful-1
F
r
r
WT Ch
G
r
r
val
H
r
r
WT Ler
I
r
r
ful-1
J
r
r
WT Ch
K
r
r
val
L
o
li
ful-1
M
o
li
val
N
li
ful-1
O
li
val

4.2.5. Genetic interactions affecting replum width

val mutants appear to possess a broader replum. A previously identified *cas1* mutant also seems to have an increased replum width. Together, *val, cas1,* and the *cbp* allele also identified in Chapter 3 provide an opportunity to examine the genetic control of replum versus valve patterning in *C. hirsuta*.

The repla of these mutant lines, and of double mutant combinations, are compared in Figure 4.12. TBO-stained transverse sections show the mature repla of WT, *cbp*, *cas1, val*, *cbp val, cas1 val*, and *cas1 cbp* (Figure 4.12 A to G). Figure 4.6H shows the mean number of replum epidermal cells in each line, giving an indication of replum width in each genetic background. Figure 4.12I shows these means as fold increases relative to the mean numbers of WT and *val* replum epidermal cells.

The repla of *cbp* siliques show no discernible differences in morphology from WT (Figure 4.12 A and B). Figure 4.12 H and I show that the mean number of replum epidermal cells is very similar in WT and *cbp*. The *cas1* replum, however, is expanded, and this mutant has aberrant “shoulders” stretching out from the central replum tissue (marked by brackets and arrows in Figure 4.12C). Compared with WT, the number of replum epidermal cells in *cas1* is much increased and this difference is strongly statistically significant (one-tailed Student’s T-test assuming unequal variance, P-value 0.0007), showing a 1.46 fold increase relative to WT (Figure 4.12I). This phenotype is partially rescued in *cas1 cbp* (Figure 4.12D), whose replum epidermal count is significantly smaller than that of *cas1* at higher than the 95% level (one-tailed Student’s T-test, assuming unequal variance, P-value 0.0122). The mean replum epidermal cell count in this

double mutant is, however, still 1.2-fold greater than that seen in WT (Figure 4.12H), significant at the 95% level with a P-value of 0.0317.

The replum of *val* siliques are also expanded (1.11-fold greater than WT)(Figure 4.12 E and I). A one-tailed Student's T-test (assuming unequal variance) gives a P-value of 0.0912, indicating that this expanded replum in *val* is significant at the 90% level but not at the 95% level. However, this could be due to the relatively large variance seen in small samples. Because *val* mutants show an extended replum, which is similar but less severe than the phenotype seen in *cas1* siliques, double mutants were generated between these lines and *val*.

The repla of these double mutants are shown in cross-section in Figure 4.6 F and G. Like *val* (Figure 4.12E), *cbp val* and *cas1 val* (Figure 4.12 F and G) also show expansion of the replum, quantified in Figure 4.6H. The repla of *cas1 val* are significantly wider than both *val* and *cas1* single mutants (one-tailed Student's T-tests, assuming unequal variance, P-values 0.0013 and 0.0339, respectively). The increase in replum width between *val* and *cas1 val* mutants (1.50 fold) is similar to the increase in replum seen between WT and the *cas1* single mutant (1.46) (Figure 4.12I). This suggests that the expanded replum of *cas1 val* double mutants is an additive effect of combining the *cas1* and *val* mutant alleles.

However, this does not appear to be the case in *cbp val* mutants. Whilst *cbp* repla are similar to WT in size (the mean *cbp* replum epidermal cell number was 0.986 times that of WT), the repla of *cbp val* double mutants are significantly wider than those of WT at the 95% level (one-tailed T-test, assuming unequal variance, P-value 0.0157). The mean number of replum epidermal cells in *cbp val* double mutants is increased 1.16 fold compared to *val* single mutants (Figure

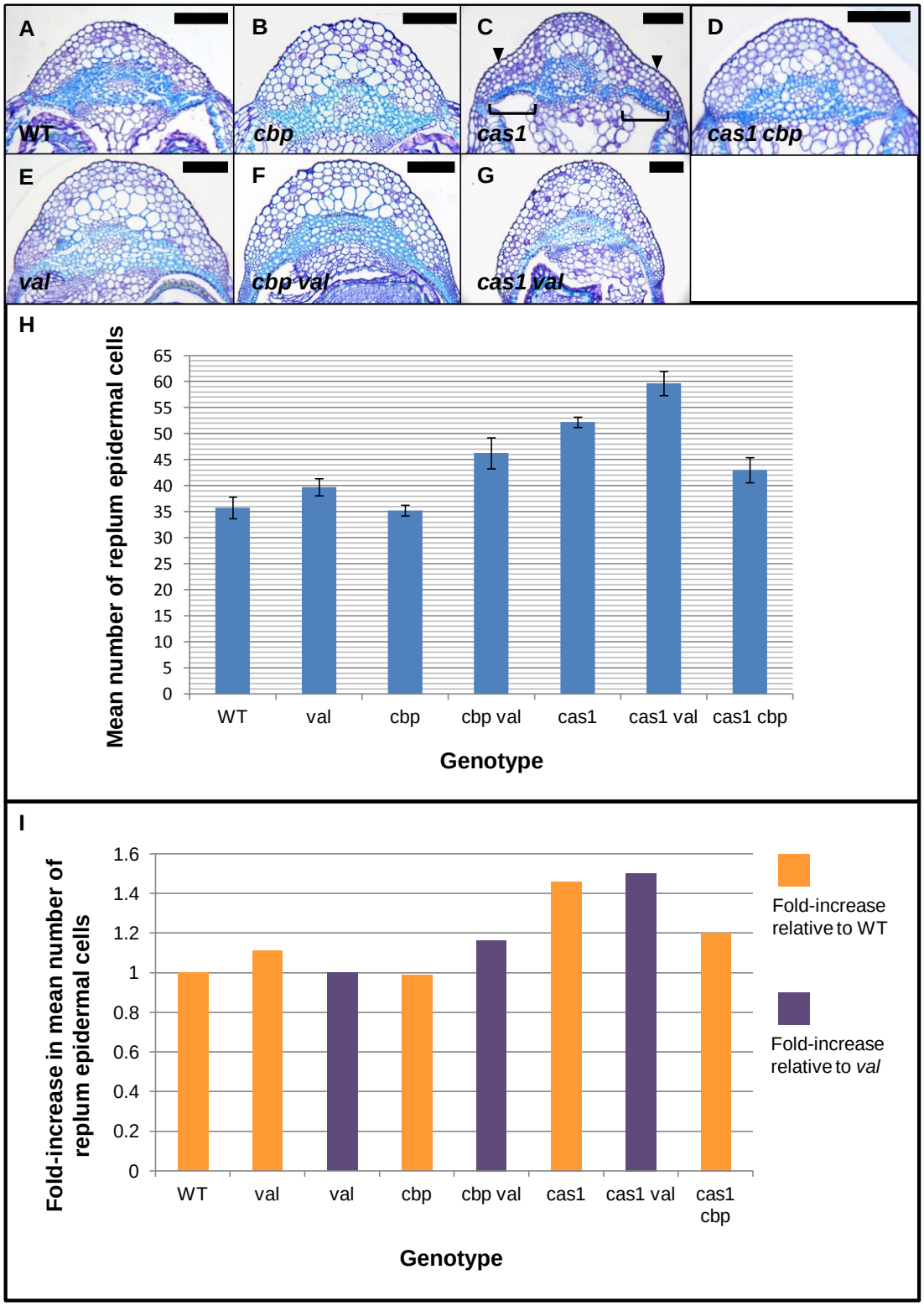

Figure 4.12 Replum morphology in genetic lines. TBO-stained plastic transverse sections of stage 17b repla from (A) WT, (B) *cbp*, (C) *cas1*, (D) *cas1 cbp*, (E) *val,* (F) *cbp val*, and (G) *cas1 val*. Bar indicates 100 µm. Arrows and brackets in (C) indicate expanded "shoulder-like" extensions in *cas1* replum. Mean replum epidermal cell counts shown in (H). For each genetic line, n was between 3 and 5 (stomatal guard cells were not counted). Error bars show standard error. (I) shows fold-increase in mean replum epidermal cell number relative to WT mean (orange) or *val* mean (purple).

4.12I). This suggests that the effect of *val* alone does not account for the expanded repla of *cbp val* mutants, indicating that a genetic interaction between *val* and *cbp* in these double mutants could underlie a further expansion of the replum beyond the phenotype of *val* single mutants.

In addition to an expanded repla, other altered morphologies were seen in *cas1* and *cas1 val* mutants (Figure 4.13).

As characterised in Chapter 3, the WT valve shows enlargement and polarised lignification of the endocarp *b* layer cells (Figure 4.13A). In *cas1* mutants, aberrant lignin deposition was observed in this layer (Figure 4.13B). Rather than showing a strict, inner-most wall-only deposition of lignin in these cells, *cas1* en*b* cells show some ectopic lignin deposition, particularly in cells proximal to vascular bundles. The valves of *cas1* siliques also appear to possess fewer cell layers.

The absence of valve tissue in *val* leads to an expansion of valve margin tissue between two expanded repla (Figure 4.13C), as will be discussed in Chapter 5. The shape of the *val* silique is further altered by the loss of *cAS1* function (Figure 4.13D). In this double mutant, the expanded replum spreads further around the silique. The valve margin tissue occupies much less space, filling-in the smaller gaps between the severely expanded repla of this double mutant.

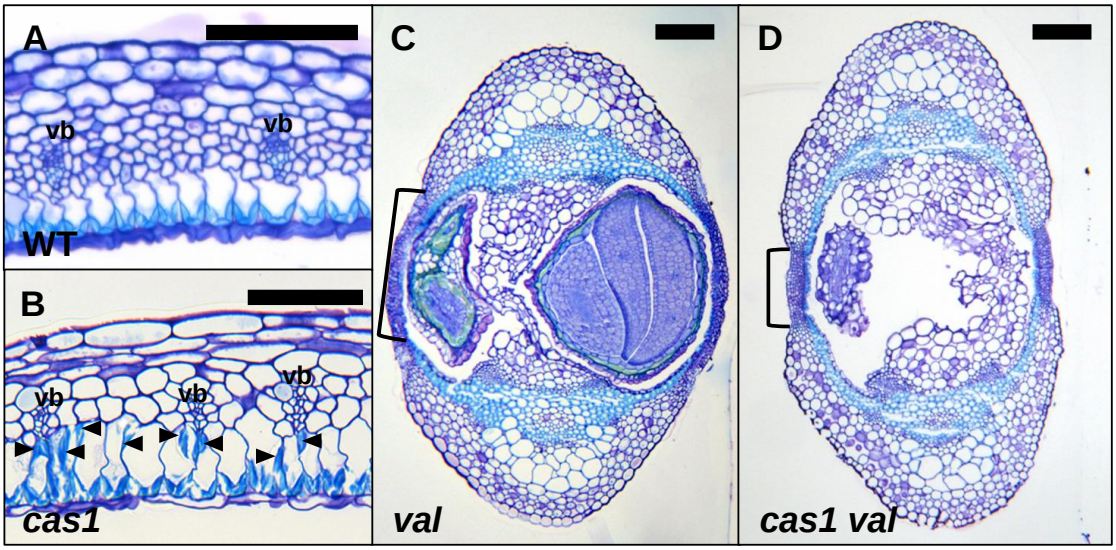

Figure 4.13 TBO-stained cross sections of *cas1* and *cas1 val* reveal other altered morphologies. Transverse sections of valve (A-B) and whole siliques (C-D) from WT (A), *cas1* (B), *val* (C), and *cas1 val* (D). Vascular bundles labelled 'vb' and arrows indicate ectopic lignification in (A) and (B). Brackets in (C) and (D) indicate expanded valve margin tissue. Bar represents 100 µm.

4.3. Discussion

valveless is an indehiscent *C. hirsuta* mutant, showing conversion of valve to valve margin. Genetic mapping delimited a 2.7 cM interval that contains the *val* locus and the *cFUL* gene. The *cFUL* gene is mutated in *val* plants, which would result in a truncated protein, and this mutation co-segregated with the *val* phenotype. The *val* mutant shares a number of morphological commonalities with *fruitfull* mutants in *A. thaliana.*Taken together, this evidence suggests that the mutation in *cFUL* is responsible for the mutant phenotypes seen in *val* plants.

Analysis of *val*, *cas1* and *cbp* mutants suggests that *C. hirsuta* shares the same regulatory framework for valve and replum specification and development as is seen in *A. thaliana*. Together, these mutants allow investigation of replum and valve development, but suggest that it is genetic changes downstream of this regulatory framework that pattern the explosive opening mechanism seen in *C. hirsuta*.

4.3.1. Genetic mapping of *valveless* in *C. hirsuta*

The mapping procedure followed is shown in Figure 4.14. Linkage was first identified between *val* and m229, a marker located towards the bottom of chromsome 8 in the *C. hirsuta* genome (Figure 4.2A). This region is homologous to chromosome 5 in *A. thaliana*. New CAPS and dCAPS markers were designed and tested in this region. Recombinants from 39 mutants were used to define a genetic interval of 25.6 cM that contained the *val* locus, flanked by markers m229 and m306, which corresponds to a syntenous region of approximately 1.04 Mb in *A. thaliana*.

Recombinants from 79 mutants were then used to narrow this genetic interval to 2.7 cM, flanked by the novel markers m690 and fd04 (Figure 4.2B). This 2.7 cM interval corresponds to a region of approximately 149 kb in *A. thaliana*. Within this 149 kb region in *A. thaliana* there are 33 genes (Figure 4.2D), a manageable number to begin looking at gene annotations in order to determine candidate genes. A variety of gene ontology categories were represented amongst these 33 genes (Table 4.3). A clear candidate was evident amongst these, *FRUITFULL*, which is known to be a key transcription factor involved in patterning the valve tissues in the *A. thaliana* silique.

Sequencing of *cFUL* identified a mutation of the fourth base of exon 5 (Figure 4.4 A to C). Here the WT cytosine has been mutated to thymine in *val* plants. This change codes for a stop codon in place of the amino acid glutamine, resulting in a truncated protein of 143 amino acids (Figure 4.4D). Comparison of cFUL protein sequences from WT and *val* shows that the truncated protein contains the MADS-box, but the premature stop codon truncates the K-box domain. This suggests that the mutant cFUL protein might still be able to bind DNA through its MADS-domain, but its ability to regulate target genes is likely to be impaired by its truncated K-box protein-protein interaction domain which is required for functional dimerisation with other MADS-box proteins.

A marker was designed to distinguish between WT *cFUL* sequences (in the Oxford accession) and mutant *cFUL* in *val* plants. This marker utilises the introduction of a novel DdeI restriction endonuclease site into *cFUL,* caused by the cytosine to thymine mutation found in *val* plants. *cFUL* amplicons from both WT Oxford and Oligosperma accessions are not cleaved by the DdeI enzyme at this site, but *cFUL* amplicons from *val* are cleaved into two products (Figure 4.5A).

This marker was then analysed in *val* mutants from the F_2 mapping population. No mutants were identified that did not have the mutant *cFUL* allele. Whilst this is not definitive evidence that the *cFUL* mutation is responsible for the *val* phenotype, the cosegregation between *val* and a known valve-patterning transcription factor that contains a mutation that introduces a stop-codon at a conserved site (Figure 4.4D) strongly implicates mutation of *cFUL* as the underlying cause of the *val* phenotype.

To confirm that the cytosine to thymine mutation identified in *cFUL* is responsible for the *val* phenotype, complementation of the mutant, and/or phenocopy through *cFUL* knock-down needs to be accomplished. A single line of *AtFUL::FUL:GUS* was analysed in the *val* background, and no complementation was observed. However, this could be due to a number of technical reasons, discussed in the next section. In a further effort to complement *val*, I have transformed the original *AtFUL::FUL:GFP* construct into *val/+* heterozygotes. Additionally, my colleague H. Hofhuis has generated a genomic *cFUL* construct and has transformed these into *val/+* heterozygotes.

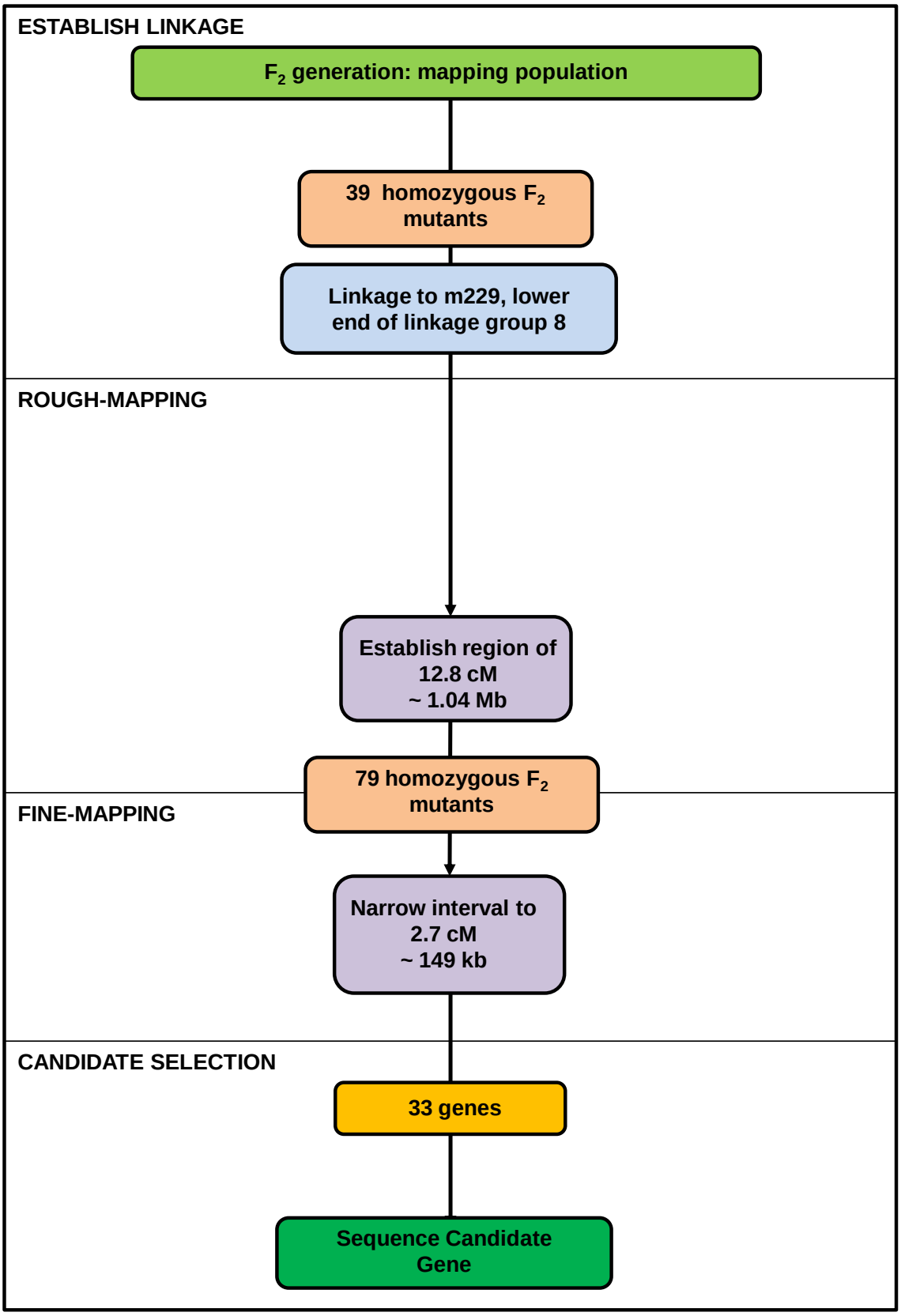

Figure 4.14 Procedure for mapping *val* in *C. hirsuta*. Physical distances are approximated from homologous region in *A. thaliana*.

4.3.2. *val* shows a conversion of valve to valve margin

val siliques appear to lack valve tissue, and instead a sunken, thin, semi-transparent region of valve margin tissue is flanked by enlarged repla (Figure 3.9 A to H). *val* siliques are indehiscent, and its seeds are narrow and cylindrical, in contrast to the flat, rounded, disc-shaped seeds of WT (Figure 3.9 I and L). The tissue that replaces valve in these mutants comprises small, undifferentiated cells, which contrast with the highly organised and differentiated cell layers of the WT valve (Figure 3.9 M-O).

SEM (Figure 4.6) and histological (Figure 4.7) analyses of developing carpels first detect morphological differences between WT and *val* as early as stage 10, when the replum starts to broaden and flatten in WT but cannot be distinguished in *val* (Figure 4.6 E and F). At stage 12, *val* mutants show less clear boundaries between replum and valve tissue than WT (Figure 4.7 G and H). These *val* phenotypes are comparable to *ful* tissues observed at the same stage in *A. thaliana* (Gu et al. 1998). Later in development, enlarged replum (Figure 4.7L) and an expanded style (Figure 4.6P) can be observed in *val* siliques, both phenotypes that are seen in some *A. thaliana ful* alleles (Ferrandiz et al. 2000; Roeder et al. 2003).

As is seen in *ful* mutants, *val* seeds are smaller than WT (Gu et al. 1998). In *val*, seeds adopt a narrower, less flattened shape, possibly as a consequence of seed-crowding within the narrower mutant silique (Figure 4.6R). DIC analysis of embryo development (Figure 4.8) in *val* mutants suggest that this altered seed shape does not reflect aberrant embryo development, and *val* embryos can be seen to develop normally until reaching the bent cotyledon stage, when the

hypocotyl often kinks, possibly due to the narrower, constricted size of *val* seeds (Figure 4.8R).

Expression of *AtIND::IND:GUS* in WT *C. hirsuta* plants clearly demarcates the valve margin tissues of the carpel from stage 12 onwards (Figure 4.9 A and C). This expression pattern implies regulatory conservation of *IND* expression between *A. thaliana* and *C. hirsuta* and allows *IND* expression to be used as a valve margin-specific marker (Liljegren et al. 2004). Expression of this construct in the *val* background is seen throughout the valve margin-like tissue that replaces the valve in these mutants (Figure 4.9 B and D). This expression pattern is the same as *IND* expression in *ful* mutants in *A. thaliana*, as seen by *in situ* hybridisation (Liljegren et al. 2004). This result can therefore be interpreted in two ways – either the valve tissue is wholly absent from *val* and has been replaced by valve margin tissue, or valve margin identity has spread into the valve, as is described in *ful* mutants (Liljegren et al. 2004).

Comparison of *val* and *ful-1* siliques reveals a number of morphological similarities and some differences (Figure 4.11). Both mutants possess expanded repla (Figure 4.11 L and M) and thin, aberrant tissue in place of WT valve (Figure 4.11 N and O). This aberrant tissue expresses *IND* in both mutants, indicating that it is of valve margin identity.

Within the repla, both mutants exhibit a spreading of lignification. *val* shows an over-proliferation of the large, circular cells that are particular to the *C. hirsuta* replum, a phenotype which bears some resemblance to the large, aberrant, rounded cells that are seen in the epidermis of the *ful-1* replum.

However, there are clear differences between the *ful-1* and *val* mutant fruit morphologies. The *ful-1* silique is severely stunted in length and has twisted repla

due to unequal growth of the valve and replum, and these phenotypes are not seen in *val*. Furthermore, the aberrant tissue between the repla is ectopically lignified, unlike the expanded valve margin tissue of the *val* mutants.

In quintuple *ind alc shp1 shp2 ful* mutants, the stunted growth and ectopic lignification seen in *ful-1* siliques is largely rescued (Liljegren et al. 2004). In these mutants, valve development is broadly restored, showing only minor defects in cell layer organisation. This result demonstrates that the conversion of valve to valve margin tissue in *ful-1* is not homeotic, and *ful-1* plants retain the ability to develop valve tissue.

Therefore, *val* and *ful-1* together suggest a different perspective from which to view the results of compromised *FUL*function in these siliques. Differences between WT and *val* gynoecium development are not detectable until stage 10 (Figure 4.6 E and F), and it is at a similar developmental stage when *FUL* expression becomes clearly visible in the flanking regions of the developing WT gynoecium. Prior to stage 10, however, the gynoecium already exists as a cylinder formed from medial and carpel tissues (Figure 4.7 A to D). Little difference is observed between WT and *val* during stages 7 to 9, suggesting that *FUL* expression around stage 10 is necessary not to specify the carpel tissues that flank gynoecium, but instead to direct differentiation of these carpel tissues from this stage onwards.

By stage 14 (Figure 4.7I), the carpels of WT fruits have differentiated into the distinct valve layers recogniseable throughout the rest of fruit development in *C. hirsuta*. These layers, however, fail to differentiate in *val* and cannot be identified at stage 14 (Figure 4.7J). Instead, the flanking regions of the *val* fruit show valve margin characteristics, developing as a thin tissue comprising layers of

lignified and non-lignified small rectangular cells (Figure 4.7N). These traits correlate with the expression of *IND* in this tissue in *val* (Figure 4.9).

These observations suggest that *FUL* directs the differentiation of the pre-existing carpel tissue in the gynoecium into the distinct layers of the valve tissue in the fruit. *ful* mutants in *A. thaliana* and *C. hirsuta* therefore show the differentiation of the entire gynoecium carpel tissue into fruit valve margin tissue, where normally *FUL* function restricts the differentiation of these small, rectangular cells to the edges of the carpel through the repression of *IND*.

Liljegren *et al.* (2004) describe the spreading of valve margin identity into the valve of *ful* mutants. Instead, the observations made in this chapter suggest that in *ful* mutants, the cells of the pre-existing carpel aberrantly differentiate into valve margin cells instead of valve cells. The carpel tissue that is necessary to form the fruit valve is present, but cannot be described as valve because it does not differentiate into the valve cell layers seen in WT. This hypothesis is illustrated in *C. hirsuta* in Figure 4.15.

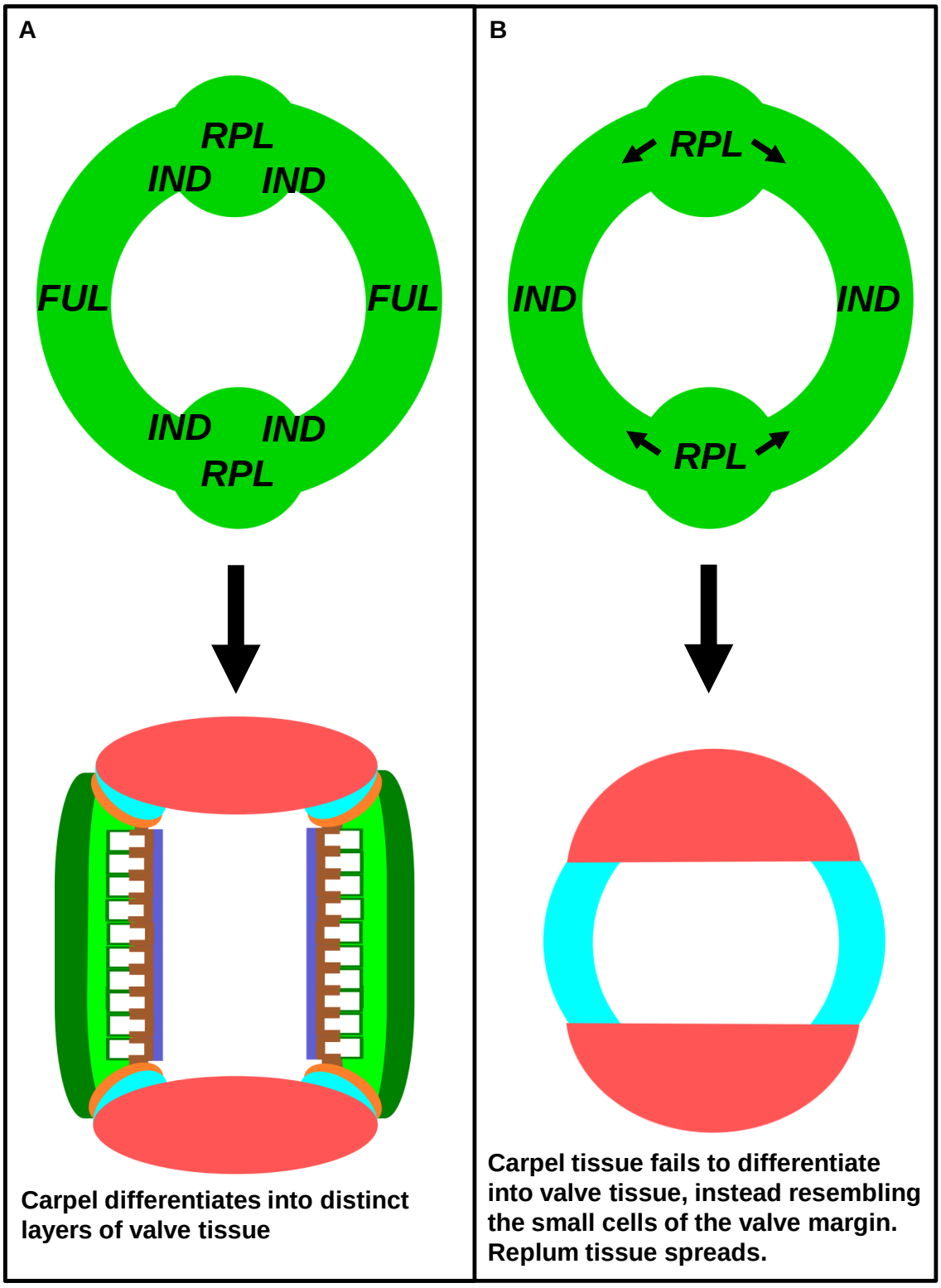

Figure 4.15 Developmental hypothesis for WT and *val*. Diagram showing predicted gene activity at stage 10 of gynoecium development, and resulting tissue phenotypes in WT (A) and *val* (B) at stage 17b.

4.3.3. Differing morphologies arising from compromised *FUL* function

Correct *FUL*function appears to be necessary in both *A. thaliana* and *C. hirsuta* to prevent the entire carpel wall tissue of the developing gynoecium from differentiating into valve margin tissue. This function of *FUL*, described in *A. thaliana* (Liljegren et al. 2004), fits perfectly with the observations of *val*made in this chapter. However, the null *ful-1* allele of *A. thaliana* differs from *val* in silique length, replum morphology, and lignification. There are several possible explanations for the differences observed between *ful* and *val* siliques.

4.3.3.1. Allelic morphs and severity in ful-1 *and* val*.*

A first, and likely, explanation for the differences between *ful-1* and *val* siliques is the severity of these two alleles. *ful-1* is a null allele, and expression of *FUL* is fully abolished in this mutant (Gu et al. 1998). From sequence analysis, however, the *cful* allele in *val* mutants is unlikely to be a null. Instead the FUL protein is truncated at the K-box (Figure 4.4D).

In *A. thaliana*, multiple *ful* alleles exist, and this allelic series in *A. thaliana* gives a gradient of *ful* phenotypes. The strongest alleles, *ful-1* and *ful-5*, produce siliques that have twisted repla and are severely stunted in length. The other alleles show less severe stunting of silique length, with the weak *ful-6* producing the longest silique (Ferrandiz et al. 2000). The intermediate *ful-4* allele shows reduced twisting of the replum, but its aberrant ‘valve’ cells remain small and unexpanded, like those of stronger mutants. In the weak *ful-6* allele, expansion of these cells is largely restored and differentiation of a dehiscence zone occurs (Ferrandiz et al. 2000).

From this allelic series, *ful-4* is the most comparable to *val*. The allele is mutated at the fifth exon-intron boundary, not far downstream from the site of the premature *FUL* stop codon in *val*. Like *val*, the siliques of *ful-4* are shorter than WT without being severely stunted, and the cells of the 'valve' region are small and unexpanded. However, whilst the replum of *ful-4* siliques is less severely distorted than in *ful-1* siliques, it still shows some twisting, unlike the replum in *val* mutants.

It is therefore plausible that the *val* fruit phenotypes are caused by a *ful* allele which, like *ful-4* in *A. thaliana*, is intermediate in strength, and that stronger *ful* alleles in *C. hirsuta* might more closely resemble the phenotypes seen in *ful-1*. To investigate this theory, *ful-4* siliques should be examined in cross-section, to determine whether the lignification phenotype of *ful-1* is absent in this mutant, as it is in *val*.

The *val* phenotype is recessive, and its failure to correctly differentiate valve is consistent with what would be expected from loss of *FUL* function. Compared with the strong phenotype of the null *ful-1*mutant, *val* appears to show a weaker loss of function phenotype, suggesting a hypomorphic allele and implying that the mutated cFUL protein still functions, albeit to a reduced extent, in *val* siliques. Quantitative reverse transcriptase PCR could be used to confirm that *cFUL* is still expressed in *val* siliques.

If *val* is a hypomorphic *cFUL* allele, we would expect the mutant cFUL transcription factor to be capable of dimerising with other MADS-box proteins and binding downstream target DNA sequences, but to a reduced extent. The fact that the MADS-box of the mutant cFUL protein is unaltered (Figure 4.4D) suggests that it retains the ability to bind to downstream target sequences.

The reduced function of the mutant cFUL protein is therefore likely the result of its truncated K-box, which could result in poorer dimerisation with partner transcription factors. Because the *A. thaliana* allelic series suggests that *val* is unlikely to be a null phenotype, this K-box must still be partially functional. Despite its truncated K-box, the mutant cFUL protein must, to some extent, still interact with other MADS-proteins, allowing some binding of downstream target sequences. However, this dimerisation is probably less effective and stable, resulting in reduced binding and a hypomorphic phenotype.

In addition to retaining some ability to dimerise with other MADS-proteins and bind DNA sequences, the mutant cFUL protein in *val* appears to dimerise with and bind to at least some of the same target proteins and DNA sequences as wild type. Were the mutant to bind new proteins and sequences, it would be expected to show dominant inheritance of neomorphic features, and this is not seen in *val* heterozygotes.

If the mutant cFUL protein was capable of binding the correct transcription factor partners and DNA sequences, but could not then correctly turn the expression of these genes on or off, we would expect to see a dominant negative phenotype, as the mutant cFUL would block the function of wild type cFUL in *val* heterozygotes. Because this is not seen, it is unlikely that the mutated *cful* allele in *val* plants is an antimorph.

The mutant *cful* allele seen in *val* therefore appears to be a recessive, loss-of-function, hypomorphic allele, and this could be the main reason underlying the differences in phenotype observed between *val* and the *A. thaliana* null mutant *ful-1*. To further test these hypotheses, a series of *C. hirsuta* mutant *ful* alleles are

needed. Such alleles could be generated by artificial microRNA-mediated knock-down, selected from a wider mutant screen, or identified in a TILLING population.

4.3.3.2. Differences in FUL *function.*

AtFUL::FUL:GUS did not rescue *val* (Figure 4.10). This result could be the consequence of biological or technical factors. Biologically, this finding could imply that the *A. thaliana FUL* gene is insufficient to rescue the *val* phenotype. This could either be due to the *val* phenotype being caused by a mutation in a different gene that is very tightly linked to *FUL*, or it could be due to divergences in *FUL* function between *A. thaliana* and *C. hirsuta*. The possibility that a different gene is responsible for the *val* phenotype could be tested by complementation. Chromatin immunoprecipitation-sequencing (ChIP-seq) could be used to test if *FUL* functions differently between the two species by identifying and comparing the direct targets of FUL in both species. Swapping genetic clones between the two species would also test this hypothesis.

Technical factors could instead explain the failure of *AtFUL::FUL:GUS* to complement *val*. Because the construct was transformed into WT *C. hirsuta* and then crossed into *val*, the data in Figure 4.10 represents only one insertion line. It is possible that had multiple independent *AtFUL::FUL:GUS* lines been generated in the *val* background, some of these would have shown complementation. It is also possible that the large β-glucoronidase C-terminal tag hindered the AtFUL protein from functioning fully.

To test which of these theories best explains the failure of *AtFUL::FUL:GUS* to complement *val*, I have transformed a population segregating *val* with the original *AtFUL::FUL:GFP* construct. This construct, which uses a GFP tag instead of the larger β-glucoronidase, may be better able to function, and in *A. thaliana* it

is capable of rescuing *ful-1* mutants (Urbanus et al. 2009). Transformation efficiency of *val* plants was very low in my hands, so by transforming a segregating population, *val* plants expressing the transgenic construct can be identified in higher numbers amongst the progeny of the transformed *val/+* heterozygotes. This should provide a large enough number of independent lines to investigate the ability of this *A. thaliana* construct to complement *val*.

4.3.3.3. Species-specific differences in IND expression or IND function

In *A. thaliana*, *FUL* acts largely through *IND* to repress valve margin identity in the valve. In *A. thaliana*, the *ful-1 ind* double mutant shows a large degree of rescue (Liljegren et al. 2004). Whilst the siliques are not as long as WT, their length is significantly less stunted than siliques of the *ful-1* single mutant. Furthermore, valve tissue is largely restored in this mutant, showing valve cell expansion, endocarp *b* formation, and no ectopic lignification. These findings show that expanded *IND* expression is responsible for a large proportion of the *ful-1* phenotypes.

AtIND::IND:GUS is expressed in *val* as in *ful*, indicating that FUL functions to repress IND in *C. hirsuta* in the same manner as in *A. thaliana*. However, *val* siliques differ from *ful-1* in their length, as well as in not ectopically lignifying the expanded valve margin tissue. Because these phenotypes are dependent on IND function in *A. thaliana*, alterations in *IND* function in *C. hirsuta* could explain the *val* phenotype. For example, the IND protein in *C. hirsuta* may function differently, activating different downstream target genes.

To test this, the phenotypes of *A. thaliana IND* and *C. hirsuta IND,* driven in WT *A. thaliana* using the *A. thaliana FUL* promoter, could be compared. Expression of *aIND* in the *A.thaliana* valve should mimic the *A. thaliana ful*

phenotype. Whether expression of *cIND* in the *A. thaliana* valve also produces this same, *A. thaliana ful*-like phenotype, or whether it results in a *C. hirsuta val*-like phenotype, will help determine the extent to which divergent *IND* function is involved in the different *ful* phenotypes observed between these species in this chapter.

This could be further investigated using comparative ChIP-seq between the two species to investigate conservation or divergence of IND target genes. Furthermore, the isolation of *ind* mutants or generation of *ind* loss of function alleles in *C. hirsuta* would be useful for investigating conservation or divergence of IND function and for determining the contribution of *IND* to the mutant phenotype seen in *val*. IND alleles may be identified as suppressors in an EMS-mutagenised *val* population that is currently being screened for suppressors and enhancers of the *val* mutant phenotype.

4.3.3.4. Differences in WT fruit structure.

A final explanation for the phenotypic differences between *ful-1* and *val* could be the different silique morphologies found in *A. thaliana* and *C. hirsuta*. Compared with *C. hirsuta*, the *A. thaliana* replum is round and narrow. The *C. hirsuta* replum, however, is much broader and constitutes a larger proportion of the total fruit tissue. Spanning this larger replum is a thick bridge of strengthened, lignified cells. In strong *A. thaliana ful* mutants, the failure of valve cells to expand stunts silique growth, forcing the replum to double-back on itself, forming the twisted, bumpy replum seen in *ful-1* fruits (Gu et al. 1998). However, the replum is broader and more heavily strengthened with lignin in *C. hirsuta*. This stiffened morphology could be harder to distort, which might explain why the replum is not twisted in *val* siliques.

4.3.4. Genetic effects on silique morphology

Analysis of the *val* mutant reveals that correct *FUL* function is necessary to pattern the explosive fruit of *C. hirsuta*. In the absence of a fully functional FUL protein, the carpel tissue fails to differentiate into the organised and distinctive cell layers identifiable in the wild-type *C. hirsuta* valve. The failure of the aberrant, valve margin-like tissue that differentiates instead to curl outwards and upwards at maturity shows that the *C. hirsuta* fruit cannot open explosive unless the carpel tissues correctly differentiate into the correct cell types of the WT valve (Figure 4.16).

As well as failing to open explosively, *val* mutants also produce smaller, narrower seeds (Figure 4.6S). Analysis of cleared *val* seeds suggests, however, that this phenotype does not arise from aberrant embryo development (Figure 4.8). Instead, the *val* embryo appears to develop normally, until it starts to be constrained by the narrow shape of the mutant seed.

The seed phenotype seen in *val* mutants could therefore arise as a result of the shape of the *val* silique. In transverse section, the mature *val* silique shows an expanded, curved replum, and a reduction in size of the flanking carpel tissue (Figure 4.7L). These siliques are noticeably thinner than WT (Figure 3.9B), and, inside these fruits, their locules are narrower, and reduced in size (Figure 4.7L). The reduced size of the *val* locule could therefore be responsible for limiting the size and shape of the mutant's seeds, as there is not sufficient space for *val* mutants to grow the flat, round, disc-shaped seeds seen in WT (Figure 4.16).

This hypothesis suggests that the broad replum and flattened valve of WT *C. hirsuta* play a role in allowing its large, disc-shaped seeds to develop. This hypothesis fits the observation in Chapter 3 that in the Brassicacean species

examined, large, flat, disc-shaped seeds correlated with flatter valves in *C. hirsuta, C. corymbosa,* and *A. lyrata* (Figure 3.6).

Analysis of the replum morphology of the *val* mutant, alongside *cas1*, *cbp*, and double mutant combinations, allowed investigation of the antagonistic model of replum versus valve patterning that has been proposed in *A. thaliana* (Alonso-Cantabrana et al. 2007).

As in *A. thaliana*, some common regulatory modules were found to pattern both leaf and fruit development in *C. hirsuta*. In both species, reduced *AS1* or *FUL* function leads to an expansion of the replum (Roeder et al. 2003; Alonso-Cantabrana et al. 2007), and double *as1 ful* mutants show extreme replum expansion (Alonso-Cantabrana et al. 2007) (Figure 4.12H). Similarly, in both species the combined loss of *AS1* and *FUL* function results in a wider replum than is seen in either single mutant (Figure 4.12H). Comparisons of replum width between WT and *cas1*, and between *val* and *cas1 val*, show a similar fold-increase, which suggests that the particularly widened replum of *cas1 val* mutants is the additive effect of the two combined alleles (Figure 4.12I).

Whilst the *cbp* replum is not significantly different in size from WT (Figure 4.12H), reduced *BP* expression in both in both *A. thaliana* and *C. hirsuta* can partially rescue the *as1* replum phenotype (Alonso-Cantabrana et al. 2007) (Figure 4.12I). However, when combined with *val*, the *cbp val* mutant has a larger replum than *val*, which is significant at the 90%, but not the 95%, level (P-value 0.0594, one-tailed Student's T-test, assumed unequal variance). This result contrasts with *cas1 bp* mutants, in which loss of *BP* function results in partial rescue of the expanded replum phenotype of *cas1* (Figure 4.6H). This suggests that, whilst *BP* overexpression is partially responsible for the replum phenotype of *cas1*, this is

not the case in *val* mutants, where loss of *BP* function appears to result in wider, rather than thinner, repla. *bp ful* double mutants have not been described in *A. thaliana*.

Analysis of *val, cas1* and *cbp* mutant combinations confirms that, as in *A. thaliana*, interactions between *FUL, AS1* and *BP* help pattern replum versus valve development in the silique. However, the broader replum phenotype seen in *cas1* siliques did not have any noticeable affect on the explosive opening mechanism of *C. hirsuta*, indicating that, alone, *AS1* and *BP* function are not of strong importance for patterning the explosive morphology of *C. hirsuta*.

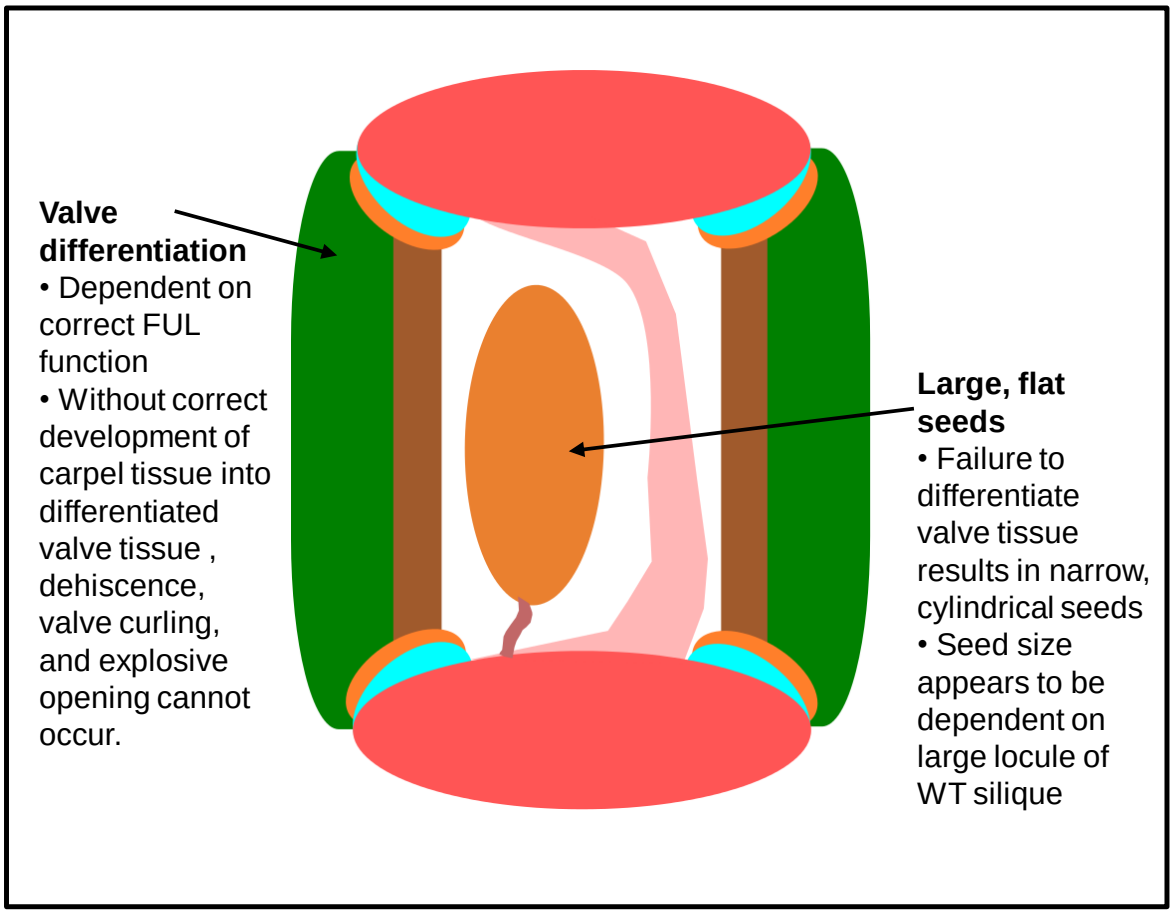

Figure 4.16 Diagram showing functions of silique features that are implied by the *val* mutant.

4.3.5. Evaluation of *C. hirsuta* genetic screen

Of the six dehiscence patterning genes identified in *A. thaliana*, only one mutant allele of *cFUL* was isolated in the EMS screen. Due to the thorough use of three screening methods – visual inspection, lignin staining, and screening for indehiscence – it seems unlikely that mutant alleles in these genes were simply undetected by the screen. The isolation of *cbp*, which shares similarities with *rpl* mutants in *A. thaliana*, suggests that had a loss of function mutation in *cRPL* occurred, it would probably have been detected.

The failure to identify any *cRPL* alleles amongst the mutant population likely stems from the number of plants screened. In *A. thaliana*, roughly 125 000 or more M_1 plants are thought to be needed for a saturation EMS mutagenesis (Haughn & Somerville 1987). Flow cytometry indicates that the *C. hirsuta* genome is 1.2 times as large as the *A. thaliana* genome. Factoring-in this increased genome size, we might expect approximately 150 000 M_1 plants to be needed for a saturation mutagenesis in *C. hirsuta*. In this mutagenesis, only 1004 M_1 seeds were planted, of which only 895 were fertile. Furthermore, the mutation rate in this mutagenesis may have been lower than is typically seen in a saturation mutagenesis in *A. thaliana*. Whilst the concentrations of EMS used (0.18% and 0.3%) are similar to the 0.2% concentration used by Jander *et al.* (2003) in their saturation mutagenesis, the incubation time was much shorter, with seeds being exposed to EMS for only 10 hours instead of 16 (Jander et al. 2003).

Jander *et al.* (2003) found that 45 000 M_1 lines were needed to have a 95% likelihood of mutating every GC basepair (Jander et al. 2003). Accounting for increased genome size, this might be expected to be around 54 000 M_1 lines in *C. hirsuta*. The number of M_1 lines screened in this mutagenesis therefore represent

approximately 1.7% of the number that would be needed to mutagenise every possible site with the same certainty. Furthermore, if, like *A. lyrata*, *C. hirsuta* has an increased GC content, this would further increase the number of plants that would need to be screened to be 95% certain of screening every possible GC basepair.

As well as due to the design of the mutant screen, the *A. thaliana* patterning genes which specify valve margin may not have been identified in this screen due to species-specific reasons. Due to its close similarity with *A. thaliana*, we can probably expect the *C. hirsuta SHP* genes to function redundantly, meaning that mutations in only one of the genes will not result in a mutant phenotype. In the case of *IND* and *ALC*, however, it is perhaps possible that the loss of function of either of these genes would not have had as large a phenotypic impact in *C. hirsuta* as they do in *A. thaliana.* Whilst silique opening in *A. thaliana* depends on the correct patterning of lignin in the dehiscence zone, in *C. hirsuta* the sudden and forceful outward curling of the valve, initiated at the silique base, might be of primary importance. It is conceivable that this curling is so forceful that it would lead to ripping along the narrower valve margin layer during silique opening, even if it was incorrectly lignified.

A further reason for why many fruit patterning genes were not identified in this screen is that more sophisticated screens were used to identify many of these genes in *A. thaliana*. Out of the genes which pattern the dehiscence zone of *A. thaliana*, only *IND* was identified by a simple, forward genetics EMS screen (Liljegren et al. 2000; Liljegren et al. 2004). *FUL* and *ALC* were both identified in screens of enhancer or gene trap lines (Gu et al. 1998; Rajani & Sundaresan 2001) and *RPL* was identified in a secondary screen conducted in the *ful* mutant

background (Roeder et al. 2003). *SHP1* and *SHP2* were the targets of reverse genetics methods – *shp1* mutants were screened for by PCR in a T-DNA insertional collection, whilst *SHP2* was targeted for knock-out using homologous recombination (Kempin et al. 1997; Liljegren et al. 2000). The identification of similarly important genes in *C. hirsuta* will therefore likely require a combination of genetic approaches. A suppressor screen is currenly being conducted (by H. Hofhuis) in the *val* mutant background, and TILLING may provide an opportunity to directly identify mutant alleles of specific genes of interest.

5. Cell layers of the *C. hirsuta* silique

5.1. Introduction

Comparative characterisation of the *C. hirsuta* and *A. thaliana* siliques reveals that, despite their contrasting dehiscence mechanisms, the explosive opening of *C. hirsuta* is not facilitated by any novel or dramatically altered structural features. The gross structural organisation of the two siliques remain remarkably similar.

However, within this shared organisation, some morphological features show smaller differences. Comparison of the *C. hirsuta* silique with other Brassicacean relatives implicates possible roles in explosive opening for *C. hirsuta*'s broader replum, flatter valves, and increased lignin deposition. In Chapter 3, studies of other Brassicacean fruits found that broader repla may correlate with valve curling, and flatter valves with larger seeds. Given the force-generating role ascribed to lignin in the model for silique dehiscence in *A. thaliana*, it seems likely that the increased lignin deposition observed in the *C. hirsuta* silique in Chapter 3 is important for its explosive opening force.

However, mutant analyses hint at the limited importance of these features in the *C. hirsuta* explosive opening mechanism. As discussed in Chapter 3, the valves of the *lig1* mutant did not lignify as wild type, and yet they were still capable of opening and curling explosively, although this does appear to have been delayed, and of slightly reduced speed and force. The analysis of replum-patterning mutant combinations in Chapter 4 revealed no effect on *C. hirsuta* dehiscence. Were replum width a key factor of central importance to the *C. hirsuta* explosive mechanism, it would be expected that the further increase in replum

width seen in *cas1* mutants would in some way perturb this mechanism, but no such effect was seen.

The only *C. hirsuta* mutant discovered whose dehiscence is severely affected is *val*. As described in Chapter 4, this mutant fails to correctly differentiate carpel wall tissue into the highly organised layers of the *C. hirsuta* valve. Unlike any other *C. hirsuta* fruit mutant identified, the altered morphology of *val* siliques renders them indehiscent, implicating the valve and its correctly differentiated layers as of central importance to explosive opening of the *C. hirsuta* silique.

5.1.1. Proposed roles of valve cell layers in *Cardamine* dehiscence

Previous studies of *Cardamine* siliques have suggested that the differing behaviours of valve cell layers within the silique are responsible for driving the explosive opening of the silique. Hayashi *et al.* proposed that the innermost endocarp *a* layer in *C. parviflora* is mucilaginous, so absorbs water and becomes swollen (Hayashi et al. 2010). They suggest that the lignified endocarp *b* layer, which sits above the endocarp *a*, is rigid and compresses the swollen endocarp *a*, until dehiscence occurs along the valve margin. They propose that when this happens, the mucilaginous layer suddenly expands, resulting in explosive outward curling of the valve. A layer of water between the endocarp *a* and the seeds is hypothesised as the agent through which energy is imparted to the seeds, resulting in their ballistic dispersal.

In their study of *C. hirsuta*, Vaughn *et al.* hypothesised that the shrinking of the middle cell layers of the valve generates the explosive force for silique opening, whilst the U-shaped lignification of the endocarp *b* cells ensures that the valve curls outwards rather than inwards (Vaughn et al. 2011). They suggested

that the endocarp *a* layer traps mucilage between itself and the endocarp *b* layer, keeping the endocarp *b* cells moist in order to maintain the flexibility of these cells or to hold them together whilst the rest of the valve dries.

In this chapter, the role of these cell layers in the explosive dehiscence mechanism of *C. hirsuta* is examined further. This includes an investigation of the endocarp *a* layer as a possible secretor of mucilage, based upon previous studies of mucilage secretion in *A. thaliana*.

5.1.2. Mucilage secretion by the A. thaliana seed epidermis

In *A. thaliana*, mucilage synthesis, its composition, its secretion, and its genetic regulation, has been well studied, particularly with reference to the seed epidermis (Haughn & Chaudhury 2005; Western 2006; Haughn & Western 2012). The seed epidermis is a single cell layer that produces a large quantity of mucilage, a thick and viscous substance high in complex polysaccharides like pectin. The role of this mucilage is unknown and it is not extruded from the seed epidermal layer unless the seed is immersed or “imbibed” in water.

The seed epidermis therefore forms a useful case study for cell layers that are specialised for mucilage production and secretion. Studies of this layer have histologically characterised the cellular changes that accompany mucilage production (Western et al. 2000; Western et al. 2001; Arsovski et al. 2009). Seed sections visualised either by transmission electron microscopy or with the histological stains toluidine blue O or ruthenium red reveal the presence of the starch-processing organelles amyloplasts in the seed epidermis layer. These amyloplasts appear to be associated with mucilage production within these cells. A large vacuole can be seen to occupy most of the cell volume and toluidine blue

O staining shows that the mucilage, which stains pink, accumulates within these vacuoles.

As the epidermis matures, a second cell wall is built within the epidermal cells. This wall is laid down around a remaining column of cytoplasm named the columella. The original, outermost cell wall later degrades, exposing mucilage which wells in the troughs of the thickened, now exposed columellae.

5.2. Results

5.2.1. *C. hirsuta* shows increased and polar silique lignin deposition

A range of techniques were used to further examine lignin deposition in the silique, focussing on the differences in *A. thaliana* and *C. hirsuta* lignin content and on *C. hirsuta* endocarp *b* lignification (Figure 5.1). Phloroglucinol can be used to stain lignin pink in whole-mount preparations (Figure 5.1 A and B). Whole-mount staining of fresh *A. thaliana* and *C. hirsuta* siliques reveals a stark difference in phloroglucinol staining intensity. Whilst pink stripes along the valve margins and repla of the *A. thaliana* fruit reflect lignification of the dehiscence zone, the entire *C. hirsuta* silique stained strongly pink. This suggests an increased deposition of lignin in *C. hirsuta* siliques.

Lignin extraction assays (conducted by A. Hay) were used to quantify this difference and revealed an increased proportion of lignin per gram of dry weight silique tissue in the *C. hirsuta* silique (Figure 5.1C). A one-tailed Student's t-Test (equal variance) gave a P-value of 0.005, showing that the increase in lignin content per gram dry weight in *C. hirsuta* is highly significant, at higher than the 99% level. However, whilst there is a significant difference in the amount of lignin deposited in *C. hirsuta* and *A. thaliana* siliques, this difference is not as large as

might have been expected. Despite the intense pink phloroglucinol staining seen in the *C. hirsuta* valve, the mean difference in lignin content between *C. hirsuta* and *A. thaliana* siliques is only 9.39 mg of lignin per gram of silique dry weight. It is possible that the increased staining of *C. hirsuta* siliques is partly an optical effect, arising due to the flatter structure of its valves.

Confocal scanning laser microscopy was used to visualise secondary wall thickening of the *C. hirsuta* endocarp *b* layer and its subsequent lignification (Figure 5.1D to M). Five successive siliques throughout stage 17 were fresh-sectioned using a cryotome. Calcofluor white was used to visualise the cellulose deposited during secondary wall thickening in these transverse sections, and lignin could be visualised by its autofluorescence. Because the lignin autoflurorescence emission spectrum overlaps with that of calcofluor white, the five siliques were first imaged only for lignin autofluorescence (green). A calcofluor white solution was then floated under the coverslip of each of these sections, which were then scanned again. Comparison of the first (Figure 5.1 D to H) and second images (Figure 5.1 I to M) across the five siliques allowed comparison of lignin and cellulose deposition throughout time. Cellulose was observed earlier than lignin, as one would expect to see in secondary wall formation, and lignin was subsequently deposited in the same pattern as the cellulose thickenings. Both cellulose and lignin deposition began as a flat U-shape at the abaxial end of the endocarp *b* cell, and this U-shape then subsequently thickened inwards.

This pattern of lignin deposition can be seen in greater detail in TBO-stained plastic sections of consecutive siliques from stage 17 (Figure 5.1N to S). The lignin, staining light blue, begins as a thin U-shape, which thickens inwards

throughout stage 17. By late stage 17b, lignification of the endocarp *b* cell has formed a tri-partite cap at the abaxial end of the cell.

Transmission electron microscopy (TEM), conducted by H. Dickinson, showed that this lignified endocarp *b* cell-cap is striated, suggesting the layers in which the lignin polymer is laid down within the cell (Figure 5.1T). TEM also indicated that by stage 17b, the endocarp *b* cells may have largely died, as no live cellular contents were observed. In the sections examined, plasma membranes that were oppressed to the cell walls were not observed, indicating that these cells have become dead, hollow tubes.

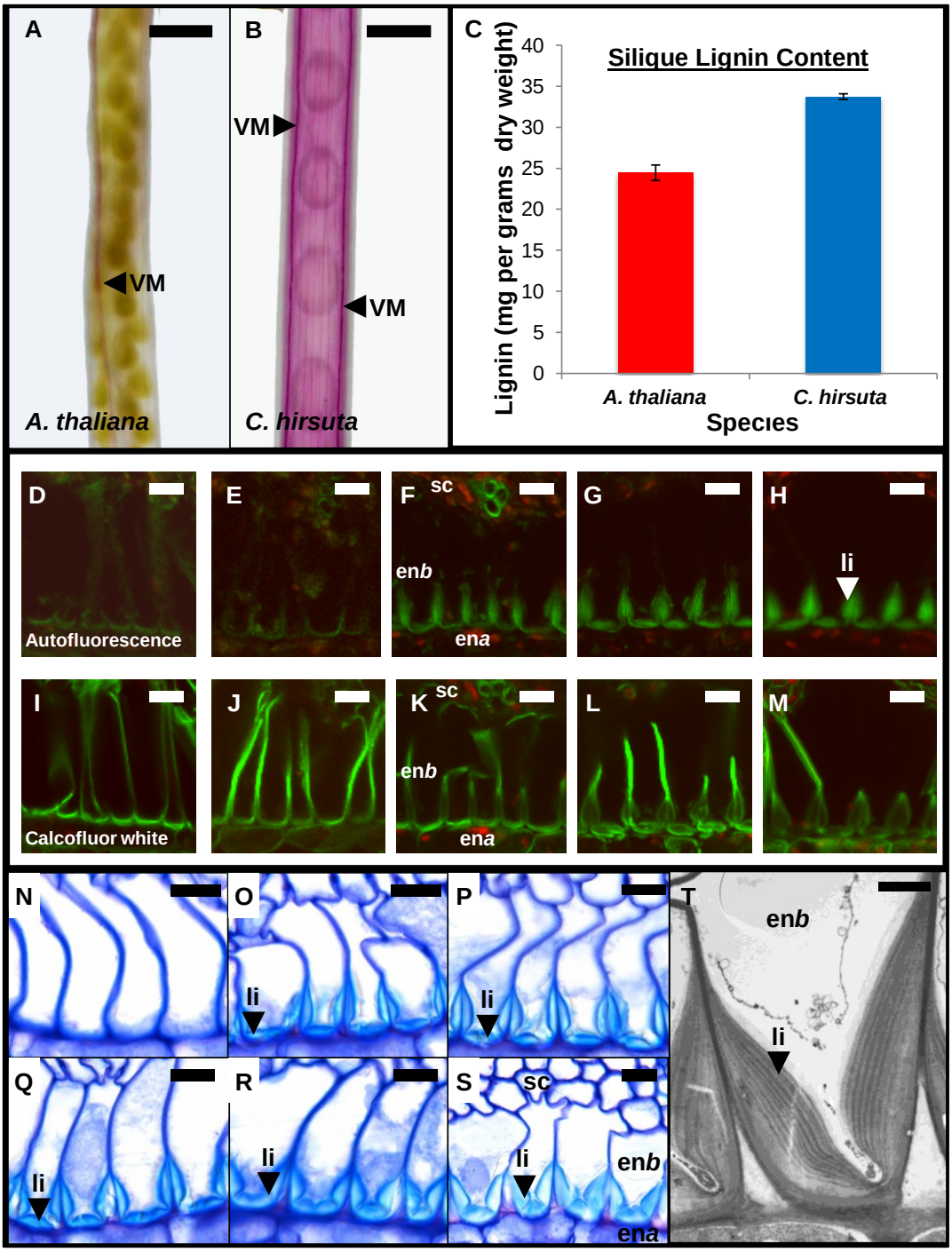

Figure 5.1 Lignin deposition in the *C. hirsuta* silique. Whole-mount phloroglucinol staining of lignin (pink) in *A. thaliana* (A) and *C. hirsuta* (B) siliques. VM indicates valve margin. Bar represents 1 mm. (C) Lignin extraction assay comparing quantity of lignin per dry weight in two species. Error bars show standard error. (D) to (T) show *C. hirsuta* in transverse section. (D) to (M) Confocal laser scanning microscopy of endocarp *b* layer. (D) to (H) show autoflourescence (green) of lignin in siliques throughout stage 17. (I) to (M) show calcofluor white staining of cellulose (green) of the corresponding siliques above. Bar represents 10 µm. (N) to (S) TBO staining illustrating progressive lignin deposition throughout stage 17. Bar represents 10 µm. (T) TEM of endocarp *b* cell, showing striations in secondary thickening, by H. Dickinson. Bar represents 2 µm. li, sc, en*b* and en*a* indicate position of lignin, sclerenchyma, endocarp *b* and endocarp *a*.

5.2.2. *C. hirsuta* valve cell layers

Comparison of the *A. thaliana* and *C. hirsuta* valve cell layers reveals a number of differences (Figure 5.2 A and B). Not only is the valve of *C. hirsuta* flatter, it is thicker. At maturity, the *A. thaliana* valve comprises a one-cell thick outer layer of exocarp, a three-cell thick layer of mesocarp, a thin layer of lignified endocarp *b* cells, and a degraded, innermost endocarp *a* layer. In total, the *A. thaliana* valve is 6 cells thick.

In contrast, the *C. hirsuta* valve is 9 to 10 cells thick. Like *A. thaliana*, it comprises an outer exocarp layer, and a three-cell thick mesocarp layer. Beneath this mesocarp layer, however, lies an additional, four-cell thick layer. Compared with the cuboidal cells of the mesocarp layer, this layer comprises more irregularly shaped cells which are small in transverse section and long and thin when viewed longitudinally. Unlike the *C. hirsuta* mesocarp cells, this sclerenchyma-like layer lacks chloroplasts and contains vascular bundles.

The *C. hirsuta* endocarp layers show stark differences with those of *A. thaliana*, in both its *a* and *b* layers. These characters – massive radial enlargement of the endocarp *b* cells, thicker and polar lignification of the endocarp *b,* and retention of the endocarp *a* layer to maturity – are of interest for their possible roles in explosive seed dispersal in *C. hirsuta*. To further investigate how these characters develop and mature, 13 successive siliques from the same plant, spanning from stage 14 to stage 17b, were fixed for plastic sectioning and TBO staining. Whole transverse sections of these siliques are shown in Figure 5.2 (panels I to T) and illustrate the radial enlargement seen during silique maturation.

Figure 5.2 Valve layers, and successive siliques from a single *C. hirsuta* plant. Grey bar represents 1 mm, white bar represents 50 mm, black bar represents 100 µm. Valve cell layers of *A. thaliana* (A) and *C. hirsuta* (B). ex = exocarp, me = mesocarp, sc = sclerenchyma-like layer, en*b* = endocarp *b*, en*a* = endocarp *a*, li = lignin. (C) to (H) Photographs illustrating stages of fruit development prior to yellowing and dehiscence. (I) to (T) TBO-stained transverse sections of successive siliques. Round brackets indicate developmental stage, square brackets indicate order of siliques. Silique 11 showed stunted growth and was excluded.

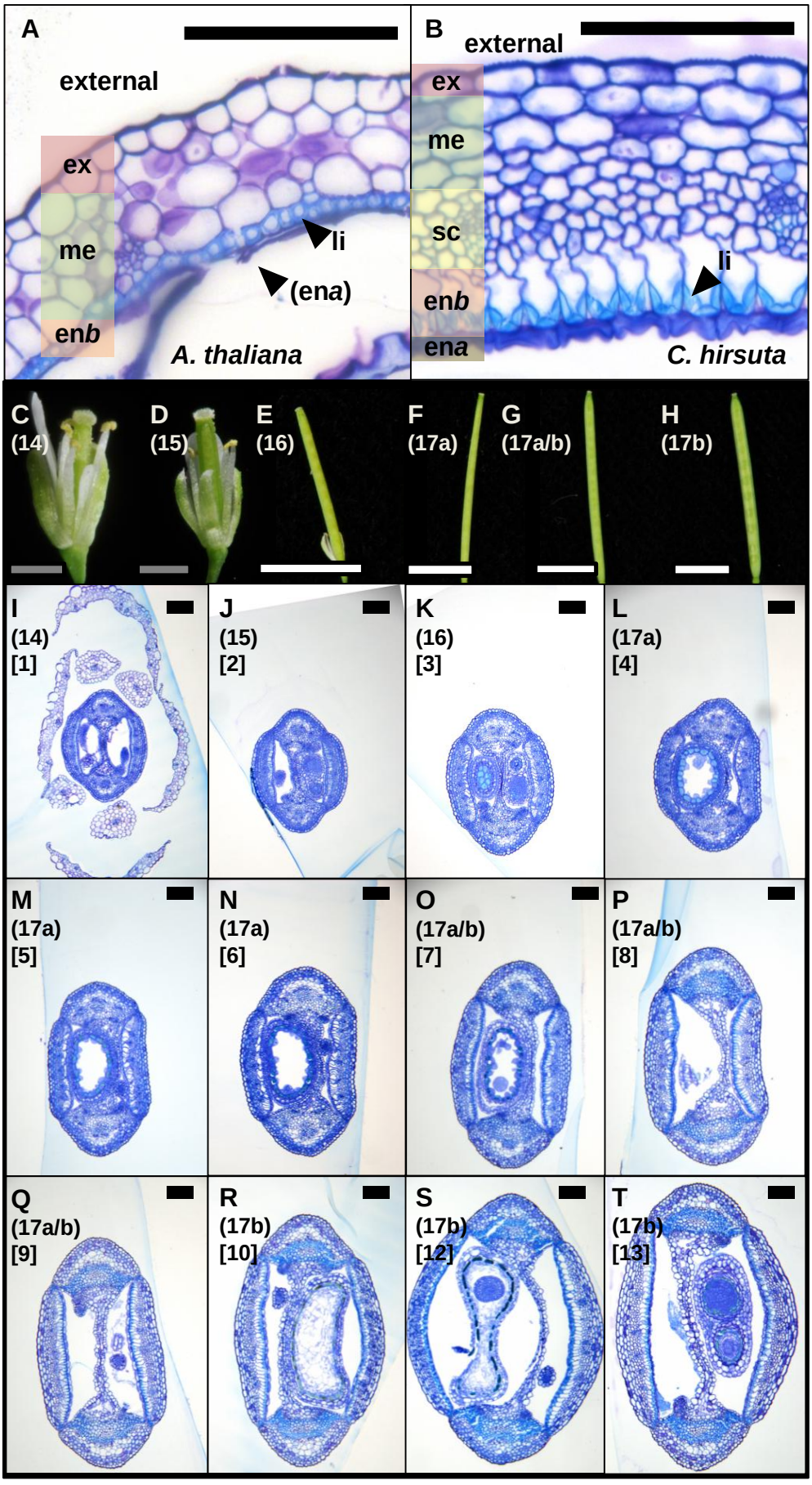
A
external
ex
me
enb
li
(ena)
A. thaliana
B
external
ex
me
sc
enb
ena
li
C. hirsuta
C
(14)
D
(15)
E
(16)
F
(17a)
G
(17a/b)
H
(17b)
I
(14)
[1]
J
(15)
[2]
K
(16)
[3]
L
(17a)
[4]
M
(17a)
[5]
N
(17a)
[6]
O
(17a/b)
[7]
P
(17a/b)
[8]
Q
(17a/b)
[9]
R
(17b)
[10]
S
(17b)
[12]
T
(17b)
[13]

5.2.3. *C. hirsuta* endocarp *b* maturation

Examination of the valves of the successive siliques shown in Figure 5.2 gives an insight into endocarp *b* growth and maturation from stage 14 to maturity (Figure 5.3). Comparison of the first 6 siliques (stage 14 – stage 17a, Figure 5.3 A to F) reveals a rapid increase in endocarp *b* cell size during these stages, which coincides with the longitudinal elongation of the fruit that occurs up until stage 17. However, the mesocarp, sclerenchyma, and exocarp layers enlarge only slightly throughout this time, highlighting a focussed and marked growth of these endocarp *b* cells during this period.

After this first phase of endocarp *b* maturation, a second phase occurs – that of lignification – across the following siliques. Lignin in the endocarp *b* is first observable at the start of the stage 17a/b transition (Figure 5.3G), and lignification inwards of the abaxial cap of the endocarp *b* cell continues throughout this transition and into stage 17b. This two-phase pattern of enlargement followed by lignification is consistent with our understanding that cells become inflexible, are unable to grow, and begin to die after lignification. The endocarp *b* appears to therefore undergo rapid enlargement prior to lignification and subsequent cell death.

During this phase of endocarp *b* maturation, the exocarp, mesocarp and schelrenchyma cells appear to expand slightly in size. This observed expansion is likely to build tension against the already enlarged endocarp *b* cells, which cannot expand further and are becoming rigid through lignification at this stage.

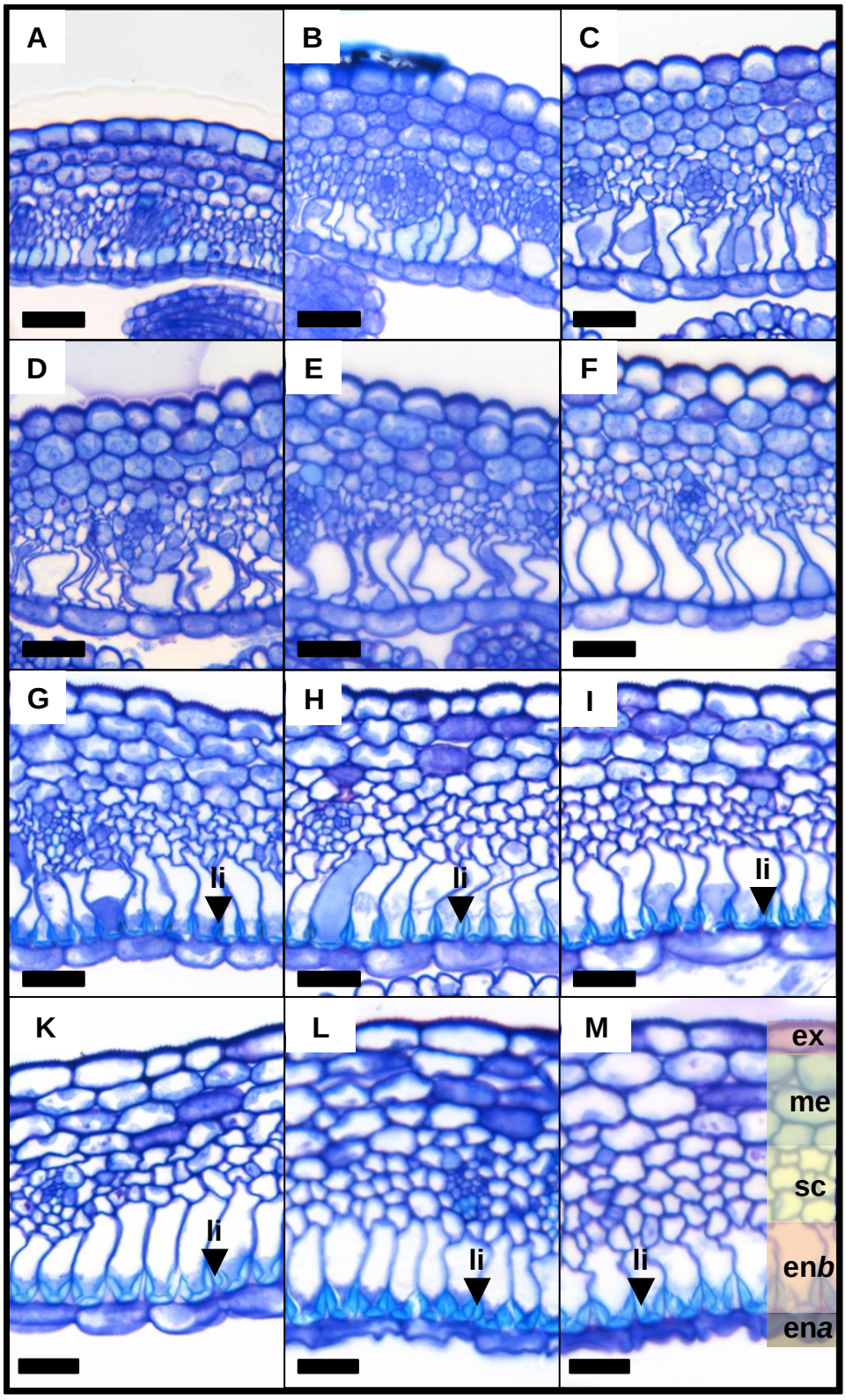

Figure 5.3 Endocarp *b* expansion from stage 14 to 17. TBO-stained transverse sections of successive siliques, from stage 14 (A) to 17b (K to M). ex, me, sc, en*b* and en*a* indicate exocarp, mesocarp, sclerenchyma, endocarp *b* and endocarp *a* layers. li indicates lignin deposition in endocarp *b* cells. Bar represents 25 µm.

The maturation of the endocarp *b* cells was further characterised using image analysis software to measure cell sizes in the sections taken from this silique series. ImagePro was used to measure the two-dimensional area of endocarp *b* cells in transverse sections. To minimise the impact of measurement errors resulting from the fixation and processing of tissue and any software calculation inaccuracies, 5 sections were measured per silique. These cell area measurements were then added together to form a total data series for each silique. The range of endocarp *b* cell area measurements can be seen in Figure 5.4A. These boxplots reveal that the endocarp *b* cells can exhibit a wide range of cell areas within one silique, particularly in siliques 12 and 13, which were at stage 17b.

However, this range of endocarp *b* areas is much reduced in the earlier stages, 14 and 15. The endocarp *b* cells which are closest to the valve margin are constrained in size by their position. To minimise the influence of these cells on the calculation of the mean endocarp *b* cell area, the lower quartile of cell measurements were removed from each silique's data series before constructing Figure 5.4B. This bar chart shows that there is a sudden increase in the mean endocarp *b* cell area between stages 15 and 16, revealing that the most marked period of endocarp *b* enlargement occurs during the main phase of apical-basal growth of the gynoecium out of the floral bud.

Both the boxplots and bar charts in Figure 5.4 show that after this rapid enlargement of endocarp *b* cells the mean endocarp *b* cell area does not change drastically. Figure 5.4B shows that the mean cell area continues to increase moderately into stage 17b. The interquartile regions in Figure 5.4A, however,

show a large degree of overlap from stage 16 onwards, suggesting a statistical degree of similarity.

It is important to note the statistical limitations of Figure 5.4. Because 13 consecutive siliques were taken from a single plant, it was not possible to include biological replicates of each silique. Whilst five sections were analysed for each silique, this will only have reduced measurement error, without having any affect upon biological noise or variation. Therefore the data displayed in Figure 5.4 represent an accurate analysis of a single silique series from one individual *C. hirsuta* plant. We can use this to discuss the growth patterns seen in this one individual, but must be cautious about applying our conclusions with statistical confidence to all *C. hirsuta* siliques.

One limitation of this method is highlighted by silique 12. In Figure 5.4Q, this silique can be seen to have rounder valves than the siliques preceding and following it. This silique seems either to have grown slightly abnormally or to have suffered some distortion during fixation and embedding in plastic. This could account for this silique's potentially anomalous data in Figure 5.4, where the endocarp *b* measurements from this silique appear to be too high and do not fit in with the general trends seen in these graphs. The biological variation or fixation error behind this could not be removed or minimised statistically because there is only one biological (and experimental) replicate for each successive silique in the series.

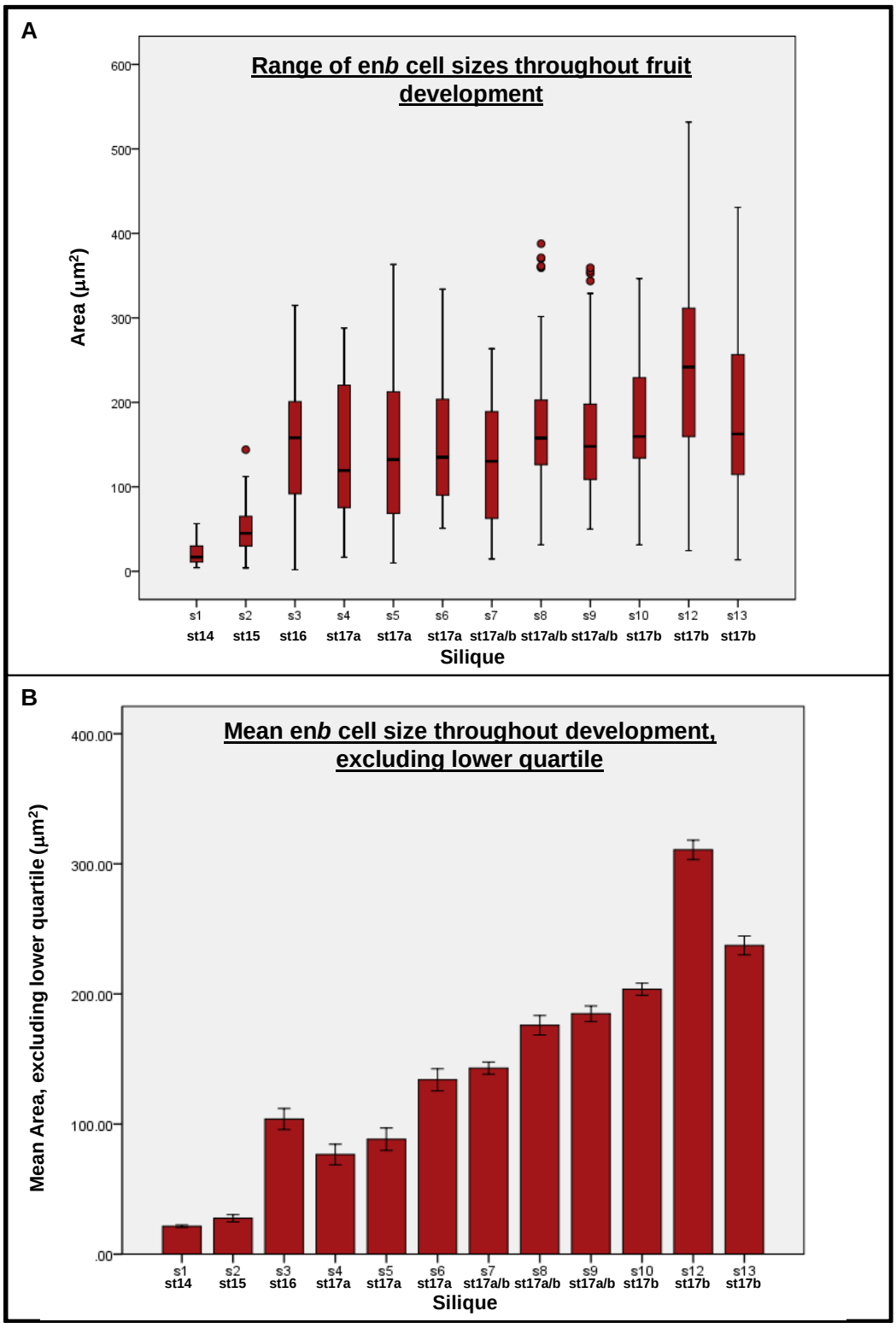

Figure 5.4 Expansion in endocarp *b* cell size throughout successive siliques. (A) Boxplots showing the range of cell sizes seen. Boxes show interquartile range, black bar indicates mean and circles represent outliers. (B) Bar chart of mean endocarp *b* cell sizes, excluding the lower quartile (which contains cells constrained in size due to proximity to valve margin). n ranged from 89 to 209. Number in silique sequence (s) and developmental stage (st) indicated on x-axis.

The data summarised in Figure 5.4 were taken from only one of the two valves of each silique. It was found that when lying directly adjacent to a seed, the area of the valve endocarp *b* cells were constrained, distorting the data. For Figure 5.4, therefore, endocarp *b* measurements were taken only from valves not immediately adjacent to a seed.

The effect of seed position on endocarp *b* size and shape is described in Figure 5.5. Longitudinal silique sections (Figure 5.5A) show that seeds are positioned down the silique on alternating sides of the septum. Transverse silique sections (Figure 5.5 B to D) show how endocarp *b* cells appear smaller and constrained in cross-sectional area when adjacent to a seed. The bar chart of mean endocarp *b* cell area in Figure 5.5E compares the endocarp *b* cells of valves immediately adjacent to a seed and those which are not, from each silique of the series. Seed-adjacent and non-seed-adjacent endocarp *b* areas are similar until stage 16, after which the endocarp *b* cell area appears to be constrained when a seed is positioned next to it. These findings suggest that the seed does not impact upon endocarp *b* cell shape and size until stage 16 because prior to this stage the developing ovule/seed is accommodated by displacement of the septum. The apparent later impact of the seed upon endocarp *b* cell size suggests that either these endocarp *b* cells are compressible, and are squashed by the developing seed, or that endocarp *b* cells in close proximity to a seed are constrained in their growth. From other histological silique sections, the former seems more likely, and the endocarp *b* layer appears to be somewhat compressible, despite the stiff lignin layer.

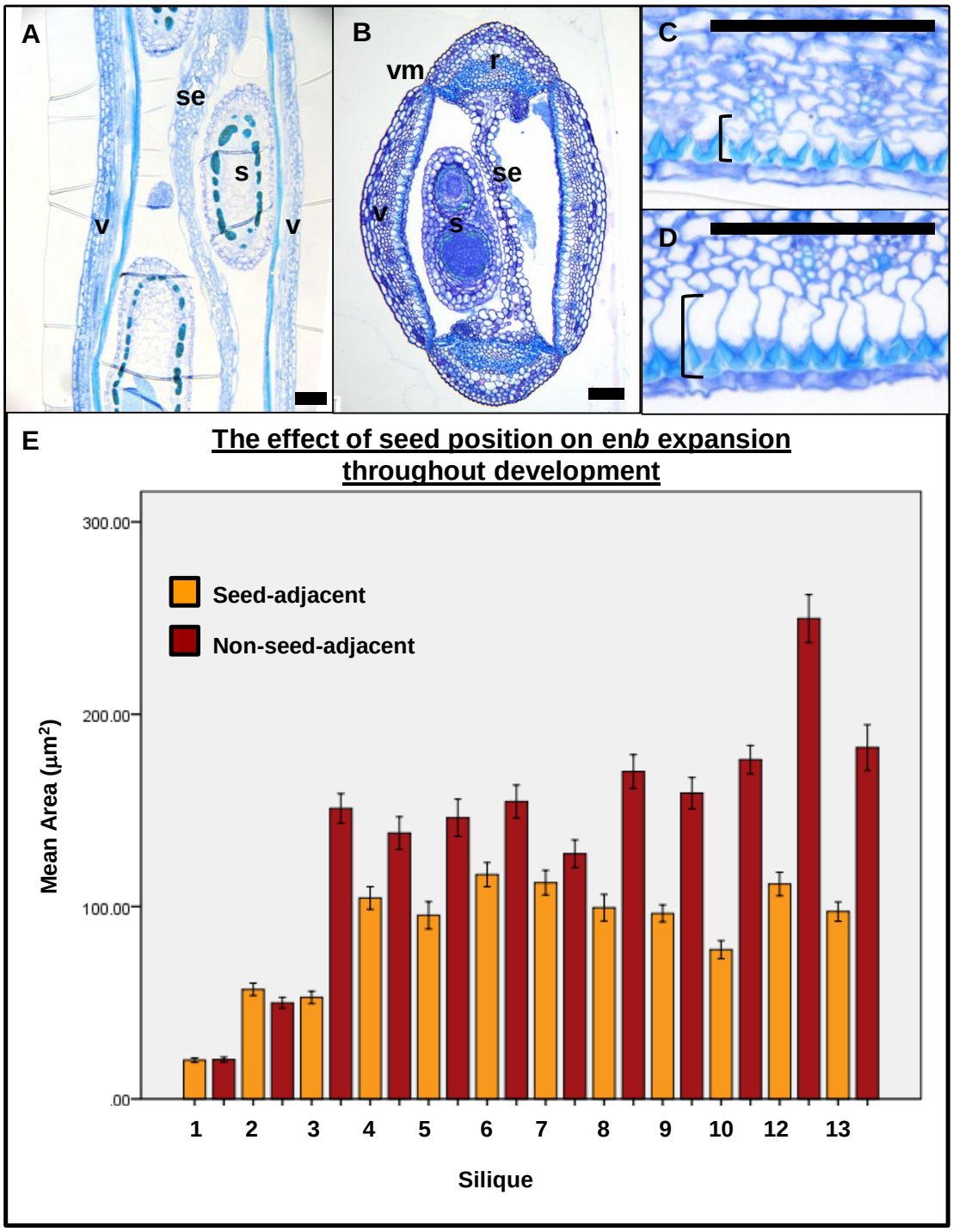

Figure 5.5 Positioning of seed adjacent to valve constrains endocarp *b* expansion. Photographs illustrating positioning of seeds in silique in longitudinal (A) and transverse (B) TBO sections. Photographs showing the difference in en*b* size (bracket) in TBO transverse sections when a seed is present (C) and absent (D). (E) Graph showing the differences in en*b* size throughout silique development. Bar represents 100 µm

5.2.4. Endocarp *a* layer retention in *C. hirsuta* siliques

In *A. thaliana*, the innermost valve cell layer, the endocarp *a*, degrades and disintegrates prior to stage 17b. However, in *C. hirsuta* this layer persists to full maturity. Histological analysis of the endocarp *a* layer throughout successive silique series (Figure 5.6) confirmed that at stage 17b these endocarp *a* cells were still structurally intact and appeared to be alive, as indicated by TBO dark-blue staining of their cytoplasm and nuclei.

A conundrum in *C. hirsuta* explosive dehiscence is how the force of the silique's opening mechanism is transferred to the seeds. Stress appears to build up within the valve tissue, resulting in its explosive curling away from the fruit, but it is not clear how this force is then transferred to the seeds, which are attached to the medial tissues of the fruit.

High speed imaging of *C. hirsuta* silique opening (conducted by A. Hay in collaboration with R. Bomphrey of the Oxford Animal Flight Group, Department of Zoology, University of Oxford) revealed that seeds adhere to the valve during explosion. This observation prompted the question: how does this adhesion between seed and valve happen?

Y. Ventikos (of the Fluidics and Biocomplexity Group, Department of Engineering Science, University of Oxford) modelled seed behaviour during valve release with a thin layer of air, water, or honey between the seed and valve. Simulations found that a layer of air or a layer of water was insufficient for the valve to pull the seeds away from the silique. A substance with a higher viscosity (such as honey), however, was sufficient to remove the seeds away from the silique during valve curling.

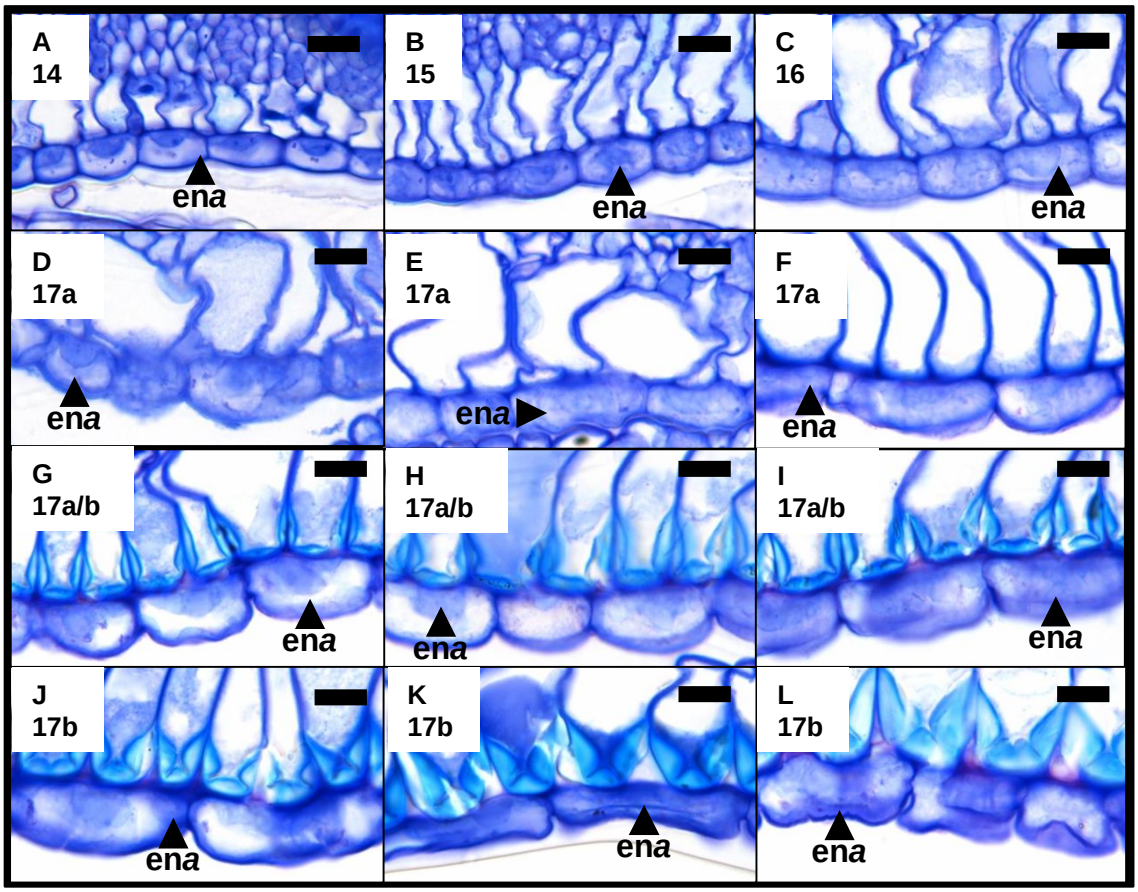

Figure 5.6 Endocarp *a* layer through silique maturation. TBO staining of transverse sections of successive siliques from Figure 5.2. Unlike *A. thaliana*, the endocarp *a* layer (denoted by "ena" and arrow) does not disintegrate by mid stage 17 and instead persists through to maturity. Developmental stages indicated, bar represents 10 µm.

The endocarp *a* layer, then, became a candidate for playing a role in this process. In *A. thaliana*, in which the endocarp *a* layer degrades prior to maturity, seeds are left to simply fall from the open silique after they abscise. The fact that *C. hirsuta* requires an added feature of valve-seed adhesion, and that it retains a cell layer at the interface between these two tissues, therefore seems potentially important, and the endocarp *a* layer in *C. hirsuta* was investigated for a potential role in this process.

The endocarp *a* layer directly contacts the seed epidermis in *C. hirsuta* (Figure 5.7A), providing a large potential surface area for adhesion between the two cell layers. One hypothesis was that the endocarp *a* layer may function as a mucilage-secreting cell layer, and histological analyses were used to identify characteristics commonly associated with the presence of muciliage or of its production and secretion. In the *A. thaliana* seed epidermis, TBO stains accumulating mucilage as pink-purple within the cells that are producing it, and the columellae stain dark blue (Western et al. 2000). However, TBO staining of the endocarp *a* layer did not indicate mucilage accumulation or columellae formation (Figure 5.7B).

Ruthenium red is a histological stain that can be used to visualise mucopolysaccharides like pectin, a constituent of both cells walls and mucilage. Ruthenium red staining of plastic sections (Figure 5.7C) and fresh free-hand sections (Figure 5.7 D and E) showed the presence of pectin in the cell walls but did not reveal an external layer of a pink secreted substance, as one would expect in the presence of a significant quantity of mucilage. When viewed longitudinally (Figure 5.7E), the endocarp *a* can be seen as a pink mesh, formed from a fine grid of cells, rather than a cell layer coated in a pectin-rich exudate.

The endocarp *a* cell layer was further analysed by TEM, conducted by H. Dickinson (Figure 5.7 G and I). The endocarp *a* was compared at both immature and mature stages with the seed epidermis (Figure 5.7 F and H), a tissue which is known to produce mucilage in *A. thaliana* (this mucilage is not secreted, however, unless the seed becomes imbibed in water). The seed epidermis possessed large vacuoles and later accumulated amyloplasts, a pattern characteristic of mucilage production. However, the vacuoles of the endocarp *a* cells were smaller and no amyloplasts became visible. TBO staining of the endocarp *a* layer (Figure 5.6) shows that these cells retain large amounts of living cytoplasm, and the large, pink-purple TBO-staining mucilage-containing vacuoles and subsequent columellae formation seen in the *A. thaliana* seed epidermis during mucilage production are not visible in this layer (Western et al. 2000). Together, these histological analyses of the endocarp *a* layer do not implicate a role for the endocarp *a* in mucilage production, nor do they observe a layer of mucilage between this cell layer and the seed epidermis.

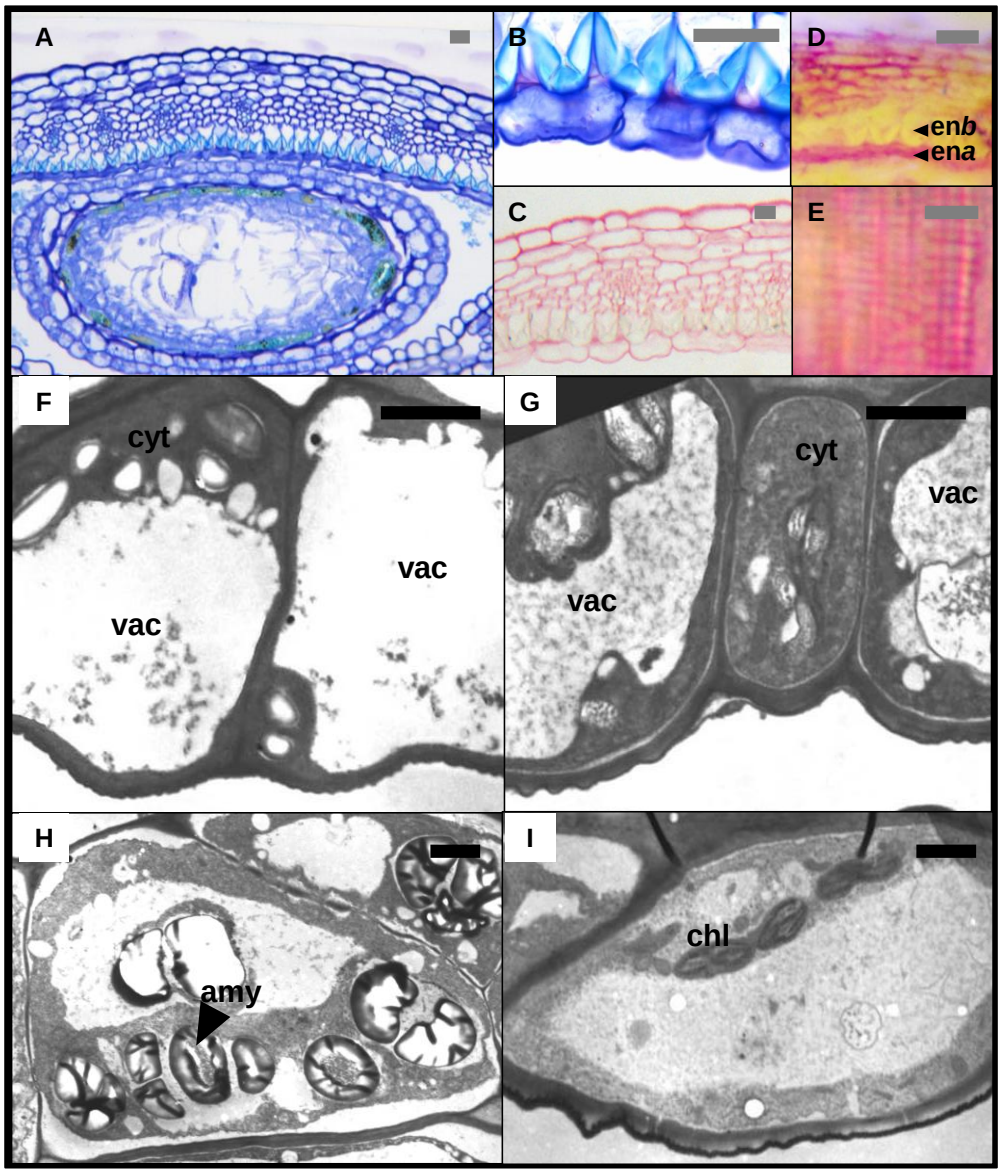

Figure 5.7 The endocarp *a* as a mucilage secreting layer? (A) to (C) Staining of plastic sections. TBO shows seed epidermis directly contacts en*a* (A) and no accumulation of mucilage or columellae formation (B). Ruthenium red stains pectin of cell walls but does not reveal a secreted mucilage layer (C). (D) and (E) Ruthenium red staining of fresh tissue. In transverse section (D), the en*a* stains pink, reflecting surface pectins. When viewed longitudinally (E), the en*a* is visible as a fine mesh, with only cell walls staining pink and no obvious mucilaginous secretion or exudate. (F) to (I) Transmission electron microscopy by H. Dickinson. (F) and (G) show immature seed epidermis and endocarp *a*, whilst (H) and (I) show the tissues at maturity. The seed epidermis shows large vacuoles (F) followed by amyloplasts (H), characteristic of seed coat mucilage production. However, en*a* vacuoles are smaller (G) and no amyloplasts are visible (I). Labels indicate vacuoles (vac), amyloplasts (amy), chloroplasts (chl), and cytoplasm (cyt). Grey bar represents 20 µm, black bar 2 µm.

Further investigation of the endocarp *a*, however, revealed that the layer itself is sticky and capable of adhering to the seed. For example, dissection of the seed from fresh silique tissue (Figure 5.8A) resulted in the additional removal of the endocarp *a* (stained pink with ruthenium red), which adheres strongly to the seed, from which it cannot be manually removed or dissected away.

TEM (by H. Dickinson) revealed the endocarp *a* cell wall to be very thick, with an outer, electron dense layer in direct and close contact with the outer wall of the seed epidermis (Figure 5.8 B and C). Where the endocarp *a* wall became detached from the seed epidermis, it could be seen to leave behind a dark residue (Figure 5.8B). When torsion was applied to the TEM specimen, the seed epidermal wall appeared to adhere so tightly to the endocarp *a* outer wall that it tore.

TBO and periodic acid-Schiff (PAS) staining of longitudinal plastic sections allowed further characterisation of the endocarp *a* layer. TBO-stained longitudinal sections through the valve layers (Figure 5.8D) showed the endocarp *a* to lie as a fine grid of cells below the light-blue staining abaxial lignified rods of the endocarp *b* cells. Along the same axis, PAS staining (conducted by S. McKim) visualised the polysaccharides of the endocarp *a* (Figure 5.8G). This staining confirmed the presence of a sugary, thick outer wall seen by TEM.

Longitudinal sections perpendicular to this, conducted along the replum-to-replum axis, gave a view of the valve cell layers and seed in profile. The seed can be seen to be closely appressed to the endocarp *a* cells (Figure 5.8E), with the thick polysaccharide wall in direct contact with the seed epidermis (Figure 5.8H). This direct contact between the seed and the endocarp *a* layer is not always seen in transverse section (for example Figure 5.2B) due to the gaps

between the seed edge and the endocarp *a* layer that occur at the rounded edges of the seed.

Longitudinal sections that view the valve in profile before (Figure 5.8F) and after (Figure 5.8I) valve curling showed that before dehiscence, the seed appears to be pushed into the valve wall, squashing the endocarp *b*, as previously suggested by comparisons of cell area measurements. After dehiscence, the valve curls outwards, with the endocarp layers now becoming the outermost face of the valve. The endocarp *a* layer can be seen to be retained by the valve, but it comes loose from the endocarp *b* in regions where a seed was previously in contact with the endocarp *a*. This implies that adhesion in these regions between the endocarp *a* and the seed epidermis causes the endocarp *a* layer to be tugged away from the endocarp *b* when the seed gathers sufficient force and momentum to break away from the endocarp *a* and disperse.

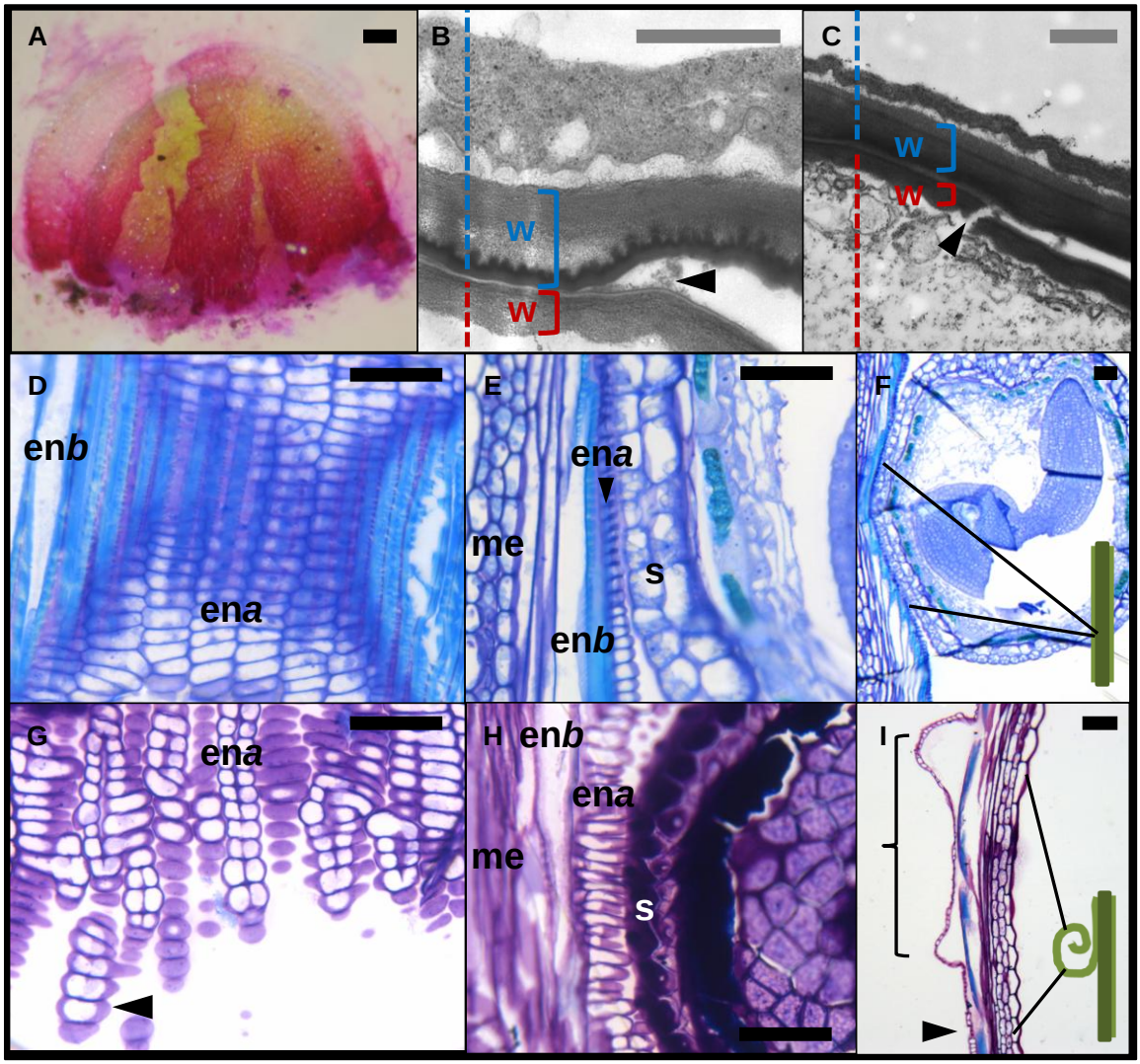

Figure 5.8 The endocarp *a* adheres to seeds until after the silique has opened. (A) Seed dissected from fresh silique. The en*a*, stained pink with ruthenium red, adheres to the seed. (B) and (C) TEM by Hugh Dickinson showing interface between en*a* (blue) and seed (red). Cell walls indicated by w and brackets. (B) The en*a* wall is very thick and contains an outer, electron dense layer which leaves residue where it has become detached (arrow). (C) When torsion is applied, tearing of the seed wall occurs (arrow), due to adhesion to en*a* wall. (D) to (I) Silique sections stained with TBO (D) to (F) and Periodic acid-Schiff (PAS) stain (G) to (I). (D) and (G) show longitudinal sections of valve inner surface. The en*a* forms a mesh (as seen in Figure 3.10E) and purple PAS staining (G) shows a thick, polysaccharide wall (arrow). This thick wall can be seen to contact the seed epidermis (E) and (H). (F) and (I) show endocarp before (F) and after (I) silique opening. The outcurled valve surface, indicated on schematic in (I) retains the en*a* (arrow), but it becomes detached from the en*b* where the seed was previously adhered and has pulled upon the layer (bracket) during seed dispersal. Black bar represents 50 μm, grey bar 1 μm.

5.2.5. Valve layers across the Brassicaceae

The valve cell layers of the 8 Brassicacean species selected in Chapter 3 are shown in transverse section in Figure 5.9. Out of all eight species, only the two *Cardamine* species show a sclerenchyma layer of valve tissue (labelled in yellow in Figure 5.9) and polar deposition of lignin within the endocarp *b* layer (Figure 5.9 A and B). This polar lignin deposition and extra valve layer of sclerenchyma can therefore be tentatively posited, along with broad repla, to contribute to the outward valve curling seen in both species. Endocarp *b* lignification in the other species is isotopic, with varying degrees of thickness. Lignification in *R. islandica*, and its absence of a sclerenchyma-like layer, closely resemble *A. thaliana*, despite the former's closer relationship to the *Cardamine* genus.

Although the two *Cardamine* species share several features, including broad repla, a scelrenchyma layer of valve tissue, and polar lignin deposition in the endocarp *b* layer, they differ in the enalrgement of this endocarp *b* cell layer. Whilst the *C. corymbosa* endocarp *b* cells are proportionally larger than in all other species (excepting *C. hirsuta*), they do not show the same degree of massive enlargement that is so striking in *C. hirsuta*. As this is the most marked morphological difference between these two *Cardamine* species, it is possible that this trait contributes to the observed differences in their silique opening, with *C. hirsuta*'s explosive opening occurring more forcefully, more reliably and being easier to trigger. However, it is alternatively possible the locule of the *C. corymbosa* is more crowded than in *C. hirsuta*, causing its seeds to press more against the valve, resulting in a higher degree of compression of the endocarp *b* layer than is seen in *C. hirsuta*.

Whilst many of the morphological features identified in *C. hirsuta* are shared only with *C. corymbosa* (with the exception of flattened valves in *A. lyrata*), retention of the endocarp *a* layer is a more widespread trait throughout the siliques examined. Only the two *Arabidopsis* species show a degraded endocarp *a* layer at maturity. This perhaps suggests that the endocarp *a* is largely maintained throughout the family but has been lost at maturity in the *Arabidopsis* species examined. If the endocarp *a* does play a role in valve-seed adhesion, it seems likely that this is a role for the endocarp *a* that has been newly acquired in the *Cardamine* lineage.

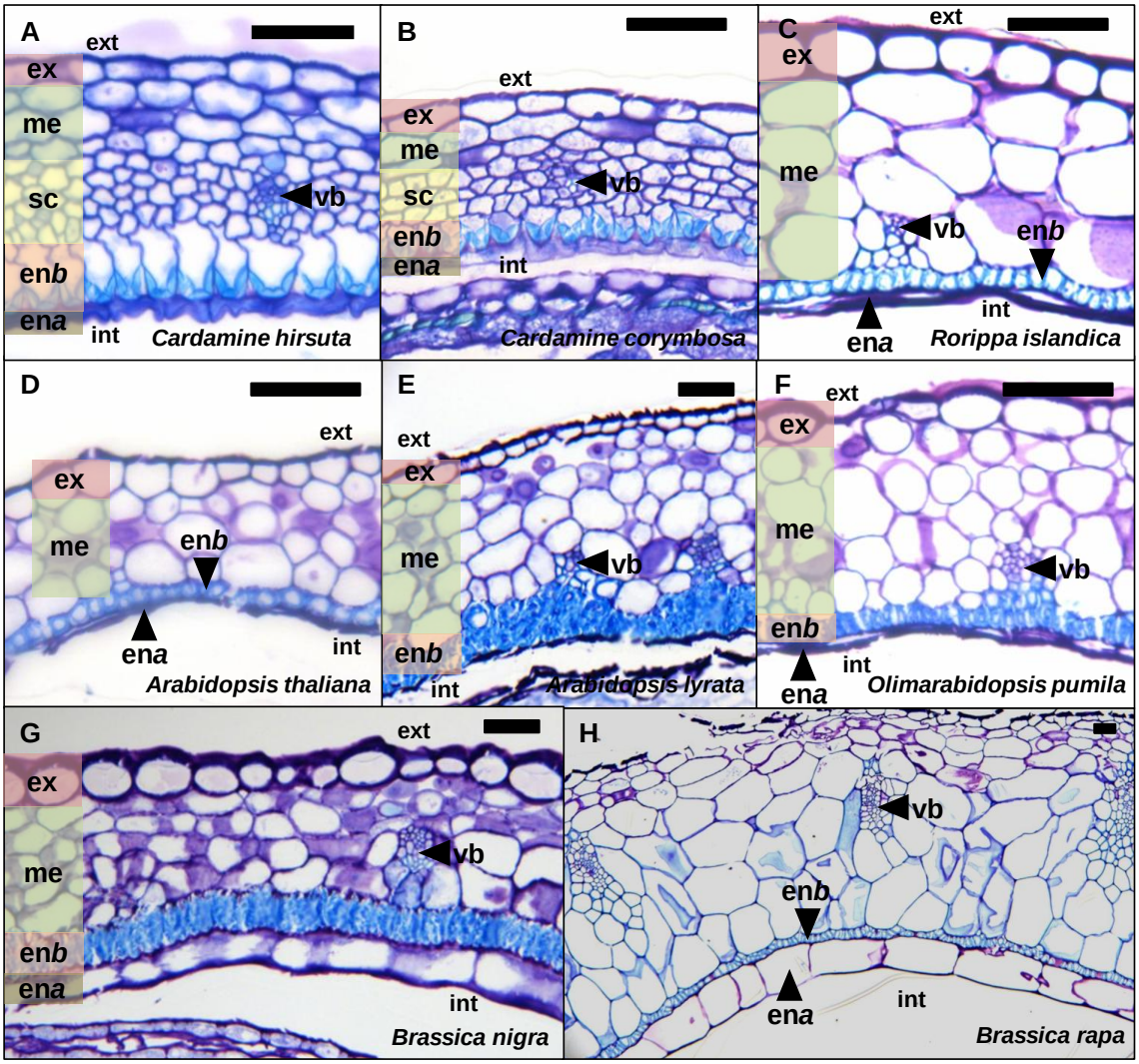

Figure 5.9 Transverse sections of Brassicacean valves. Plastic sections of mature fruits, stained with TBO. External (ext) and internal (int) surfaces of valves are labelled. (A) *Cardamine hirsuta*, (B) *Cardamine corymbosa*, (C) *Rorippa islandica*, (D) *Arabidopsis thaliana*, (E) *Arabidopsis lyrata*, (F) *Olimarabidopsis pumila*, (G) *Brassica nigra*, (H) *Brassica rapa*. ex = exocarp, me = mesocarp, sc = sclerenchyma-like layer, en*b* = endocarp *b*, en*a* = endocarp *a*, vb = vascular bundle. Bar represents 50 µm.

5.3. Discussion

5.3.1. Possible roles for *C. hirsuta* valve cell layers in explosive dehiscence

Despite their different dehiscence modes, both *C. hirsuta* and *A. thaliana* fruits comprise the same gross morphology of lignified repla, flanking valve tissue, and a valve margin that forms the dehiscence zone. Within these tissues there are clear differences, with *C. hirsuta* possessing broader repla and flatter valves. However, most of the morphological differences between the fruits of the two species are seen in the cell layers of the valve tissue, and these are summarised in Figure 5.10.

Comparison with *A. thaliana* reveals that lignin deposition in increased in the *C. hirsuta* silique, and that within the valve this lignin is deposited solely within the endocarp *b* cell layer (Figure 5.1). Unlike all other Brassicacean siliques examined, this lignin is not deposited isotopically within *Cardamine* endocarp *b* cells, and is instead laid down within U-shaped secondary thickenings at the innermost, abaxial faces of these cells only (Figure 5.9). Because the increased lignin deposition seen in *C. hirsuta* is only greater than in *A. thaliana* by 9.29 mg per gram dry weight, it may be that the pattern of secondary thickening in the endocarp *b* layer contributes more to the explosive opening mechanism than the increased lignin content does alone. This hypothesis is supported by the *lig1* mutant described in Chapter 3, which undergoes U-shaped secondary thickening of the endocarp *b* cells (data not shown) without subsequent lignification, and still opens explosively, albeit delayed and possibly with less force.

A second valve layer feature which is shared by *C. hirsuta* and *C. corymbosa*, but was not seen in any of the 6 other Brassicacean species

examined, was the presence of a four-cell thick additional cell layer, situated between the mesocarp and endocarp *b* layers (figures 5.2 and 5.9). As the two *Cardamine* species both show outward curling of the valve, it is possible that the polar thickening of the endocarp *b* layer and the extra layer of sclerenchyma-like tissue within the valve are related to this trait (outlined in Figure 5.10).

Across stage 17b, the *C. hirsuta* silique broadens, coinciding with a swelling of the excocarp, mesocarp and sclerenchyma cells (Figure 5.3). This swelling may cause tension between these valve layers and the already enlarged and lignified endocarp *b* layer. Whilst the polar lignification of these endocarp *b* cells is seen in both *C. hirsuta* and *C. corymbosa*, endocarp *b* size is one of the only clear differences between *C. hirsuta* and *C. corymbosa* silique morphology (Figure 5.9). It is therefore possible that the larger endocarp *b* cells of *C. hirsuta* might be responsible for the increased sensitivity, reliability, and force of the explosive mechanism that is seen in this species.

When the valve explosively curls outward, the endocarp *a* cells appear to mediate seed adhesion, pulling the seeds along with the valve, and out from the fruit (Figure 5.8). Rather than secreting mucilage, the endocarp *a* layer appears to instead possess thick, sticky, polysaccharide-rich cell walls (figures 5.7 and 5.8). Whilst an endocarp *a* cell layer is found in the mature siliques of multiple Brassicacean species, it appears to have acquired this novel function in *C. hirsuta* (Figure 5.9).

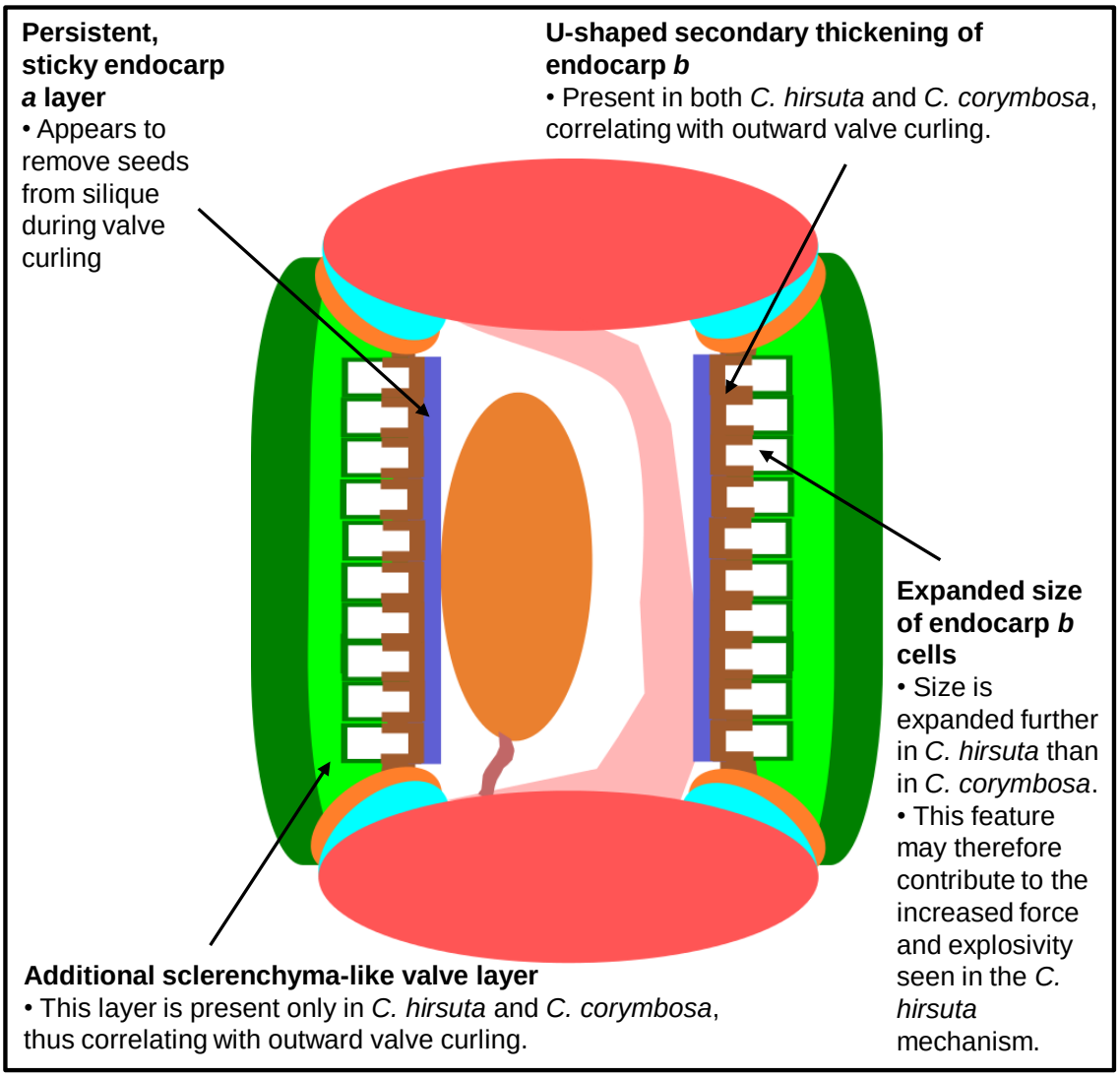

Figure 5.10 Hypothesised roles of valve layers in explosive *C. hirsuta* silique opening

5.3.2. Discussion of previous *Cardamine* cell layer studies

During the course of the research presented in this thesis, two papers examining the explosive dispersal mechanism of the *Cardamine* genus were published. The first of these focussed on describing the dispersal characteristics of the *Cardamine parviflora* silique (Hayashi et al. 2010), whilst the second sought to explain the explosive opening of *C. hirsuta* siliques in terms of endocarp *b* and *a* morphology (Vaughn et al. 2011).

Hayashi *et al.* observed the persistence of the *Cardamine* endocarp *a* cell layer to maturity, an anatomical feature that is not seen in *A. thaliana*, describing this as “the primary difference” between *Cardamine* siliques and those of other Brassicaceae. The observations presented in this chapter show that the retention of the endocarp *a* layer to maturity in *Cardamine* siliques is neither the only difference between the siliques of *C. hirsuta* and other species, nor is this trait unique to the *Cardamine* genus.

Vaughn *et al.* (2011) observed the U-shaped lignification patterns of the *C. hirsuta* endocarp *b* cells. In their paper, they state that the only differences seen between the siliques of *A. thaliana* and *C. hirsuta* are the contrasting anatomies of the endocarp *b* and *a* layers. The analyses conducted in this chapter identify the large expansion of endocarp *b* cell size, and the presence of an additional, sclerenchyma-like cell layer, as further features that are seen in *C. hirsuta* but not in *A. thaliana*.

Hayashi *et al*. proposed that the *Cardamine* opening mechanism arises from the differing properties of a bilayer, formed from endocarp tissues. They propose that the endocarp *a* layer, which they observed to be mucilaginous, absorbs water and becomes swollen (Hayashi et al. 2010). They suggested that

the lignified endocarp *b* layer functions to compress this endocarp *a* layer, until dehiscence occurs along the dehiscence zone, resulting in the sudden expansion of the endocarp *a* layer, causing outward curling of the valve. Hayashi *et al*. hypothesised that a layer of water may exist between the valve and the seeds that is responsible for imparting energy from the valve to the seeds in *C. parviflora*.

However, biomechanical modelling suggests that a layer of water would not be viscous enough to pull the seeds out of the *C. hirsuta* fruit as its valves curl. Furthermore, the analyses conducted in this chapter failed to identify any characteristics associated with mucilage production in the endocarp *a* cells (figures 5.6, 5.7 and 5.8). This finding also conflicts with the suggestion made by Vaughn *et al.* that the endocarp *a* functions to keep the endocarp *b* cells moist by trapping mucilage between the two cell layers (Vaughn et al. 2011). The fact that the endocarp *a* layer also persists to maturity in the indehiscent Brassica species examined also suggests that the maintenance of this layer is unlikely to be a key driver of explosive dehiscence.

An alternative model to those of Hayashi *et al.* and Vaughn *et al.*, that takes into account the further observations made in this and the previous two chapters is presented in the next chapter.

6. Discussion

Successful dispersal, to varying degrees, is crucial to the success of all extant species. Within plants, seed dispersal is a vital opportunity for otherwise sessile organisms to move and spread to new areas. Explosive seed dispersal is a particularly dramatic means for doing this, and is widespread throughout the plant kingdom. However, most scientific investigations of explosive seed dispersal have sought to describe this trait ecologically or mechanically. Of the limited number of developmental analyses of explosive seed dispersal, none have been underpinned by genetics.

This thesis establishes *C. hirsuta* as a well-characterised, genetically tractable model for studying explosive seed dispersal. The exploding morphology of the *C. hirsuta* fruit is characterised in detail, and compared with other fruits of differing seed dispersal modes across the Brassicaceae. Mutants affecting fruit development and seed dispersal are identified and characterised in a genetic screen, and the first *C. hirsuta* fruit mutant to be mapped, *valveless*, is presented.

6.1. *C. hirsuta* achieves explosive seed dispersal through modification of conserved silique tissues

Morphological characterisation of the *C. hirsuta* fruit reveals that it shares the same organisation of tissues that is seen in the siliques of other Brassicacean species, including *A. thaliana*. The *C. hirsuta* silique comprises two fused carpels, separated by repla. The valve tissue of these carpels, plus the two repla, together surround the two locules of the fruit, which are separated by a false septum of medial tissues, which run from replum to replum.

As well as showing the same organisation of fruit tissues as other Brassicacean species, *C. hirsuta* siliques also open along a dehiscence zone

which shows homology to *A. thaliana* and *Brassica* species. This dehiscence zone incorporates two types of valve margin tissues – lignified valve margin cells, and a "separation layer" of non-lignified valve margin cells.

Despite these similarities, differences in the cellular differentiation of *C. hirsuta* fruit tissues accompany its dramatically different mechanism of fruit opening. Of the Brassicacean siliques characterised, the *A. thaliana* mode of dehiscence – splitting of the silique along the dehiscence zone, eventual loss of valves, exposure of the seeds, and passive dispersal – seems likely to be ancestral. The indehiscence seen in the *Brassica* genus is probably the result of artificial selection of these crop plants, and explosive opening of siliques appears to be a novel adaptation in the *Cardamine* genus. In *C. hirsuta*, the dehiscence zone does not gradually open to expose the seeds, but instead it rips apart as the valve springs outwards and upwards from the silique.

The *C. hirsuta* silique differs from that of *A. thaliana* in a range of features. The flatter valves possess an additional tissue layer of sclerenchyma cells, a persistant endocarp *a* cell layer, and greatly enlarged, polarly lignified layer of endocarp *b* cells – none of which are observed in the *A. thaliana* silique. Together, these morphological differences allow the explosive propulsion from the silique of *C. hirsuta*'s larger, flatter seeds. These morphological changes represent *Cardamine* lineage-specific morphological adaptations for explosive seed dispersal that have occurred within the context of a broadly similar fruit plan that is seen across the Brassicaceae family.

Characterisation of *C. hirsuta* fruit development therefore shows that dramatic changes to seed dispersal mode can be brought about through minor modifications of fruit morphology. Figure 6.1A summarises the roles hypothesised

in this thesis that the modified tissues of the *C. hirsuta* silique play in its explosive seed dispersal mechanism.

Explosive pod shatter evolved in *C. hirsuta* without the gain of entirely novel fruit tissues. The *C. hirsuta* silique has a similar dehiscence zone to other Brassicaceae species, and modifications to the valve, particularly the endocarp *b* cell layer, seem sufficient to power the explosive opening of the *C. hirsuta* silique.

6.2. Proposed model for explosive pod shatter in *C. hirsuta*

In collaboration with H. Hofhuis, I propose a model for explosive pod shatter in *C. hirsuta* which is driven by the differing behaviours of the valve exocarp, mesocarp, sclerenchyma-like, and endocarp *b* cells during swelling and shrinking. This model is illustrated in the numbered steps of Figure 6.1B.

The excocarp, mesocarp and previously undescribed sclerenchyma cells appear to swell during the broadening of the silique that is seen during the later part of stage 17 (Figure 5.3). Because the lignified, secondarily thickened inner cell walls of the endocarp *b* layer are unable to expand, this creates tension.

During subsequent drying, the shape of a cell determines whether it contracts or bends. The small, cuboidal cells of the exocarp and mesocarp contract inwards, whereas the long sclerenchyma and endocarp *b* cells bend. This rapid cell shape deformation releases the built up stress and causes explosive opening.

As suggested by Vaughn *et al.*, the deposition of lignin only at the innermost wall of the endocarp *b* cells means that they can only bend outwards, not inwards, and this could in theory explain the outward curling of the valve seen in *C. hirsuta*. However, the *lig1* mutant shows that U-shaped secondary

thickenings are sufficient to cause this, and lignin deposition within these wall thickenings appears only to increase the sensitivity and force of the mechanism.

As the valve curls outwards, driven by bending of the endocarp *b* and sclerenchyma-like layers, and powered by the release of tensions built by the earlier differential swelling of the valve tissue layers, the persistent, sticky endocarp *a* adheres to the seeds, pulling them away with the valve and out of the silique. When the removed seeds gather sufficient momentum, they break away from the endocarp *a*, and fall to their newly dispersed locations.

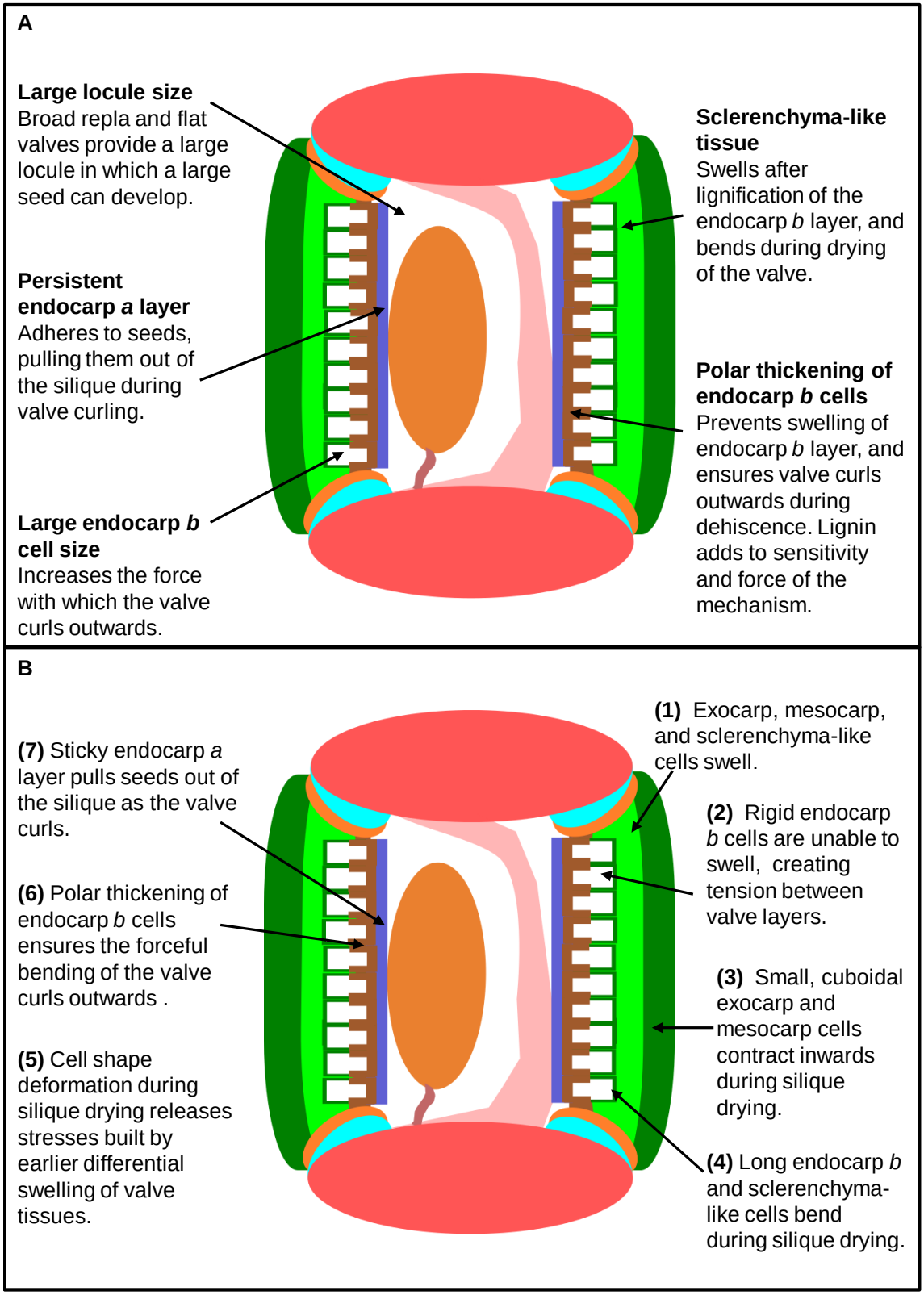

Figure 6.1 Hypothesised roles of silique features (A) and model for explosive opening (B).

6.3. *val* allows comparison of genetics of silique patterning in *C. hirsuta* and *A. thaliana*

The *val* mutant, which is tightly linked to a mutation in *cFUL*, enables some comparison of the genetic control of dehiscence tissue patterning between *C. hirsuta* and *A. thaliana*. In *A. thaliana*, *FUL* is crucial for correct valve development, and compromised FUL function results in a spreading of valve margin properties into the valve region. This aspect of the *A. thaliana* dehiscence-patterning model applies too to *C. hirsuta*, and the valve region of *val* mutant siliques is replaced by valve margin cells. This finding suggests that the *A. thaliana* model also applies to *C. hirsuta*, a species with a different fruit opening mechanism.

The *val* mutant therefore suggests that the *A. thaliana* model for silique patterning is robust. Testing of this model in a new species with a different fruit opening mechanism found that the principles of the *A. thaliana* model also apply in *C. hirsuta*. As in *A. thaliana*, correct valve differentiation cannot occur in the absence of factors that prevent valve margin identity. Additional investigations could test this model further by determining whether replum differentiation in *C. hirsuta* also requires the correct restriction of valve margin-specifying factors, as it does in *A. thaliana*. The finding that the *A. thaliana* model for silique patterning can be extended to *C. hirsuta* suggests that the genetic modifications that contribute to explosive pod shatter in *C. hirsuta* are downstream of the regulatory network that patterns the silique tissues. This hypothesis is in keeping with the finding that the overall morphological plan of the *C. hirsuta* fruit is the same as in other Brassicacean species, and that the main differences observed between the

siliques of *C. hirsuta* and *A. thaliana* are modifications of cell layers within the same shared tissues.

6.4. Future Research Directions

The most immediate area for further investigation is the cloning of *val*. If the transformation of *val* with a genomic *cFUL* construct (experiment conducted by H. Hofhuis) shows full complementation of the mutant phenotype, this will confirm that the mutation of *cFUL* is the cause of the *val* silique phenotypes. Once this has been established, the extent of conservation of *FUL* function between *C. hirsuta* and *A. thaliana* can be investigated. A genomic *aFUL* construct (*FUL::FUL:GFP*, gift from G. Angenent) can be used to perform a reciprocal swap – expression of *aFUL* in *val* and *cFUL* in *ful-1* – to test the extent of functional conservation between the two genes. Further investigation of *FUL* function in *C. hirsuta* would also benefit from the isolation of additional *cful* alleles, particularly null alleles.

The *val* mutant also provides a starting point from which to begin investigating the function of other genes in *C. hirsuta* fruit development. A suppressor/enhancer screen in *val* has been conducted by H. Hofhuis to identify other genes of importance to patterning the *C. hirsuta* valve, and *IND, ALC* and *RPL* alleles are expected to be identified as repressors of the *val* phenotype. Of greater importance to understanding explosive dehiscence in *C. hirsuta*, however, will be previously unidentified *ful* suppressors of particular importance to patterning the tissue layers of the *C. hirsuta* valve. Transcriptional profiling of WT and *val* fruits is another approach to identify genes potentially regulated by *FUL*.

In this thesis, a number of specific tissue or cellular morphologies were identified within the *C. hirsuta* silique which may be responsible for controlling various different aspects of the species's explosive seed dispersal phenotype. My

colleague H. Hofhuis is part of a multidisciplinary collaboration to model explosive pod shatter which will test the hypothesised functions of these morphologies and provide detailed understanding of the mechanics of the explosive dispersal of *C. hirsuta* seeds.

To further understand explosive seed dispersal in *C. hirsuta* in an evolutionary context, wider sampling of the Cardamineae, particularly the *Cardamine* genus, would be needed. Comparison of *Cardamine* species with differing silique opening mechanisms would allow more precise correlation of morphological features with aspects of the explosive opening of *C. hirsuta*. Wider, well-informed sampling across the Cardamineae and the Camelineae might provide more data for inferring how explosive *Cardamine* siliques transitioned from an ancestral *Arabidopsis*-like silique.

Finally, to understand the conditions under which the ballistic seed dispersal method of *C. hirsuta* is advantageous, ecological field experiments are needed. To understand the adaptive significance of *C. hirsuta's* dispersal mechanism, measures of dispersal, survival, competitive and reproductive successes in various conditions are needed, both in *C. hirsuta* and in a species showing the ancestral dispersal phenotype, such as *A. thaliana*.

References

Alonso-Cantabrana, H. et al., 2007. Common Regulatory Networks in Leaf and Fruit Patterning Revealed by Mutations in the Arabidopsis ASYMMETRIC LEAVES1 Gene. *Development*, 134(14), pp.2663–2671.

Al-Shehbaz, I., Beilstein, M. & Kellogg, E., 2006. Systematics and phylogeny of the Brassicaceae (Cruciferae): an overview. *Plant Systematics and Evolution*, 259(2), pp.89–120.

Arnaud, N. et al., 2010. Gibberellins Control Fruit Patterning in Arabidopsis Thaliana. *Genes & Development*, 24(19), pp.2127–2132.

Arnaud, N. et al., 2011. The Same Regulatory Point Mutation Changed Seed-Dispersal Structures in Evolution and Domestication. *Current Biology*, 21(14), pp.1215–1219.

Arsovski, A.A. et al., 2009. AtBXL1 Encodes a Bifunctional B-D-Xylosidase/A-L-Arabinofuranosidase Required for Pectic Arabinan Modification in Arabidopsis Mucilage Secretory Cells. *Plant Physiology*, 150(3), pp.1219–1234.

Bailey, C.D. et al., 2006. Toward a Global Phylogeny of the Brassicaceae. *Molecular Biology and Evolution*, 23(11), pp.2142–2160.

Barkoulas, M. et al., 2008. A developmental framework for dissected leaf formation in the Arabidopsis relative Cardamine hirsuta. *Nature Genetics*, 40(9), pp.1136–1141.

De Bary, A., 1887. *Comparative morphology and biology of the Fungi, Mycetozoa and bacteria*, Clarendon Press (Oxford).

Beattie, A.J. & Lyons, N., 1975. Seed Dispersal in Viola (Violaceae): Adaptations and Strategies. *American Journal of Botany*, 62(7), pp.714–722.

Beaumont, K.P., Mackay, D.A. & Whalen, M.A., 2009. Combining distances of ballistic and myrmecochorous seed dispersal in Adriana quadripartita (Euphorbiaceae). *Acta Oecologica*, 35(3), pp.429–436.

Beer, T. & Swaine, M.D., 1977. On the theory of explosively dispersed seeds. *New Phytologist*, 78(3), pp.681–694.

Beilstein, M.A. et al., 2010. Dated molecular phylogenies indicate a Miocene origin for Arabidopsis thaliana. *Proceedings of the National Academy of Sciences*, 107(43), pp.18724–18728.

Beilstein, M.A., Al-Shehbaz, I.A. & Kellogg, E.A., 2006. Brassicaceae Phylogeny and Trichome Evolution. *American Journal of Botany*, 93(4), pp.607–619.

Benjamins, R. et al., 2001. The PINOID Protein Kinase Regulates Organ Development in Arabidopsis by Enhancing Polar Auxin Transport. *Development*, 128(20), pp.4057–4067.

Bert, V. et al., 2000. Zinc tolerance and accumulation in metallicolous and nonmetallicolous populations of Arabidopsis halleri (Brassicaceae). *New Phytologist*, 146(2), pp.225–233.

Bortiri, E., Jackson, D. & Hake, Sarah, 2006. Advances in maize genomics: the emergence of positional cloning. *Current Opinion in Plant Biology*, 9(2), pp.164–171.

Bowman, J. L. et al., 1999. 4 Molecular Genetics of Gynoecium Development in Arabidopsis. In *Current Topics in Developmental Biology*. Academic Press, pp. 155–205.

Brand, U. et al., 2000. Dependence of Stem Cell Fate in Arabidopsis on a Feedback Loop Regulated by CLV3 Activity. *Science*, 289(5479), pp.617–619.

Bruggemann, E. et al., 1996. Analysis of fast neutron-generated mutants at the Arabidopsis thaliana HY4 locus. *The Plant Journal*, 10(4), pp.755–760.

Bullock, J.M., Kenward, R.E. & Hails, R.S., 2002. *Dispersal Ecology: 42nd Symposium of the British Ecological Society*, British Ecological Society.

Byrne, M.E. et al., 2000. Asymmetric leaves1 mediates leaf patterning and stem cell function in Arabidopsis. *Nature*, 408(6815), pp.967–971.

Byrne, M.E. et al., 2003. Phyllotactic Pattern and Stem Cell Fate Are Determined by the Arabidopsis Homeobox Gene BELLRINGER. *Development*, 130(17), pp.3941–3950.

Canales, C. et al., 2010. Weeds of change: Cardamine hirsuta as a new model system for studying dissected leaf development. *Journal of Plant Research*, 123(1), pp.25–33.

De Candolle, A.P., 1821. Cruciferae. *Systema Naturale*, 2, pp.139–700.

Chambers, J.C. & MacMahon, J.A., 1994. A Day in the Life of a Seed: Movements and Fates of Seeds and Their Implications for Natural and Managed Systems. *Annual Review of Ecology and Systematics*, 25, pp.263–292.

Chauvaux, N. et al., 1997. The Role of Auxin in Cell Separation in the Dehiscence Zone of Oilseed Rape Pods. *Journal of Experimental Botany*, 48(7), pp.1423–1429.

Christensen, S.K. et al., 2000. Regulation of Auxin Response by the Protein Kinase PINOID. *Cell*, 100(4), pp.469–478.

Clements, D.R. et al., 2008. The biology of invasive alien plants in Canada. 9. Impatiens glandulifera Royle. *Canadian Journal of Plant Science*, 88(2), pp.403–417.

Clobert, J. et al. eds., 2001. *Dispersal*, Oxford: Oxford University Press.

Couvreur, T.L.P. et al., 2010. Molecular Phylogenetics, Temporal Diversification, and Principles of Evolution in the Mustard Family (Brassicaceae). *Molecular Biology and Evolution*, 27(1), pp.55–71.

Darwin, C., 1860. *On the Origin of Species by Means of Natural Selection: Or, The Preservation of Favoured Races in the Struggle for Life*, J. Murray.

Davies, T.J. et al., 2004. Darwin's Abominable Mystery: Insights from a Supertree of the Angiosperms. *Proceedings of the National Academy of Sciences of the United States of America*, 101(7), pp.1904–1909.

Deegan, R.D., 2012. Finessing the Fracture Energy Barrier in Ballistic Seed Dispersal. *Proceedings of the National Academy of Sciences*, 109(14), pp.5166–5169.

DeRose-Wilson, L.J. & Gaut, B.S., 2007. Transcription-related mutations and GC content drive variation in nucleotide substitution rates across the genomes of Arabidopsis thaliana and Arabidopsis lyrata. *BMC Evolutionary Biology*, 7(1), p.66.

Dieckmann, U., O'Hara, B. & Weisser, W., 1999. The evolutionary ecology of dispersal. *Trends in Ecology & Evolution*, 14(3), pp.88–90.

Dinneny, J.R. et al., 2004. The Role of JAGGED in Shaping Lateral Organs. *Development*, 131(5), pp.1101–1110.

Dinneny, J.R., Weigel, D. & Yanofsky, Martin F, 2005. A Genetic Framework for Fruit Patterning in Arabidopsis Thaliana. *Development*, 132(21), pp.4687–4696.

Dinneny, J.R., Weigel, D. & Yanofsky, Martin F, 2006. NUBBIN and JAGGED Define Stamen and Carpel Shape in Arabidopsis. *Development*, 133(9), pp.1645–1655.

Dinneny, J.R. & Yanofsky, Martin F, 2004. Drawing lines and borders: how the dehiscent fruit of Arabidopsis is patterned. *BioEssays, BioEssays*, 27, 27(1, 1), pp.42, 42–49, 49.

Duckett, J.G. et al., 2009. Exploding a myth: the capsule dehiscence mechanism and the function of pseudostomata in Sphagnum. *New Phytologist*, 183(4), pp.1053–1063.

Durbak, A.R. & Tax, F.E., 2011. CLAVATA Signaling Pathway Receptors of Arabidopsis Regulate Cell Proliferation in Fruit Organ Formation as Well as in Meristems. *Genetics*, 189(1), pp.177–194.

Edwards, J. et al., 2005. Botany: A record-breaking pollen catapult. *Nature*, 435(7039), pp.164–164.

Ferrandiz, C., 2011. Fruit Structure and Diversity. In *Encyclopedia of Life Sciences (eLS)*. Chichester: John Wiley & Sons, Ltd.

Ferrandiz, C. et al., 2000. Redundant regulation of meristem identity and plant architecture by FRUITFULL, APETALA1 and CAULIFLOWER. *Development*, 127(4), pp.725 –734.

Ferrándiz, C., Liljegren, S.J. & Yanofsky, Martin F., 2000. Negative Regulation of the SHATTERPROOF Genes by FRUITFULL During Arabidopsis Fruit Development. *Science*, 289(5478), pp.436 –438.

Franzke, A. et al., 2009. Arabidopsis family ties: molecular phylogeny and age estimates in Brassicaceae. *Taxon*, 58(2), pp.425–437.

Franzke, A. et al., 2011. Cabbage family affairs: the evolutionary history of Brassicaceae. *Trends in Plant Science*, 16(2), pp.108–116.

Friedman, C.M.R. & Sumner, M.J., 2009. Maturation of the Embryo, Endosperm, and Fruit of the Dwarf Mistletoe Arceuthobium americanum (Viscaceae). *International Journal of Plant Sciences*, 170(3), pp.290–300.

Friis, E.M., Chaloner, W.G. & Crane, P.R., 1987. *The Origins of angiosperms and their biological consequences*, Cambridge University Press, Cambridge.

Friis, E.M., Pedersen, K.R. & Crane, P.R., 2006. Cretaceous angiosperm flowers: Innovation and evolution in plant reproduction. *Palaeogeography, Palaeoclimatology, Palaeoecology*, 232(2–4), pp.251–293.

Friml, J. et al., 2004. A PINOID-Dependent Binary Switch in Apical-Basal PIN Polar Targeting Directs Auxin Efflux. *Science*, 306(5697), pp.862–865.

Galván-Ampudia, C.S. & Offringa, R., 2007. Plant evolution: AGC kinases tell the auxin tale. *Trends in Plant Science*, 12(12), pp.541–547.

Gälweiler, L. et al., 1998. Regulation of Polar Auxin Transport by AtPIN1 in Arabidopsis Vascular Tissue. *Science*, 282(5397), pp.2226–2230.

Girin, T. et al., 2010. Brassicaceae INDEHISCENT genes specify valve margin cell fate and repress replum formation. *The Plant Journal*, 63(2), pp.329–338.

Girin, T. et al., 2011. INDEHISCENT and SPATULA Interact to Specify Carpel and Valve Margin Tissue and Thus Promote Seed Dispersal in Arabidopsis. *The Plant Cell Online*, 23(10), pp.3641–3653.

Girin, T., Sorefan, K. & Østergaard, L., 2009. Meristematic Sculpting in Fruit Development. *Journal of Experimental Botany*, 60(5), pp.1493–1502.

Gompel, Nicolas et al., 2005. Chance caught on the wing: cis-regulatory evolution and the origin of pigment patterns in Drosophila. *Nature*, 433(7025), pp.481–487.

Goujon, M. et al., 2010. A new bioinformatics analysis tools framework at EMBL-EBI. *Nucleic Acids Research*, 38(Web Server), pp.W695–W699.

Govaerts, R., 2001. How Many Species of Seed Plants Are There? *Taxon*, 50(4), pp.1085–1090.

Greene, E.A. et al., 2003. Spectrum of Chemically Induced Mutations From a Large-Scale Reverse-Genetic Screen in Arabidopsis. *Genetics*, 164(2), pp.731–740.

Griffiths, A.J.F. et al., 2012. *Introduction to genetic analysis* 10th ed.., New York: WHFreeman and Co.

Grini, P.E. et al., 1999. Isolation of Ethyl Methanesulfonate-Induced Gametophytic Mutants in Arabidopsis thaliana by a Segregation Distortion Assay Using the Multimarker Chromosome 1. *Genetics*, 151(2), pp.849–863.

Groszmann, M. et al., 2011. SPATULA and ALCATRAZ, are partially redundant, functionally diverging bHLH genes required for Arabidopsis gynoecium and fruit development. *The Plant Journal*, 68(5), pp.816–829.

Gu, Q. et al., 1998. The FRUITFULL MADS-box gene mediates cell differentiation during Arabidopsis fruit development. *Development*, 125(8), pp.1509 – 1517.

Hamilton, W.D. & May, R.M., 1977. Dispersal in stable habitats. *Nature*, 269, pp.578–581.

Harper, J.L., Lovell, P.H. & Moore, K.G., 1970. The Shapes and Sizes of Seeds. *Annual Review of Ecology and Systematics*, 1, pp.327–356.

Haughn, G. & Chaudhury, A., 2005. Genetic analysis of seed coat development in Arabidopsis. *Trends in Plant Science*, 10(10), pp.472–477.

Haughn, G.W. & Somerville, C.R., 1987. Selection for herbicide resistance at the whole plant level. In H. M. LeBaron et al., eds. *Applications of Biotechnology to Agricultural Chemistry*. Washington DC: American Chemical Society, pp. 98–108.

Haughn, George W. & Western, T.L., 2012. Arabidopsis Seed Coat Mucilage is a Specialized Cell Wall that Can be Used as a Model for Genetic Analysis of Plant Cell Wall Structure and Function. *Frontiers in plant science*, 3.

Hay, A. & Tsiantis, M., 2006. The genetic basis for differences in leaf form between Arabidopsis thaliana and its wild relative Cardamine hirsuta. *Nature Genetics*, 38(8), pp.942–947.

Hayashi, M., Feilich, K.L. & Ellerby, D.J., 2009. The Mechanics of Explosive Seed Dispersal in Orange Jewelweed (Impatiens Capensis). *Journal of Experimental Botany*, 60(7), pp.2045–2053.

Hayashi, M., Gerry, S.P. & Ellerby, D.J., 2010. The Seed Dispersal Catapult of Cardamine Parviflora (Brassicaceae) Is Efficient but Unreliable. *American Journal of Botany*, 97(10), pp.1595–1601.

He, F. et al., 2012. Widespread Interspecific Divergence in Cis-Regulation of Transposable Elements in the Arabidopsis Genus. *Molecular Biology and Evolution*, 29(3), pp.1081–1091.

Heywood, V.H. et al., 2007. *Flowering plants families of the world.* V. H. Heywood, ed., Royal Botanic Gardens, Kew.

Hintz, Maren et al., 2006. Catching a 'Hopeful Monster': Shepherd's Purse (Capsella Bursa-Pastoris) as a Model System to Study the Evolution of Flower Development. *Journal of Experimental Botany*, 57(13), pp.3531–3542.

Hovenkamp, P.H. et al., 2009. Spore movement driven by the spore wall in an eusporangiate fern. *Grana*, 48(2), pp.122–127.

Howe, H.F. & Smallwood, J., 1982. Ecology of Seed Dispersal.

Hu, T.T. et al., 2011. The Arabidopsis lyrata genome sequence and the basis of rapid genome size change. *Nature Genetics*, 43(5), pp.476–481.

Hua, S. et al., 2009. Sequence, expression divergence, and complementation of homologous ALCATRAZ loci in Brassica napus. *Planta*, 230(3), pp.493–503.

Ingold, C.T., 1965. *Spore liberation.*, Clarendon Press (Oxford).

Ino, I. & Yourno, J., 1974. X-ray mutagenesis: Base-pair deletion at a frameshift hotspot in Salmonella. *Journal of Molecular Biology*, 85(2), pp.301–307.

Jacobs, B.S. & Lesmeister, S.A., 2012. Maternal environmental effects on fitness, fruit morphology and ballistic seed dispersal distance in an annual forb. *Functional Ecology*.

Jander, G. et al., 2002. Arabidopsis Map-Based Cloning in the Post-Genome Era. *Plant Physiology*, 129(2), pp.440–450.

Jander, G. et al., 2003. Ethylmethanesulfonate Saturation Mutagenesis in Arabidopsis to Determine Frequency of Herbicide Resistance. *Plant Physiology*, 131(1), pp.139–146.

Jenkins, H. & Tsiantis, M.S., 2010. *The genetics of leaflet development in the Arabidopsis relative Cardamine hirsuta*.

Jeong, S., Rokas, A. & Carroll, Sean B., 2006. Regulation of Body Pigmentation by the Abdominal-B Hox Protein and Its Gain and Loss in Drosophila Evolution. *Cell*, 125(7), pp.1387–1399.

Kandasamy, M.K., Nasrallah, J. B & Nasrallah, M. E, 1994. Pollen-Pistil Interactions and Developmental Regulation of Pollen Tube Growth in Arabidopsis. *Development*, 120(12), pp.3405–3418.

Katoh, K., Asimenos, G. & Toh, H., 2009. Multiple Alignment of DNA Sequences with MAFFT. In D. Posada & J. M. Walker, eds. *Bioinformatics for DNA Sequence Analysis*. Methods in Molecular Biology™. Humana Press, pp. 39–64.

Kempin, S.A. et al., 1997. Targeted disruption in Arabidopsis. *Nature*, 389(6653), pp.802–803.

Kim, Y., Schumaker, K.S. & Zhu, J.-K., 2006. EMS Mutagenesis of Arabidopsis. In J. Salinas & J. J. Sanchez-Serrano, eds. *Arabidopsis Protocols*. Methods in Molecular Biology. Humana Press, pp. 101–103.

Ko, J., Kim, W. & Han, K., 2009. Ectopic expression of MYB46 identifies transcriptional regulatory genes involved in secondary wall biosynthesis in Arabidopsis. *The Plant Journal*, 60(4), pp.649–665.

Koch, M., Al-Shehbaz, I.A. & Mummenhoff, K., 2003. Molecular Systematics, Evolution, and Population Biology in the Mustard Family (Brassicaceae). *Annals of the Missouri Botanical Garden*, 90(2), pp.151–171.

Koch, M., Haubold, B. & Mitchell-Olds, T., 2001. Molecular Systematics of the Brassicaceae: Evidence from Coding Plastidic matK and Nuclear Chs Sequences. *American Journal of Botany*, 88(3), pp.534–544.

Koch, M.A., Haubold, B. & Mitchell-Olds, T., 2000. Comparative Evolutionary Analysis of Chalcone Synthase and Alcohol Dehydrogenase Loci in Arabidopsis, Arabis, and Related Genera (Brassicaceae). *Molecular Biology and Evolution*, 17(10), pp.1483–1498.

Koch, M.A. & Kiefer, M., 2005. Genome Evolution Among Cruciferous Plants: A Lecture from the Comparison of the Genetic Maps of Three Diploid species—Capsella Rubella, Arabidopsis Lyrata Subsp. Petraea, and A. Thaliana. *American Journal of Botany*, 92(4), pp.761–767.

Konieczny, A. & Ausubel, F.M., 1993. A procedure for mapping Arabidopsis mutations using co-dominant ecotype-specific PCR-based markers. *The Plant Journal*, 4(2), pp.403–410.

Konishi, S. et al., 2006. An SNP Caused Loss of Seed Shattering During Rice Domestication. *Science*, 312(5778), pp.1392–1396.

Koornneeff, M., Dellaert, L.W.M. & Van der Veen, J.H., 1982. EMS- and radiation-induced mutation frequencies at individual loci in Arabidopsis thaliana (L.) Heynh. *Mutation Research/Fundamental and Molecular Mechanisms of Mutagenesis*, 93(1), pp.109–123.

Kovalchuk, I., Kovalchuk, O. & Hohn, B., 2000. Genome-wide variation of the somatic mutation frequency in transgenic plants. *The EMBO Journal*, 19(17), pp.4431–4438.

Krieg, D.R., 1963. Ethyl Methanesulfonate-Induced Reversion of Bacteriophage T4rii Mutants. *Genetics*, 48(4), pp.561–580.

Küpper, H. et al., 2000. Cellular compartmentation of cadmium and zinc in relation to other elements in the hyperaccumulator Arabidopsis halleri. *Planta*, 212(1), pp.75–84.

Kumaran, M.K., Bowman, John L & Sundaresan, V., 2002. YABBY Polarity Genes Mediate the Repression of KNOX Homeobox Genes in Arabidopsis. *The Plant Cell Online*, 14(11), pp.2761–2770.

Kusaba, M. et al., 2001. Self-Incompatibility in the Genus Arabidopsis: Characterization of the S Locus in the Outcrossing A. Lyrata and Its Autogamous Relative A. Thaliana. *The Plant Cell Online*, 13(3), pp.627–643.

Lamesch, P. et al., 2011. The Arabidopsis Information Resource (TAIR): improved gene annotation and new tools. *Nucleic Acids Research*.

Larkin, M.A. et al., 2007. Clustal W and Clustal X version 2.0. *Bioinformatics*, 23(21), pp.2947–2948.

Levin, S.A. et al., 2003. The Ecology and Evolution of Seed Dispersal: A Theoretical Perspective. *Annual Review of Ecology, Evolution, and Systematics*, 34, pp.575–604.

Li, X. et al., 2001. A fast neutron deletion mutagenesis-based reverse genetics system for plants. *The Plant Journal*, 27(3), pp.235–242.

Li, X. & Zhang, Y., 2002. Reverse genetics by fast neutron mutagenesis in higher plants. *Functional & Integrative Genomics*, 2(6), pp.254–258.

Lihová, J. et al., 2006. Worldwide Phylogeny and Biogeography of Cardamine Flexuosa (Brassicaceae) and Its Relatives. *American Journal of Botany*, 93(8), pp.1206–1221.

Liljegren, S.J. et al., 2004. Control of Fruit Patterning in Arabidopsis by INDEHISCENT. *Cell*, 116(6), pp.843–853.

Liljegren, S.J. et al., 2000. SHATTERPROOF MADS-box genes control seed dispersal in Arabidopsis. *Nature*, 404(6779), pp.766–770.

Livingstone, C.D. & Barton, G.J., 1993. Protein sequence alignments: a strategy for the hierarchical analysis of residue conservation. *Computer applications in the biosciences : CABIOS*, 9(6), pp.745–756.

Long, J.A. et al., 1996. A member of the KNOTTED class of homeodomain proteins encoded by the STM gene of Arabidopsis. *Nature*, 379(6560), pp.66–69.

Lukowitz, W., Gillmor, C.S. & Scheible, W.-R., 2000. Positional Cloning in Arabidopsis. Why It Feels Good to Have a Genome Initiative Working for You. *Plant Physiology*, 123(3), pp.795–805.

Mable, B.K. & Adam, A., 2007. Patterns of genetic diversity in outcrossing and selfing populations of Arabidopsis lyrata. *Molecular Ecology*, 16(17), pp.3565–3580.

Macnair, Mark R et al., 1999. Zinc Tolerance and Hyperaccumulation Are Genetically Independent Characters. *Proceedings of the Royal Society of London. Series B: Biological Sciences*, 266(1434), pp.2175–2179.

Mandel, M.A. & Yanofsky, M. F, 1995. The Arabidopsis AGL8 MADS Box Gene Is Expressed in Inflorescence Meristems and Is Negatively Regulated by APETALA1. *The Plant Cell Online*, 7(11), pp.1763–1771.

Meakin, P.J. & Roberts, J.A., 1990a. Dehiscence of Fruit in Oilseed Rape (Brassica Nap Us L.) II. THE ROLE OF CELL WALL DEGRADING ENZYMES AND ETHYLENE. *Journal of Experimental Botany*, 41(8), pp.1003–1011.

Meakin, P.J. & Roberts, J.A., 1990b. Dehiscence of Fruit in Oilseed Rape (Brassica Napus L.) I. ANATOMY OF POD DEHISCENCE. *Journal of Experimental Botany*, 41(8), pp.995–1002.

Michaels, S.D. & Amasino, R.M., 1998. A robust method for detecting single-nucleotide changes as polymorphic markers by PCR. *The Plant Journal*, 14(3), pp.381–385.

Michniewicz, M. et al., 2007. Antagonistic Regulation of PIN Phosphorylation by PP2A and PINOID Directs Auxin Flux. *Cell*, 130(6), pp.1044–1056.

Mitsuda, N. et al., 2007. NAC Transcription Factors, NST1 and NST3, Are Key Regulators of the Formation of Secondary Walls in Woody Tissues of Arabidopsis. *The Plant Cell Online*, 19(1), pp.270–280.

Mitsuda, N. et al., 2005. The NAC Transcription Factors NST1 and NST2 of Arabidopsis Regulate Secondary Wall Thickenings and Are Required for Anther Dehiscence. *The Plant Cell Online*, 17(11), pp.2993–3006.

Mitsuda, N. & Ohme-Takagi, M., 2008. NAC transcription factors NST1 and NST3 regulate pod shattering in a partially redundant manner by promoting secondary wall formation after the establishment of tissue identity. *The Plant Journal*, 56(5), pp.768–778.

Müller, A., 1961. Zur Charakterisierung der Blüten und Infloreszenzen von Arabidopsis thaliana (L.) Heynh. *Genetic Resources and Crop Evolution*, 9(1), pp.364–393.

Mummenhoff, K. et al., 2009. Lepidium as a Model System for Studying the Evolution of Fruit Development in Brassicaceae. *Journal of Experimental Botany*, 60(5), pp.1503–1513.

Narbona, E., Arista, M. & Ortiz, P.L., 2005. Explosive Seed Dispersal in Two Perennial Mediterranean Euphorbia Species (Euphorbiaceae). *American Journal of Botany*, 92(3), pp.510–516.

Nathan, R., 2006. Long-Distance Dispersal of Plants. *Science*, 313(5788), pp.786–788.

Nathan, R. et al., 2009. Seed Dispersal. In *Encyclopedia of Life Sciences (eLS)*. Chichester: John Wiley & Sons, Ltd.

Neff, M. M., Turk, E. & Kalishman, M., 2002. Web-based primer design for single nucleotide polymorphism analysis. *Trends in Genetics*, 18(12), pp.613–615.

Neff, Michael M. et al., 1998. dCAPS, a simple technique for the genetic analysis of single nucleotide polymorphisms: experimental applications in Arabidopsis thaliana genetics. *The Plant Journal*, 14(3), pp.387–392.

Nemhauser, J.L., Feldman, L.J. & Zambryski, P.C., 2000. Auxin and ETTIN in Arabidopsis Gynoecium Morphogenesis. *Development*, 127(18), pp.3877–3888.

Nole-Wilson, S., Azhakanandam, S. & Franks, R.G., 2010. Polar auxin transport together with AINTEGUMENTA and REVOLUTA coordinate early Arabidopsis gynoecium development. *Developmental Biology*, 346(2), pp.181–195.

Nutt, P. et al., 2006. Capsella as a model system to study the evolutionary relevance of floral homeotic mutants. *Plant Systematics and Evolution*, 259(2), pp.217–235.

Ohno, C.K. et al., 2004. The Arabidopsis JAGGED Gene Encodes a Zinc Finger Protein That Promotes Leaf Tissue Development. *Development*, 131(5), pp.1111–1122.

Van Ooijen, J.W., 2006. *JoinMap (R) 4, Software for the calculation of genetic linkage maps in experimental populations.*, Wageningen, Netherlands: Kyazma B.V.

Ori, N. et al., 2000. Mechanisms that control knox gene expression in the Arabidopsis shoot. *Development*, 127(24), pp.5523–5532.

Østergaard, L., 2009. Don't 'leaf' now. The making of a fruit. *Current Opinion in Plant Biology*, 12(1), pp.36–41.

Østergaard, L. et al., 2006. Pod shatter-resistant Brassica fruit produced by ectopic expression of the FRUITFULL gene. *Plant Biotechnology Journal*, 4(1), pp.45–51.

Paetsch, M., Mayland-Quellhorst, S. & Neuffer, B., 2006. Evolution of the self-incompatibility system in the Brassicaceae: identification of S-locus receptor kinase (SRK) in self-incompatible Capsella grandiflora. *Heredity*, 97(4), pp.283–290.

Page, D.R. & Grossniklaus, U., 2002. The art and design of genetic screens: Arabidopsis thaliana. *Nature Reviews Genetics*, 3(2), pp.124–136.

Pautot, V. et al., 2001. KNAT2: Evidence for a Link Between Knotted-Like Genes and Carpel Development. *The Plant Cell Online*, 13(8), pp.1719–1734.

Pei, C. et al., 2011. Fine mapping and analysis of a candidate gene in tomato accession PI128216 conferring hypersensitive resistance to bacterial spot race T3. *Theoretical and Applied Genetics*, 124(3), pp.533–542.

Perrins, J., Fitter, A. & Williamson, M., 1993. Population Biology and Rates of Invasion of Three Introduced Impatiens Species in the British Isles. *Journal of Biogeography*, 20(1), pp.33–44.

Peters, J.L., Cnudde, F. & Gerats, T., 2003. Forward genetics and map-based cloning approaches. *Trends in Plant Science*, 8(10), pp.484–491.

Petrasek, J. et al., 2006. PIN Proteins Perform a Rate-Limiting Function in Cellular Auxin Efflux. *Science*, 312(5775), pp.914–918.

Van der Pijl, L., 1972. *Principles of dispersal in higher plants* 2nd ed., Springer-Verlag.

Prud'homme, B., Gompel, N. & Carroll, S. B., 2007. Colloquium Papers: Emerging principles of regulatory evolution. *Proceedings of the National Academy of Sciences*, 104(suppl_1), pp.8605–8612.

Prud'homme, Benjamin et al., 2006. Repeated morphological evolution through cis-regulatory changes in a pleiotropic gene. *Nature*, 440(7087), pp.1050–1053.

Ragni, L. et al., 2008. Interaction of KNAT6 and KNAT2 with BREVIPEDICELLUS and PENNYWISE in Arabidopsis Inflorescences. *The Plant Cell Online*, 20(4), pp.888–900.

Rajani, S. & Sundaresan, V., 2001. The Arabidopsis myc/bHLH gene ALCATRAZ enables cell separation in fruit dehiscence. *Current Biology*, 11(24), pp.1914–1922.

Roberts, M.L. & Haynes, R.R., 1983. Ballistic seed dispersal in *Illicium* (*Illiciaceae*). *Plant Systematics and Evolution*, 143(3), pp.227–232.

Robles, P. & Pelaz, S., 2005. Flower and fruit development in Arabidopsis thaliana. *International Journal of Developmental Biology*, 49, pp.633–643.

Roeder, A.H.K., Ferrándiz, C. & Yanofsky, Martin F., 2003. The Role of the REPLUMLESS Homeodomain Protein in Patterning the Arabidopsis Fruit. *Current Biology*, 13(18), pp.1630–1635.

Roeder, A.H.K. & Yanofsky, M. F., 2006. Fruit Development in Arabidopsis. *The Arabidopsis Book*, 4, p.e0075.

Rogers, L.A. et al., 2005. Comparison of lignin deposition in three ectopic lignification mutants. *New Phytologist*, 168(1), pp.123–140.

Rousset, F. & Gandon, S., 2002. Evolution of the distribution of dispersal distance under distance-dependent cost of dispersal. *Journal of Evolutionary Biology*, 15(4), pp.515–523.

Rozen, S. & Skaletsky, H., 1999. Primer3 on the WWW for General Users and for Biologist Programmers. In S. Misener & S. A. Krawetz, eds. *Bioinformatics Methods and Protocols*. Methods in Molecular Biology. Humana Press, pp. 365–386.

Säll, T. et al., 2004. Mode of reproduction in Arabidopsis suecica. *Hereditas*, 141(3), pp.313–317.

Schemske, D.W., 1978. Evolution of Reproductive Characteristics in Impatiens (Balsaminaceae): The Significance of Cleistogamy and Chasmogamy. *Ecology*, 59(3), pp.596–613.

Schierup, M.H. et al., 2001. Identification and Characterization of a Polymorphic Receptor Kinase Gene Linked to the Self-Incompatibility Locus of Arabidopsis Lyrata. *Genetics*, 158(1), pp.387–399.

Schiessl, K. et al., 2012. JAGGED Controls Growth Anisotropy and Coordination between Cell Size and Cell Cycle during Plant Organogenesis. *Current Biology*, 22(0), pp.1–8.

Schmitt, J., Ehrhardt, D. & Swartz, D., 1985. Differential Dispersal of Self-Fertilized and Outcrossed Progeny in Jewelweed (Impatiens capensis). *The American Naturalist*, 126(4), pp.570–575.

Schoof, H. et al., 2000. The Stem Cell Population of Arabidopsis Shoot Meristems Is Maintained by a Regulatory Loop between the CLAVATA and WUSCHEL Genes. *Cell*, 100(6), pp.635–644.

Schranz, M.E., Lysak, M.A. & Mitchell-Olds, T., 2006. The ABC's of comparative genomics in the Brassicaceae: building blocks of crucifer genomes. *Trends in Plant Science*, 11(11), pp.535–542.

Schulz, O.E., 1936. Cruciferae. In A. Engler & H. Harms, eds. *Die natürlichen Pflanzenfamilien*. Leipzig, Germany: Willhelm Engelmann, pp. 227–658.

Scofield, S., Dewitte, W. & Murray, J.A.H., 2007. The KNOX gene SHOOT MERISTEMLESS is required for the development of reproductive meristematic tissues in Arabidopsis. *The Plant Journal*, 50(5), pp.767–781.

Scotland, R.W. & Wortley, A.H., 2003. How many species of seed plants are there? *Taxon*, 52(1), pp.101–104.

Semiarti, E. et al., 2001. The ASYMMETRIC LEAVES2 Gene of Arabidopsis Thaliana Regulates Formation of a Symmetric Lamina, Establishment of Venation and Repression of Meristem-Related Homeobox Genes in Leaves. *Development*, 128(10), pp.1771–1783.

Sessions, R.A. & Zambryski, P.C., 1995. Arabidopsis Gynoecium Structure in the Wild and in Ettin Mutants. *Development*, 121(5), pp.1519–1532.

Shen, Y.-J. et al., 2004. Development of Genome-Wide DNA Polymorphism Database for Map-Based Cloning of Rice Genes. *Plant Physiology*, 135(3), pp.1198–1205.

Shimamura, M., Yamaguchi, T. & Deguchi, H., 2008. Airborne sperm of Conocephalum (Conocephalaceae). *Journal of Plant Research*, 121(1), pp.69–71.

Siegfried, K.R. et al., 1999. Members of the YABBY Gene Family Specify Abaxial Cell Fate in Arabidopsis. *Development*, 126(18), pp.4117–4128.

Sikora, P. et al., 2011. Mutagenesis as a Tool in Plant Genetics, Functional Genomics, and Breeding. *International Journal of Plant Genomics*, 2011, pp.1–13.

Simons, P., 1992. *The action plant : movement and nervous behaviour in plants.*, Oxford: Blackwell.

Skotheim, J.M. & Mahadevan, L., 2005. Physical Limits and Design Principles for Plant and Fungal Movements. *Science*, 308(5726), pp.1308–1310.

Smyth, D. R., Bowman, J. L & Meyerowitz, E. M, 1990. Early Flower Development in Arabidopsis. *The Plant Cell Online*, 2(8), pp.755–767.

Soltis, P.S. & Soltis, D.E., 2004. The Origin and Diversification of Angiosperms. *American Journal of Botany*, 91(10), pp.1614–1626.

Sorefan, K. et al., 2009. A regulated auxin minimum is required for seed dispersal in Arabidopsis. *Nature*, 459(7246), pp.583–586.

Sorensen, A.E., 1986. Seed Dispersal by Adhesion. *Annual Review of Ecology and Systematics*, 17, pp.443–463.

Spence, J. et al., 1996. 'Pod shatter' in Arabidopsis thaliana, Brassica napus and B. juncea. *Journal of Microscopy, Journal of Microscopy*, 181, 181(2, 2), pp.195, 195–203, 203.

Spielman, M. et al., 1997. TETRASPORE is required for male meiotic cytokinesis in Arabidopsis thaliana. *Development*, 124(13), pp.2645–2657.

Sporne, K.R., 1974. *The Mysterious Origin of Flowering Plants*, Oxford Univ, Press.

Stamp, N.E., 1989. Efficacy of Explosive vs. Hygroscopic Seed Dispersal by an Annual Grassland Species. *American Journal of Botany*, 76(4), pp.555–561.

Stamp, N.E., 1984. Self-Burial Behaviour of Erodium Cicutarium Seeds. *Journal of Ecology*, 72(2), pp.611–620.

Stamp, N.E. & Lucas, J.R., 1983. Ecological correlates of explosive seed dispersal. *Oecologia*, 59(2), pp.272–278.

Sundberg, S., 2010. Size matters for violent discharge height and settling speed of Sphagnum spores: important attributes for dispersal potential. *Annals of Botany*, 105(2), pp.291–300.

Swaine, M.D. & Beer, T., 1977. Explosive seed dispersal in Hura crepitans L. (Euphorbiaceae). *New Phytologist*, 78(3), pp.695–708.

Taylor, P. et al., 2006. High-speed pollen release in the white mulberry tree, Morus alba L. *Sexual Plant Reproduction*, 19(1), pp.19–24.

The Arabidopsis Genome Initiative, 2000. Analysis of the genome sequence of the flowering plant Arabidopsis thaliana. *Nature*, 408(6814), pp.796–815.

The UniProt Consortium, 2012. Reorganizing the protein space at the Universal Protein Resource (UniProt). *Nucleic Acids Research*, 40, pp.D71–D75.

Thoma, S. et al., 1994. Tissue-Specific Expression of a Gene Encoding a Cell Wall-Localized Lipid Transfer Protein from Arabidopsis. *Plant Physiology*, 105(1), pp.35–45.

Thoquet, P. et al., 2002. The molecular genetic linkage map of the model legume Medicago truncatula: an essential tool for comparative legume genomics and the isolation of agronomically important genes. *BMC Plant Biology*, 2(1), p.1.

Tiffney, B.H., 1984. Seed Size, Dispersal Syndromes, and the Rise of the Angiosperms: Evidence and Hypothesis. *Annals of the Missouri Botanical Garden*, 71(2), pp.551–576.

Trail, F., 2007. Fungal cannons: explosive spore discharge in the Ascomycota. *FEMS Microbiology Letters*, 276(1), pp.12–18.

Trail, F. et al., 2002. Physiological and environmental aspects of ascospore discharge in Gibberella zeae (anamorph Fusarium graminearum). *Mycologia*, 94(2), pp.181–189.

Trail, F., Gaffoor, I. & Vogel, S., 2005. Ejection mechanics and trajectory of the ascospores of Gibberella zeae (anamorph Fuarium graminearum). *Fungal Genetics and Biology*, 42(6), pp.528–533.

Urbanus, S.L. et al., 2009. In planta localisation patterns of MADS domain proteins during floral development in Arabidopsis thaliana. *BMC Plant Biology*, 9, p.5.

Vaughn, K.C., Bowling, A.J. & Ruel, K.J., 2011. The Mechanism for Explosive Seed Dispersal in Cardamine Hirsuta (Brassicaceae). *American Journal of Botany*, 98(8), pp.1276–1285.

Vogel, S., 2005. Living in a physical world II. The bio-ballistics of small projectiles. *Journal of Biosciences*, 30(2), pp.167–175.

Webster, T.R., 1995. Demonstrating Spore Dispersal in the Spikemoss, Selaginella martensii. *The American Biology Teacher*, 57(2), pp.83–86.

Weigel, D. & Glazebrook, J., 2006. Forward Genetics in Arabidopsis: Finding Mutations that Cause Particular Phenotypes. *Cold Spring Harbor Protocols*, 2006(5), p.pdb.top1.

Western, T.L., 2006. Changing spaces: the Arabidopsis mucilage secretory cells as a novel system to dissect cell wall production in differentiating cellsThis review is one of a selection of papers published in the Special Issue on Plant Cell Biology. *Canadian Journal of Botany*, 84(4), pp.622–630.

Western, T.L. et al., 2001. Isolation and Characterization of Mutants Defective in Seed Coat Mucilage Secretory Cell Development in Arabidopsis. *Plant Physiology*, 127(3), pp.998–1011.

Western, T.L., Skinner, D.J. & Haughn, George W., 2000. Differentiation of Mucilage Secretory Cells of the Arabidopsis Seed Coat. *Plant Physiology*, 122(2), pp.345–356.

White, T.J. et al., 1990. Amplification and direct sequencing of fungal ribosomal RNA genes for phylogenetics. In M. A. Innis et al., eds. *PCR protocols: A guide to methods and applications*. San Diego, California: Academic Press, pp. 315–322.

Wu, H. et al., 2006. The INDEHISCENT protein regulates unequal cell divisions in Arabidopsis fruit. *Planta*, 224(4), pp.971–979.

Yano, S., 1997. Silique burst of*Cardamine scutata* (Cruciferae) as a physical inducible defense against seed predatory caterpillars. *Researches on Population Ecology*, 39(1), pp.95–100.

Yatsu, Y., Kachi, N. & Kudoh, H., 2003. Ecological distribution and phenology of an invasive species, Cardamine hirsuta L., and its native counterpart, Cardamine flexuosa With., in central Japan. *Plant Species Biology*, 18(1), pp.35–42.

Zhao, F.J. et al., 2000. Zinc hyperaccumulation and cellular distribution in Arabidopsis halleri. *Plant, Cell & Environment, Plant, Cell & Environment*, 23(5), pp.507–514.

Zhong, R. et al., 2008. A Battery of Transcription Factors Involved in the Regulation of Secondary Cell Wall Biosynthesis in Arabidopsis. *The Plant Cell Online*, 20(10), pp.2763–2782.

Zhong, R., Richardson, E. & Ye, Z.-H., 2007a. The MYB46 Transcription Factor Is a Direct Target of SND1 and Regulates Secondary Wall Biosynthesis in Arabidopsis. *The Plant Cell Online*, 19(9), pp.2776–2792.

Zhong, R., Richardson, E. & Ye, Z.-H., 2007b. Two NAC domain transcription factors, SND1 and NST1, function redundantly in regulation of secondary wall synthesis in fibers of Arabidopsis. *Planta*, 225(6), pp.1603–1611.

Zhou, J. et al., 2009. MYB58 and MYB63 Are Transcriptional Activators of the Lignin Biosynthetic Pathway During Secondary Cell Wall Formation in Arabidopsis. *The Plant Cell Online*, 21(1), pp.248–266.